

The Crustal and Upper Mantle Shear
Velocity Structure of Eastern North
America from the Joint Inversion
of Receiver Function and
Surface-Wave Dispersion

Mohammed Saeed Fnais

A Dissertation Presented to the Faculty of the Graduate
School of Saint Louis University in Partial
Fulfillment of the Requirements for the
Degree of Doctor of Philosophy

2004

COMMITTEE IN CHARGE OF CANDIDACY:

Professor Robert B. Herrmann,
Chairperson and Advisor

Assistant Professor Keith Koper,

Assistant Professor Lupei Zhu

Acknowledgments

I dedicate this dissertation to my family, my parents, and my friends, here and in Saudi Arabia, who care for and are concerned about me. Their calls and prayers always supported me during my study. I am glad now to share this work with them. It is a great opportunity to mention Mr. Hussain Ahmed Jaber (the leading teacher in my town) for his time and effort to spread education and knowledge there.

I would like to express my special thanks to my adviser Dr. Robert B. Herrmann for his constant advice and guidance throughout this study. Dr. Herrmann is not only my academic adviser, but also advised me on my special life as a student and researcher. I still remember that day when he went with me to the department of Mathematics to set my wife's schedule. I also share the moment of happiness with all faculty in the department who asked me every other day about my study. I would like to thank Dr. Keith Koper for sharing his time with me during my research from the beginning and spending time reading this dissertation. I, also, thank Dr. Lupei Zhu for his valuable advice and for teaching me new interpretation techniques.

This dissertation would not be accomplished without data sets from the following data centers: IRIS (the Incorporated Research Institutions for Seismology), USNSN (United States National Seismic Network), CNSN (Canadian National Seismic Network) and POLARIS (Portable Observatories for Lithospheric Analysis and Research Investigating Seismicity). Also, a special thanks

are due to Dr. Karen Fischer and Dr. Michael Wysession for providing me with the FLED data. It is also a great opportunity to thank every one whose products (surface-wave dispersion curves) were part of this research.

Finally, some words that I never forget are "Do not let people say Saeed Fnais educated every one in his small town, but forgot to educate his children," my father said. My mother said "every night I think of you and your kids so do not let me be tired for nothing." My uncles, brothers and sisters asked me to finish as soon as possible so we will have the chance to live together again. My wife said to me "I miss my family, my friends, and I travel with you to share with you every moment, so please give me the best gift when your study is accomplished." I thank my children, Khaled and Tesneem, for everything you did (make me busy when I want to get rest), but after all you are the best thing in my life. To I would like ask from my father and my mother "SAMEHONI", I need your prayers.

Table of Contents

CHAPTER 1: Introduction

1.1	The Problem	1
1.2	Review of Related Literature	6
1.2.1	Plate tectonic setting and main tectonic elements of North America	6
1.2.2	Crustal thickness, average crustal velocity, and P_n velocity	8
1.2.3	Inversion for Crustal Properties	11
	Receiver function	11
	Surface wave dispersion	13
	Joint inversion of receiver function and dispersion curve	16

CHAPTER 2: Geology and Geophysics of Eastern North America

2.1	Crustal and Upper-mantle Structure	20
2.1.1	Canadian Shield	20
2.1.2	Central United States	27
2.1.3	The Appalachian Provinces	32
2.2	The Seismicity and Seismotectonics	38
2.2.1	Canadian Shield	38
2.2.2	Central United States	39
2.2.3	The Appalachian Provinces	41

CHAPTER 3: Crustal Structure of the Eastern North America from Receiver Functions

3.1	Receiver Function	43
3.1.1	Receiver function estimation	43
	The source equalization procedure	43
	Iterative deconvolution	48
3.2	Receiver Function Interpretation	50
3.2.1	Ray parameter sensitivity	51
3.2.2	Changing crustal velocity	53
3.2.3	Shallow low-velocity structure	53
3.3	Data Analysis	56
3.3.1	Receiver function data analysis	64
3.4	Crustal Thickness and Data Analysis	68

CHAPTER 4: Joint Inversion of Receiver Function and Surface-Wave Dispersion

4.1	Surface Wave Dispersion Curves	89
-----	--	----

4.1.1	Introduction	89
4.1.2	Love and Rayleigh Waves	90
4.1.3	Dispersion in surface Waves	91
	Group velocity	93
4.1.4	Inversion of dispersion curves	94
4.1.5	Group and phase velocity estimation	97
4.2	Joint Inversion of Receiver Function and Surface-Wave Dispersion	101
4.2.1	Introduction	101
4.2.2	Inversion procedure	102
4.3	Joint Inversion Processing	106
4.4	Lithospheric Structure of the Canadian Sites	108
4.4.1	The Canadian Shield (Eastern Canada)	108
	Northern (Canadian) Appalachians	109
	Grenville Province	112
	Superior Province	117
4.4.2	Canadian High Arctic region	120
4.4.3	Southwestern Canada	121
4.4.4	Northwestern Canada	126
4.5	Lithospheric Structure of the U. S. Sites	132
4.5.1	Coastal Plain	132
4.5.2	The Appalachian Orogen	136
4.5.3	Central United States (late Proterozoic)	149
CHAPTER 5: Conclusion		
5.1	Crustal Structure	168
5.2	Crustal Thickness	170
5.3	Comparison of Joint Inversion Models to Crustal Refraction Models	175
5.3.1	Structure near DRLN	175
5.3.2	Structure near GAC and NCB	176
5.3.3	Structure near SLM	178
5.4	Future Work	182
APPENDIX : Stacked Receiver Functions for all Stations.....		184
References.....		196
Vita Auctoris.....		213

List of Tables

Table 3.1: Reference model used to compute the synthetic receiver function	51
Table 3.2: Reference model used to compute the synthetic receiver function	53
Table 3.3: United States National Seismic Network (USNSN) and IRIS stations used in this study	57
Table 3.4: New Madrid network (NM) stations used in this study	58
Table 3.5: Canadian National Seismic Network (CNSN) and POLARIS - NWT (Portable Observatories for Lithospheric Analysis and Research Investigating Seismicity) stations used in this study	59
Table 3.6: FLED stations used for this study. The project ran for 15 month starting Spring, 2001	61
Table 3.7: MOMA stations used for this study. The stations ran for one year 1995-1996	63
Table 3.8: Locations of stations used in this study with the estimated crustal thickness (h) and V_P/V_S	85
Table 5.1: A comparison of crustal thickness estimates	170

List of Figures

Figure 1.1: Locations of permanent and temporary (MOMA (MM) and FLED (FA) arrays) broadband seismic stations in Eastern North America used in this study	3
Figure 1.2: North America crustal Provinces (Hoffman, 1989)	4
Figure 2.1: Index map of the eastern North America tectonic units, geologic provinces, and location of major basins (Braile, 1989 modified after Hoffman, 1989).	21
Figure 3.1: Comparison between the iterative deconvolution (time-domain) and the frequency-domain deconvolution for $\alpha = 1.0$. Top panel shows receiver function computed by time-domain deconvolution. The bottom panel shows the receiver function computed using frequency-domain deconvolution.	49
Figure 3.2: Study of the effect of changing ray parameter from 0.04 sec/km to 0.08 sec/km for Gaussian filter parameter $\alpha = 1.0$. For comparison, all traces are plotted to the same scale.	52
Figure 3.3: The effect of changing the crustal velocity with fixed ray parameter and halfspace velocity. The V_P/V_S ratio was fixed. A Gaussian filter parameter $\alpha = 1.0$ is used.	54
Figure 3.4: The effect of a shallow low velocity on receiver function for different values of surface layer thickness. A Gaussian filter parameter $\alpha = 2.5$ is used.	55
Figure 3.5: The FLED seismic stations used in this study	60
Figure 3.6: The MOMA seismic stations used in this study	62
Figure 3.7: Azimuthal equidistant projection of all teleseismic events location which used for this study. The two inner circles show the distances of $30^\circ < \Delta < 90^\circ$ for a reference site in the central US. . .	65
Figure 3.8: An example of the actual and rotated seismogram (the east-west component (E), the north-south component, the vertical component (Z), the radial component (R), and the tangential component (T)) used to compute the receiver functions	66

- Figure 3.9: Radial and Transverse receiver functions as a function of back azimuth in degree. The left panel corresponds to radial receiver functions while the right panel shows the corresponding tangential receiver function. The plot shows a clear P_s phase as well as multiple phases. The signal on the tangential component can be due to a non-horizontal interface, slightly improper back azimuth or anisotropy. This is an example of a group one (k) of receiver functions. The traces correspond to an $\alpha = 2.5$ 69
- Figure 3.10: Radial and Transverse receiver functions as a function of back azimuth in degree. The left panel corresponds to radial receiver functions while the right panel shows the corresponding tangential receiver function. The plot shows a clear P_s phase, but no consistent multiple phases. This is an example of the second group (-) of receiver functions. The traces correspond to an $\alpha = 2.5$ 70
- Figure 3.11: Radial and Transverse receiver functions as a function of back azimuth in degree. The left panel corresponds to radial receiver functions while the right panel shows the corresponding tangential receiver function. The plot shows the effect of the thick sediment layer on the computed receiver function. Although, we have enough receiver functions, the P_s phase cannot be picked accurately. Also, a large shift in the P arrival is seen, which is an indication of interference of several pulses within the width of the Gaussian function. The traces correspond to an $\alpha = 2.5$. This is an example of the third group (X) receiver functions. 71
- Figure 3.12: The best estimate P_s time delay (for $p = 0.06$ s/km) picked for the Moho P_s converted phase using radial receiver function for station HRV. 75
- Figure 3.13: The best estimate V_p/V_s ratio (k) for the radial receiver function (HRV). 75
- Figure 3.14: The best estimate P_s time delay (for $p = 0.06$ s/km) picked for the Moho P_s converted phase from the radial receiver function for station LSCT. 76
- Figure 3.15: The estimate V_p/V_s ratio (k) from the radial receiver function for station LSCT. for this station I use the average value. . . . 76
- Figure 3.16: The receiver function at FA22 is affected by the sediment layer that no P_s time can be picked. 77
- Figure 3.17: The estimate V_p/V_s ratio (k) at FA22 can not be accurate and is excluded. 77

Figure 3.18: P_s time delay (for $p = 0.06$ s/km) for Eastern North America stations used in this study. The red circle is above average and the blue circle is below average. The map show a pattern with a low than average in the Coastal Plain and high values toward the midcontinent. The uncertainties are represented by the size of the cross 78

Figure 3.19: V_P/V_S for Eastern North America stations used in this study. The red circle is above average and the blue circle is below average. The map show a pattern with a low than average in the Coastal Plain and high values toward the midcontinent. The uncertainties are represented by the size of the cross 79

Figure 3.20: Radial receiver function for station HRV as a function of ray parameter in s/km. Red lines show Moho P_s , and the later $P_pP_m s$. The upper panel shows the $s(h, k)$ from stacking the receiver functions. The elliptical shape shows the best estimate of both V_P/V_S ratio k and the corresponding crustal thickness h . This station stack shows a well defined maximum. 81

Figure 3.21: Radial receiver function for station LSCT as a function of ray parameter in s/km. Red lines show Moho P_s , and the later $P_pP_m s$. The upper panel shows the best estimate V_P/V_S ratio (k) . . 82

Figure 3.22: Radial receiver function for station FA22 (FLED Arrays) as a function of ray parameter in s/km. Red lines show Moho P_s , and the later $P_pP_m s$. The upper panel shows the best estimate V_P/V_S ratio (k). The ringing in the receiver functions does not permit an unambiguous estimate of the desired parameters. 83

Figure 4.1: The final shear velocity model inverted from receiver function and surface-wave dispersion of Rayleigh group and phase velocity. This model compares the structure for two stations from CNSN located on the northern Appalachians. For LMN the numbers 13 / 14 / 4 indicate that the number of receiver functions used with $\alpha = 0.5 / 1.0 / 2.5$ 111

Figure 4.2: The final shear velocity model inverted from receiver function and surface-wave dispersion of Rayleigh group and phase velocity. This model show four stations from CNSN 115

Figure 4.3: The final shear velocity model inverted from receiver function and surface-wave dispersion of Rayleigh group and phase velocity. This model show stations from CNSN that are located on the southern Canada (Grenville Province) 117

Figure 4.4: The final shear velocity model inverted from receiver function and surface-wave dispersion of Rayleigh group and phase velocity. This model show four stations from CNSN located southeastern Canada (Superior Province)	119
Figure 4.5: The final shear velocity model inverted from receiver function and surface-wave dispersion of Rayleigh group and phase velocity. This model show two stations from CNSN on the Arctic Region	122
Figure 4.6: The final shear velocity model inverted from receiver function and surface-wave dispersion of Rayleigh group and phase velocity. This model compares four stations from the CNSN located in south-southwestern Canada.	124
Figure 4.7: The final shear velocity model inverted from receiver function and surface-wave dispersion of Rayleigh group and phase velocity. This model compares four stations from POLARIS Network .	128
Figure 4.8: The final shear velocity model inverted from receiver function and surface-wave dispersion of Rayleigh group and phase velocity. This model compares four stations from POLARIS Network .	129
Figure 4.9: The final shear velocity model inverted from receiver function and surface-wave dispersion of Rayleigh group and phase velocity. This model compares four stations from POLARIS	130
Figure 4.10: The final shear velocity model inverted from receiver function and surface-wave dispersion of Rayleigh group and phase velocity. This model compares three stations from POLARIS	131
Figure 4.11: The final shear velocity model inverted from receiver function and surface-wave dispersion of Rayleigh group and phase velocity. This model compares stations located On the Coastal Plain East of the U.S.	133
Figure 4.12: The final shear velocity model inverted from receiver function and surface-wave dispersion of Rayleigh group and phase velocity. This model compares stations located on southern coastal plain of the U.S.	135
Figure 4.13: The final shear velocity model inverted from receiver function and surface-wave dispersion of Rayleigh group and phase velocity. This model compares stations located on the northern Appalachian	138

Figure 4.14: The final shear velocity model inverted from receiver function and surface-wave dispersion of Rayleigh group and phase velocity. This model compares stations located on the northern Appalachian	139
Figure 4.15: The final shear velocity model inverted from receiver function and surface-wave dispersion of Rayleigh group and phase velocity. This model compares stations located on the central Appalachian	143
Figure 4.16: The final shear velocity model inverted from receiver function and surface-wave dispersion of Rayleigh group and phase velocity. This model compares stations located on the southern Appalachian	144
Figure 4.17: The final shear velocity model inverted from receiver function and surface-wave dispersion of Rayleigh group and phase velocity. This model compares stations located on the southern Appalachian	147
Figure 4.18: The final shear velocity model inverted from receiver function and surface-wave dispersion of Rayleigh group and phase velocity. This model compares stations located on the southern Appalachian	148
Figure 4.19: The final shear velocity model inverted from receiver function and surface-wave dispersion of Rayleigh group and phase velocity. This model compares stations located on the central Midcontinent	152
Figure 4.20: The final shear velocity model inverted from receiver function and surface-wave dispersion of Rayleigh group and phase velocity. This model compares stations located on the central Midcontinent	153
Figure 4.21: The final shear velocity model inverted from receiver function and surface-wave dispersion of Rayleigh group and phase velocity. This figure compares models for stations located on the central Midcontinent	156
Figure 4.22: The final shear velocity model inverted from receiver function and surface-wave dispersion of Rayleigh group and phase velocity. This figure compares models at stations located on the central Midcontinent	157

Figure 4.23: The final shear velocity model inverted from receiver function and surface-wave dispersion of Rayleigh group and phase velocity. This figure compare models for stations located on the central Midcontinent	160
Figure 4.24: The final shear velocity model inverted from receiver function and surface-wave dispersion of Rayleigh group and phase velocity. This figure compares models for stations located on the central Midcontinent	161
Figure 4.25: The final shear velocity model inverted from receiver function and surface-wave dispersion of Rayleigh group and phase velocity. This figure compares models at stations located on the central Midcontinent	163
Figure 4.26: The final shear velocity model inverted from receiver function and surface-wave dispersion of Rayleigh group and phase velocity. This figure compares models for stations located on the central Midcontinent	165
Figure 4.27: The final shear velocity model inverted from receiver function and surface-wave dispersion of Rayleigh group and phase velocity. This figure compare models for stations located on the central Midcontinent	166
Figure 4.28: The final shear velocity model inverted from receiver function and surface-wave dispersion of Rayleigh group and phase velocity. This figure compares models for stations located on the central Midcontinent	167
Figure 5.1: The model compares between the final model from this study with the final model from Hughes et al. (1992).	176
Figure 5.2: The model compares between the stacked receiver function for DRLN (ray parameter p 0.04-0.08 and $\alpha=1.0$) with the synthetic receiver function estimated from the final model from Hughes et al. (1992) and the final model from the joint inversion techniques (ray parameter $p=0.06$ and $\alpha = 1.0$).	177
Figure 5.3: The plot compares the final model inverted from this study for NCB and different models as indicated by the model captions. All models reflect the present of the high velocity layer in the middle crust.	179

Figure 5.4: Compression between the synthetic receiver function computed from the refraction model and the joint inversion final model (ray parameter $p=0.06$ and $\alpha=1.0$) and the stacked receiver function for NCB station (ray parameter p 0.04-0.08 and $\alpha=1.0$).	179
Figure 5.5: The final model inverted using joint inversion is in good agreement with the final model from Catchings (1999).	180
Figure 5.6: The synthetic receiver function computed from the final model for both refraction method (Catchings, 1999) and joint inversion techniques (ray parameter $p =0.06$ and $\alpha=1.0$) and the stacked receiver function for SLM as a function of ray parameter (ray parameter p 0.04-0.08 and $\alpha=1.0$). Both receiver function have the same features with different amplitude.	181
Figure A.1: Stacked receiver functions as a function of ray parameters. .	186
Figure A.2: Stacked receiver functions as a function of ray parameters. .	187
Figure A.3: Stacked receiver functions as a function of ray parameters. .	188
Figure A.4: Stacked receiver functions as a function of ray parameters. .	189
Figure A.5: Stacked receiver functions as a function of ray parameters. .	190
Figure A.6: Stacked receiver functions as a function of ray parameters. .	191
Figure A.7: Stacked receiver functions as a function of ray parameters. .	192
Figure A.8: Stacked receiver functions as a function of ray parameters. .	193
Figure A.9: Stacked receiver functions as a function of ray parameters. .	194
Figure A.10: Stacked receiver functions as a function of ray parameters. .	195

Chapter 1

Introduction

1.1 The Problem

Among the oldest and most fundamental problems in seismology are determining the velocity-depth relation accurately, ascertaining the nature of discontinuities within the Earth, and translating this information into knowledge of the materials that constitute the interior of the earth. The crust, which occupies the outermost shell of the Earth, has always been of great interest to seismologists. In addition, knowledge of crustal structure is a prerequisite for obtaining precise information on the nature of the Earth's interior below the Moho discontinuity. The crust can be defined as the outer shell of the earth laying above the level at which the P-wave velocity increases rapidly or discontinuously to values in excess of 7.8 km/sec.

The seismic structure of the crust and upper mantle provides critical information regarding lithospheric composition and evolution. There are large variations in fundamental properties such as crustal and upper mantle velocity structure, and the depth to the lithospheric/asthenospheric boundary. The seismic velocity structure of major tectonic regions provides important constraints on theories for the formation and evolution of the Earth crust. For the first part of the 20th century, most studies on velocity structure were restricted to the determination of one-dimensional models of the solid Earth and of differ-

ent regions within it. Recently, with the introduction of better data and computational methods, seismologists were able to determine three-dimensional velocity models with better resolution of finer feature in the Earth. Geophysicists study the seismic velocity structure of the crust and upper mantle to determine the composition and thickness of the outer layer of the earth and to be able to accurately locate earthquakes and understand them.

In the past years much progress has been made toward understanding the nature and evolution of the different tectonic provinces of North America. Previous studies gave different Earth models for North America, but neither the teleseismic P-wave delay times nor active source surveys have had the earthquake source and station density required to determine the detailed velocity structure of the sub-crustal lithosphere (Mooney and Meissner, 1991 and 1992; Holbrook et al., 1992; Christensen and Mooney 1995). The overall structure of these regions cannot be measured directly and a reliable estimate of their structure requires a combination of data from a number of discrete studies. Most of our information about the seismic velocity structure of North America has been obtained by refraction and reflection methods which are more localized. With the development of long period seismometers it is possible to obtain more information about the sub-surface properties through surface and body waves.

North America is an ideal region to obtain detailed and reliable seismological information and increase our understanding of continental tectonics: it has a large number of modern, broadband, digital seismographs (Figure 1.1) and

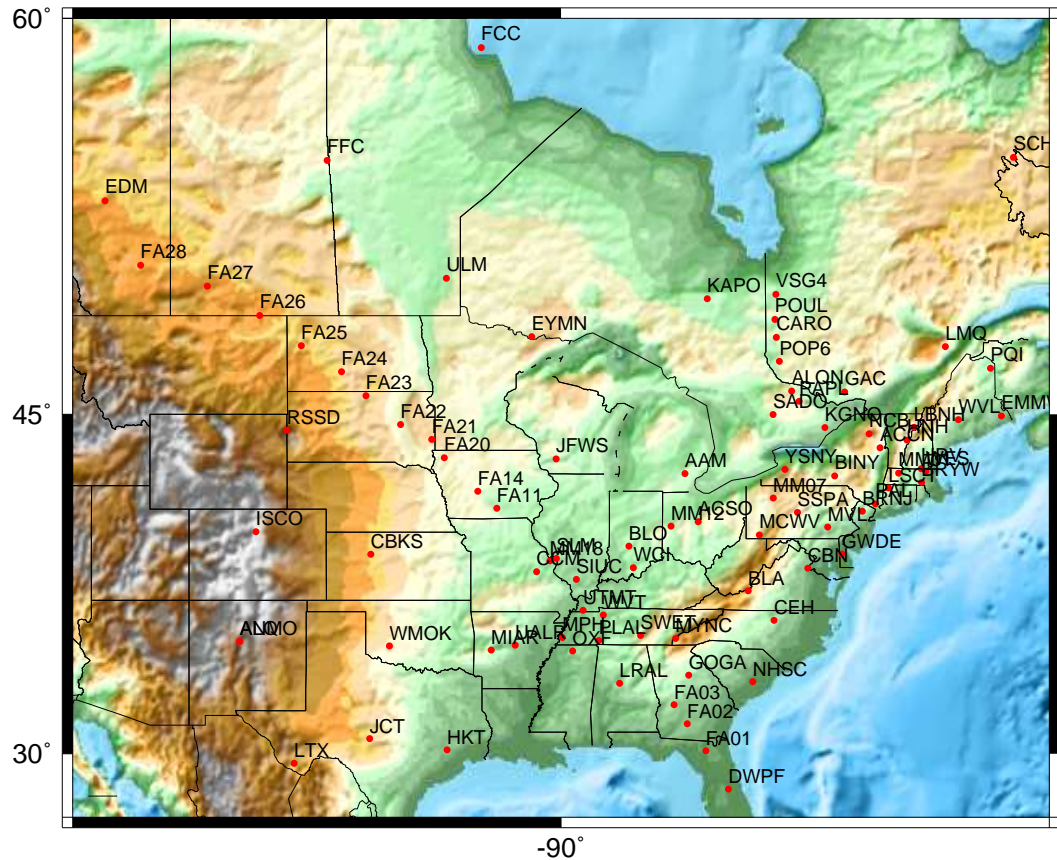


Figure 1.1: Locations of permanent and temporary (MOMA (MM) and FLED (FA) arrays) broadband seismic stations in Eastern North America used in this study

high seismicity on its southern and western borders.

Studies during the recent years have clearly shown that the physical properties of the upper mantle beneath North America vary significantly from east to west and that the details of this variation correlate with the major tectonic provinces of the continents. The western part of North America includes the subduction zones in the Pacific Northwest, a major strike-slip boundary along the coast of California, the wide continental extension in the Basin and Range, and the Rocky Mountains. The eastern side of the continent hosts the older Ap-

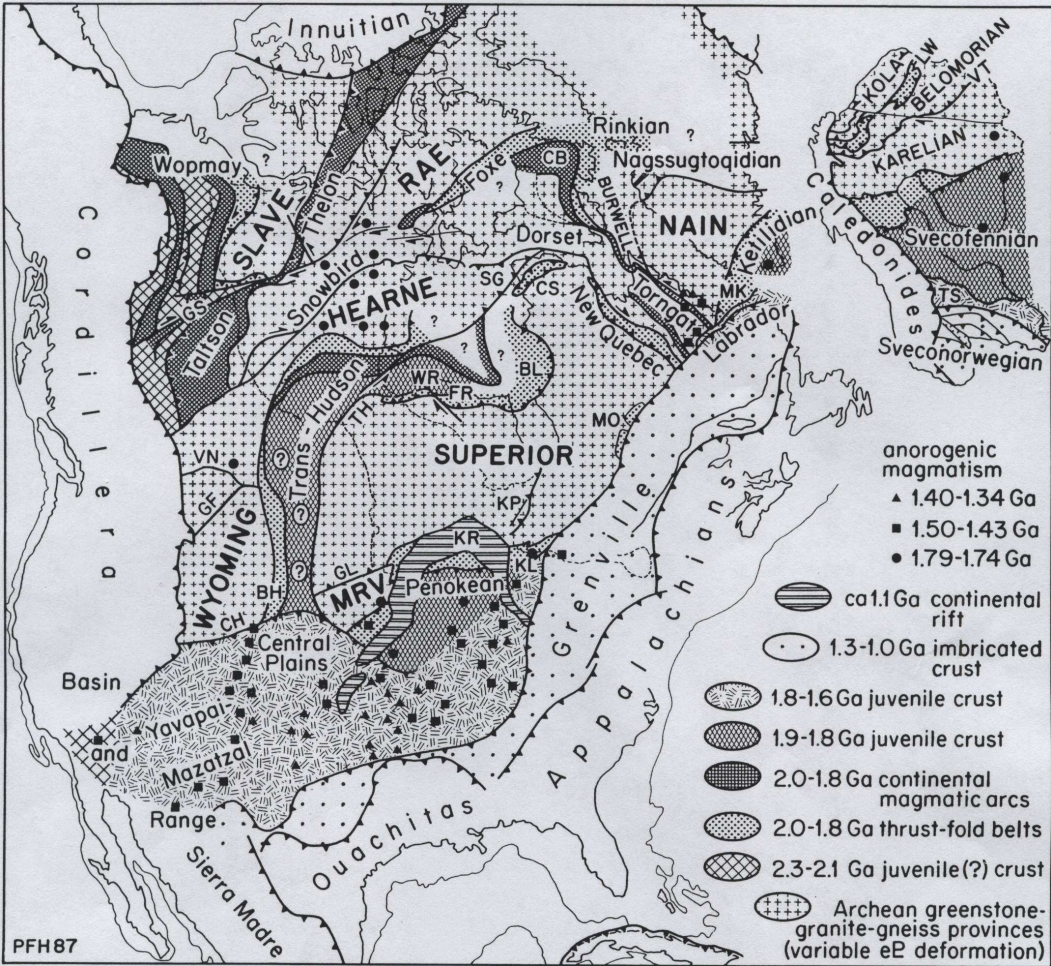


Figure 1.2: North America crustal Provinces (Hoffman, 1989)

palachian Mountains as well as the shields and platforms that comprise the eastern conterminous U.S. and Canada (Figure 1.2).

Although, numerous seismic reflection and refraction studies have been conducted in North America, few shear-wave velocity models are available that cover a large enough area to develop crustal velocity models that are representative of the North America. Although the wealth of information provided by numerous geophysical and geological surveys of the North America has greatly increased our knowledge and understanding of this region, the deep struc-

ture (>40 km) is still largely unknown and poses many interesting questions. Again, these studies were not evenly distributed. The fundamental goal of this study is to use modern broadband seismic data to estimate certain crust and upper mantle properties: depth to Moho, average crustal V_P/V_S ratio, and the use of receiver functions to define the sharpness of the Moho transition. The relationship of these parameters to crustal age and tectonic history will be considered.

The teleseismic P-wave receiver function is sensitive to the shear-velocity structure and has been used to resolve boundaries to depths of 60 km (e.g. Owens, 1987). It provides site specific information and is sensitive to both dip angle and direction of interface geometry (e.g. Cassidy, 1992). Rayleigh waves are known to be sensitive mainly to the shear-wave velocity, and with long enough wavelength they can penetrate the upper mantle. Potentially, joint inversion can provide accurate shear-wave velocity structure to better understand the elastic moduli and densities of the study regions. Since both receiver functions and surface wave dispersion curves are sensitive to the same medium parameters, a joint inversion of the two techniques should reduce the uncertainties associated with the individual inversion of each data set and minimize the dependence of the final results the initial model. It is hoped that a systematic study of crustal features will show regional variations that can then be related to our current knowledge about the crust. The detailed shear-wave velocity structure determined for each site will may be the starting point for defining the three-dimensional nature of the crust.

1.2 Review of Related Literature

1.2.1 Plate tectonic setting and main tectonic elements of North America

Plate tectonics provide a widely accepted model for understanding crustal structure. North America is an old continent. The North America Craton, known as Laurentia, has been coherent since 1.7 Ga and included Greenland and Northwest Scotland until their separation in the late Cretaceous. The Western quarter of North America is characterized by strong tectonic interaction between the southwest-moving North American plate and the adjoining Pacific, Juan De Fuca, and Cocos plates, which have different directions and velocities of absolute movement. Interplate boundaries fall into three types, convergent, extensional, and transform, depending on the direction and geometries of plate interaction. The eastern three-fourths of the North America continent are within the North American Plate and is characterized by low levels of historical seismicity, although there are some patches of higher seismicity, such as New Madrid, Missouri, and the Charlevoix- La Malbaie- Saugenay region of the St. Lawrence valley (Engdahl and Rinehart, 1988). The Midplate province is within the eastern part of North America stable continental plate and has a nearly uniform compressional stress field, maximum horizontal compression being oriented in an east-northeast direction of absolute plate velocity (Zoback and Zoback, 1991).

Unlike the midplate region, stress orientations in interplate settings are typically more diverse, and the direction of maximum horizontal compressive

stress do not show the remarkable correlation with stress-release pattern that is typical in the eastern and central United States (Dart and Zobach, 1988; Zobach et al., 1989; Zobach and Zobach, 1991). However, within the classic Basin and Range sub-province in the Cordilleran extension province, the Walker Lane belt of western Nevada has a component of superimposed shear that appears to be related to the San Andreas transform fault. At least two-thirds of the relative motion between the North America and the Pacific plate in California occurs on the San Andreas Fault system (Allen, 1981; Minster and Jordan, 1978; Sieh and Jahns, 1984). In southern California, the plate boundary is a complex fault system with deformation spread over four major faults, including the San Andreas fault itself, and numerous minor ones.

The stable craton of North America includes the Precambrian outcrops of the Canadian and Greenland Shields, their subsurface extension and their platform cover, which is subdivided into a number of sedimentary basins and arches (Bally, 1989; Hoffman, 1989). In the southwestern United States, the craton and its cover have been deformed and are involved in local basement uplifts of either the Paleozoic Wichita-Ancestral Rocky Mountain system, or the Laramide southern Rocky Mountains (Oldow et al, 1989; Arbenz, 1989). The Precambrian basement also extends well underneath the Paleozoic and Mesozoic-Cenozoic folded belts of much of North America (Rast, 1989; Trettin, 1989).

1.2.2 Crustal thickness, average crustal velocity, and P_n velocity

The seismic structure of the crust and upper mantle provides critical information regarding lithospheric composition and evolution. Large variations in fundamental properties such as crustal thickness, average velocity, and Poisson's ratio are interpretable in terms of processes which have formed and modified the lithosphere. Much of what we know about the seismic structure of the lithosphere has been accumulated over the past 30 years from seismic refraction profiles and the surface wave studies.

The crustal thickness of North America which varies by more than a factor of two from about 25 to 55 km (Mooney and Braile, 1989) is known from seismic refraction/reflection profiles. Mooney and Braile (1989) noted that the crust generally thickens from the coast to the continental interior and increases in thickness with age. North American crustal thickness can be divided into the following geological age provinces:

1. The crust is 30 to 35 km along most of the east coast and about 25 to 30 km along the west coast of the North America. These differences reflect the contrasting process of evolution by rifting on the east coast and accretion on the west coast.

2. Proceeding from the near-shore to the interior of the continent, there is a continuous gradual crustal thickening from about 30 to 40 to 45 km in eastern North America with a more complex pattern on the western side where magmatic and tectonic processes have been recently active.

3. Volcanic regions such as Cascade Range, Columbia Plateau, Snake River Plain, Mexican volcanic belt, Wrangell Mountains, and Alaska are characterized by a crust thickness of 40 to 45 km.

4. The Basin and Range of the western United States is characterized by a crustal thickness of only 30 to 35 km. This thickness is similar to that of extended crust worldwide and suggests that continental extension produces a characteristic crustal structure.

5. The Archean and Proterozoic crust of the continental interior have crustal thicknesses that range from 35 to 55 km, with an average thickness greater than the North American mean of 36 km.

A recent study by Chulick and Mooney (2002) improved resolution of the structure relative to previous work. They showed a thin crust in the Basin and Range province and a thicker crust in the Great Plains (United States). Nevertheless, their maps also reveal new features. They resolved a northward extension of thin crust from the Basin and Range province into the western Canada Cordillera. A crustal thickness less than 40 km in much of northern Canada including the region of Hudson Bay, was shown. Finally, the average crustal thickness estimated is 36.7 km, with a standard deviation of 8.4 km.

The average P-wave velocity varies from one province to another indicating the composition and evolution of the crust. Braile et al. (1989) presented a regional variation in seismic properties of the crust and upper-mantle. Their contour maps show a significant correlation between crustal thickness and the seismic velocity. The eastern portion is characterized with both thick crust (42

km), high P-wave velocity (6.5 km/sec) and a Pn velocity of about 8.1 km/sec. The Basin and Range province in the western portion has both thin crust (30 km) and anomalously low upper-mantle velocities (7.8 km/sec). In general, a significant correlation is seen between the distribution of the Pn velocities and the crustal thickness. Except for the Colorado Plateau, higher Pn velocities are usually associated with thicker crust. Much of the continental interior of North America is underlain by mantle with a Pn of 8.1 km/sec. Chulick and Mooney (2002) presented high Pn values (8.2 km/sec) following a north-to-south trend under the Great Plains, lower Pn values (8.0 km/sec) under the Midwest and 8.1 km/sec under the Appalachians and the Gulf Coast.

There are substantially fewer measurements of whole-crust S-wave velocity (S_c) than of P-wave (P_c) velocity. The contour maps of S_c indicate high S-wave velocities (> 3.7 km/sec) under the Craton and Platform in central and eastern North America and low S-wave velocities (< 3.4 km/sec) found under parts of western North America (Chulick and Mooney, 2002). The low P_c region in the west corresponds to regions with high heat flow and thinned crust. Intermediate values of S_c correlate with the Rocky Mountains and the Atlantic and Gulf coastal plains. The average S_c for the continental of North America is equal to 4.6 km/sec (Chulick and Mooney, 2002).

1.2.3 Inversion for Crustal Properties

Receiver function

Most detailed investigations of crustal structure use multiple seismic recordings, and only a few techniques have been developed to study local shear-wave velocities in the crust and upper mantle beneath isolated three-component stations. The most widely used tool is called receiver function analysis (Langston, 1979, 1981; Ammon and Zandt, 1993; Cassidy, 1995). The teleseismic P-wave receiver function is defined as the filter which converts the P-wave motion observed on the vertical component to that observed on the radial component. The beauty of this definition is that while the teleseismic P waveforms contain information related to the source time history, source orientation, near-source structure, mantle-path effect, and the local receiver structure, the receiver function itself only contains information about the local structure beneath the seismograph station. The receiver function waveform is a composite of P-to-S converted waves that reverberate in the structure beneath the seismometer. The initial arrival indicates how the initial P wave is partitioned into radial and vertical components at the surface. This is followed by a Ps phase which arises from pronounced impedance contrasts such as the Moho and later phases reverberated between the surface and the impedance contrasts such as PpPms, PpSmS+PsPms, and PsSms (Last et al., 1997).

The amplitude and arrival times of phases in a given receiver function provide information about the travel time from the interface to the surface and

the properties of the velocity contrast. Receiver function inversions for shear-wave velocity structure are non-unique because there is a very little absolute-velocity information contained in the receiver functions. A significant trade-off exists between the depth of an interface and the average wave velocity above it that is known as the velocity-depth trade-off (Ammon et al., 1990). Ammon et al (1990) urged, "All future receiver function studies perform non-uniqueness analysis to exclude velocity models that do not fit the other a priori geophysical constraints obtained from refraction, reflection, earthquake travel-time, and surface-wave data where available."

Receiver functions can be used to estimate the geometry of seismic reflectors (Langston, 1979; Langston, 1981; Cassidy et al., 1998), the shear-wave velocity distribution within the crust and the upper mantle (Ammon et al 1990; Ammon and Zandt, 1993; Tomfohrde and Nowack, 2000), the nature of the crust-mantle boundary (Owens et al, 1984), and the estimation of the average Poisson's ratio in the crust (Zandt and Ammon, 1995; Zhu and Kanamori, 2000). Owens et al (1984) used receiver functions to invert shear-wave velocity structure beneath the station RSCP located in the Cumberland Plateau, Tennessee. The results indicated that a thick transition between lower crustal and upper mantle velocities exists in the depth range of 40 to 55 km, consistent with early refraction work in the area. Their results reveal significant rapid lateral changes in the mid-crustal structure beneath the station, which may be associated to the cause of the east continent gravity high located northeast of the station.

The Ammon and Zandt (1993) study revealed a 1-D velocity structure from the inversion of the receiver function recorded at the station LAC southern Mojave block, California. The structure is relatively simple and consists of an approximately 30 to 34 km thick crust with a relatively sharp crust-mantle boundaries and a change in velocity from about 3.5 km/sec to 4.6 km/sec over a depth range of 4 to 6-km. Receiver functions from broadband teleseismic P waveform recorded at station MNV, near Mina, Nevada, were inverted for the shear-wave velocity structure beneath the station (Mangino et al., 1993). They obtained a 1-D crustal models with a vertical resolution comparable to the PASSCAL (Program for Array Seismic Studies of the Continental Lithosphere) Basin and Range models. They showed a smooth positive gradient in the mid-to-lower crust with the top of the crust-mantle boundary as 34 to 36 km depth, reaching upper-mantle velocities of 7.8 to 7.9 km/sec between 38 and 40 km. The thicker lower crust may be representative of a transition zone between typical extensional Basin and Range province crust to the east and a thicker Sierra block to the west of station MNV.

Surface wave dispersion

Surface waves are generally the strongest arrival recorded at teleseismic distances and they provide constraints on the Earth's shallow structure. For both Rayleigh and Love waves the displacement amplitude decays exponentially with depth in the half-space. That surface-wave motions are the largest of any arrivals on the seismogram results from the 2-D geometric spreading of

the surface wave relative to the 3-D spreading that affects the body waves. For a homogeneous half-space the velocity of Rayleigh wave does not depend on frequency, but for a layered or vertically inhomogeneous structure, the Rayleigh wave is dispersive. Love waves are always dispersive because they require at least a low-velocity layer over a half-space to exist. Because Love wave particle motion is parallel to the surface, a complete separation of Rayleigh- and Love-wave surface motion occurs in isotropic media. Love waves travel faster and arrive on the transverse component ahead of the Rayleigh wave, which arrives on the vertical and radial components.

Both Rayleigh- and Love-waves have provided important information on the properties of the crust and upper mantle in the various regions of the Earth (Mitchell and Herrmann, 1979). Because of their sensitivity to shear-wave velocity structure, they provide information that is often difficult to obtain from body-wave studies. Most surface-wave studies of crust and upper mantle structure have used either phase or group velocities. The phase and group velocities provide information on the long-wavelength vertical averages of the shear-wave velocity structure between any given station pair. In surface-wave studies, one must distinguish between the phase- and group-velocity. Both velocities are identical if the media is non-dispersive and the seismic pulse that propagates outward from the source will travel without a change in shape. In contrast, when the media is dispersive, each frequency component will travel with its own characteristic velocity and the group velocity is the velocity associated with a packet of waves of a given frequency (Kovach, 1978). Block

and Hales (1968), developed new techniques to determine the phase velocities from the digitized seismograms from pairs of stations. One of these techniques is to Fourier analyze the sum (or difference) of the two seismograms after time shifting in steps to correspond to steps in phase velocity. Another technique is to pass both seismograms through a narrow bandpass digital filter centered at various periods and from the cross product of the filtered seismogram, after time shifting. These new techniques of phase velocity determination take advantage of much of the information contained in the surface-waves train that the peak and trough method failed to exploit.

Inversion of the surface-wave dispersion curves began in the 1960s with the development of the numerical techniques and remains a powerful tool to investigate Earth structure. The measurements of these dispersion curves are complex because the seismogram consists of a complex sum of normal modes, multipathing, and background noise. Surface wave dispersion measurements constrain averages of the absolute shear wave velocity that reach deeper structure with increasing period (Juliá et al., 2000). A study of surface wave dispersion provides a much better determination of shear velocity structure compared to seismic refraction. In contrast, seismic refraction gives better determination of compressional velocity structure and thus the methods are complementary. The study of surface waves covers long paths and yields information on a range of depths in the upper mantle that may be difficult to determine by body wave techniques in the presence of a low velocity channel (Brune and Dorman, 1963).

Joint inversion of receiver function and dispersion curve

A single geophysical technique cannot uniquely constrain subsurface geologic features. In order to accurately estimate the detailed subsurface Earth structure, researchers usually combine geophysical and geological methods. Although receiver function analysis is a valuable resource for obtaining local crustal and upper mantle shear velocities beneath three-component broadband digital stations, the inversion for shear velocity structure is non-unique (velocity-depth trade-off). Receiver function inversions have some limitations that make it practical to use another technique such as surface-wave dispersion curve for better results. Receiver functions are contaminated by scattering, anisotropy, and dipping layers. Large velocity variations are usually well constrained by receiver function analysis, but broad velocity transitions are not easily resolved (Cassidy, 1992). The size of Ps conversions is primarily a function of velocity contrast across layer interface but is not sensitive to absolute velocity or smooth variations in velocity over depth (Langston, 1994). On the other hand, surface-wave dispersion curves are sensitive to the average shear wave velocity structure rather than to seismic discontinuities.

The phase and group velocities provide information on the long-wavelength vertical averages of the shear wave structure between any given station pair, which is absent in receiver functions. Thus, a combination of surface wave dispersion curves and receiver functions provides constraints on the shear velocity of the propagation medium that improve those provided by either of the

data sets considered separately, and helps to avoid over interpretation of single data sets. Recently researchers have successfully inverted surface wave dispersion and receiver function together (Özalaybey et al., 1997, Juliá et al., 2000) reducing the lack of uniqueness of each individual data set and minimizing the dependence of the final result on the initial model. This technique takes advantage of average-velocity information utilized in the surface wave method and the differential velocity information included in the receiver function method to minimize the non-uniqueness problem (Özalaybey et al., 1997). The inversion of the receiver function and surface wave dispersion are successful because both measurements are consistent and complementary (Juliá et al., 2000).

In order to understand the results and to give good interpretation, it is important to know the geology of the area. Before launching into the seismological aspects, a literature review is given in Chapter 2. The focus of this review will be on the seismic properties of the crust. This review is important because it provides content for discussing the results described in the next chapters.

Chapter 3 provides detailed presentation of the data used in this study with the summary of station location (latitudes and longitudes). The data request and preparation processes are discussed in this chapter with an explanation of how to estimate the receiver functions. Chapter 3 also provides a an overview of how receiver functions are used to define crustal features. The crustal thicknesses with V_P/V_S ratio for each station examined in this dissertation are estimated in this chapter.

Chapter 4 applies the joint receiver function - surface wave dispersion inversion technique. Since surface-wave dispersion is used to provide a constraint to the inverted model, I review some of its properties in this chapter. The surface-wave dispersion curves used in this study are from taken from Stevens and Adams (1999) and the Harvard group and phase velocities. The main part of this chapter discusses and applies the joint inversion of receiver function and surface-wave dispersion curves. A detailed discussion of the inverted velocity model is presented for each tectonic provinces. includeCHAP1/intro

Chapter 2

Geology and Geophysics of Eastern North America

During the past half-century, geophysical studies have provided models describing the petrology, chemistry, and structure of the continental crust and upper-mantle. Much of what we know about the seismic structure of the lithosphere has been accumulated over the past 30 years from seismic refraction profiles and the surface wave studies. Large variations in fundamental seismic properties such as crustal thickness, average velocity, and Poisson's ratio are interpretable in terms of processes which have formed and modified the lithosphere.

Until recently, models of the earth were based on the assumption of lateral homogeneity of the mantle. Now, it is clear that there is significant lateral heterogeneity not only in the crust, but also in the mantle. Geophysical studies have clearly shown that the physical properties and composition of the crust and upper-mantle beneath North America vary significantly from east to west and that the details of this variations correlate with the major tectonic provinces of the continent.

In this chapter I will compare the different geological provinces in terms of geophysical and tectonic characteristics, e.g., crustal thickness, seismic velocity, heat flow, gravity, seismicity, and evolution. Figure 2.1 shows the mid-continent region of the conterminous United State and southern Canada (Braile,

1989). Principal tectonic units, geologic provinces, and location of major basins are delineated.

2.1 Crustal and Upper-mantle Structure

The seismic structure of the crust and upper mantle yields critical information concerning lithospheric composition and evolution. By the crustal and upper-mantle structure, I mean the distribution of the elastic constants, seismic wave velocities, and density. To understand crustal generation and evolution, it is important to know the structure and composition of the crust. The last two decades have seen a remarkable increase in the application of seismic methods for studying the crust and upper-mantle. Most of our knowledge about the physical properties of the crust and upper-mantle is derived from the seismic refraction and reflection methods combined with surface-wave studies and teleseismic waveform modeling.

2.1.1 Canadian Shield

Shield areas such as the Canadian Shield are stable regions with low relief, with few earthquakes, no volcanism, and low heat flow. The Canadian Shield has been stable for more than half a billion years and many of the exposed rocks are very old as indicated from the geological studies. It has large geologic provinces with nearly uniform elevation. The main two provinces are the Grenville and Superior Precambrian provinces.

The Grenville province is characterized by moderate to high grade meta-

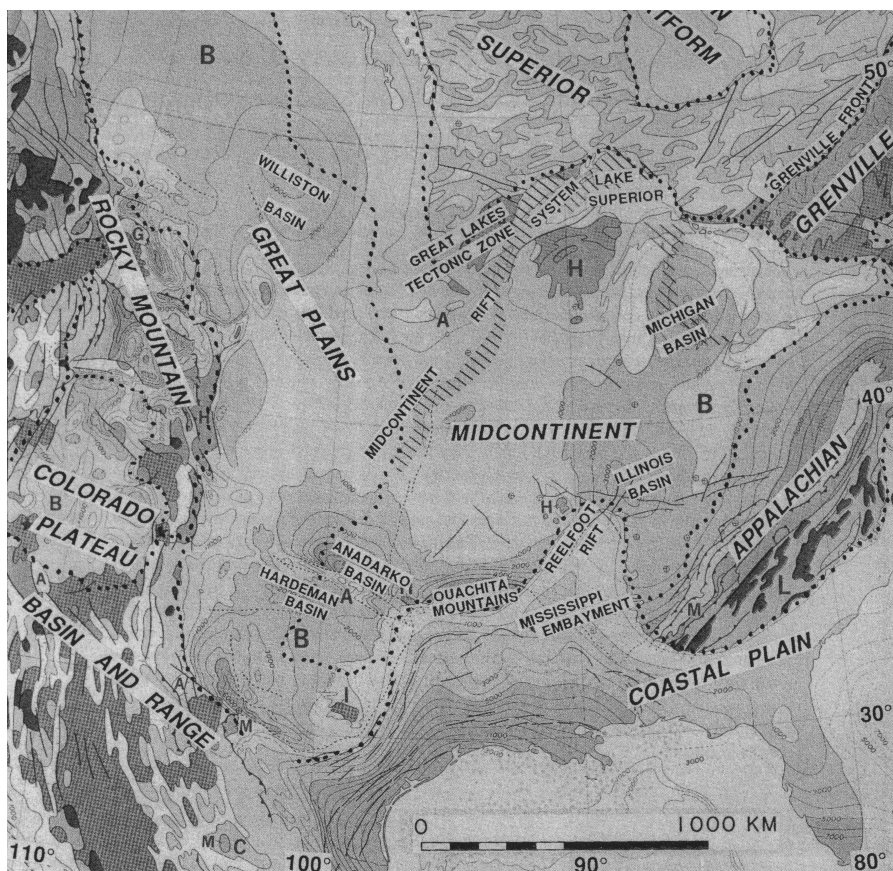


Figure 2.1: Index map of the eastern North America tectonic units, geologic provinces, and location of major basins (Braile, 1989 modified after Hoffman, 1989).

morphism and a complex structural style that is evidence of strong and deep erosion (Berry and Fuchs, 1973). The Superior province is characterized by granitic intrusions. Hodgson (1953) proposed that the Canadian Shield consists of a single crustal layer of 35 km thickness with P-wave velocity of 6.25 km/sec overlying the mantle with P-wave velocity of 7.9-8.2 km/sec. The velocity of the phase L_g is 3.7 km/sec. Brune and Dorman (1963) measured the phase velocities in the Canadian Shield for the period range 3 to 90 seconds for Rayleigh waves and 12 to 60 seconds for Love waves by phase correlation of wave trains. They found an increase in velocity with depth and they divided the crust to three layers with an upper 6 km thick layer with shear velocity 3.47 km/sec, a middle thick layer with shear velocity 3.64 km/sec, and a lower 18.7 km thick crustal layer with a shear wave velocity of 3.85 km/sec. The shear velocity on the upper 80 km of the mantle was 4.72 km/sec. Other studies have proposed that the Superior Lake province has a Moho depth at 30 km under the western end, rapidly drops to a depth greater than 50 km under its eastern half (Berry and West, 1966 and Smith, 1966).

The study made by Mereu and Hunter (1969) consists of a detailed analysis of the first arrival seismic data obtained from the project Early Rise Superior-Churchill line and also from the Lake Nipigon-Smooth Rock Falls area of the Canadian Shield. The main results showed that the Moho at the Superior Lake is relatively flat and horizontal throughout most of the Superior province at a depth of 30 to 35 km. They also indicated rapid thickening of the crust of 40 to 50 km under the younger Churchill province, which may be due to mantle

material having been extruded at the surface during the Churchill orogeny giving rise to high density rocks and the observed gravity high in the region. Delandro and Moon (1982) indicated that the Moho beneath the boundary zone between the Superior and Churchill provinces dips down toward the west and that there exists a complicated lateral seismic structure in the upper crustal and mid crustal depths. Their ray tracing results also indicate that there may exist a zone of negative velocity gradient along the boundary zone at the depth range of 4-13 km. This study showed that the depth to Moho discontinuity increases from 37 km in the north to 43 km in the south. The upper crust and P_n velocities in the two provinces appear to be quite similar (Green et al., 1980). The main characteristics that distinguish the Churchill provinces from the Superior provinces in southern Canada are the strongly reflecting 7 km/sec lower crustal layer and the relatively thicker crust. A distinct layer with velocity of 7.1 km/sec has been postulated for the Superior province by Gurbuz (1970). On the other hand, the crust thickens within the boundary zone from 41 km in the Superior province to about 46 km in the Churchill province.

Berry and Fuchs (1973) studied the Superior and Grenville provinces of the NE Canadian Shield by using a large scale seismic refraction experiment data applying two different techniques: first, by using a modification of the time-term approach and, second, by interpreting the individual seismic profiles. They investigated the possible differences in the gross crust and upper mantle structure between the Grenville and Superior Precambrian provinces

to find an explanation for the major gravity anomaly that is centered along the boundary, or front, between the provinces. They concluded that the average velocity of the crust is 6.57 ± 0.03 km/sec and appears to be the same over the whole region. The crustal thickness varies from 48 to 29 km with the average thickness in the Superior being 34 km compared to 39 km in the Grenville to the south. This study showed that the Conrad discontinuity lies at a depth of 14 km in the Superior, 21 km in the Grenville and 24 km along Grenville Front. The material below the Conrad discontinuity has a velocity from 6.5 to 6.8 km/sec. Godlewski and West (1977) found the shear velocity structure to be 3.55 km/sec for the upper crust as would be expected from the abundance of fresh, exposed crystalline rock. The upper mantle shear velocity of 4.6 km/sec, is slightly lower than the typical value for other shield areas.

Morel et al. (1987) modeled eight reversed seismic refraction profiles using two-dimensional ray tracing techniques to match the time and amplitude of primary and coherent secondary arrivals across the Phanerozoic Williston sedimentary basin that overlies the margins of the Superior and Wyoming Archean cratons and the Proterozoic Trans-Hudson orogen. They found that the velocities increase smoothly from 6.1 km/sec beneath the Paleozoic sediments to 6.2-6.4 km/sec at depths of 8-13 km. Near this depth there is generally a change in gradient with velocities increasing smoothly to 6.5-6.8 km/sec at depths varying from 28 to 40 km. An upper mantle velocity of 8.0-8.4 km/sec is encountered at the crust-mantle boundary in the depth range 41-48 km. Green et al. (1985) has revealed a zone of a prominent reflection dipping to the west at 30-40° in

the vicinity of Thompson fault.

Recently, the crustal structure of the eastern Grenville and Makkovik provinces was determined using two onshore-offshore reflection seismic lines of the Litho-probe Eastern Canadian Shield Onshore-Offshore Transect (Func et al., 2001). A correlation between a high gravity in the Hawke River terrain and the increased P-wave velocity in the upper 30 km of the crust (6.2-6.7 km/sec in the upper and middle crust and 6.9-7.1 km/sec in the lower crust) has been indicated. The adjacent Groswater Bay has a P-wave velocity of 6.0-6.55 km/sec in the upper and middle crust and 6.6-6.95 km/sec in the lower crust. A thick high-velocity lower crustal (15-20 km) wedge consisting of an upper layer (7.1-7.4 km/sec) and a lower layer (7.6-7.8 km/sec) underlie the entire Grenville crust. The Cartwright Arch is characterized by velocity of 6.4 km/sec and 4 km thick sediment sequences (4.3-5.7 km/sec) in the surrounding basin. The Grenville front is characterized by a decrease of velocity in the Makkovik province (5.8-6.4 km/sec) in the upper and middle crust and (6.65-6.85 km/sec) in the lower crust and a gradual thickening of the crust from 30 km in Grenville province to 35 km in the Makkovik province (not including the high velocity lower crust).

It is generally accepted that the crustal thinning produces the marked change in Bouguer anomalies from negative values over continents to positive values over oceans. However, this relationship is not always systematic in continental areas, i.e., in Lake Superior and Hudson Bay, where gravity anomalies computed for crustal models exhibit values that are much larger than those mea-

sured and there is little correlation between the computed and observed gravity profiles (Weber and Goodacre, 1968). Goodacre (1972) noted that throughout most of Canada the regional Bouguer anomaly is inversely proportional to the depth of the crust-mantle boundary. Along the Grenville front to the southwest of Wabash lies one of the strongest gravity anomalies in eastern Canada (Berry and Fuchs, 1973). Massive granites in the upper crust have been suggested by Innes (1957) to be the source of the anomaly while Grant (1968) has proposed that low density, perhaps numetamorphosed sediments might be the present. Tanner (1969) suggests that the anomaly can be interpreted as a compensated structure in the Grenville consisting of a dense layer within the upper crust underlain by a crust thicker than the more normal one in the Superior province to the north. Gravity profiles across the Superior-Grenville and Slave-Churchill boundaries indicate that the Proterozoic crust consistently thicker and slightly denser than the crust of the adjacent Archean province (Gibb and Thomas, 1976).

The correlation between mean heat flow and crustal thickness indicates that the total crustal heat production increases with crustal thickness, but there is no evidence in bulk compositional data for the crust to support this hypothesis (Morgan and Gosnold, 1989). In the Prairie Basin area of Canada the heat flow is complex and there is much discussion of the role of fluid flow in the observed heat-flow pattern (Jessop, 1990b). In the Canadian Shield the heat flow is generally between 40 and 50 mWm^{-2} , and local heat flow depends on the local value of crustal heat production. In eastern Canada, a low heat

flow in the Grenville terrain is associated with a crust generally low in heat production, possibly due to deep erosion and removal of an upper crustal radioactive heat source after the Precambrian collision of the Grenville terrain with North America (Blackwell et al., 1991).

2.1.2 Central United States

By the central United States (mid-continent), I mean the area bounded approximately by the Appalachian Mountains on the east, the front range of the Rocky Mountains on the west, and the Gulf Coastal Plain on the south (Figure 2.1). The central United States has been relatively undeformed since Precambrian time (Braile, 1989). Denison et al. (1984) indicated that during Precambrian time the central United States crust accreted by collision and welding of continental margin volcano/sedimentary belts and then was modified by superimposed orogenic thermal-tectonic events later orogenic processes. This region is probably composed mostly of Middle Proterozoic crust produced during events that took place 1.9-1.7 Ga (Bickford et al., 1986). However, drilling and limited outcrop data has indicated that an extensive province of younger felsic volcanic (1.3-1.4 Ga) and plutonic rocks covers the southern part of this region from Missouri and Arkansas to Colorado and New Mexico (Hatcher et al., 1987). Most of this region is characterized generally as a platform region, mantled by Paleozoic and later sedimentary rocks, and only slightly disturbed since Paleozoic time. The present sedimentary rocks cover range in thickness from zero meters in the region of Ozark Dome to more than 3,000 meters in

the region of the Denver Basin (Moss, 1936). Therefore, most of the sediments that cover this region are Paleozoic and Mesozoic age with younger sediments restricted to river valleys and glacial deposits (Baquer and Mitchell, 1998).

Stewart (1968) presented general features for the crustal structure in Missouri as follow: (1) velocity increases rapidly in the upper 3 km of the crust then gradually to a depth of about 18 km, which may represent a crust composed of granitic materials as concluded by Birch (1958); (2) the velocity increases between 18 and 39 km; (3) the lower half of the crust is characterized by a velocity of 6.5 to 7.1 km/sec and (4) the crustal thickness is about 43 km. McCamy and Meyer (1966) reported upper crust velocities of 6.2 km/sec along a refraction profile between Cape Girardeau, Missouri, and Little Rock, Arkansas, with 7.4 km/sec in the lower crust, 8.3 km/sec for the uppermost mantle, and a crustal thickness of 45 km. Qualls (1965) reported velocities of 6.0 km/sec in the upper half of the crust, 7.2 km/sec in the lower half of the crust, 8.1 km/sec for the upper mantle, and a crustal thickness to be 51 km in Oklahoma. Interpretation of strong secondary phases as refractions suggests an intermediate velocity layer of 7 km/sec or slightly higher in Southern Missouri and 8.0 for the upper mantle (Stewart, 1968). Estimates of crustal thickness from the phase velocity of Rayleigh waves is 35 to 41 km in the Interior Plains region with the higher values occurring under the higher Plains in the western part (Ewing and Press, 1959).

Kurita (1973) studied the regional variations in the structure of the crust in the Central United States from P-wave spectra and summarized the following

features: (1) The crust thickens from 33 to 41 to 47 km from near the Gulf of Mexico, to the intersection of the Gulf coastal plains and the interior plains, and the midst of the interior plains, respectively. It thins to about 41 km near the intersection of the interior plains and the Superior upland. (2) There is a sedimentary layer having a compressional velocity of about 3.0 km/sec and thickness of 3 km near the coast of the Gulf of Mexico and tapering out to the north, while a near-surface layer with velocity of about 4.7 to 5.4 km/sec and having a thickness of about 1 to 3 km is a prevailing feature elsewhere. (3) In each of the regions in (1), the silicic upper crust has a P-velocity of about 6.0 to 6.5 km/sec. (4) The mafic lower crust with the velocity of about 6.9 to 7.0 km/sec and thickness of about 10 km is a common feature possibly except for the midst of the interior plains, whereas a velocity of 7.4 km/sec is probable, implying an inclusion of ultramafic rocks. (5) The uppermost mantle velocity of 8.1 km/sec increases to 8.15 km/sec as we move from near the coast of the Gulf of Mexico to the north.

The proposed model of the Mississippi Embayment (McCamy and Meyer, 1966) contains a sedimentary wedge thickening to the south associated with Cretaceous and younger Mississippi Embayment sediments. A typical upper-crust layer (with P-wave velocity of 6.2 km/sec) is present, but is anomalously thin. Below this upper crustal layer, a thick layer of a typical lower-crustal velocity is underlain by a high velocity (7.4 km/sec) lower-crustal layer just above the Moho discontinuity. Ervin and McGinnis (1975) proposed that a late Precambrian rift underlies the Mississippi Embayment and that the rifting

event produced the high-velocity lower-crustal layer.

Different studies suggest that the crustal thickness in this region is about 40 km. Kurita (1979) studied a 40 second segment of the teleseismic P-phase that contains most of the information on the crustal layering with this amount of crustal thickness. The assumed P-wave velocity for most of the previous studies in the uppermost mantle is 8.1 km/sec. The thinnest crust is found in the northeast adjacent to Canada that also has the lowest average crustal velocity (Hinze and Braile, 1988). The thickest crust is found immediately east of the eastern margin of the Rocky Mountains in the vicinity of the Great Plains with two recognized maxima, one centered over eastern Colorado and the other over the boundary between Montana and North Dakota. Another area of regionally thickened crust is observed in Minnesota, Wisconsin, and Iowa approximately along the axis of the northern portion of the mid-continent geophysical anomaly. A zone of thickened crust is also observed extending easterly from the southern Great Plains across northern Texas, Oklahoma, and Arkansas into the northern Mississippi Embayment, and northeasterly along the eastern margin of the Appalachian.

The mean crustal velocities of the mid-continent (6.5 km/sec) imply an average composition between granite (approximately 6.1 km/sec) and diorite (approximately 6.7 km/sec) with mafic crust at depth (Hinze and Braile, 1988). The average upper mantle compressional velocity in the mid-continent are roughly 8.1 km/sec with observed high P_n velocity (> 8.2 km/sec) in the northern Great Plains and the southern portion of Mississippi Embayment and Mis-

Mississippi River Delta. Black and Braile (1982) suggest that the variation in continental P_n velocity may be primarily related to the temperature at the Moho discontinuity and, thus, the relatively constant P_n velocity in the mid-continent region may be related to the average heat flow of the craton.

The presence a high-velocity lower-crustal layer has been considered to be a characteristic of the Mississippi Embayment and an anomalous feature (Braile, 1989). A thinned upper crust and uplifted lower-crustal rocks (or intrusion of high velocity rocks into the upper crust) beneath the Mississippi Embayment appear to be the principal anomalous structure of the region that may be the cause of the long-wavelength positive regional gravity anomaly that trends northeast ward along the Embayment. In fact, the Mississippi Embayment is underlain by a late Precambrian rift and the rift event produced the high-velocity lower-crustal layer. Warren et al. (1966) used seismic refraction survey data (along a line trending north from Ansley to Oxford in southern Mississippi) to study the crustal structure for this region. They suggested that the complicated crustal structure might be due to the intermingling of two major geotectonic trends, the Appalachian and the Ouachita. Low to zero values of regional free- air gravity anomaly indicated that the region is near isostatic equilibrium. For their crustal model to be in isostatic equilibrium, the density must increase in the upper mantle below southern Mississippi.

Heat flow and associated thermal regimes in the continental United State are related to the tectonic evolution and physical properties of the continental lithosphere (Morgan and Gosnold, 1989). East of the Rockies, normal heat

flow is interpreted to reflect a stable thermal regime with regional variation and heterogeneity in upper crustal heat production. Although, regions with recent tectonic activity commonly have higher heat flow than more stable regions, no direct correlation between surface heat flow and "tectonic ages" is comparable to the tectonic age-heat flow-elevation relationship (Morgan and Gosnold, 1989). They revealed that changes in crustal thickness associated with extension or compression may result in a change in the thickness parameter associated with the upper crustal radiogenic heat production and/or the vertical distribution of the heat-producing elements. In the central stable region of the United State the heat flow is generally between 40-50 mWm^{-2} , and local heat flow depends on the local value of crustal heat production (Blackwell et al., 1991). The only anomalous area is in Arkansas and Louisiana where high heat-flow values are found with no obvious explanation (Smith and Dees, 1982 and Blackwell et al., 1991)

2.1.3 The Appalachian Provinces

The Appalachian province consists of the eroded core of a Paleozoic mountain chain, which extends at least 3000 km from the southeastern United States to Newfoundland (Musacchio et al., 1997). The earliest study for calculating V_p and V_s velocities of the northern Appalachian was conducted by Lee (1941), who studied both the primary and secondary arrivals for both P- and S-waves. The average crustal thickness was 36 km, and V_p increased from 6.1 km/sec at the base of the crust with a fairly high estimated value for P_n

velocity of 8.43 km/sec. Taylor and Toksoz (1982) indicated that the northern Appalachian are composed of a relatively thick crust (40 km).

Klemperer and Luetgert (1985) interpreted the refraction line data collected in Maine and Southeastern Quebec in 1984 using both ray tracing and near a vertical reflection technique. The upper crust shows localized low-velocity zones with the P-velocity ranging from 5.7 to 6.3 km/sec and relatively high P-velocity of 6.8 to 7.2 km/sec for the lower crust. Analysis of the reflected arrival using synthetic seismograms indicated that the crust increased in thickness from 32 km near the coast to 42 km in northeast Maine (Luetgert et al., 1987).

A seismic refraction survey centered at the Cumberland Plateau Observatory (CPO) was performed by the U.S. Geological Survey (Borcherdt and Roller, 1966) to provide a detailed study of the crust and the upper mantle in the region. The survey was carried out along two 400-km long lines, one from Burnside, Kentucky to Moulton, Alabama, and the other from Fort Campbell, Kentucky to Gainesville, Georgia, intersecting each other at CPO near McMinnville, Tennessee. They estimated that the thickness of the crust is about 40 km near CPO and that the crust-mantle boundary has an apparent dip of about 2 degrees to the southwest along the Burnside- Moulton profile. The crustal thicknesses at the two survey lines are 34 and 51 km, respectively. Along the Fort Campbell-Gainesville profile, only the last 150 km section crosses the Valley and the Blue Ridge provinces. The crustal thickness within the two geological provinces is estimated between 40 and 45 km.

A P-wave travel-time study, using six central Appalachian earthquakes, was

conducted by Bollinger (1970). Seismograms collected from WWSSN stations, LRSM stations, and some university stations operating in the region were employed in the study. Since the stations covered a greater part of the eastern U.S. along the Appalachian, the model derived represents an average crustal velocity for the eastern U.S. Mathur (1971) used Rayleigh wave dispersion and travel-time studies to investigate the crustal structure in the southeastern U.S. the model which he proposed consists of two layers over a half-space. A crustal thickness of 40 km was determined. In the following year, Long and Marthur (1972) presented an average southern Appalachian crustal structure within the triangular arrays formed by the WWSSN stations SHA, OXF, BLA and ATL from the dispersion of Rayleigh waves. They proposed an average S-wave velocity model with a crust-mantle boundary at 40 km.

Using southeastern United States earthquakes and quarry blasts in his study area, Kean (1979) developed a regional and local crustal velocity model for the southern Piedmont province of Georgia and South Carolina. The Moho depths reported for the regional and the local models are 36.6 and 33.0 km, respectively. Prodehl et al. (1984) reinterpreted the data collected by the U.S. Geological Survey (1984) using modern digitizing and stacking techniques. The velocities are somewhat similar to those indicated by the previous studies. Instead of sharp crustal boundaries, velocity transition zones were suggested. The estimated crustal thickness, under the Southern Appalachians, is between 49-50 km, while in the Cumberland Plateau the crustal thickness is 55 km. In contrast to the root zone predicted by James et al. (1968), they indicated that

the crust thickened westward into the Cumberland Plateau.

Owens et al. (1984) performed a detail analysis of broadband teleseismic P-waveform in the Cumberland Plateau region. By stacking the horizontal components of teleseismic P-waveforms and using inverse modeling techniques, they presented two S-wave velocity models, each consisting of 28 layers with a thickness varying from 1.5 to 3.0 km. The velocities are 2.14 km/sec at the top layer and 4.71 km/sec in the upper mantle, at a depth of about 60.0 km. Based on their results, they claimed that the crust-mantle boundary is a laminated velocity structure in the depth range between 40-55 km. This is similar to the velocity transition zone designated by Prodehl et al. (1984).

The over all crustal thickness ranges from 33 to 55 km. Generally, the thinner crusts are reported in the Piedmont or the Coastal Plain provinces whereas the thicker crusts are observed in the Appalachian mountains and the Cumberland Plateau provinces. Bollinger and Carts (1980) showed that the average crustal velocities range from 6.0 to 6.57 km/sec for the P-waves velocity and 3.47 to 3.76 km/sec for the S-waves velocity. On the basis of the crustal velocity models discussed previously, crustal layers with lower velocities are observed as thin layers near the surface, whereas thicker layers with higher velocities are generally establish at greater depth. A possible low-velocity layer in the upper crust below 10 km has been suggested in at least two studies conducted in the southern Appalachian near the Piedmont province (Cook, 1979; Long, 1979) on the basis of seismic reflection and refraction data. Taylor et al. (1989) proposed that the Pn velocity of the Appalachian in the New England region

is approximately 8.1 km/sec. In New York and Pennsylvania the observed P_n velocity is 8.14 km/sec (Dorman and Ewing, 1962).

In general, the gravity and magnetic anomalies show a very good correlation with geologic features in the Appalachian provinces. The prominent feature in the regional field in the northern Appalachian are a low over the tectonic Klippe in eastern New York, a low over the white Mountains in the northern New Hampshire, and a northeast-trending low over the Connecticut valley synclinorium in Vermont and western Main (Taylor, 1989). A north-northeast-trending gravity high is found in western Connecticut, western Massachusetts, western Vermont, and extending into Quebec; it is associated with the Precambrian uplifts and the serpentinite belt. Simmons (1964) found a gravity low over the anorthosite bodies in the Adirondack Mountain region due to their low density ($2.72g/cm^3$) relative to surrounding Precambrian rocks ($2.82g/cm^3$). The gravity high in the northern Adirondacks is covered by Paleozoic sedimentary rocks and is thought to be due to a buried intrusive mass at a depth of approximately 3 km (Taylor, 1989).

In the southern Appalachians, many gravity models have been proposed to explain the large negative anomaly over the Appalachian Plateau and Blue Ridge and the steep gradient anomaly over the Piedmont by (1) crustal thickening beneath the regional negative related to a mountain root (James et al., 1968) (2) crustal thinning beneath the positive possibly related to rifting (Sugarman, 1981) and (3) a more or less uniformly thick crust with anomalous higher density bodies in either the upper crust or lower crust (Hutchinson et

al., 1983). Crustal thickness data combined with Hutchinson et al. (1983) gravity models suggest that the source of the large Appalachian negative anomaly is primarily crustal thickening of 7 to 10 km, which represents a mountain root that may be partly the result of the Paleozoic crustal loading by thin-skinned tectonics. The steep gradient and the positive anomaly characterizing the southern Appalachian can be modeled by three different structures in the vicinity of North Carolina: a suture zone, a mantle upwrap, and a shallow body (Hutchinson et al., 1983). Another gravity modeling study suggesting some flexure of the lithosphere is necessary to compensate for the mass load of the Appalachian (Karner and Watts, 1983). This is consistent with what they consider to be the dominant action of mountain building, the emplacement of abducted blocks/flakes. The effective elastic lithosphere thickness beneath the southern Appalachian was found to be between 80 and 130 km.

A linear relationship between heat flow and heat production (Birch et al., 1968) suggests an enrichment of radioactive elements in the upper crust. This relationship helps isolate mantle heat-flow from the near-surface radiogenic component. Heat-flow maps of eastern North America indicate that central New England is characterized by a north-northeast-trending zone of high heat flow. Jaupast et al. (1982) suggested that heat flow measurements in New England reflect variations in near-surface radiogenic heat production and that no deep-seated thermal perturbation from the most recent orogenic events or magmatic episodes are evident in the heat flow data. Low heat-flow values in the Adirondak Mountains are mainly confined to the Precambrian anorthosites,

which are very low in radioactive elements (Birch et al., 1968). Generally, heat-flow values are less than 60 mWm^{-2} east of the Cordillera except in the Appalachian Mountains where higher than average heat-flow values are associated with areas of high crustal radioactivity (Blackwell et al., 1991).

2.2 The Seismicity and Seismotectonics

2.2.1 Canadian Shield

Much of this area appears to be substantially aseismic, although it contains several zones of significant seismicity and a few other regions of lower-level seismicity (Adams and Basham, 1991). Adams and Basham clustered the seismicity of the southern part of the continental region into four zones; western Quebec, Charlevoix, the lower St. Lawrence and the northern Appalachian. Significant clusters of earthquakes occur in the Grenville province in western Quebec and extend into eastern Ontario across the Ottawa River. They note that most earthquakes occurring in this regions have magnitudes $M=4.3$ or less except the 1932 earthquake near Montreal ($M=6$), 1945 earthquake near lake Timiskaming ($M=6.2$), and 1944 earthquake near Cornwall, Ontario ($M=5.6$). In 1983 the ($M=5.2$) Goodnow, earthquake occurred on an extension of the exposed Grenville provinces into the Adirondacks of New York state. For western Quebec the seismicity appears to occur in two bands: one trending slightly west to north east along the Ottawa River to Ottawa and extending southeast to Cornwall and east to Montreal associated with rift faults (Forsyth, 1981), and a second trending slightly north to northwest extending from Montreal to

the Baskatong Reservoir due to crustal fractures forming during the passage of North America over a hot spot between 140 and 120 Ma (Crough, 1981). Almost all focal mechanisms have near-horizontal P-axes, and are thrust earthquakes (Adams et al., 1988 ; Adams and Basham, 1991).

The Charlevoix zone is historically the most active in eastern Canada. Most earthquakes are confined under the St. Lawrence River with focal depths between 5 and 25 km (Adams and Basham, 1991). In general, the derived P-axes lie in the east quadrant and the mechanisms represent thrust and combination thrust/strike-slip faulting. The lower St. Lawrence earthquakes occur mainly under the St. Lawrence River and may involve the old rift faults (Adams and Basham, 1991). The zone has magnitude 3 and 4 earthquakes with hypocentral depths 10 to 20 km (Adams et al., 1988). These focal mechanisms have P-axis orientations only slightly less variable than at Charlevoix and indicate thrust faulting. Adams and Basham (1991) reported that the northern Appalachian region is a zone of relatively uniform seismicity. Focal mechanisms of most recorded earthquakes indicated thrust faulting with focal depths from shallow to 19 km deep.

2.2.2 Central United States

The central United States has been relatively stable tectonically for roughly the past billion years and characterized by nearly horizontal stress field and northeast- trough east- striking axis of maximum compressive stress (Herrmann, 1977; Dewey et al., 1989a). The seismicity rate of the central United

State is low compared to that in more active regions of North America such as California (Mitchell et al., 1991). For mid-plate regions, earthquakes are enigmatic because they cannot easily be associated with major deformation, as can earthquakes near plate margins. The two areas of recurrent large earthquakes (m_b 6.0 or larger) are the New Madrid area in southern Missouri, northeastern Arkansas, and northwestern Tennessee, and the La Malbaie-Charlevoix area of the St. Lawrence River Valley (Hatcher et al., 1987). New Madrid and La Malbaie-Charlevoix earthquakes exceed rate of recurrence and size expected seismic activity for an intraplate region but are not near or within a recognized active plate margin.

Most earthquakes have strike-slip, oblique-reverse, or reverse fault mechanisms. Previous studies such as the finite-element modeling of tectonic plates (Richardson et al., 1979) and qualitative reasoning (Zoback and Zoback, 1981) point to ridge-push and/or drag forces at the base of the North America plates as the most likely sources of the mid-plates stress field (Dewey et al., 1989a). The Central United States has focal mechanisms for earthquakes that range from the upper few kilometers to not more than 30 km with magnitude less than 4.5 (Zoback and Zoback, 1981). The location of earthquakes of m_b (4.5) led them to classify 11 zones in the Central United States as seismogenic; New Madrid fault zone, the Wabash valley fault zone, the Ozark uplift, the Illinois basins, the Michigan basin, the Cincinnati Findlay arch, the Kankakee, the Lake Superior tectonic zone, the Namaha uplift, the Wichita seismic zone, and the Ouachita seismic zone.

All of the earthquakes of m_b (5.9) in the Central United State since 1811, have occurred in the New Madrid fault zone. Fault plane solutions for the New Madrid seismic zone indicate that right- lateral strike-slip motion characterizes the northeast - southwest - trending portion of the fault zone and mixed motion (strike-slip and reverse motion) characterizes the north-northwest-trending segment (Herrmann, 1979). The Wabash fault zone, which lies in the eastern part of Illinois basin, has the largest earthquakes to have occurred in the twentieth century in the Central United State ($m_b=5.5$). Fault-plane solutions for earthquakes in the Ozark uplift (great principal stress direction is close to vertical) and along the Ouachita frontal thrust (oriented northwest-southeast) may indicate that the Ozark are still uplifting and that thrust motion is still occurring on the Ouachita front.

2.2.3 The Appalachian Provinces

Bollinger et al. (1991) presented a map showing the seismicity in the southern United States and its relation to geologic provinces. Most of the recorded earthquakes in the southern Appalachian are concentrated beneath the Valley and Ridge provinces, near the western edge of that part of the Appalachian in which thin-skin over thrusting has carried eugeosynclinal or miogeosynclinal rock over Precambrian basement or platform deposits on Precambrian basements (Dewey et al., 1989a). The focal-depth for earthquakes in this region is concentrated between 8 and 16 km with the largest earthquake of magnitude 5.8 (Nuttli et al., 1979). The Appalachian Highlands have earthquakes

distributed from the Virginia-West Virginia border area southwestward into central Alabama and northeasterly trending lineation in eastern Tennessee and in Giles County, Virginia (Bollinger et al., 1991). The Appalachian Piedmont province accounts for about 13 percent of the regional seismicity with focal depths to 15 km and average depth of 9 km. The Atlantic Coastal Plain province has the largest earthquake in the southeastern United State during historical times ($M_b=6.7$) with an epicentral depth of 20 to 30 km (Bollinger et al., 1991). The focal-mechanism solution indicates a north-northeast maximum compressive stress and northwest trend perpendicular to the northeasterly tectonic fabric of the adjoining Piedmont and Appalachian Highland (Bollinger et al., 1991).

The northern Appalachians are characterized by moderate seismicity throughout its recorded history. The main cause of these earthquakes is not clear but there is evidence that some of these earthquakes are related to a combination of stress caused by plate-tectonic processes (Ebel and Kafka, 1991). Focal depths are primarily within the upper half of the crust with average depth of 9 km. The regional maximum compressive stress is essentially horizontal and trends approximately east-west (Ebel and Kafka, 1991).

Chapter 3

Crustal Structure of the Eastern North America from Receiver Functions

3.1 Receiver Function

3.1.1 Receiver function estimation

The source equalization procedure

In the time domain, the observed P-wave arriving at a station from a teleseismic event is the composite of the seismic source function, the impulse response of the recording instrument, and the impulse of the locale (near-receiver) earth structure. In order to combine the information contained in many events, each with a different seismic source function, an estimate of the receiver function requires an effective means of isolating the source effect from the observed seismograms. The source equalization procedure proposed and discussed by Langston (1979) is an effective procedure to isolate the local earth structure effects. Deep events with simple pulse like waveforms on the vertical component are preferred because later P-to-S conversions on the horizontal components can be then investigated directly. In the time domain, the three components of the seismic response at any one receiver station due to a plane P-wave arriving from a teleseismic event, $D(t)$, can be theoretically represented by

$$D(t) = I(t) * S(t) * E(t) \quad (3.1)$$

where;

$I(t)$ is the impulse response of the recording instrument,

$E(t)$ is the impulse response of the local earth structure,

$S(t)$ is the seismic source function, and

$*$ is the convolution operator.

Given that the earth structure beneath a station will produce phase conversions of the P-to-S type, the horizontal components of ground motion will, in general, be quite different from the vertical component. Thus, equation would be

$$\begin{aligned}
 D_V(t) &= I_V(t) * S(t) * E_V(t) \\
 D_R(t) &= I_R(t) * S(t) * E_R(t) \\
 D_T(t) &= I_T(t) * S(t) * E_T(t)
 \end{aligned}
 \tag{3.2}$$

where subscripts V , R and T represent vertical, radial and tangential components respectively. Langston (1979) indicated that the vertical component of ground motion for a steeply-incident P-wave consists of a large direct P-arrival followed by minor P-to-S conversions and crustal reverberations. Langston's (1979) source equalization method assumed that $D_V(t)$ behaves mostly like one Dirac delta function $\delta(t)$

$$E_V(t) \approx \delta(t) \tag{3.3}$$

Langston (1979) examines this assumption for a layer over a half space

assuming that;

$$E_V = \alpha_1 \delta(t - \tau_1) + \alpha_2 \delta(t - \tau_2) \quad (3.4)$$

where the first term is the direct P arrival and the second term is reverberated P. The form of $E_V(t)$ is valid for angle of incidence appropriate for teleseismic distances. Thus, for different angles of incidence, the amplitude and arrival times will vary. Langston (1997) showed that the inverse operation of $E_V(t)$, E_V^{-1} , is given by;

$$E_V^{-1}(t) = \frac{1}{\alpha_1} \delta(t + \tau_1) - \frac{\alpha_2}{\alpha_1^2} \delta(t + 2\tau_1 - \tau_2) + 0 \left(\frac{\alpha_2^2}{\alpha_1^2} \right) \quad (3.5)$$

In the frequency domain;

$$E_V^{-1}(t) \longrightarrow \frac{1}{E_V(\omega)},$$

and by letting $\alpha_1 = 1$ and $\tau_1 = 0$

Assuming that the vertical and horizontal instrument responses are equal and from (2) and (3), we can approximate $S(t)$ by

$$D_V(t) = S(t) * I(t) \quad (3.6)$$

Thus, $D_V(t)$ contains all the factors that we wish to remove from the seismogram. From (4) it is evident that the functions $D_R(t)$ and $D_T(t)$ could be estimated from the three-component seismogram by deconvolving the vertical signal from the horizontal radial and tangential components. The resulting $E_R(t)$ and $E_T(t)$ are assumed to be a property of the local receiver structure. In

the frequency domain, we have

$$\begin{aligned} H_R(\omega) &= \frac{D_R(\omega)}{D_V(\omega)} = \frac{E_R(\omega)}{E_V(\omega)} \approx E_R(\omega) \\ H_T(\omega) &= \frac{D_T(\omega)}{D_V(\omega)} = \frac{E_T(\omega)}{E_V(\omega)} \approx E_T(\omega) \end{aligned} \quad (3.7)$$

where $D(\omega)$ and $E(\omega)$ are Fourier transform of $D(t)$ and $E(t)$, respectively. $E_R(\omega)$ can be approximated by $H_R(\omega)$ only if $E_V(\omega)$ is close to delta function for teleseismic. Since real data contains noise, this method is unstable. Stability is achieved by dividing the Fourier Transform of the radial component by that of the vertical component after introducing a water-level spectral fill to the amplitude spectrum of the vertical component.

The water-level helps to avoid instabilities generated by a very small number troughs in the spectrum (Helmberger and Wiggins, 1971; Clayton and Wiggins, 1976). The final expression for the radial receiver function (deconvolution) in the frequency domain is as follows

$$\begin{aligned} H_R(\omega) &= \frac{D_R(\omega)D_V^*(\omega)}{\phi(\omega)}G(\omega) \\ H_T(\omega) &= \frac{D_T(\omega)D_V^*(\omega)}{\phi(\omega)}G(\omega) \end{aligned} \quad (3.8)$$

where

$$\phi(\omega) = \max \{D_V(\omega)D_V^*(\omega), c \max [D_V(\omega)D_V^*(\omega)]\}$$

and

$$G(\omega) = \xi \exp\left(\frac{-\omega^2}{4\alpha^2}\right)$$

The variable ($c \leq 1.0$) is the minimum allowable spectral amplitude of the vertical component, the water-level; * indicates complex conjugate, ξ normalizes the Gaussian filter to the unit amplitude in the time domain; and α is the Gaussian factor which control the width of the Gaussian pulse (used to remove high frequency noise). For broadband teleseismic data, the appropriate value for α is between 3 and 7. An α value of 3 removes frequencies higher than ~ 0.5 Hz; an α value of 7 removes frequencies higher than ~ 2 Hz (Cassidy, 1992). A value of α from 1 to 3 may be used to examine the lower-frequency (0.1 to 0.5 Hz) component of the data.

Clayton and Wiggins (1976) demonstrated the relationship between the water-level parameter and the trade-off arrival time and amplitude resolution. If $c = 0$, equation (6) reduces to equation (5), the deconvolution is the best estimate of the true amplitude response and provides the best arrival time resolution. If $c = 1$, equation (6) is the scale cross-correlation of $D_R(t)$ and $D_V(t)$, and thus is a least-square estimate of the true arrival amplitude at the sacrifice of arrival time resolution (Helmberger and Wiggins, 1971; Owens, 1984). Because our interest is in relative amplitudes of phase within a single seismogram, are chooses c to be as small as possible in hopes of better resolving

relative arrival times and to minimize the effect of the water-level on the solution (Owens, 1984).

Iterative deconvolution

Ligorria and Ammon (1999) introduced an iterative deconvolution technique to compute the receiver function based on the Kikuchi and Kanamori (1982) source time function estimation algorithm. The reason for considering a new technique is illustrated in Figure 3.1 which shows the result of the water level deconvolution in the lower panel. There is noise before the first pulse 0 sec. A broad low frequency trough on either side of the first arrival peak at 0_s is an artifact of frequency domain deconvolution. Gurrola et al. (1995) indicated that since the side lobes about the main peak are expected to be symmetric, they suspect that later peaks and troughs are impinged upon side lobes of the primary peak. The foundation of a time-domain iterative technique is a least-squares minimization of the difference between the Gaussian filtered observed horizontal seismogram and a predicted signal generated by the convolution of an iteratively updated spike train with the vertical component seismogram (Ligorria and Ammon, 1999). They prefer this technique for several reasons. First, for a noise contaminated signal, the technique can perform better than the frequency domain (water-level) technique, since the resulting receiver function (constructed by a sum of Gaussian pulses) does not exhibit the long-period instability usually observed on the frequency domain approximation. Second, it does not require an additional choice of the optional stabilization deconvolu-

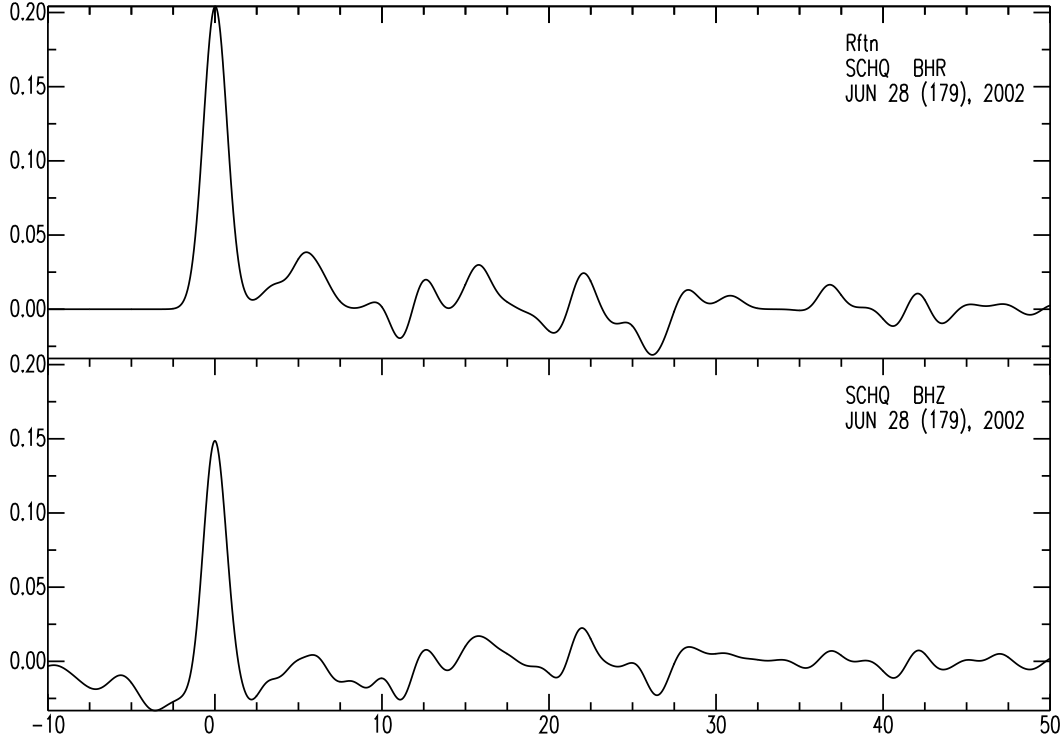


Figure 3.1: Comparison between the iterative deconvolution (time-domain) and the frequency-domain deconvolution for $\alpha = 1.0$. Top panel shows receiver function computed by time-domain deconvolution. The bottom panel shows the receiver function computed using frequency-domain deconvolution.

tion. Third, it constructs a causal receiver function, which is generally lost in the water-level frequency domain deconvolution.

The goal of the technique is to minimize the difference between the observed signal and the predicted (synthetic) signal generated by convolution of an iteratively updated spike train with the unperturbed response of the propagation medium.

The spike wavelet train sought is the receiver function, $h(t)$, which is convolved with the vertical component of motion, $v(t)$, to obtain the radial component of motion, $r(t)$. In the iterative deconvolution process, we compute an iterative receiver function, $h_i(t)$, which will be equivalent to $h(t)$ if the misfit

between $r(t)$ and the deconvolution of $h_i(t)$ with $v(t)$ is below a preset tolerance level. In order to construct $h_i(t)$, a series of time lagged Gaussian pulses are added. Next, the convolution of the current estimate of the receiver function with the vertical component seismogram, and the procedure is repeated to compute other spike lags and amplitude (Ligorria and Ammon, 1999). For each spike addition of the misfit between the vertical component seismogram and receiver function convolution and the radial component seismogram is reduced. The process is halted is when the reduction in misfit with additional spike becomes insignificant (Ligorria and Ammon, 1999). The misfit is saved as one indication of the quality of the receiver function.

3.2 Receiver Function Interpretation

The resolution of receiver function technique has increased with the utilization of digital broadband data (Owens and Crosson, 1988). This increased resolution of fine structure extends to an increased sensitivity of receiver function to shallow structure interfaces with high-velocity contrast (i.e. the sedimentary cover-basement rock contact). The purpose of these numerical examples are to study the effect of different parameters such as shallow structure, ray parameter, and velocity effects on broadband receiver function. To examine the effects of different structure on receiver function, synthetic receiver functions were computed for a single-layer over a half-space. Here both the layer and half-space are considered isotropic and homogeneous. Such numerical examples help to track the pulse amplitude difference as we change the structure.

Table 3.1: Reference model used to compute the synthetic receiver function

H(KM)	VP(KM/S)	VS(KM/S)	RHO(GM/CC)
40.00	6.00	3.50	2.70
00.00	8.00	4.70	3.30

Ammon et al (1990) showed that the sequence of initial arrivals in the receiver function could be interpreted in terms of rays propagating through a simple crustal model. The first arrival, denoted by P in Figure 3.2, arises because of the partition of the incident P wave into vertical and radial components at the surface. The subsequent arrivals correspond to the partition of S waves incident. The timing of the arrival can be used to define the paths. An P_s corresponds to an S-wave created by conversion of the teleseismic P wave into S at the Moh. Later arrivals correspond to crustal reverberations, with the final leg of the ray being of type S . Given this association, we can examine features that control the arrival times and amplitudes for the following reference model.

width=5.5in(left) The receiver function correspond to the model to the right. (right) Simplified ray diagram showing the major P-to-S converted phases that comprise the receiver function for a single layer over a half-space (Ammon et al., 1990)receiver.eps

3.2.1 Ray parameter sensitivity

Figure 3.3 considers the effect of changing the ray parameter. Since the ray parameter is related to angle of incidence, the smaller ray parameter would correspond to data from large teleseismic distances. As the ray parameter in-

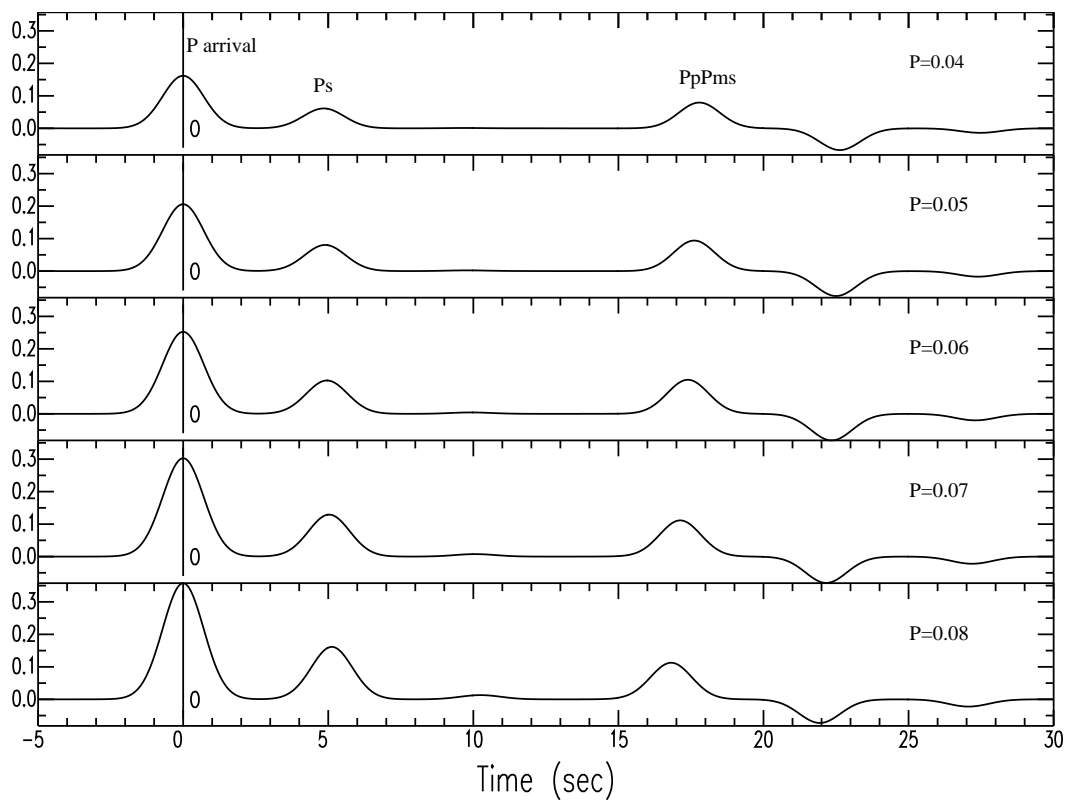


Figure 3.2: Study of the effect of changing ray parameter from 0.04 sec/km to 0.08 sec/km for Gaussian filter parameter $\alpha = 1.0$. For comparison, all traces are plotted to the same scale.

Table 3.2: Reference model used to compute the synthetic receiver function

H(KM)	VP(KM/S)	VS(KM/S)	RHO(GM/CC)
0.600	1	1	1
40.00	6.00	3.50	2.70
00.00	8.00	4.70	3.30

creases, all amplitudes increase with increasing ray parameter. In addition the arrival of later pulses, such as $PpPms$, becomes shorter with increasing ray parameter.

3.2.2 Changing crustal velocity

Figure 3.4 shows the effect of changing the crustal velocity in the top layer with fixed ray parameter and halfspace. The ratio of P wave amplitude and the Ps conversion is very sensitive to the crustal velocity. It is clear that as crustal velocity decreases the amplitude of the first bump is reduced. The arrival time of the Ps converted and multiple phases and amplitude also increases as the crustal velocity decreases.

3.2.3 Shallow low-velocity structure

The amplitude and arrival time of the P wave arrival and Ps converted and multiples are sensitive to the shallow velocity structure beneath the recording station. Since some of the stations I used for this research are located in sedimentary basins, it is important to examine the effect of shallow structure on receiver function. For this purpose, I inject a low-velocity structure (0.6 km, 1.5 km, and 2.5 km) in the upper most crust (Table 3.2).

The effects of shallow structure on broadband teleseismic P waveforms have

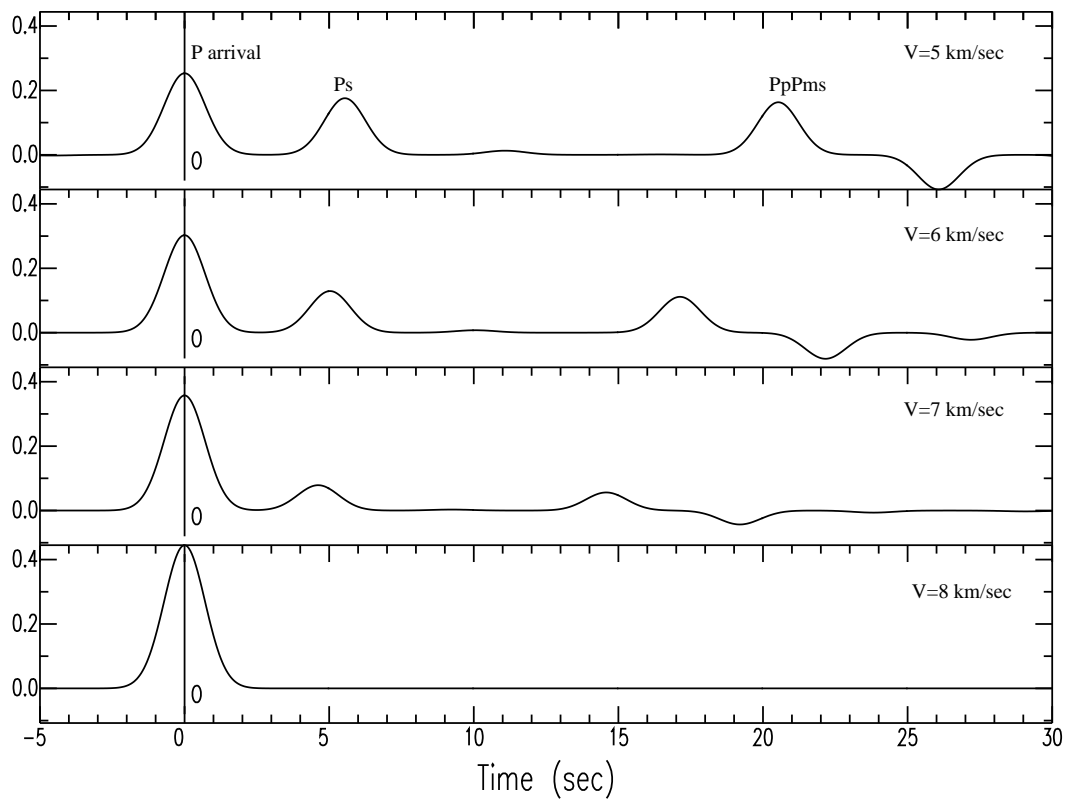


Figure 3.3: The effect of changing the crustal velocity with fixed ray parameter and halfspace velocity. The V_P/V_S ratio was fixed. A Gaussian filter parameter $\alpha = 1.0$ is used.

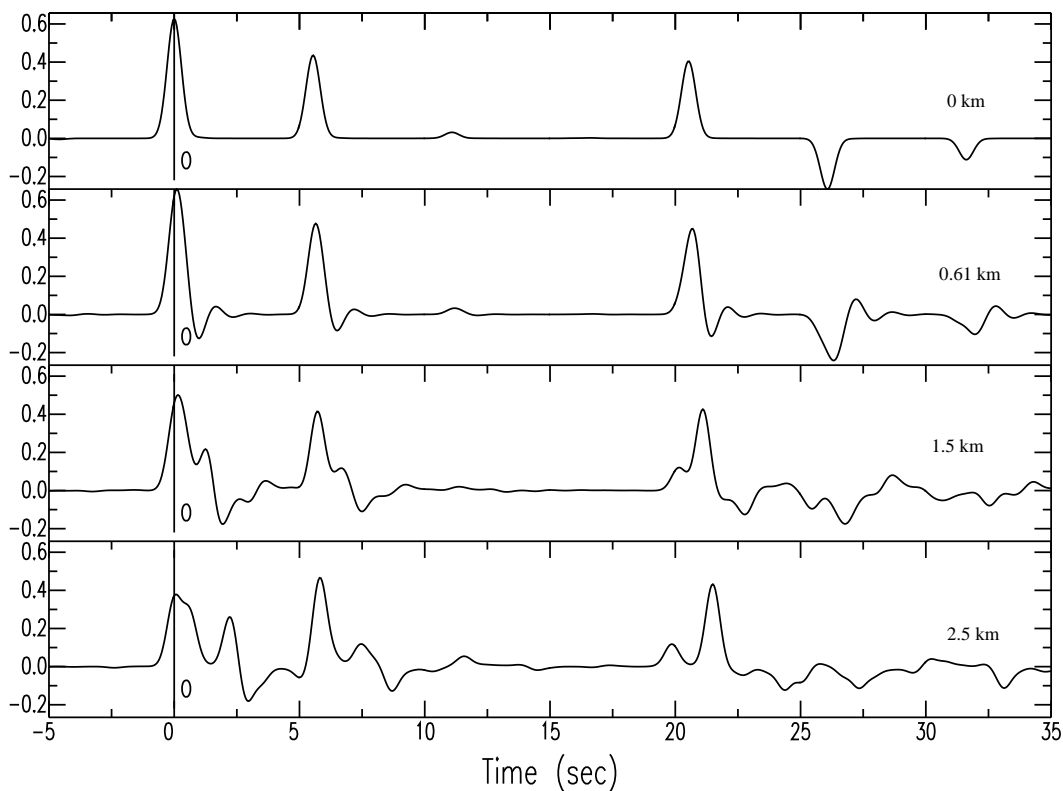


Figure 3.4: The effect of a shallow low velocity on receiver function for different values of surface layer thickness. A Gaussian filter parameter $\alpha = 2.5$ is used.

been documented by Owens and Crosson (1988) and Cassidy (1992). They indicated that shallow, high-velocity contrast interfaces are obviously a source of problems when using broadband teleseismic receiver function to model deeper structure.

Figure 3.5 shows the effect of such structure on the receiver function. Addition conversions at the base of the low velocity layer increase the duration of the direct P contribution. As the layer thickness, or equivalently the S-wave travel time in the low velocity layer, increases, the signal complexity increases. The first pulse is no longer symmetric about zero lag. In addition the crustal reverberation phases, e.g., $PpPms$ become less distinct.

3.3 Data Analysis

The number of broadband seismic stations in North America has increased dramatically over the last few years. However, these stations are not evenly distributed, and large gaps exist in some areas. While station density is greatest crossing the Midcontinent Rift in Iowa because of the FLED deployment and the Reelfoot Rift because of permanent networks, we note that no single station existed between Cathedral Cave (CCM) and Edmonton before 1998. The variety of tectonic provinces and the increased number of broadband seismic stations make this region applicable for any new method to be tested.

To accomplish this study I used all data available at the Incorporated Research Institutions for Seismology Data Management Centers (IRIS-DMC) recorded by different networks such as United State Geological Survey (USGS, Table 3.3), data provided data recorded by the USNSN, the New Madrid seismic network (NM, Table 3.4) operated by Saint Louis University, and the Canadian National Seismic Network (CNSN, Table 3.5). In addition to the permanent stations, I used temporary stations such as Missouri-Massachusetts array (MOMA, Table 3.6) and Florida-Edmonton array (Table 3.7 and Figure 3.5). It is obvious that I good coverage of the study area, a coverage better than possible even five years ago.

Table 3.3: United States National Seismic Network (USNSN) and IRIS stations used in this study

Station	Latitude	Longitude	Location
AAM	+42.3011	-83.6566	Ann Arbor, Michigan
ACSO	+40.2318	-82.9820	Alum Creek State Park, Ohio
ANMO	+34.9462	-106.4567	Albuquerque, New Mexico
BINY	+42.1993	-75.9861	Binghamton, New York
BLA	+37.2113	-80.4210	Blacksburg, Virginia
CBKS	+38.8140	-99.7373	Cedar Bluff, Kansas
CBM	+46.9325	-68.1208	Caribou, Maine
CCM	+38.0557	-91.2446	Cathedral Cave, Missouri
CEH	+35.8908	-79.0927	Chapel Hill, North Carolina
DWPF	+28.110	-81.4327	Disney Wilderness Preserve, Florida
EYMN	+47.9461	-91.4950	Ely, Minnesota
GOGA	+33.4111	-83.4666	Godfrey, Georgia
GWDE	+38.8256	-75.6171	Greenwood, Delaware
HKT	+29.9618	-95.8384	Hockley, Texas
HRV	+42.5060	-71.5580	Harvard, Massachusetts
JCT	+30.4794	-99.8022	Junction, Texas
JFWS	+42.9142	-90.2480	Jewell Farm, Wisconsin
LBNH	+44.2401	-71.9258	Lisbon, New Hampshire
LSCT	+41.6783	-73.2243	Lakeside, Connecticut
LTX	+29.3338	-103.6669	Lajitas, Texas
MCWV	+39.6581	-79.8456	Mont Chateau, West Virginia
MIAR	+34.5453	-93.5765	Mount Ida, Arkansas
MYNC	+35.0738	-84.1278	Murphy, North Carolina
NCB	+43.9708	-74.2236	Newcomb, New York
NHSC	+33.1066	-80.1778	New Hope, South Carolina
OXF	+34.5118	-89.4092	Oxford, Mississippi
RSSD	+44.1204	-104.0361	Black Hills, South Dakota
SSPA	+40.6358	-77.8880	Standing Stone, Pennsylvania
WCI	+38.2290	-86.2940	Wyandotte Cave, Indiana
WMOK	+34.7378	-98.7810	Wichita Mountains, Oklahoma
WVT	+36.1300	-87.8300	Waverly, Tennessee
YSNY	+42.4758	-78.5375	Yorkshire, New York

Table 3.4: New Madrid network (NM) stations used in this study

Station	Latitude	Longitude	Location
BLO	+39.1719	-086.5222	Bloomington, Indiana
MPH	+35.1230	-089.9320	Memphis, Tennessee
PLAL	+34.9823	-088.0754	Pickwick Lake, Alabama
SIUC	+37.7148	-089.2174	Carbondale, Illinois
SLM	+38.6361	-090.2364	St. Louis, Missouri
UALR	+34.7753	-092.3436	Little Rock, Arkansas
USIN	+37.9650	-087.6660	Evansville, Indiana
UTMT	+36.3423	-088.8642	Martin, Tennessee

The FLED array spanned a great variety of North American provinces, allowing for study of several regions of interest. The array consisted of 28 seismometers installed between Florida and Edmonton and operated for 15 months starting Spring 2001. Figure 3.5 shows that the array crosses from the Atlantic Coastal Plain passes through the Mississippi Embayment and continues through the Midcontinent Rift in Iowa.

Stations FA04 through FA07 cross the southernmost end of the Appalachian mountains (Figure 3.5), where crustal rocks vary from sedimentary to high-grad metamorphic, and from felsic to ultramafic, with considerable late Paleozoic and Mesozoic rifting and thrust faulting, particularly on the western edge (Costain et al., 1989). Stations FA14 through FA17 cross the Precambrian Midcontinent Rift that has been filled in with volcanic and intrusive rocks and covered by sedimentary deposit (Cannon et al., 2001). Further to the northwest, stations FA23 through FA25 fall within the Trans-Hudson orogen and stations FA26 and FA27 cross the Williston Basin.

The MOMA array consisted of 18 seismometers extending from the stable

Table 3.5: Canadian National Seismic Network (CNSN) and POLARIS - NWT (Portable Observatories for Lithospheric Analysis and Research Investigating Seismicity) stations used in this study

Station	Latitude	Longitude	Location
DLBC	58.4372	-130.0272	DEASE LAKE, British Columbia
DRLN	49.256	-57.5042	Deer Lake, Newfoundland, Canada
EDM	53.2217	-113.35	EDMONTON, Alberta
FCC	58.7616	-94.0866	FORT CHURCHILL, Manitoba
FFC	54.725	-101.9783	Flin Flon, Canada
FRB	63.7467	-68.5467	Iqaluit, N.W.T. Canada
GAC	45.7033	-75.4783	Glen Almond, Quebec, Canada
INK	68.3067	-133.52	Inuvik, N.W.T. Canada
KAPO	49.4504	-82.5079	KAPUSKASING, Ontario
KGNO	44.2272	-76.4934	KINGSTON, Ontario
LMN	45.852	-64.806	CALEDONIA MTN., New Brunswick
LMQ	47.5483	-70.3267	LA MALBAIE, Quebec
RES	74.687	-94.9	Resolute, N.W.T. Canada
SADO	44.7694	-79.1417	SADOWA, Ontario
SCHQ	54.8319	-66.8336	Schefferville, Quebec, Canada
ULM	50.2499	-95.8750	LAC DU BONNET, Manitoba
WALA	49.0586	-113.9115	WATERTON LAKE, Alberta
ACKN	64.9915	-110.8781	ACHILLES LAKE , NWT
BOXN	63.8521	-109.7169	BOX LAKE , NWT
CAMN	63.7321	-110.8989	CAMSELL LAKE , NWT
COWN	65.2679	-111.1859	CONTWYOTO LAKE 2 , NWT
DVKN	64.5092	-110.3096	DAVIK MINE , NWT
EKTN	64.6984	-110.6096	EKATI MINE , NWT
GLWN	64.7253	-109.3303	EKATI MINE , NWT
IHLN	63.3052	-110.8911	NDIAN HILL LAKE , NWT
KNDN	63.4192	-109.2013	KENNADY LAKE , NWT
LDGN	64.5785	-110.5224	LAC DE GRAS NORTH , NWT
LGSN	64.3337	-110.1307	LAC DE GRAS SOUTH , NWT
MCKN	64.1980	-110.2131	MACKAY LAKE NORTH , NWT
MGTN	63.6855	-109.5911	MARGARET LAKE , NWT
MLON	63.9695	-109.8953	MARLO LAKE , NWT
NODN	63.9607	-110.9601	NODINKA NARROWS , NWT
SNPN	63.5178	-110.9077	SNAP LAKE , NWT
YMBN	64.8742	-111.5325	YAMBA LAKE , NWT
YNEN	65.0883	-111.0500	YAMBA LAKE NORTH EAST , NWT



Figure 3.5: The FLED seismic stations used in this study

Table 3.6: FLED stations used for this study. The project ran for 15 month starting Spring, 2001

Station	Latitude	Longitude	Location
FA01	+29.9166	-082.5827	O'Leno St Park, High Springs, FL
FA02	+32.0549	-084.2152	Reed Bingham St Park, Adel, FL
FA03	+32.0549	-084.2152	Georgia Southwestern St Un, Americus, GA
FA04	+32.7510	-084.9206	Calloway Gardens, Pine Mountain, GA
FA05	+33.5728	-085.1094	St Un of West Georgia, Carrollton, GA
FA06	+33.9848	-085.9923	Gadsden St Comm College , Gadsen, AL
FA07	+34.7312	-086.7104	Huntsville, AL
FA08	+37.3155	-089.5293	Southeast MO St Un, Cape Girardeau, MO
FA09	+39.4885	-091.7861	Mark Twain St Park, Stoutsville, MO
FA10	+40.1035	-092.6695	Kirksville, MO
FA11	+40.8192	-093.2865	Corydon, IA
FA12	+41.1388	-093.7109	Green Pine Wildlife Area, Osceola, IA
FA13	+41.3125	-094.0077	Winterset, IA
FA14	+41.5448	-094.2642	Dexter, IA
FA15	+41.7716	-094.4651	Springbrook St Park, Guthrie Center, IA
FA16	+41.8926	-094.5984	Coon Rapids, IA
FA17	+42.0348	-094.8379	Swan Lake St Park, Carroll, IA
FA18	+42.3021	-095.0490	Black Hawk St Park, Lake View, IA
FA19	+42.5115	-095.3486	Schaller, IA
FA20	+42.9696	-095.9765	Alton, IA
FA21	+43.7380	-096.6236	EROS Data Center, Sioux Falls, SD
FA22	+45.5503	-099.9841	Huron Univ, Huron, SD
FA23	+45.5503	-099.9841	Lake Hiddenwood St Park, Selby, SD
FA24	+46.5318	-101.2400	Flasher, ND
FA25	+47.5820	-103.2988	Theodore Roosevelt Ntl. Park, Medora, ND
FA26	+48.7908	-105.4309	Scoby City Hall, Scoby, MT
FA27	+49.9422	-108.1081	Simmie, Saskatchewan, Canada
FA28	+50.7608	-111.5237	Brooks, Alberta, Canada

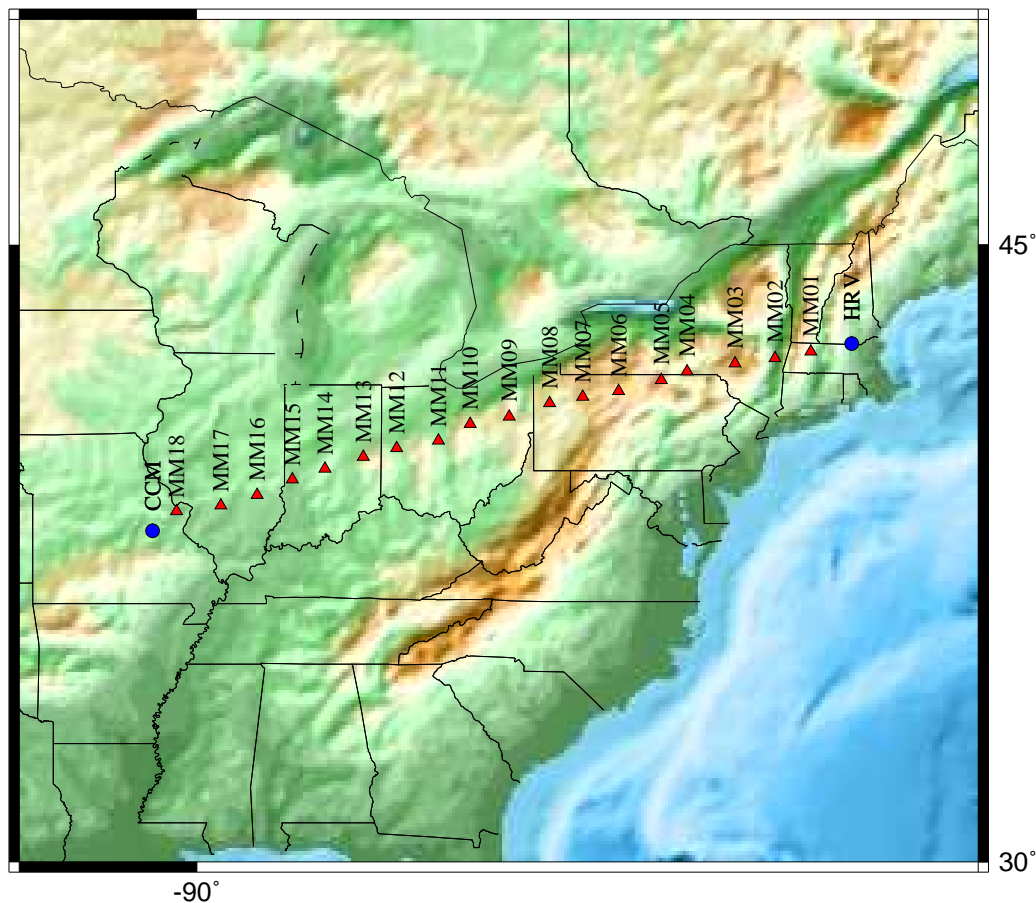


Figure 3.6: The MOMA seismic stations used in this study

Midcontinent craton across the Appalachian to the eastern terrains (Figure 3.6). The seismometers were evenly spaced between permanent stations CCM and HRV and operated for 1 year (1995-1996). This geometry is ideally suited to provide a transect of the crust and upper mantle across the eastern United States. The MOMA array can detail the transition of the lithosphere among these very different tectonic regions, including a variation in the depth to the Moho (Wyssession et al., 1996).

Table 3.7: MOMA stations used for this study. The stations ran for one year 1995-1996

Station	Latitude	Longitude	Location
MM01	+42.3175	-072.7117	North Hampton, Massachusetts
MM02	+42.1660	-073.7186	Hudson, New York
MM03	+42.0387	-074.8461	Roscoe, New York
MM04	+41.8530	-076.1979	LeRaysville, Pennsylvania
MM05	+41.6530	-076.9219	Gleason, Pennsylvania
MM06	+41.3914	-078.1266	Emporium, Pennsylvania
MM07	+41.2571	-079.1350	Sigel, Pennsylvania
MM08	+41.1095	-080.0681	Slippery Rock , Pennsylvania
MM09	+40.7911	-081.2055	East Canton, Ohio
MM10	+40.6147	-082.3031	Bellville, Ohio
MM11	+40.2214	-083.1947	Columbus, Ohio
MM12	+40.0439	-084.3724	Laura, Ohio
MM13	+39.8316	-085.3114	Spiceland, Indiana
MM14	+39.5494	-086.3947	Brooklyn, Indiana
MM15	+39.2945	-087.3134	Terra Haute, Indiana
MM16	+38.9219	-088.3045	Lake Newton, Illinois
MM17	+38.6694	-089.3255	Lake Carlyle, Illinois
MM18	+38.5286	-090.5686	Tyson, Missouri
MO18	+38.5143	-090.5643	Tyson (bunker), Missouri

3.3.1 Receiver function data analysis

Broadband teleseismic data for earthquakes recorded by both temporary and permanent stations for the period (1995-2002) are used to compute receiver functions. The data are selected based on the following criteria:

- (1) Epicentral distance between $30^\circ < \Delta < 90^\circ$ (Figure 3.7). At epicentral distances less than 30° , seismograms are complicated and dominated by multiple high-frequency seismic arrivals sampling the earth's structure at depths between 70 to 600 km below the surface. For earthquakes more than 90° distant, the effect of the core-mantle transition zone on seismograms becomes significant and the direct P is very close to the reflected P_cP phase
- (2) magnitude greater than 5.5, and
- (3) Good signal-to-noise ratio on seismograms.

Figure (3.8) shows typical 3 component seismograms east-west, north-south, and vertical (E, N, and Z) accompanied with the rotated traces (R and T) for a good earthquake that met all the criteria to compute receiver function.

The original 3 component seismograms are rotated to radial (R), tangential (T), and vertical (Z) components. The receiver functions for each event are calculated using the iterative time-domain deconvolution method (Herrmann and Ammon, 2003). Each receiver function was deconvolved using 100 iterations with a limiting error of 0.001 for Gaussian factors of 0.5, 1.0 and 2.5. To reduce the influence low-frequency noise on receiver function, all the receiver functions were high-pass filtered with a two-pass Butterwoth 0.02 Hz corner

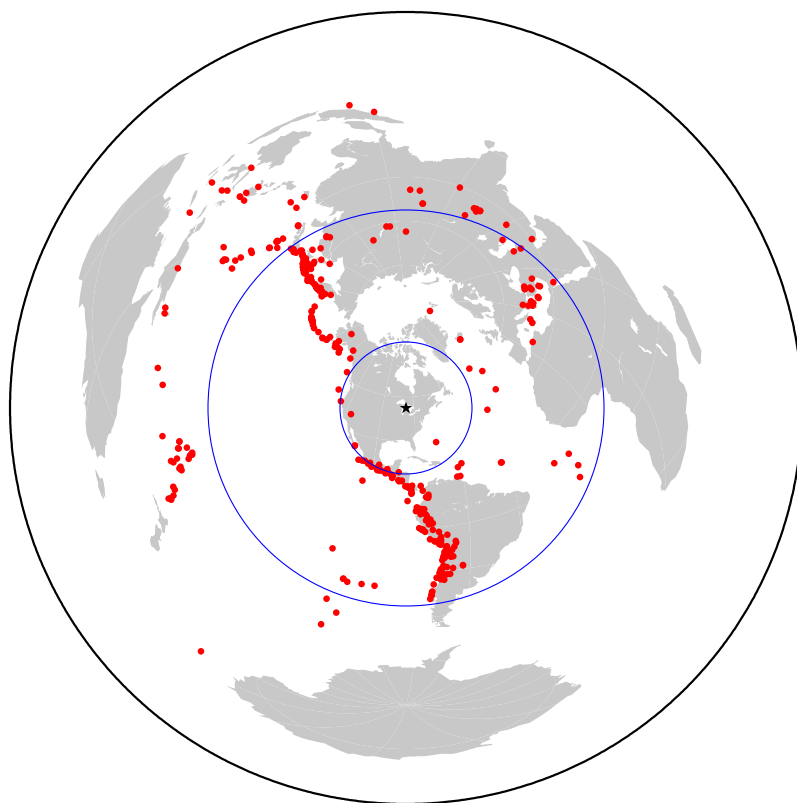


Figure 3.7: Azimuthal equidistant projection of all teleseismic events location which used for this study. The two inner circles show the distances of $30^\circ < \Delta < 90^\circ$ for a reference site in the central US.

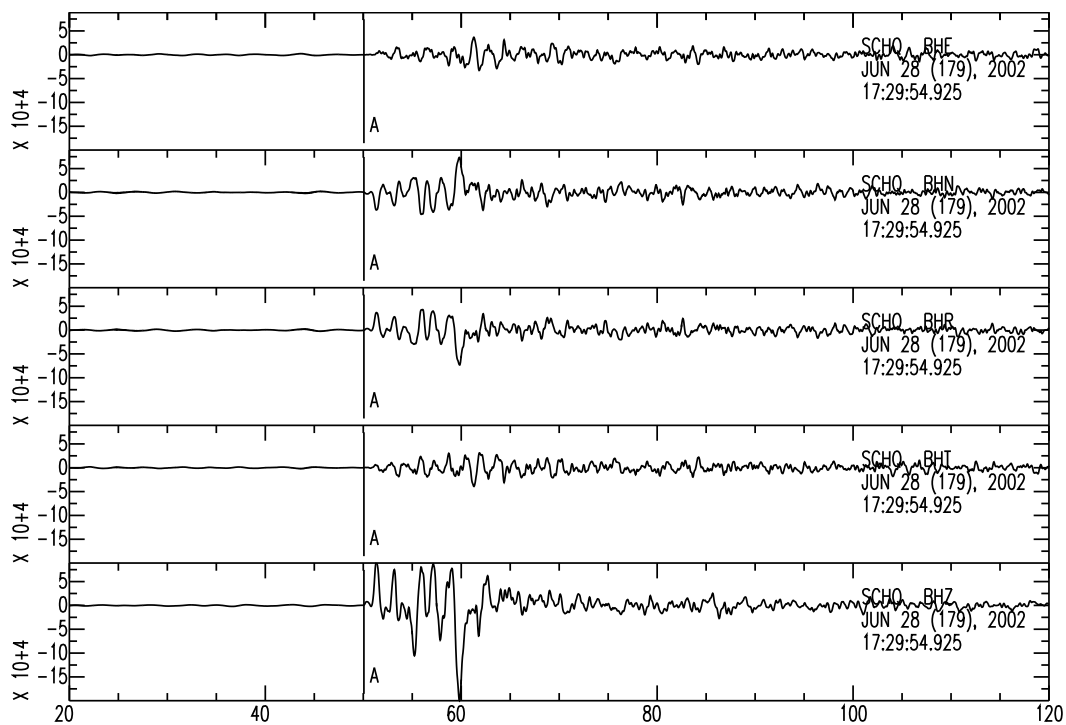


Figure 3.8: An example of the actual and rotated seismogram (the east-west component (E), the north-south component, the vertical component (Z), the radial component (R), and the tangential component (T)) used to compute the receiver functions

frequency filter.

3.4 Crustal Thickness and Data Analysis

The detailed structure of the Moho has been one of the most important targets in earth sciences since its discovery by Mohorovicic (1910). Seismic refraction and reflection techniques have provided relatively high resolution images regarding the physical and structural properties of the Earth's lower crust and upper mantle. The detailed architecture of the crust-mantle transition is the most significant asset in unraveling the lithospheric processes that are involved in extension and in collision zones and provide key knowledge in processes like crustal growth, accretion and delamination. (Hale and Thompson 1982).

The receiver functions for each station are plotted and tested for signal-to-noise ratio. The receiver functions for all stations used on this study can be divided into three groups. The first group is characterized by a clear P_s phase and clear multiples marked with the letter k as shown in Tables (3.8-3.11). The second group is characterized by a good P_s phase but do not have a clear multiples or may not have a large number of receiver function (-). The third group are characterized a poor P_s phase and/or multiples with (letter X). The third group may have large number of receiver functions, but the direct P arrival is affected by the thick sedimentary layer which causes a shift on the P time arrival. Figures 3.9-3.11 show both the radial and the tangential receiver function for three stations as an example of the three groups (one example from each group).

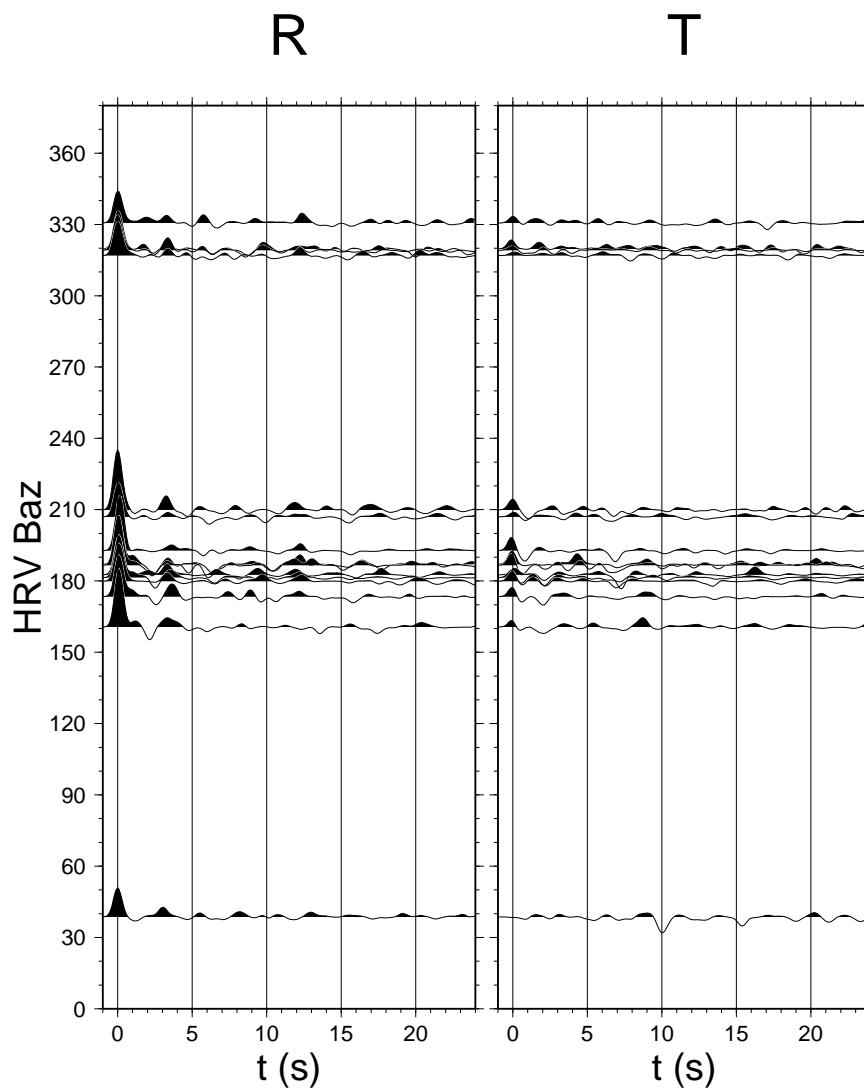


Figure 3.9: Radial and Transverse receiver functions as a function of back azimuth in degree. The left panel corresponds to radial receiver functions while the right panel shows the corresponding tangential receiver function. The plot shows a clear P_s phase as well as multiple phases. The signal on the tangential component can be due to a non-horizontal interface, slightly improper back azimuth or anisotropy. This is an example of a group one (k) of receiver functions. The traces correspond to an $\alpha = 2.5$.

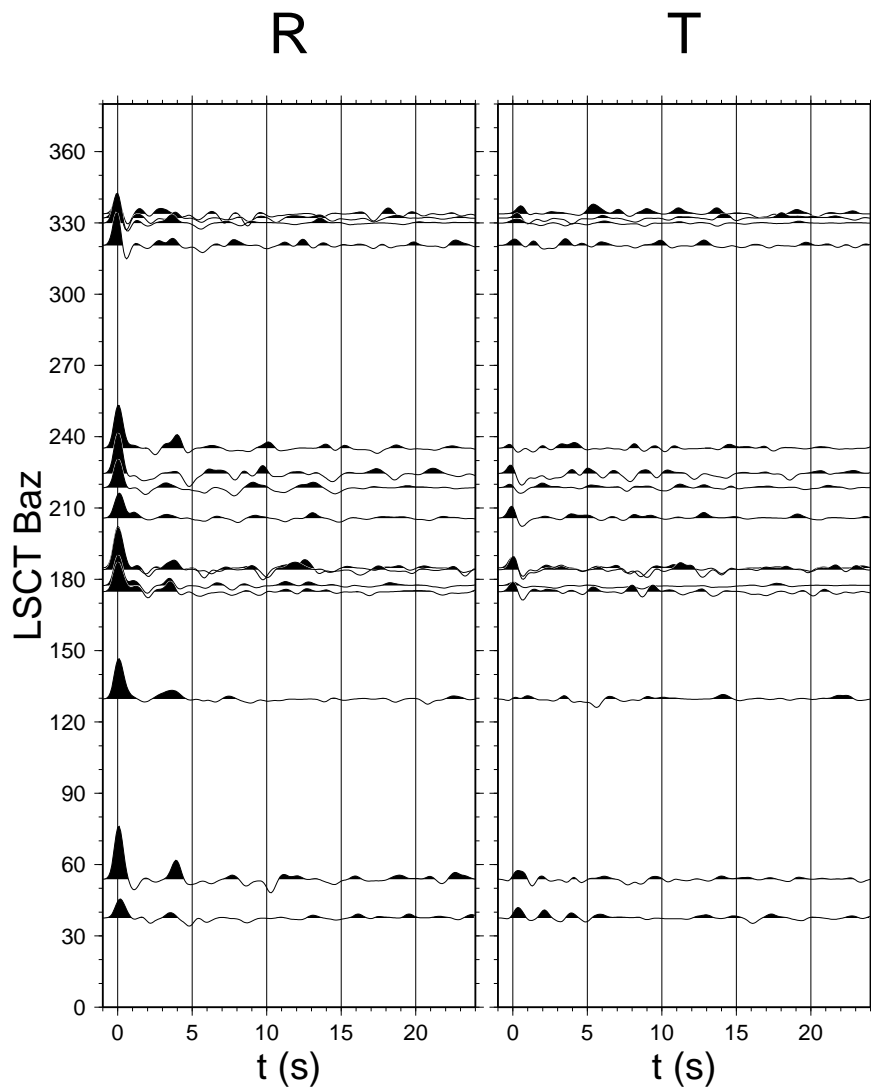


Figure 3.10: Radial and Transverse receiver functions as a function of back azimuth in degree. The left panel corresponds to radial receiver functions while the right panel shows the corresponding tangential receiver function. The plot shows a clear P_s phase, but no consistent multiple phases. This is an example of the second group (–) of receiver functions. The traces correspond to an $\alpha = 2.5$.

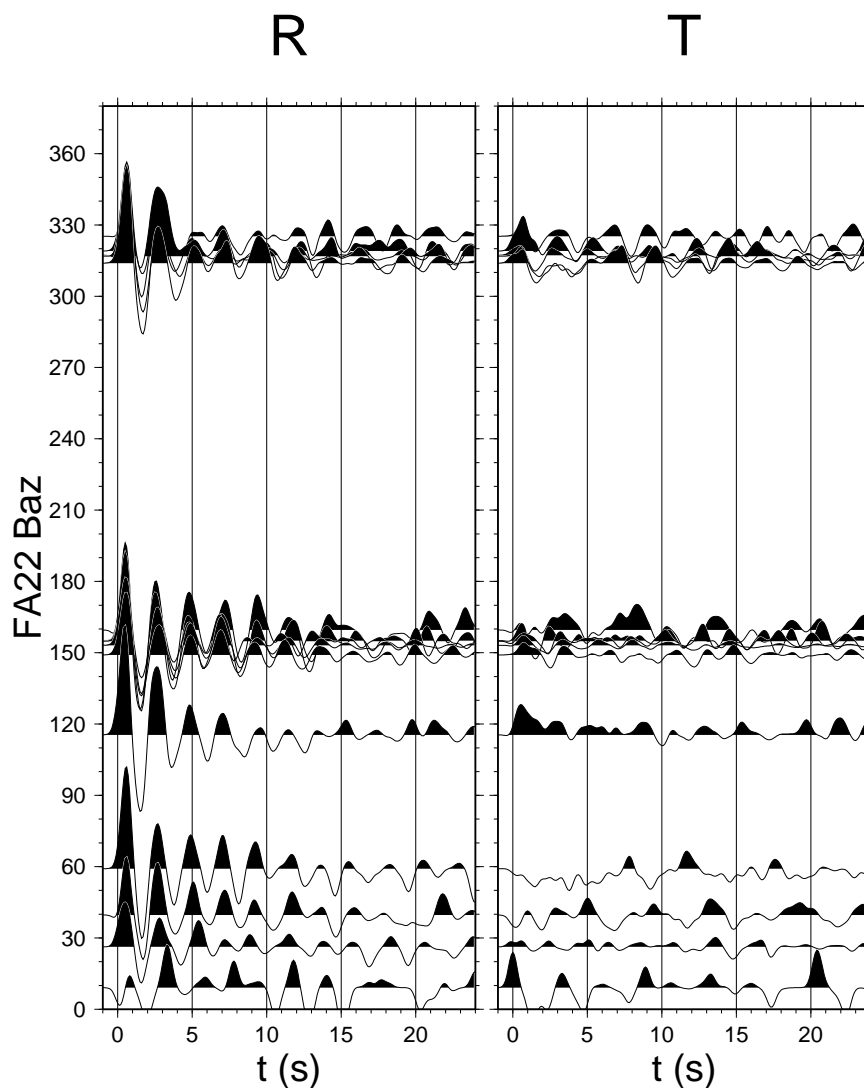


Figure 3.11: Radial and Transverse receiver functions as a function of back azimuth in degree. The left panel corresponds to radial receiver functions while the right panel shows the corresponding tangential receiver function. The plot shows the effect of the thick sediment layer on the computed receiver function. Although, we have enough receiver functions, the P_s phase cannot be picked accurately. Also, a large shift in the P arrival is seen, which is an indication of interference of several pulses within the width of the Gaussian function. The traces correspond to an $\alpha = 2.5$. This is an example of the third group (X) receiver functions.

Since 1997, different studies have provided valuable information using receiver function (Langston, 1977; Ammon, 1991; Zandt et al., 1995; Zandt and Ammon, 1995; Zhu, 1998; Zhu and Kanamori, 2000). Zandt and Ammon (1995) used a simplified method based on the relationship of the ratio of the $P_s - P$ time and the $PpPms - P_s$ times to the value of V_P/V_S and the crustal thickness and Poisson's ratio. Using this method, it is easy to estimate the crustal thickness (h) using the P_s converted travel time (t_{P_s}), assuming a value for V_p and using the Poisson's ratio to compute The corresponding V_S . Zhu (1998) used the time delay between the direct P arrival and the Moho P-to-S conversion to estimate the crustal thickness:

$$h = \frac{t_{P_s}}{\sqrt{V_s^{-2} - p^2} - \sqrt{V_p^{-2} - p^2}} \quad (3.9)$$

where;

h is the crustal thickness

t_{P_s} is the time delay for the Moho conversion P_s phase

V_S is the shear velocity

V_P is the compressional velocity and

p is the ray parameter.

The amplitude and delay of these P_s conversions provide information on the depth to the discontinuity and the change in seismic properties across the discontinuity. The amplitude of the P_s conversion does not depend directly on the absolute value of the velocities across the interface, but rather on the seis-

mic impedance across the interface. Because of the absence of information on absolute crustal velocity, the interface depth is not very well estimated (trade-off between thickness and average crustal velocities. Thus, the dependence of h on V_P or V_S is not strong as long as the ratio $k = V_P/V_S$ remains constant.

To address this problem Zhu (1998) and Zhu and Kanamori (2000) used the time delay for the secondary converted phases (t_{PpPms}) that provides an additional measurement

$$h = \frac{t_{PpPms}}{\sqrt{V_s^{-2} - p^2} - \sqrt{V_p^{-2} - p^2}} \quad (3.10)$$

Thus the k value can be estimated using

$$k = \sqrt{\frac{(t_{Ps} + t_{PpPms})^2 + (2ph)^2}{(t_{Ps} - t_{PpPms})^2 (2ph)^2}} \quad (3.11)$$

The identification of the Moho P_s conversion is made mainly with the following criteria (1) its expected delay of about 5 second with respect to the direct P arrival for shield areas where the crust is about 40 km thick and (2) its moveout with epicentral distance. The P_s converted phase has a moveout that depends on the epicentral distance; that is, the time difference $P_s - P$ decreases with decreasing angle of the P-wave at the interface. Other phases, such as the surface reflected $PpPms$, have the opposite moveout: its delay in relation to the direct P arrival increases with epicentral distance and so can be distinguished from the P_s conversion (for more details see the synthetic example discussed previously in this chapter).

From the previous equations it is important to pick the time for each phase accurately. The time delay for each station was checked separately and examined for the Moho P_s time delay. The delay of these converted phases with respect to the direct P arrival are listed in Tables 3.8-3.11). After picking the time delay for each station, the V_P/V_S ratio provides a second check. Since some stations may show different possible candidates for the PpP_{ms} , it is important to check for the V_P/V_S ratio before estimating the crustal thickness. Figures 3.12-3.16 show both the time delay and the V_P/V_S estimates for the previous stations (HRV, LSCT, FA22). To obtain the time delay, the P_s delay figures show the result of a stack of receiver functions corrected to a common ray parameter of 0.06 s/km. A simple crustal model is assumed, but the measured delay time is not very sensitive to the model since many of the data are centered near this ray parameter. To obtain the V_P/V_S figure, each stack results from shifting by an amount based on the predicted arrival times of the P_s and later multiples using the observed P_s delay as an additional constraint. When the stacks are simple in appearance, e.g., for HRV and LSCT for the P_s time delay and HRV for the V_P/V_S ratio, the delay time and ratio can be confidently determined.

Figures 3.18 and 3.18 show the P_s time delay for a ray parameter of 0.06 s/km and the expected V_P/V_S ratio for all the used stations. The symbol sizes and colors are chosen relative to the average values of the time delay (average = 4.5 sec) and the average value of the V_P/V_S ratio (1.78), respectively.

The difficulty in identifying the Moho P_s and the multiples and measuring

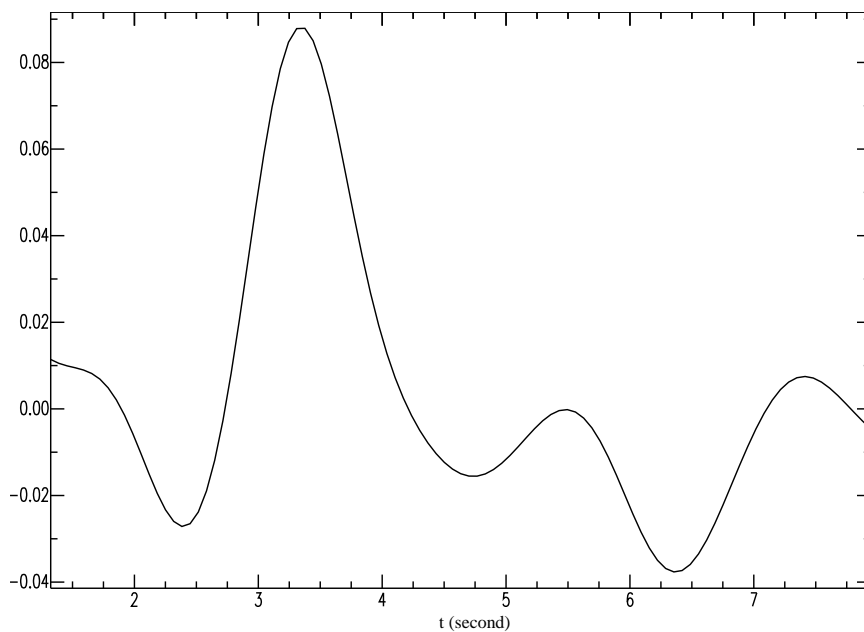


Figure 3.12: The best estimate P_s time delay (for $p = 0.06$ s/km) picked for the Moho P_s converted phase using radial receiver function for station HRV.

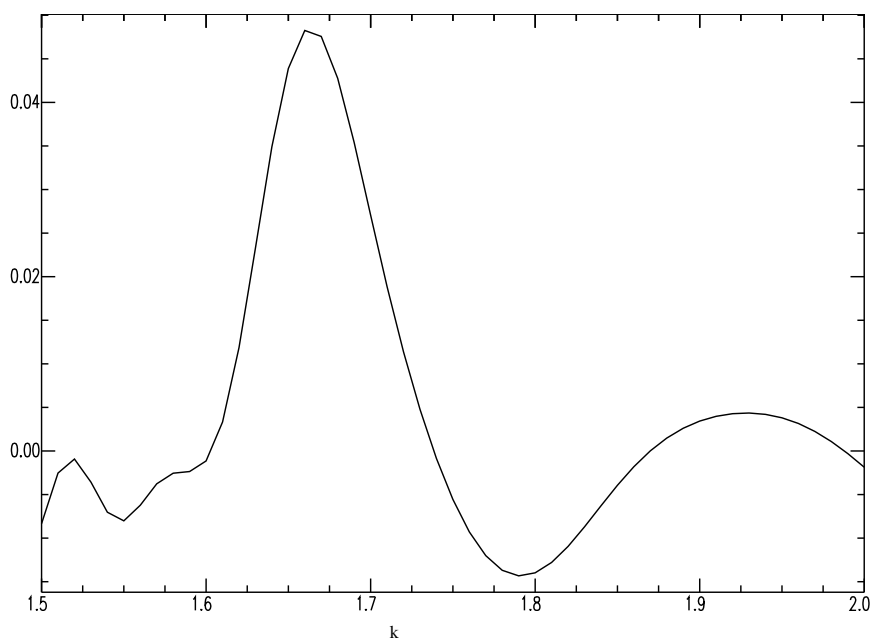


Figure 3.13: The best estimate V_p/V_s ratio (k) for the radial receiver function (HRV).

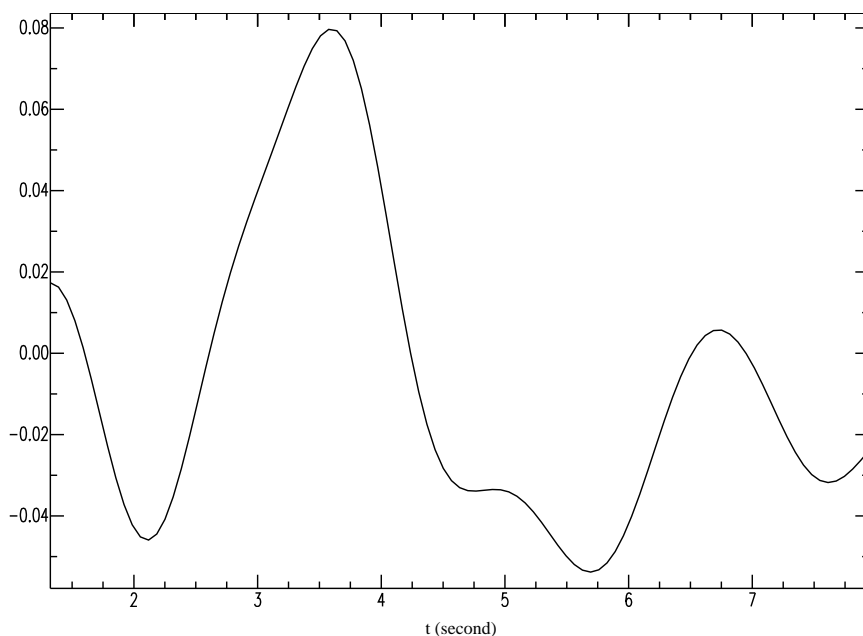


Figure 3.14: The best estimate P_s time delay (for $p = 0.06$ s/km) picked for the Moho P_s converted phase from the radial receiver function for station LSCT.

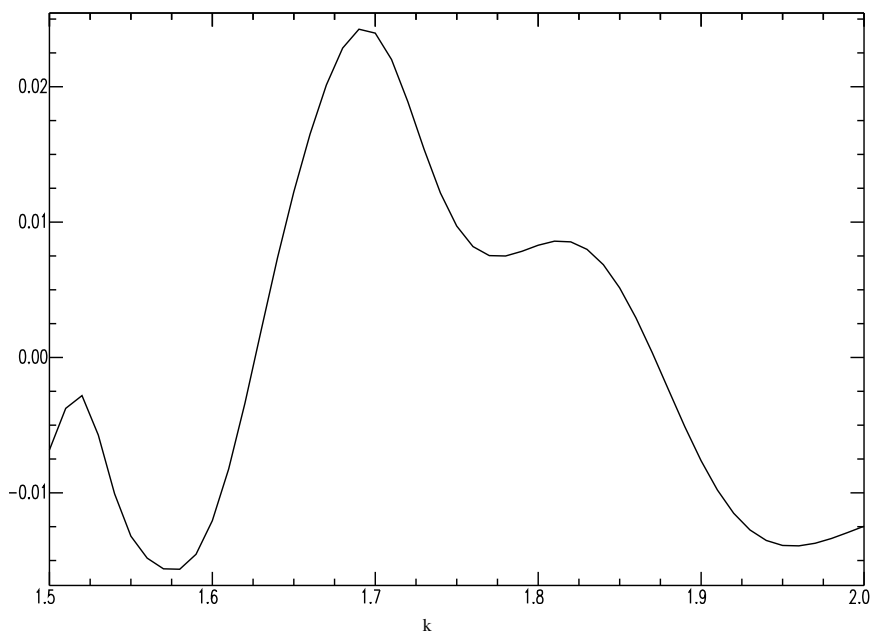


Figure 3.15: The estimate V_P/V_S ratio (k) from the radial receiver function for station LSCT. for this station I use the average value.

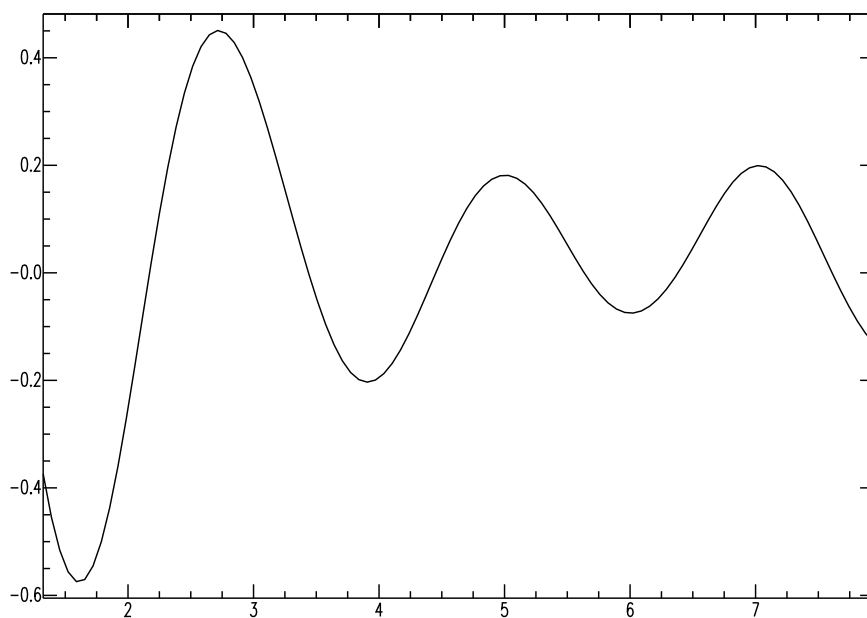


Figure 3.16: The receiver function at FA22 is affected by the sediment layer that no P_s time can be picked.

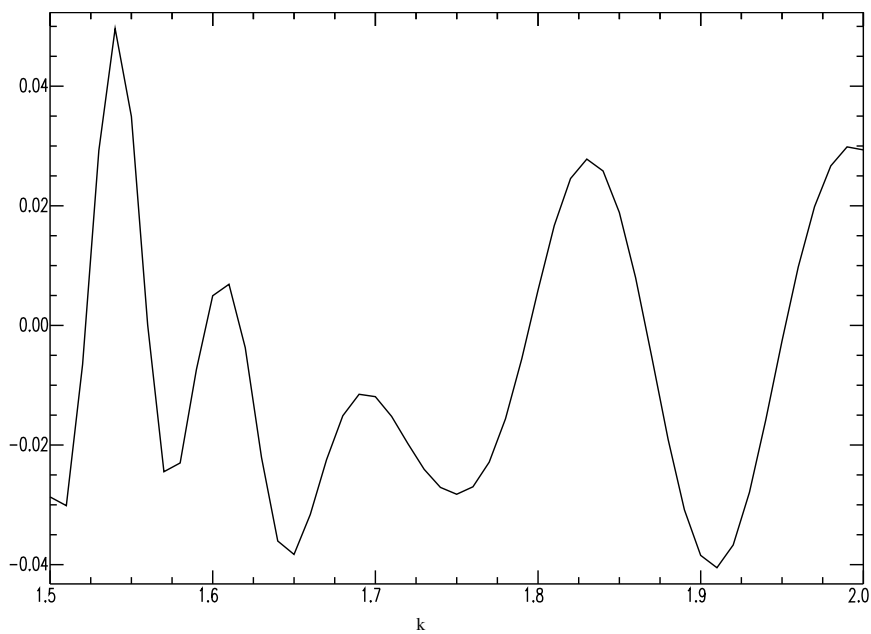


Figure 3.17: The estimate V_P/V_S ratio (k) at FA22 can not be accurate and is excluded.

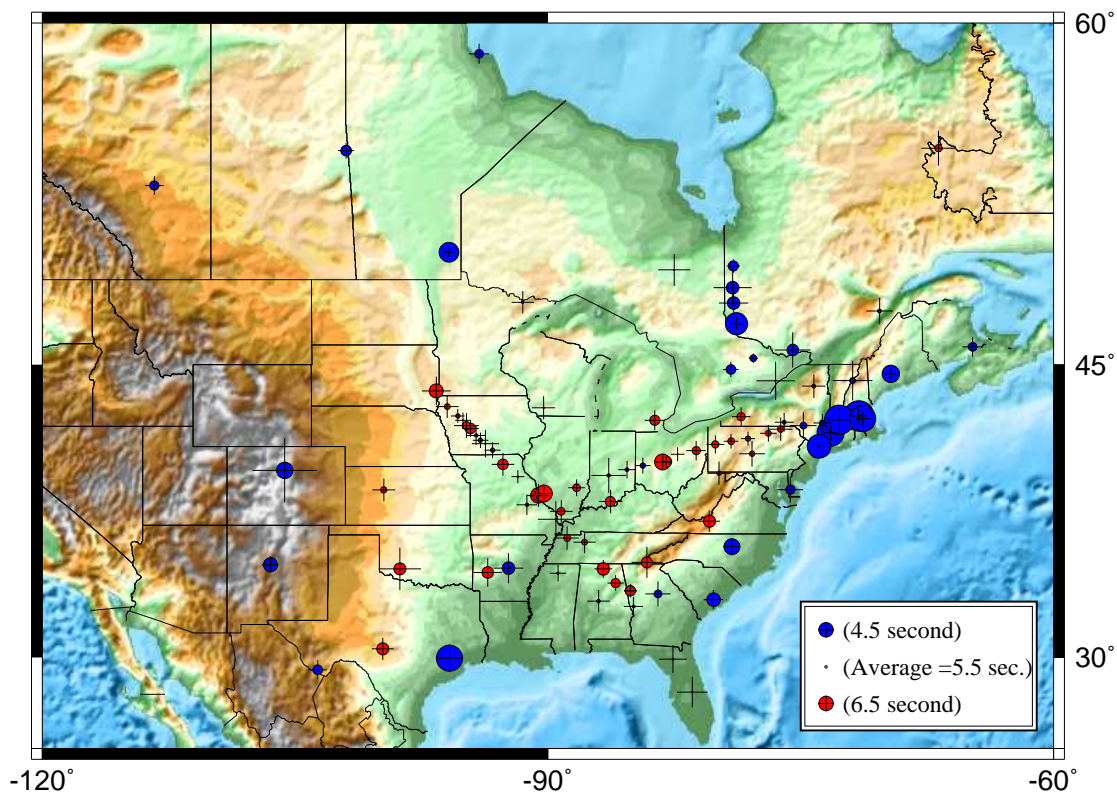


Figure 3.18: P_s time delay (for $p = 0.06$ s/km) for Eastern North America stations used in this study. The red circle is above average and the blue circle is below average. The map show a pattern with a low than average in the Coastal Plain and high values toward the midcontinent. The uncertainties are represented by the size of the cross

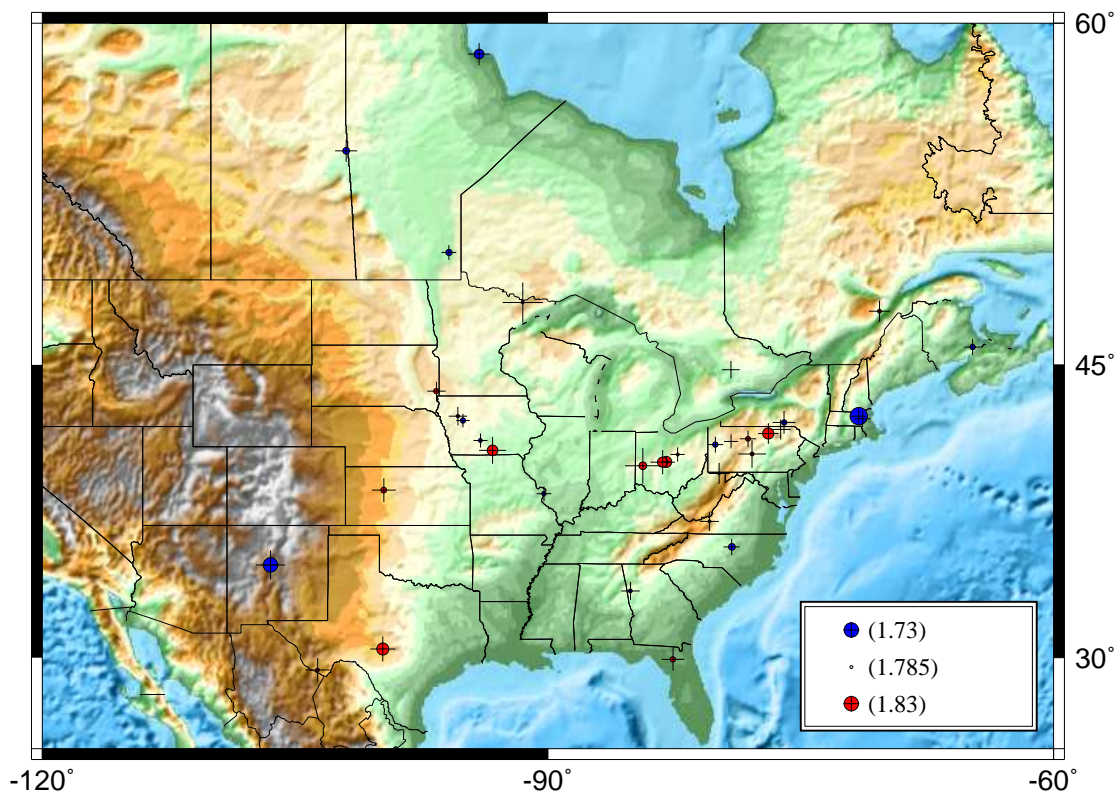


Figure 3.19: V_P/V_S for Eastern North America stations used in this study. The red circle is above average and the blue circle is below average. The map shows a pattern with a low than average in the Coastal Plain and high values toward the midcontinent. The uncertainties are represented by the size of the cross

their arrival times on a single receiver function trace can be due to the background noise, scattering from crustal heterogeneities, and P-to-S conversions from subcrustal discontinuities. However, the time relation for both the Moho P_s converted phase and the multiples (P_pPms and $P_pSs + P_sP_s$) can be used to estimate the V_P/V_S ratio and the depth, h , of the interface simultaneously by adding values of the receiver functions at predicted times t_1 , t_2 , and t_3 for a reasonable range of values of k and h . This $h - k$ domain stacking (Zhu and Kanamori, 2000) is defined as

$$s(h, k) = w_1r(t_1) + w_2r(t_2) - w_3r(t_3) \quad (3.12)$$

where $r(t)$ is the radial receiver function

t_1 , t_2 , and t_3 are the predicted P_s , P_pPms and $P_pSs + P_sP_s$ arrival times corresponding to crustal thickness h and V_P/V_S ratio k .

The w_1 , w_2 , and w_3 are the weighting factors to be applied to the multiples arriving at the times t_1 , t_2 , and t_3 . Figures 3.20-3.22 show the resultant stacks obtained for those stations. The best estimates of crustal thicknesses and V_P/V_S ratio are found when the three phases stack coherently.

Crustal thickness at each station is then computed using equation (3.9) from the Moho t_{P_s} converted phase and V_P/V_S for stations belong to the first group, assuming the average crustal P velocity of 6.3 km/sec. For stations belonging to the second group the V_P/V_S ratio is assumed to be the average (1.78) and the Moho thickness is computed accordingly. The final results with the stan-

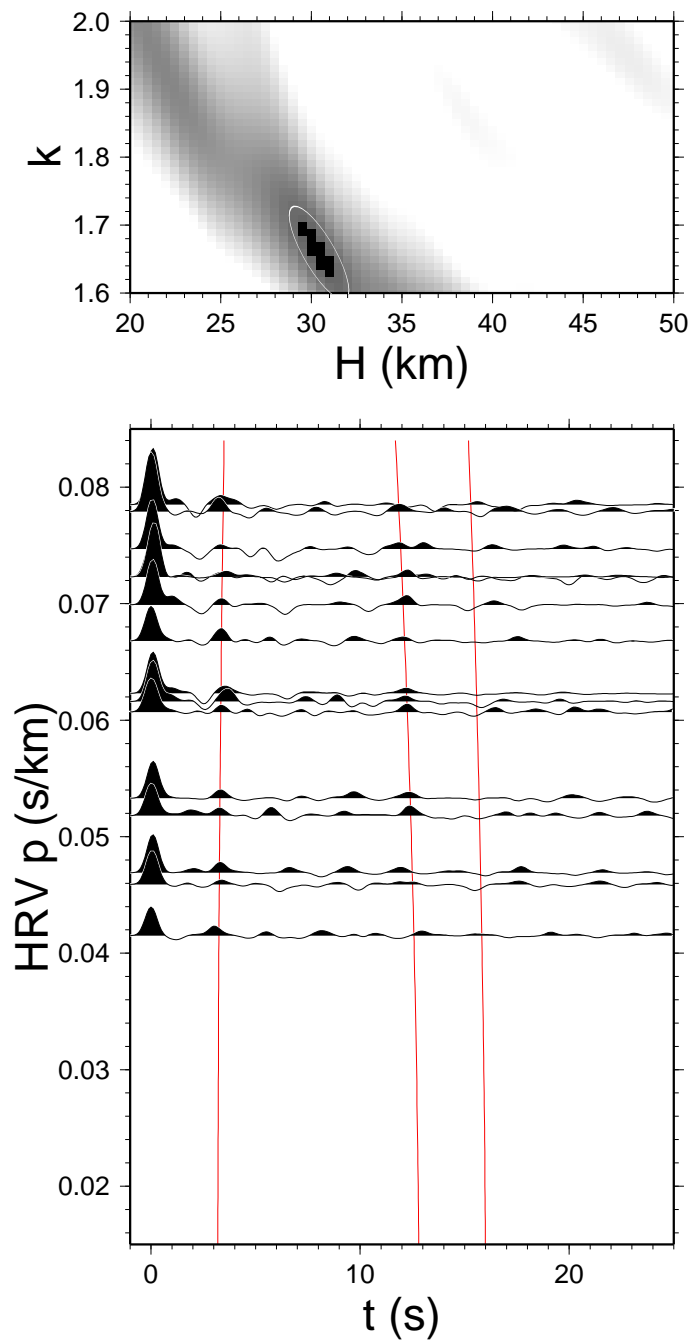


Figure 3.20: Radial receiver function for station HRV as a function of ray parameter in s/km . Red lines show Moho P_s , and the later $P_p P_m s$. The upper panel shows the $s(h, k)$ from stacking the receiver functions. The elliptical shape shows the best estimate of both V_P/V_S ratio k and the corresponding crustal thickness h . This station stack shows a well defined maximum.

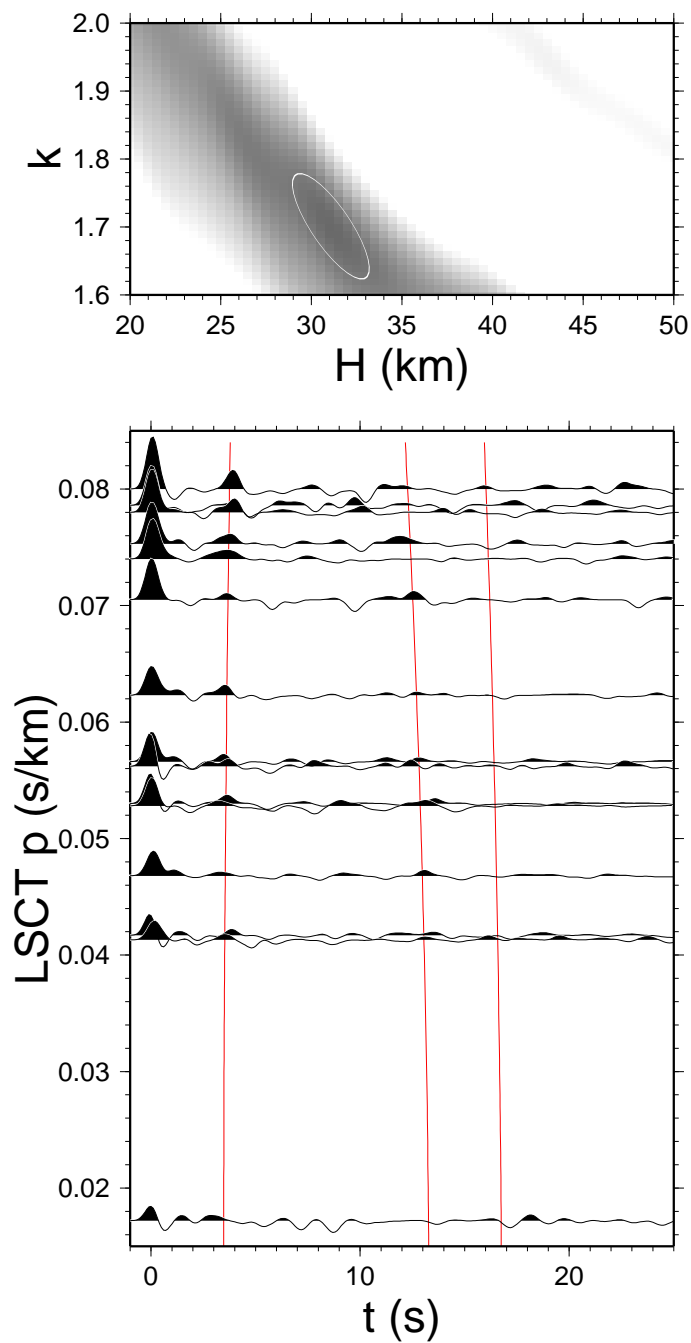


Figure 3.21: Radial receiver function for station LSCT as a function of ray parameter in s/km. Red lines show Moho P_s , and the later PpP_{ms} . The upper panel shows the best estimate V_P/V_S ratio (k)

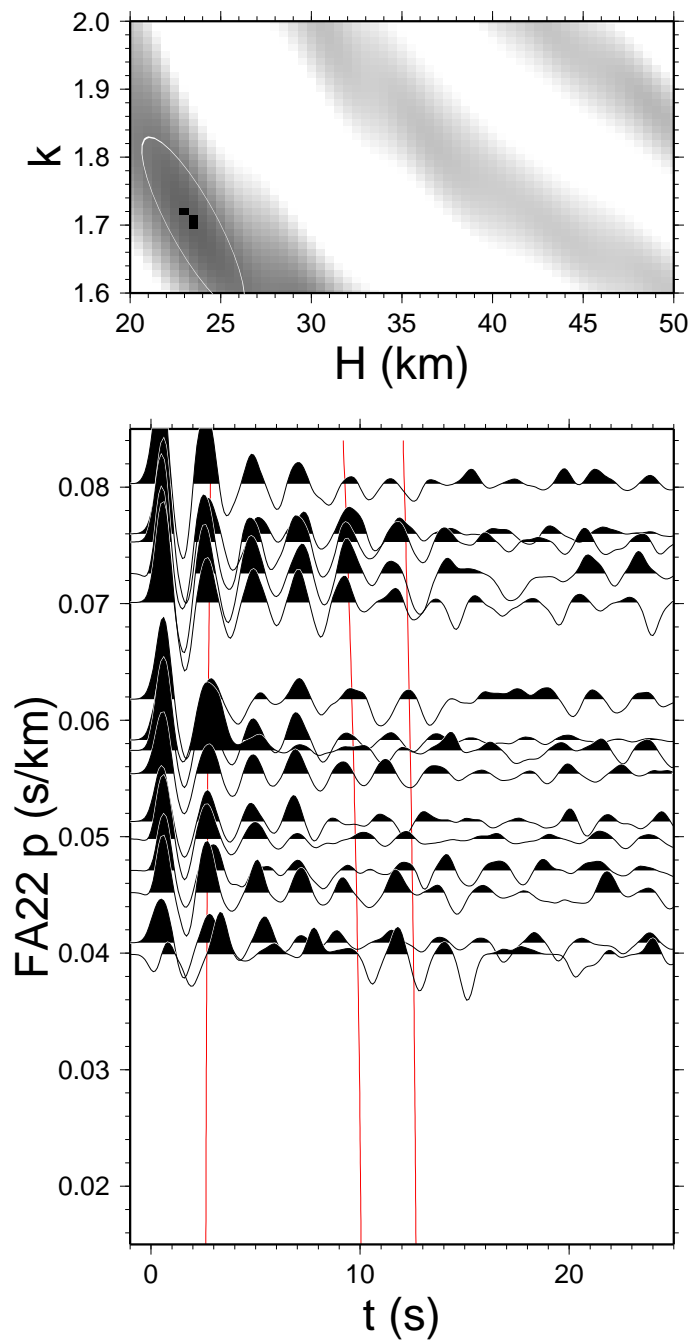


Figure 3.22: Radial receiver function for station FA22 (FLED Arrays) as a function of ray parameter in s/km. Red lines show Moho P_s , and the later $P_pP_m s$. The upper panel shows the best estimate V_P/V_S ratio (k). The ringing in the receiver functions does not permit an unambiguous estimate of the desired parameters.

dard error are listed in Table 3.8. Figure 3.23 shows the crustal thicknesses estimated for all the stations in groups 1 and 2.

We observe some interesting patterns. First the interior of the United States typically shows Moho depths greater than 40 km. The eastern coast and New England have Moho depths less than 40 km. There seems to be a sharp drop in Moho depth in northeastern Pennsylvania. Southern Canada also has depths less than 35 km. Some stations, such as ACSO and MM11, have a Moho depth that is significantly different than neighboring stations. Some variation in Moho depth is seen along the FLED line in Iowa.

Table 3.8: Locations of stations used in this study with the estimated crustal thickness (h) and V_P/V_S

STA	Lat(°)	Lon(°)	Elev(m)	Events	h (km)	t_{Ps} (s)	V_p/V_s	Group
AAM	42.30	-83.66	249	40	47.32 ±3.61	6.15	1.78	–
ACSO	40.23	-82.98	288	18	47.94 ±2.10	6.23	1.78	–
ALQ	34.94	-106.46	1849	46	38.96 ±2.36	4.52	1.70 ±0.04	k
ALQN	45.74	-78.19	0	2	–	5.14	–	X
ANMO	34.95	-106.46	1740	33	39.64 ±3.45	4.50	1.68 ±0.07	k
BINY	42.20	-75.99	498	71	46.00 ±3.56	5.72	1.75 ±0.05	k
BLA	37.21	-80.42	634	65	48.32 ±3.92	6.28	1.78	–
BLO	39.17	-86.52	246	35	–	7.05	–	X
CARO	47.92	-78.98	330	7	35.44 ±5.31	4.61	1.78	–
CBKS	38.81	-99.74	677	6	43.10 ±3.94	5.88	1.83 ±0.06	k
CCM	38.06	-91.24	222	51	43.93 ±3.70	5.71	1.78	–
CEH	35.89	-79.09	152	6	35.57 ±3.30	4.36	1.74 ±0.04	k
DRLN	49.26	-57.50	238	60	33.10 ±2.87	4.05	1.74 ±0.06	k
DWPF	28.11	-81.43	-142	35	35.94 ±4.76	5.41	1.91 ±0.07	k
EDM	53.22	-113.35	730	30	37.05 ±3.35	4.82	1.79 ±0.10	k
EYMN	47.95	-91.50	475	38	41.73 ±4.13	5.28	1.76 ±0.09	k
FA01	29.92	-82.58	-4	19	40.90 ±4.83	5.55	1.82 ±0.05	k
FA02	31.17	-83.53	39	6	–	6.41	–	X
FA03	32.05	-84.22	89	76	–	5.09	–	X
FA04	32.75	-84.92	175	16	43.55 ±3.49	5.66	1.78	–
FA05	33.57	-85.11	303	14	47.29 ±2.33	6.15	1.78	–
FA06	33.98	-85.99	134	19	46.77 ±2.85	6.08	1.78	–
FA07	34.73	-86.71	178	21	48.62 ±3.21	6.32	1.78	–
FA08	37.32	-89.53	118	16	41.53 ±6.50	5.40	1.78	–
FA09	39.49	-91.79	159	19	42.83 ±2.35	5.57	1.78	–
FA10	40.10	-92.67	2187	15	47.56 ±4.10	6.18	1.78	–
FA11	40.82	-93.29	295	13	44.44 ±2.88	5.78	1.78	–

k: station has clear P_s and multiples

–: station has good P_s but no multiples

X: station has poor P_s

Table 3.8: *continued*

STA	Lat(°)	Lon(°)	Elev(m)	Events	h (km)	t_{Ps} (s)	Vp/Vs	Group
FA12	41.14	-93.71	271	7	42.75 ±4.89	5.56	1.78	–
FA13	41.31	-94.01	252	25	44.35 ±2.78	5.76	1.78	–
FA14	41.54	-94.26	308	9	43.93 ±3.45	5.71	1.78	–
FA15	41.77	-94.47	303	25	–	6.66	–	X
FA16	41.89	-94.60	331	18	47.63 ±2.99	6.19	1.78	–
FA17	42.03	-94.84	361	34	46.32 ±4.48	6.02	1.78	–
FA18	42.30	-95.05	351	35	41.79 ±2.76	5.43	1.78	–
FA19	42.51	-95.35	390	18	44.28 ±2.49	5.75	1.78	–
FA20	42.97	-95.98	395	32	45.12 ±4.14	5.86	1.78	–
FA21	43.74	-96.62	456	26	49.46 ±5.16	6.43	1.78	–
FA22	44.36	-98.22	379	30	–	5.00	–	X
FA23	45.55	-99.98	538	12	–	5.55	–	X
FA24	46.53	-101.24	557	20	–	6.54	–	X
FA25	47.58	-103.30	578	24	–	6.59	–	X
FA26	48.79	-105.43	724	21	–	6.07	–	X
FA27	49.94	-108.11	883	8	–	6.63	–	X
FA28	50.76	-111.52	618	23	–	5.67	–	X
FCC	58.76	-94.09	39	22	40.73 ±3.95	4.86	1.72 ±0.05	k
FFC	54.73	-101.98	338	51	38.75 ±3.10	4.73	1.74 ±0.0	k
GAC	45.70	-75.48	62	16	37.72 ±6.71	4.66	1.75 ±0.05	k
GOGA	33.41	-83.47	150	65	38.94 ±4.63	4.92	1.76 ±0.05	k
GWDE	38.83	-75.62	19	30	29.77 ±3.73	4.84	1.99 ±0.11	k
HKT	29.96	-95.84	-413	85	38.95 ±6.90	3.65	1.56 ±0.05	k
HRV	42.51	-71.56	180	10	30.33 ±3.12	3.34	1.66 ±0.03	k
ISCO	39.80	-105.61	2743	20	46.69 ±16.26	4.33	1.56 ±0.04	k
JCT	30.48	-99.80	591	70	43.79 ±3.62	6.29	1.87 ±0.06	k
JFWS	42.91	-90.25	335	28	42.69 ±4.19	5.55	1.78	–
KAPO	49.45	-82.51	210	64	41.62 ±5.79	5.41	1.78	–

k: station has clear Ps and multiples–: station has good Ps but no multiplesX: station has poor Ps

Table 3.8: *continued*

STA	Lat(°)	Lon(°)	Elev(m)	Events	h (km)	t_{Ps} (s)	Vp/Vs	Group
KGNO	44.23	-76.49	89	21	42.50 ±6.89	5.52	1.78	–
LBNH	44.24	-71.93	367	64	30.97 ±5.71	5.05	1.99 ±0.16	k
LMN	45.85	-64.81	363	20	39.13 ±3.76	4.85	1.75 ±0.04	k
LMQ	47.55	-70.33	419	19	42.60 ±4.60	5.72	1.81 ±0.05	k
LRAL	33.03	-87.00	130	8	43.84 ±4.03	5.70	1.78	–
LSCT	41.68	-73.22	318	22	27.67 ±2.86	3.60	1.78	–
LTX	29.33	-103.67	1013	48	35.85 ±3.34	4.81	1.81 ±0.06	k
MCWV	39.66	-79.85	280	75	43.23 ±4.11	5.74	1.80 ±0.05	k
MIAR	34.55	-93.57	207	74	38.49 ±4.10	6.26	1.99 ±0.14	k
MM01	42.32	-72.71	122	21	26.49 ±4.17	3.44	1.78	–
MM02	42.17	-73.72	134	36	38.97 ±3.22	5.06	1.78	–
MM03	42.04	-74.85	670	39	32.33 ±4.00	5.00	1.94 ±0.09	k
MM04	41.85	-76.20	473	34	45.37 ±4.21	5.90	1.78	–
MM05	41.65	-76.92	701	40	45.17 ±3.02	5.87	1.78	–
MM06	41.39	-78.13	647	24	44.78 ±2.51	5.82	1.78	–
MM07	41.26	-79.14	518	46	45.72 ±2.64	5.94	1.78	–
MM08	41.11	-80.07	381	43	45.90 ±3.26	5.97	1.78	–
MM09	40.79	-81.21	357	35	46.39 ±3.51	6.03	1.78	–
MM10	40.61	-82.30	346	34	41.73 ±2.49	5.42	1.78	–
MM11	40.22	-83.19	283	37	50.44 ±2.64	6.56	1.78	–
MM12	40.04	-84.37	305	36	39.24 ±2.88	5.10	1.78	–
MM13	39.83	-85.31	337	19	40.00 ±3.17	5.20	1.78	–
MM14	39.55	-86.39	290	31	43.70 ±6.29	5.68	1.78	–
MM15	39.29	-87.31	190	15	–	6.76	–	X
MM16	38.92	-88.30	165	27	46.11 ±3.05	5.99	1.78	–
MM17	38.67	-89.33	143	34	–	6.70	–	X
MM18	38.53	-90.57	185	28	47.87 ±3.83	6.53	1.83 ±0.04	k
MO18	38.51	-90.56	161	4	47.53 ±3.13	6.18	1.78	–

k: station has clear P_s and multiples–: station has good P_s but no multiplesX: station has poor P_s

Table 3.8: *continued*

STA	Lat(°)	Lon(°)	Elev(m)	Events	h (km)	t_{Ps} (s)	Vp/Vs	Group
MPH	35.12	-89.93	93	41	—	5.11	—	X
MYNC	35.07	-84.13	550	34	47.87 ±5.57	6.22	1.78	—
NCB	43.97	-74.22	500	25	37.99 ±3.63	5.73	1.91 ±0.05	k
NHSC	33.11	-80.18	12	11	34.87 ±3.49	4.53	1.78	—
OXF	34.51	-89.41	101	26	43.00 ±2.94	5.59	1.78	—
PAL	41.00	-73.91	91	5	29.36 ±0.49	3.82	1.78	—
PAPL	45.32	-77.81	—	3	38.43 ±1.66	4.99	1.78	—
PLAL	34.98	-88.08	165	36	—	4.12	—	X
POP6	46.95	-78.82	—	6	30.15 ±2.65	3.92	1.78	—
POUL	48.63	-79.04	—	4	35.27 ±6.86	4.58	1.78	—
PQI	46.67	-68.02	180	5	—	5.86	—	X
RSSD	44.12	-104.04	2060	31	—	4.58	—	X
SADO	44.77	-79.14	243	22	36.68 ±2.74	4.78	1.78	—
SCHQ	54.83	-66.83	501	48	45.89 ±6.24	5.96	1.78	—
SIUC	37.71	-89.22	137	62	46.20 ±4.02	6.00	1.78	—
SLM	38.64	-90.24	161	44	51.09 ±3.23	6.64	1.78	—
SSPA	40.64	-77.89	252	96	43.26 ±4.47	5.82	1.81 ±0.06	k
SWET	35.22	-85.93	581	11	—	6.94	—	X
UALR	34.78	-92.34	138	29	35.34 ±5.39	4.59	1.78	—
ULM	50.25	-95.88	281	40	33.25 ±2.11	4.09	1.74 ±0.03	k
UTMT	36.34	-88.86	120	26	45.53 ±4.23	5.92	1.78	—
VSG4	49.63	-79.00	—	5	36.68 ±2.38	4.77	1.78	—
WCI	38.23	-86.29	506	48	47.45 ±4.24	6.17	1.78	—
WES	42.38	-71.32	60	7	28.25 ±2.48	3.67	1.78	—
WMOK	34.74	-98.78	486	67	48.40 ±7.64	6.29	1.78	—
WVL	44.56	-69.66	—	4	32.94 ±1.87	4.26	1.78 ±0.05	k
WVT	36.13	-87.83	157	71	45.02 ±4.00	5.85	1.78	—
YSNY	42.48	-78.54	628	19	46.46 ±3.34	6.04	1.78	—

k: station has clear P_s and multiples—: station has good P_s but no multiplesX: station has poor P_s

Chapter 4

Joint Inversion of Receiver Function and Surface-Wave Dispersion

4.1 Surface Wave Dispersion Curves

4.1.1 Introduction

Surface wave signals are generally the strongest arrivals recorded at teleseismic distances. They provide some of the best constraints on the Earth's crust and upper mantle structure. Their waveforms are more complicated than body waves. They travel more slowly and decay less with distance than body waves and they are dispersed. Interpreting surface-wave dispersion measurements provides an important method for determining the shear-wave velocity variation in the Earth. Modern studies of surface waves and their application in structure interpretation were propelled by Haskell's (1953) matrix formulation of the multi-layered system period equation, which made possible rapid, accurate computation of dispersion curves for complex models.

The modern use of seismic surface waves for studying crustal and upper mantle structure started in the 1950s. Several studies on observations of surface waves are available for both global and regional models. Regional surface wave studies of the crust and upper mantle were reviewed by Ewing et al. (1972); Kovach, (1966); Seidel and Müller, (1977). Brune (1969) and Knopoff (1972) presented surface wave dispersion for different tectonic provinces. Kovach (1978) provided an overview of how surface-wave data from earthquakes

are analyzed to infer details of the earth structure over particular propagation paths. Experimental methods for measuring surface wave dispersion, including the Fourier phase methods, the time correlation method, the band-pass filtering method, the group delay time method, and various digital moving window techniques, were described by Kovach (1978).

Surface wave data exhibit distinctive observational characteristics in different tectonic provinces. Shield areas have the highest values of shear wave velocities with depth and a relatively and a relatively weak mantle low-velocity zone. On the other hand, rift areas have much lower upper-mantle shear-wave velocities and a very pronounced low velocity zone (Kovach, 1978).

4.1.2 Love and Rayleigh Waves

The displacement field created by a stress difference is completely accounted for by propagating body waves, P and S including (S_H and S_V components) waves for linear-elastic, isotropic, homogeneous media. These wave fields become increasingly complex when discontinuous material, anisotropy and inhomogeneity are present. One of basic attributes of the Earth, the presence of the Earth's free surface, strongly affects the seismic wave field. The free surface of an elastic medium has the special stress environment defined by the vanishing of surface normal traction. Because all seismic wave measurements are made at or near the free surface, it is critical to understand free surface effects in order to interpret seismograms.

The two types of surface waves are known as Love and Rayleigh waves. At

the Earth's surface, both incident and reflected seismic waves instantaneously coexist, and the entire motion involves the sum of their respective amplitudes. Love waves are formed by the constructive interference of reflected SH waves at the free surface due to internal layering of the earth that traps SH reverberations near the surface. Rayleigh waves are the result of incident P and S_V plane wave interference at the free surface and travel along the surface. Fundamental mode Rayleigh waves travel along the surface with a retrograde elliptical particle motion at the surface and change to prograde with depth, passing through a node when there is no radial motion at all. Both Love and Rayleigh waves travel slower than body waves and appear later in the seismogram with Love waves arriving slightly before the Rayleigh waves.

4.1.3 Dispersion in surface Waves

Dispersion is observed in the frequency dependent travel times of surface waves, resulting from the increase of velocity with depth. In general, short period surface waves travels slower than long period waves. Long periods are more sensitive to the faster velocities found deeper in the earth. Both Love waves and Rayleigh waves exhibit dispersion and are used to estimate shear-velocity variations in the crust and upper mantle.

In a homogeneous elastic half-space with no damping, Rayleigh waves propagate along the surface of the body at a constant, frequency independent, phase velocity. In a layered or vertically heterogeneous half-space different frequency surface waves propagate with different phase velocities and different wave-

lengths. Each harmonic component of an observed signal has a velocity called phase velocity, $C(\omega)$, defined by Dziewonski and Hales (1972) as the instantaneous velocity of the plane waves at a given frequency:

$$C(\omega) = \frac{\omega}{k(\omega)} \quad (4.1)$$

where;

ω (The angular frequency) $= 2\pi f$

f = frequency

For a given angular frequency (ω), $C(\omega)$ depends on the medium parameters such as layer thickness (h), density (ρ), shear and compressional velocity (P and/or S) Wave disturbances with wide spectrum of periods interfere with each other producing constructive or destructive patterns that influence the total ground motion. Constructive patterns propagate along the surface as a wave packets with well defined group velocities, $U(\omega)$, which depend on the medium parameters and variation in phase velocity with frequency.

All surface waves, except Rayleigh waves, in an isotropic half-space, exhibit dispersion, with the apparent velocity along the surface depending on frequency (Lay and Wallace, 1995). The observed dispersion can be compared to theoretical dispersion to find the best fitting structure beneath an area of interest. It has been suggested that Love wave dispersion contributes less information about Earth structure than Rayleigh wave dispersion (Braile and Keller, 1975) . Both phase and group velocity dispersion curves contribute

generally the same information about the earth structure (Der et al., 1970; Wiggins, 1972). However, due to the nature of group velocity as a differential of phase velocity, small perturbations in phase velocity show up as larger variations in group velocity.

Group velocity

Group velocity is a dispersive characteristic where constructive patterns travel along the surface as wave packets. Group velocity dispersion curves can be used to define velocity structure. In the 1960s, the development of numerical techniques has resulted in significant progress in making dispersion curves measurements (Dziewonski and Hales, 1972). In general, many factors make the measurements of these dispersion curves complicated such as multipathing and background noise.

The group velocity, U , of a wave is defined by the angular frequency, ω , and the wavenumber, k , as

$$\begin{aligned} U &= \frac{d\omega}{dk} \\ &= C + k \frac{dC}{dk} \end{aligned} \quad (4.2)$$

where; C is the phase velocity. We can substitute $k = \frac{\omega}{C}$ and

$$\frac{dC}{dk} = \frac{dC}{d\omega} \frac{d\omega}{dk} = \frac{dC}{d\omega} U. \quad (4.3)$$

Then, at a particular frequency, we can express the group velocity as

$$U = \frac{C}{1 - \left(\frac{\omega}{C}\right)\left(\frac{dC}{d\omega}\right)} \quad (4.4)$$

Therefore, if we know the phase velocity dispersion, $C(\omega)$, across some frequency range, we can easily calculate the group velocity, $U(\omega)$, across that range (Larson and Ekström, 2001).

The group velocities of fundamental mode Rayleigh waves can be determined from observations by using Multiple Filter Analysis (MFT). Dziewonski et al. (1969) proposed Multiple Filter Analysis (MFT) to compute group velocity dispersion curves for a specific mode from complex multi-mode dispersion signal. The presence of multipathing in a surface train will bias conventional methods including MFT for estimating group velocities such that they will be determined slow (Jin and Herrin, 1980). This MFT technique is widely used and provides a sufficient number of group velocities to yield a continuous dispersion curve in an appropriate period interval from any dispersed wave train (Dziewonski et al., 1969; Herrmann, 1973; Bonner and Herrin, 1999).

4.1.4 Inversion of dispersion curves

Observed seismograms are a combination of source radiation, propagation path effects and recording instruments effects. Seismograms can be used to analyze the subsurface geology in two ways: by forward modeling or inversion of parameters derived from waveform. The approach to compute the forward problem is to start with an approximate model and make changes to the assumed parameterization, until the observed and predicted seismograms are

matched. Usually this method can be solved using trail and error modifications. On the other hand, the forward problem is important to inversion problems, since it provides the starting point for inversion.

Since the relationship between phase-and/or group velocities at a given frequency and the properties of the propagation path is not simple, a numerical procedure must be performed to compute one from the other to invert for the earth model. An implicit theoretical relationship exists between wave-type, mode, phase and group velocities and structural earth parameters such as density (ρ), layer thickness h , shear-wave velocity (β), and compressional-wave velocity (α). Generally, the inversion of a dispersion curve is a nonlinear process which can be linearized by applying Taylor's expansion to both phase and group velocities about a starting Earth model and neglecting higher-order terms in the difference between observed phase velocity $C(\beta, \alpha, \rho)$ and predicted phase velocities $C(\beta_0, \alpha_0, \rho_0)$ to relate the difference between observed and model predicted phase velocity dispersion as

$$C(\beta, \alpha, \rho) - C(\beta_0, \alpha_0, \rho_0) = \left. \frac{\partial C}{\partial \beta} \right|_{\beta_0} (\Delta\beta) + \left. \frac{\partial C}{\partial \alpha} \right|_{\alpha_0} (\Delta\alpha) + \left. \frac{\partial C}{\partial \rho} \right|_{\rho_0} (\Delta\rho) \quad (4.5)$$

and between observed and predicted group velocity dispersion as

$$U(\beta, \alpha, \rho) - U(\beta_0, \alpha_0, \rho_0) = \left. \frac{\partial U}{\partial \beta} \right|_{\beta_0} (\Delta\beta) + \left. \frac{\partial U}{\partial \alpha} \right|_{\alpha_0} (\Delta\alpha) + \left. \frac{\partial U}{\partial \rho} \right|_{\rho_0} (\Delta\rho) \quad (4.6)$$

where;

C is the phase velocity

U is the group velocity

α_0, α is the P-wave velocity; and β_0, β is the S-wave velocity

ρ is the density.

The non-linear inversion of the dispersion for a velocity model is easy because of the limited data sets usually used. The resulting model depends upon the starting model and constraints applied in the inversion. If the objective is that the model tell something about the Earth, it is necessary that the starting model be realistic at depth and that the model not be permitted to change in regions not controlled by the data set. The result of the inversion must be carefully evaluated.

4.1.5 Group and phase velocity estimation

In this research I used the Rayleigh-wave group and phase velocities Stevens and Adams (1999) and Harvard models. Stevens and Adams (1999) performed a global tomographic inversions to determine the shear velocity as a function of depth in discrete cells ($1^{\circ}x1^{\circ}$), each cell associated with a particular Earth model type. Each model consists of plane layers with a uniform compressional and shear velocities, density, and attenuation. The layer depths extended to about 200km. In their model, the shear velocity was treated as a free parameter which was estimated by tomographic inversion of observations of phase and group velocity dispersion curves. Their surface wave dispersion has the following characteristics:

- 1) They use a data set of 84,966 phase velocity measurements taken from Curtis et al. (1996).
- 2) The group velocities they used were derived from Stevens and McLaughlin (1988) and augmented with more recent measurements for a total of 1500 path at 6 frequencies from 0.02-0.06 Hz.
- 3) The surface wave phase and group velocity dispersion curves from underground nuclear test sites (Stevens, 1986; Stevens and Mclaughlin, 1988) computed from earth models for 270 path at 10 frequencies 0.015-0.06 Hz.
- 4) Phase and group velocity measurements obtained from western Asia and Saudi Arabia from Mitchell et al. (1996).
- 5) Global phase velocity model of Ekström et al. (1996) for 9 periods (35-150

second) computed for each 5° grid block.

6) Group velocity measurements obtained for Eurasia (Ritzwoller et al., 1996 and Levshin et al., 1996) for frequencies between 0.004 and 0.1 Hz with 500-5000 paths/frequency.

7) Group velocity measurements for South America and Antarctica from the University of Colorado (Vdovin et al., 1999 and Ritzwoller et al., 1996).

Pérez, (2001) tested the differences between the dispersion curves obtained for Rayleigh waves and the Stevens' global earth model for paths in the continental U.S. She found that for periods between 13 to 160 seconds the Stevens' model reproduces the observations very well (within $\pm 3.3\%$ at 20 seconds). For periods longer than 160 seconds, the Stevens' model delineate a linearly increasing tendency to overestimate the group velocity ($12 \pm 2.5\%$). In his model, Stevens based the inversion for these periods on the PREM model for layers deeper than 200 km. For periods ≤ 13 seconds, the model underestimates observed group velocities.

In the Harvard study, the Rayleigh wave group velocity was computed from the global model introduced by Larson and Ekström (1999). They used over than 50,000 minor-arc and 5,000 major-arc observations to construct a high-resolution surface-wave group-velocity model of the Earth for both Rayleigh and Love waves in the period 35-175 seconds. They made some assumptions to construct the images:

1) The surface waves are assumed to follow the great circle paths between the earthquakes and the stations.

2) The model corresponds to an azimuthally isotropic approximation of the actual Earth. In most areas of the world the anisotropy has been shown to be small with respect to isotropic structure, especially at long wavelengths (Larson and Ekström, 1999)

3) They do not account for mislocation of earthquakes or errors in station time because these effects can be neglected as constraint by other works (Ritzwoller and Levshin, 1998).

The phase match filter technique was used to measure the group velocity. The data were decimated by excluding low quality values and then inverted for degree 40 spherical harmonic coefficients. The inversion process was determined from individual measurements of group velocity in two steps. First, they invert for a long-wavelength model. The basis functions are spherical harmonics up to degree 12, described by 196 spherical harmonic coefficients, which results in a model with a minimum wavelength of 3000 km. As a result, the variance of the data were reduced by 70-95% depending on period. Second, they inverted for a higher degree (40) spherical harmonic map which allows for the description of features as small as 500 km. The second step accounted only for a reduction on the remaining variance of the data of about 10%.

The global surface-wave tomography models have some characteristics which make them good candidates for starting model in a regional studies (Mejia, 2001; Larson and Ekström, 1999). First, the global models do not have a large errors at the boundaries of the target region because the global model works for a sphere. Second, the global model uses a great circle path to estimate the

observation of velocities at longer periods.

Based on the same principles used for the global models, the regional models for Eurasia were calculated by Ritzwoller and Levshin (1998). Although, the resolution on a regional tomography increases with decreasing periods Ritzwoller and Levshin (1998) inverted measurements of surface waves propagating along 9,000 paths to produce a detailed $1^\circ \times 1^\circ$ grid of fundamental-model Rayleigh- and Love-wave group velocities for Asia. Their result presents group velocity maps from 20 to 200 seconds period for Rayleigh waves and from 20 to 175 seconds for Love waves. The average uncertainty for both is about 0.030-0.040 km/sec independent of frequency. Resolution is estimated from checkerboard tests with an average of 5° to 7.5° but degrade at periods above about 100 seconds.

For our study, we use the Stevens and Adams (1999) code to predict group velocities at our sites and also the Harvard phase and group velocity predictions. We feel confident in doing this because Pérez checked the Stevens and Adams (1999) predictions for many paths in our study region. We realize that additional dispersion data, especially at the shorter periods, would be very useful. These data should be available in a few years,

4.2 Joint Inversion of Receiver Function and Surface-Wave Dispersion

4.2.1 Introduction

A study of crustal and upper mantle structure beneath North America helps seismologists to visualize the effect of different tectonic episodes on the formation of the continental lithosphere. Different models have been introduced to explain the nature and evolution of North America, but no teleseismic P-wave delay times or active source surveys have had the source and station density required to determine the detailed velocity structure of the subsurface for the entire continent (Mooney and Meissner, 1991, 1992; Holbrook et al., 1992a; Christensen and Mooney, 1995). Since we cannot model the overall structure of this region directly, it is important to combine different data from a number of discrete studies. Combining seismic data (receiver function and surface-wave dispersion) in joint inversion is an obvious approach to improve estimates of earth structure. Although, numerous seismic reflection/refraction studies have been conducted in North America, these have been primarily P-wave studies so that few shear-wave velocity models are available. The existing do not cover a large enough area or do not have the resolution to develop crustal velocity models to be representative of the expected continental variation in structure.

Although the receiver function is sensitive to the shear-velocity structure and has been used successfully to resolve boundaries at different depths and provide site specific information about the dip angle and direction of interface geometry (Langston, 1979, 1995; Owens, 1984, 19987; Ammon et al., 1990;

Ammon and Zandt, 1993; Cassidy, 1992, 1995; Zandt et al., 1995; Zandt and Ammon 1995), its inversion for shear-wave velocity structure is non-unique (velocity-depth trade-off) since there is very little absolute-velocity information contained in the receiver function (Ammon et al., 1990). On the other hand, Rayleigh waves are known to be sensitive mainly to the shear-wave velocity and with longer wavelength they can penetrate the upper mantle, but lack the resolution to define crustal layers. The surface-wave shear-velocity information is essentially absent in the receiver function. Özalaybey et al. (1997) proposed that the non-uniqueness problem can be addressed by combining receiver function inversion with surface-wave dispersion. Thus, to combine data in an inversion, the data have to be sensitive to the same physical quantities and that they sample or average structure over a comparable length scales (Özalaybey et al., 1997; Juliá et al., 2000; Ammon et al., 2002).

4.2.2 Inversion procedure

The joint inversion for both receiver function and surface-wave dispersion curves (Rayleigh group-and phase-velocity) attempts to simultaneously invert a set of observation that are sensitive to the same parameters of the media that they travel through (Herrmann and Ammon, 2003 and Juliá et al., 2000, Özalaybey et al., 1997). This joint inversion process can be expressed by the following equation (see page 5-1 Herrmann and Ammon, 2002):

$$S = \frac{(1-p)}{N_r} \sum_{i=0}^{N_r} \left(\frac{O_{r_i} - P_{r_i}}{\sigma_{r_i}} \right) + \frac{p}{N_s} \sum_{j=0}^{N_s} \left(\frac{O_{s_j} - P_{s_j}}{\sigma_{r_j}} \right) \quad (4.7)$$

where;

O_{r_i} Observed receiver function at time t_i

P_{r_i} Predicted receiver function at time t_i

σ_{r_i} Standard error of observation at t_i

O_{s_j} j^{th} observed surface-wave dispersion

P_{s_j} j^{th} predicted surface-wave dispersion point

σ_{s_j} Standard error of j^{th} surface-wave observation

N_r Total number of receiver function points N_s Total number of surface-waves dispersion points p Influence factor, $0 \leq p \leq 1$.

The system of the entire set of observation (receiver function and surface-wave dispersion) may be expressed as

$$Y = AX$$

where $Y = m \times 1$ matrix of data points, A is an $m \times n$ matrix which relates the observations to the model parameters, and X is an $n \times 1$ vector of unknown model perturbation. The equation cannot be satisfied by every data point. Thus, the simplest method for solving the linear inverse problem is based on the length of the estimated model parameters and the predicted data $Y^{pre} = AX^{est}$. In the least-square principle, a set of model parameters (X) is considered to be a valid solution if it will minimize the sum of the square of the residuals (ϵ). The residual can be defined as the difference between the observed and predicted models. Mathematically the minimization function can be expressed as

$$E = \epsilon^T \epsilon = (AX - Y)^T (AX - Y)$$

The minimization process can be simplified by introducing the singular value decomposition, which is an orthogonal transformation of the matrix A into three matrices as

$$A = U \Lambda V^T$$

where U is an $m \times m$ orthogonal matrix with the eigenvectors of A in the columns, $V = n \times n$ orthogonal matrix, and $\Lambda = m \times n$ upper left diagonal matrix and are non-negative and are called singular values (Menke, 1984). The solution can be written as

$$X = V \Lambda U^T Y$$

or, if each column of U and V represent orthogonal vectors u_j and v_j , then X will be expressed as a sum of k orthogonal vectors v_j

$$X = \sum_{j=1}^k \frac{u_j^T y}{\Lambda_j} v_j$$

Identically zero eigenvalues are ignored in the decomposition of A (Crosson, 1976). In practice, the very small eigenvalues are encountered because of numerical errors. In a situation where the problem is poorly constrained at least one of the singular values λ_j will be small causing an excessive magnification of the corresponding vector v_j . Ideally, we seek a solution procedure that results in the suppression of those model components associated with small or near-

zero eigenvalues. This could be solved by the damped least-squares method (Levenberg, 1944; Marquardt, 1963) which involves the addition of the scale identity matrix to the original least-square problem for which the solution vector is

$$X = (A^T A + \sigma^2 I)^{-1} A^T Y$$

where

σ^2 is the damping value, I is an identity matrix, and T indicates transpose. Changing σ controls the relative importance given to the prediction error and solution length. The solution vector X can be given in term of the eigenvectors and eigenvalue of matrix A using singular value as

$$X = V(\Lambda^2 + \sigma^2 I)^{-1} \Lambda U^T Y$$

If the damping σ is increased, it will impose more weight on minimizing the solution norm and less on the least-squares residuals. We can reduce the problem of the stochastic least-squares to standard least-squares problem by letting $\sigma^2 = 0$.

In the standard damped least-squares problem the resolving kernel matrix R can be evaluated to know how closely the estimated model is to the true model. The resolution matrix can be expressed as

$$R = V(\Lambda^2 + \sigma^2 I)^{-1} \Lambda^2 V^T$$

If $R = I$, then each model parameters is uniquely determined. If R is not an identity matrix, then the estimates of the model parameters are weighted averages of the true model parameters.

The standard deviation in the model solution is tested by using the covariance matrix which given as

$$C = V(\Lambda^2 + \sigma^2 I)^{-1} \Lambda^2 (\Lambda^2 + \sigma^2 I)^{-1} V^T$$

This formula relates the error in the solution vector to the error in the data vector. The introduction of the damping parameter σ in the solution stabilizes the solution by reducing the covariance matrix C , but it degrades the solution matrix R .

Herrmann and Ammon (2002) implemented this algorithm in their program *joint96*. This program also adds the options of smoothing and constraints on each individual layer. These options permit deriving a smooth model and also one that only departs from the initial starting model because the data require such a departure.

4.3 Joint Inversion Processing

I applied the joint inversion technique (*joint96*) to the North America seismic network (Figure 1.1). The inverted data include receiver functions at three low pass filter frequencies, roughly $f = 0.5, 1.0, \text{ and } 2.5$ Hz corresponding to $\alpha = 0.5, 1.0$ and 2.5 , respectively. Rayleigh fundamental-mode group-and-phase velocities between 4 and 200 second are taken from work of Stevens and Adams

(1999) and Harvard. The starting model is a modified version of the *ak135* earth model of Kennett et al. (1995). This modified version consisted in having the upper 50 km of the model replaced by the model values at a depth of 50 km; this starting model was chosen without a crustal layer so that the data would be able to totally control the image of the crustal velocities with no bias from the initial model.

To give better estimate of the crust and upper mantle properties, I was careful in selecting the data. For a station to be used, it must have recorded at least 4 teleseisms from which receiver functions were computed. The high quality receiver were functions estimated using an iterative time-domain approach (Ligorria and Ammon, 1999). The first step in this method is to test the original waveform and select the best quality records (small background noise). The second step is to pick the P-wave manually. The third step is to compute the receiver function using the iterative time-domain deconvolution. The final step is to select the good receiver functions based on the match between the radial receiver function and the vertical component. This uniform inversion procedure was applied at each stations. In addition, I used the goodness of fit factor output as part of the interactive deconvolution and also used those receiver functions for which 90% and 80% of the observed radial P-wave signal was accounted for, for $\alpha = 0.5$ and 1.0 and $\alpha = 2.5$, respectively.

For the receiver functions the inversion is applied to time window between -5 and 20 seconds. Layer weighting is used to force constraints onto the inversion to have a smooth upper crust and fixed lower crust with a transition

starting at 50 km. The velocities at the bottom of the model, at a depth of 600 km, were fixed. The model was not permitted to change must at depths greater than 100 km, but could do so if the data required. The p factor (equation 5.7) was chosen to give more weight to the receiver function ($p = 0.15$). This value was arrived at through experimentation. I started the first inversion with a slightly higher damping to avoid an overshoot in the first model estimate and for the remaining inversion a small damping was used. For each data set, I performed 30 iterations. The V_P/V_S ratio was fixed throughout the model to those of the initial model because of the greater sensitivity to shear-wave velocities. In later interpretation, to define the location of the Moho, I used the depth at which the shear-wave velocity became 4.2 km/s; this was necessary since, as we will see, not all inverted models had sharp discontinuities in velocity at depths at which we would expect a Moho.

4.4 Lithospheric Structure of the Canadian Sites

4.4.1 The Canadian Shield (Eastern Canada)

Archean-early Proterozoic-crust of Canada is sampled by the stations SADO, KGNO, PAPL, ALQN, GAC, CARO, POP6, POUL, VSG4, KAPO, LMQ, SCHQ, FRB, DRLN, LMN, LMQ, and LBNH. The depths to Moho were indicated using the travel time for the Ps phase based on the method proposed by Zandt and Ammon (1995). Mooney and Braile (1989) proposed that the Archean and Proterozoic crust of the continental interior has a crustal thickness that ranges from 35 to 55 km with an average thickness of 36 km (39 km as estimated from

receiver function in this study). As discussed earlier, a receiver function gives a good estimate for the crustal thickness in this region.

Northern (Canadian) Appalachians

The inversion method was carried out in the northern Appalachians using two stations (LMN and DRLN) as part of the CNSN (Figure 4.1). The central mobile belt of the Newfoundland Appalachian orogen is the manifestation of different tectonic processes that formed the Northern Appalachians within a cycle of continental rifting, oceanic spreading, and continental collision culminating in the transpressional Appalachian orogeny (Hughes et al., 1994). A lateral and continuous zone of polydeformed meta-sedimentary and island arc volcanic rocks are identified by characteristic age, lithologic, and structural signatures (Williams and Hatcher, 1983). The station DRLN is located above the seismic refraction/wide-angle reflection profile shot point-12. Four geologic zones can be recognized across the Newfoundland Appalachian orogen: the Humber zone, the Dunnage zone, the Gander zone, and The Avalon zone. The station DRLN samples the Dunnage zone located in the central Newfoundland, characterized by vestiges of Early Paleozoic island arc volcanic rocks and flysch sediments deposited on Ordovician ophiolitic assemblages thought to be allochthonous upon basement of continental aspect (Hughes et al., 1994).

The Dunnage zone is also characterized by positive gravity anomalies with superimposed localized lows related to granitic intrusive (Miller, 1990 and Hughes et al., 1994). Hughes et al., (1994) showed that the Deer Lake basin

(Devonian / Carboniferous basin) is modeled as step-sided asymmetric bodies about 2 km deep and characterized by velocities in the range 4.2-4.6 km/sec. Beneath the surface layer they divided the crust into three layers with a crustal thickness of 35 km. The upper crust has a compressional velocity of 5.6 km/sec and a rock composition of Granite-Granodiorite. The middle crust extends to 25 km depth with the Granodiorite-diorite rock composition and compressional velocity of 6.4 km/sec. The lower crust extends to about 35 km depth and a velocity of 7.2 km/sec. The receiver function shows a crustal thickness of about 32 km. The inverted shear velocity model reveals a surface velocity of 3.1 km/sec. The inverted model is not stable, a rapid increase for the 10 km from 3.1 to 3.35 km/sec for the first 5 km and from 3.35 to 3.65 km/sec to a depth of 10 km. The middle crust extends from 10 to 22 km with average velocity of 3.65 km/sec. The lower crust for this model has a low velocity layer and a gradational crust-mantle transition from 30 to 48 km deep.

The station LMN in central New Brunswick lies within the Appalachian Orogen. The closest seismic refraction lines to this station are 200 km to the north-northeast (Dainty et al., 1966) and about 300 km to the west-southwest (Hennett et al., 1991) which indicate a relatively simple crust with a Moho depth estimated at 42 and 36 km, respectively. Joint inversion at this station reveals a surface shear velocity of 3.15 km/sec and a rapid increase to 3.7 km/sec at 4 km depth. The model shows a high velocity layer for depths from 4 to 10 km with high shear velocity of 3.9 km/sec. The upper crust has a velocity of 3.65 km/sec and extends to 20 km depth. A sharp discontinuity is seen

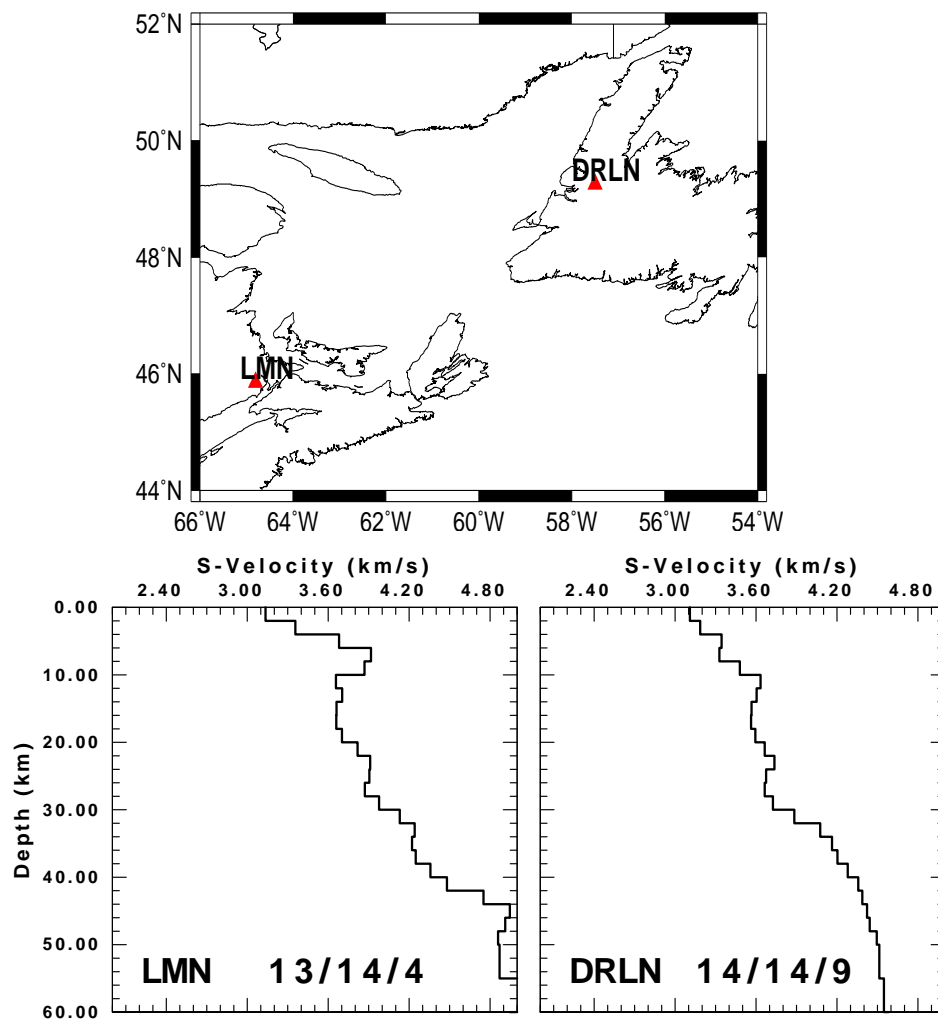


Figure 4.1: The final shear velocity model inverted from receiver function and surface-wave dispersion of Rayleigh group and phase velocity. This model compares the structure for two stations from CNSN located on the northern Appalachians. For LMN the numbers 13 / 14 / 4 indicate that the number of receiver functions used with $\alpha = 0.5 / 1.0 / 2.5$.

between the upper and the middle crust. The velocity gradually increases between the middle and lower crust which has a thickness of about 8 km. This station has a sharp crust-mantle transition as indicated from the receiver function and the joint inversion model.

Grenville Province

The Carthage - Colton mylonite zone, an intense ductile shear and igneous intrusion, divides the southern Grenville province into two subprovinces - the Central Meta-sedimentary Belt (amphibolites facies metasediments) to the west and the granulite facies metaplutonic of the Central Granulite Terrane to the east (Hughes and Luetgert, 1992). It was accreted to the Superior province during the Grenvillian orogenic cycle between 1160 and 970 Ma (Rivers et al., 1989; Rondenay et al., 2000). Most parts of Grenville province in Ontario have been locus of several seismic studies (Green et al., 1988; Winardhi and Mereu, 1997; Forsyth et al., 1994a, 1994b; Rondenay et al., 2000; Zelt et al., 1993) which have greatly increased the knowledge of the subsurface structure of this region. The Grenville province in Ontario is separated from the Archean Superior province and Paleo - proterozoic southern province to the northwest by the Grenville Front tectonic zone where the Grenville rocks were thrust over the Superior (White et al., 1993).

The stations GAC, PAPL and ALQN are located in the Central Meta-sedimentary Belt Terran (CMB) of the Grenville province that comprises the youngest terrains of the Precambrian Canadian Shield (Rondenay et al., 2000). To the west

of the Central Meta-sedimentary Belt is the Central Gneiss Belt (CGB) which is associated with the station SADO. The CMB is characterized by a series of highly sheared calc-silicate marbles, quartzites, metaevaporite, and polydeformed magmatitic gneisses belonging to the Grenville supergroup (Hughes and Luetgert, 1992). During the Grenvillian cycle the Central Meta-sedimentary Belt was pervasively deformed and metamorphosed to amphibolite/granulite facies suggestive of paleopressures and temperatures of 400-600 MPa/600°C (Wiener et al., 1984).

The 1982 refraction/wide-angle reflection experiment across the Central Meta-sedimentary Belt suggests that the crust is 40 km thick and is characterized by anomalously high seismic velocities (Mereu et al., 1986), which agrees well with the Moho depth estimated in this study (40-42 km). Mereu et al. (1986) indicated that the upper crust has a relatively low vertical gradient with shear velocity of 6.4 km/sec at the surface increasing to 6.7 km/sec at 23 km depth and the velocity of the lower crust of 6.7-7.1 km/sec at 40 km depth. Berry and Fuchs (1973) found that the crust in the Central Meta-sedimentary Belt is composed of two layers with velocities of 6.2-6.4 km/sec for the upper crust and 6.6-7.1 km/sec for the lower crust with a thick transitional zone across which seismic velocity increases from 7.1-8.5 km/sec between depths of 36-50 km.

The inverted models show a simple three layer crust with a low velocity layer for the structure underneath the station PAPL (Figure 4.2). The average shear-wave velocity for the uppermost crust is 3.45 km/sec with a rapid

increase in the velocity from 3.3 at the surface to 3.55 km/sec at 4 km depth. The middle crust has an average shear velocity of 3.6 km/sec and extends from 4-22 km depth. The lower structure beneath station GAC may sample a sharp mid-crustal discontinuity ($\Delta V_s=0.2$ km/sec) at 22-24 km depth, however, more high-quality data are needed to confirm this. A gradual transition zone extends between the depths 38-50 km where the shear velocity increases from 4.0 to 4.6 at 50 km depth. The crustal structure beneath PAPL has a surface layer shear velocity of 3.5 km/sec and reaches 3.6 km/sec at 4.0 km depth. The inverted shear velocity model shows a constant shear velocity 3.6 km/sec extending to 10 km depth. A low velocity zone may be identified between depths 10 to 14 km. The lower crust has an average shear velocity of 3.75 km/sec with the crust-mantle transition zone extending from 36-42 km depth. The highest shear velocity for this station is 4.5 km/sec.

Additional estimates for the Central Meta-sedimentary Belt is available from the inverted shear velocity model at KGNO (Kingston, Ontario) south of GAC (Figure 4.3). As mentioned earlier, the crustal thickness beneath this station is 41 km which is in a good agreement with the average crustal thickness for the Grenville province. The surface shear velocity increases from 3.25 km/sec at the surface to 3.6 km/sec at 4 km depth. A low velocity layer is present beneath this station from 10-16 km depth. Also, the model indicates a gradational increase in the velocity from 16-20 km which represents the middle crust. The lower crust has an average shear velocity of 3.95 km/sec and extends from 20-40 km where we have the beginning of the gradual transition

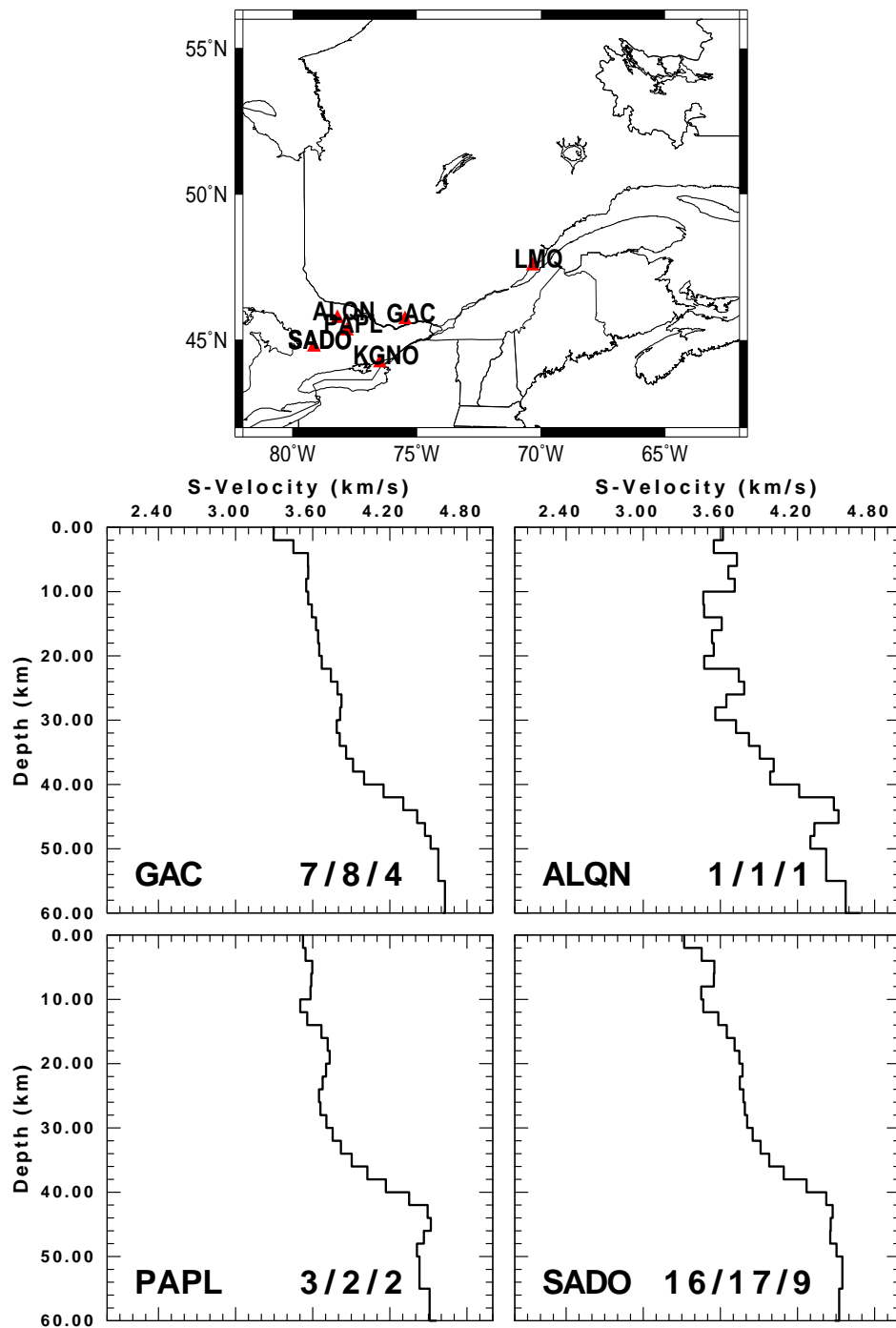


Figure 4.2: The final shear velocity model inverted from receiver function and surface-wave dispersion of Rayleigh group and phase velocity. This model show four stations from CNSN

zone for about 8 km extending from 40-48 km with high velocity of 4.6 km/sec. The upper crust of the Central Gneiss Belt (SADO) indicates that the seismic velocity increases from 3.3 at the surface to 3.6 km/sec for the upper 4 km. The structure beneath SADO has a constant upper crust velocity of 3.57 km/sec to 8 km depth. This station is nearest to PAPL and by comparing the inverted models it seems that both have the same crustal structure. The inverted model at SADO shows a low velocity layer in the upper crust from (3.4 km/sec) at depths 8-12 km that may confirm the presence of this layer as indicated at PAPL. The transition zone for this region is gradual with a shear velocity increases from 3.9 km/sec at 32 km depth to 4.5 km/sec at 42 km depth.

Stations LMQ and SCHQ are located in the northeastern Grenville province. In the northeastern Grenville, crustal thickening resulted in tectonic burial and high-pressure metamorphism of a variety of middle and upper crustal rocks including the aforementioned gabbros and anorthosites (Hurich et al., 2001). The northeastern Grenville is dominated by a strong inverse metamorphic gradient from the foreland toward the interior of the province ranging. Station SCHQ samples the foreland which comprises a Paleo - proterozoic continental margin sequence, exposed in the Labrador Trough and its Archean basement. Both LMQ and SCHQ show the same velocity model for the upper 10 km (Figure 4.3). The surface velocity beneath these stations is 3.35 km/sec and increases rapidly to 3.65 km/sec at depth of 4 km. Both models indicated a high velocity layer at depths from 4 to 10 km with an average shear velocity of 3.7 km/sec. At station SCHQ, it is easy to identify the middle and lower

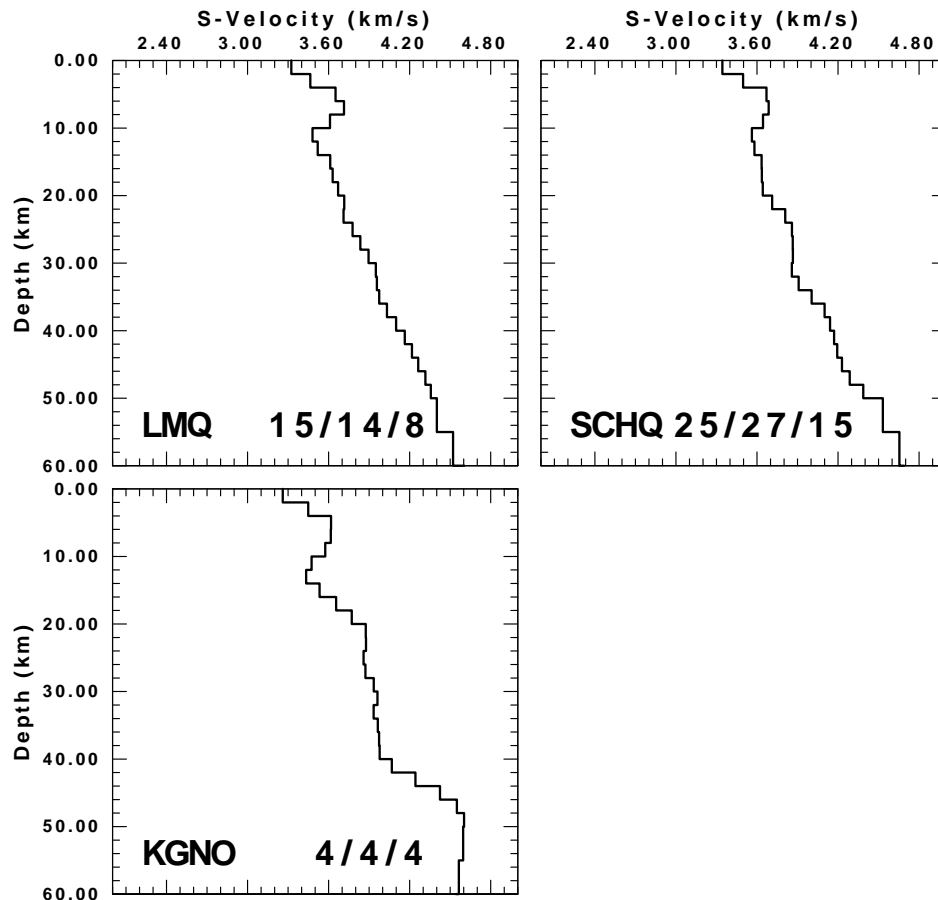


Figure 4.3: The final shear velocity model inverted from receiver function and surface-wave dispersion of Rayleigh group and phase velocity. This model show stations from CNSN that are located on the southern Canada (Grenville Province)

crust, whereas it is not easy at LMQ. Both models show a gradual crust mantle transition zone with the Moho depth of 38-42 km as indicated from the receiver function.

Superior Province

The Grenville Front is a major tectonic boundary exposed on the Canadian Shield. The front, which results from the Late Proterozoic Grenville orogeny separates the weakly deformed Archean and Early Proterozoic foreland from

the highly deformed terrains of the Grenville province (Kellett et al., 1993). To the north are the stations POP6, POUL and VSG6 in the Abitibi subprovince, the largest Archean greenstone Terrane in the world. The crustal thickness for this region shows a crustal thinning of 35-36 km relative to 40-42 km in Grenville Province as indicated from the receiver function analysis. Previous seismic studies (Winardhi et al., 1997; Rondenay et al., 2000) revealed that a thinning of the crust occurs north of the Grenville Front, 32-34 km, relative to 39-43 km in the Grenville Province.

The final shear velocity models show an increase in the seismic velocity with in the upper crust with average shear velocity of 3.6 km/sec (Figure 4.4). At station POP6 a low shear velocity of 2.95 km/sec and increases to 3.6 km/sec in the upper 2 km. In general those stations do not show a simple crust and the inverted models are inconsistent. Kellett et al. (1993) suggested that the absence of a large gravity anomaly over this section of the Grenville Front (Rivers et al. 1989) is evidence that the crustal blocks are in isostatic equilibrium. Thus, the thinning of the crust at this area must be accompanied by an increase in the average density of the middle to upper crust to preserve the isostatic balance. The station KAPO (Kapuskasing, Ontario) is located to the west of these stations and has enough receiver functions which will give more constrained inverted model.

The Kapuskasing uplift situate in the south central Superior Province is an oblique cross section of Archean crust exposed by a major thrusting event in the Early Proterozoic times (Boland and Ellis, 1990). The Kapuskasing struc-

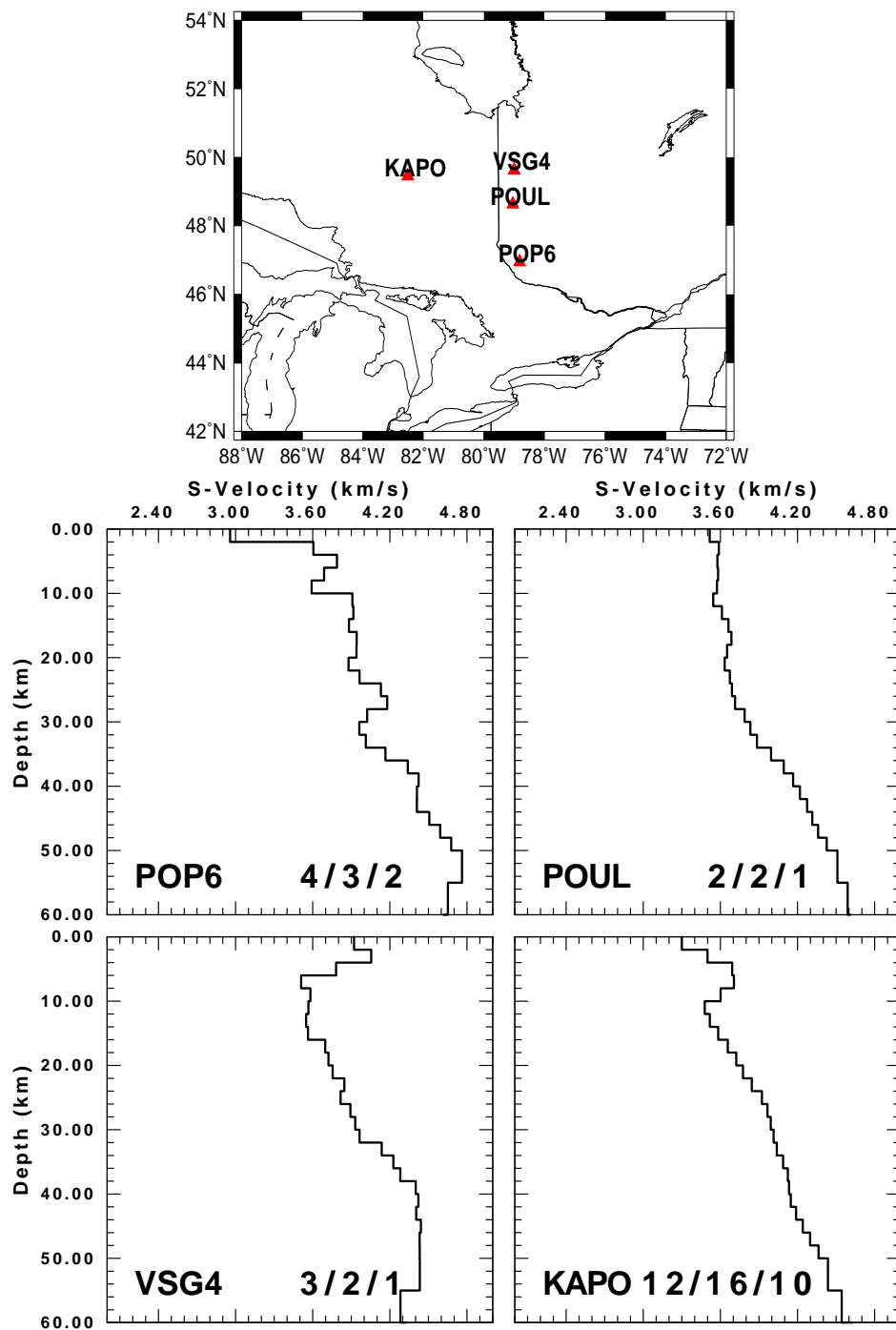


Figure 4.4: The final shear velocity model inverted from receiver function and surface-wave dispersion of Rayleigh group and phase velocity. This model show four stations from CNSN located southeastern Canada (Superior Province)

tural zone consists of high-grade metamorphic rocks that extends for about 500 km across the Superior Province and marked a pronounced Bouguer gravity high and distinctive aeromagnetic (Fountain et al., 1990) features. The structure of this region has included thinning of granitic upper crustal layer, mid-to Late Proterozoic rifting, a suture between the eastern and western Superior Province, textural transcurrent faulting, and an east-verging thrust exposing an oblique crustal cross section (Percival and West, 1993).

The inverted model shows a rapid shear velocity increase from 3.3 km/sec to 3.7 km/sec for the first 4 km. The model, also, shows a low velocity layer from 8 to 18 km depth. The middle crust has a gradational velocity from 3.7 to 3.9 km/sec for the depths from 18-24 km. The lower crust extends from 24 to 34 km with shear velocity of 3.9-4.1 km/sec. Boland and Ellis (1990) used the data from the 1984 seismic refraction experiment, which crossed Kapuskasing uplift and Abitibi (east-west line). The line passes through the stations VSG4 and POUL to the east and the station KAPO to the west. They suggested that the presence of a low velocity and low density layer of tonalites under the surface greenstones has been established and can account for the low-velocity zones imaged along the Abitibi profile (Boland and Ellis, 1990).

4.4.2 Canadian High Arctic region

The Canadian High Arctic is complex, with episodes of geosynclinal and orogenic development shaping the lithospheric structure since the Late Proterozoic (Darbyshire, 2003). The northern Canadian Shield consists of Archean

and Proterozoic structure, consisting of a set of Archean provinces bounded by younger magmatic arcs, suture zone and fold belts (Hoffman, 1989). Two stations sampled the crustal structure in this region, RES and FRB (Figure 4.5). The middle crust at FRB is characterized by gradational velocity increasing from 3.6 km/sec at 20 km depth to 3.75 km/sec at 26 km depth. The lower crust has a shear velocity of 4.0 km/sec and extends from 26 to 42 km depth. The crust-mantle transition zone is sharp where the velocity increases from 4.0 to 4.4 km/sec for the depth from 42 to 44 km. The sharp transition zone is clearly present from both the receiver function and the inverted model.

Inverted model revealed from the station RES shows a gradual transition zone with a velocity increase from 4 to 4.55 km/sec for depths from 32 to 46 km. The velocity model has a surface velocity of 2.65 km/sec which increases rapidly to 3.5 km/sec at depth 6 km. A high velocity layer is seen in the upper crust from 12 to 18 km depth with an average shear velocity of 3.85 km/sec. A gradational increase in the shear velocity in the lower crust layer starts at depth of 20 km and deepens to 32 km with highest velocity of 4.6 km/sec. This model suggests a low velocity zone for the upper mantle for depths 50 to 56 km and shear velocity of 4.4 km/sec.

4.4.3 Southwestern Canada

The western part of the Canadian Shield is composed of Archean and Proterozoic crustal and is largely buried beneath Phanerozoic sedimentary rocks of the Western Canada Sedimentary Basin (Eaton, 1996). The Archean and Pro-

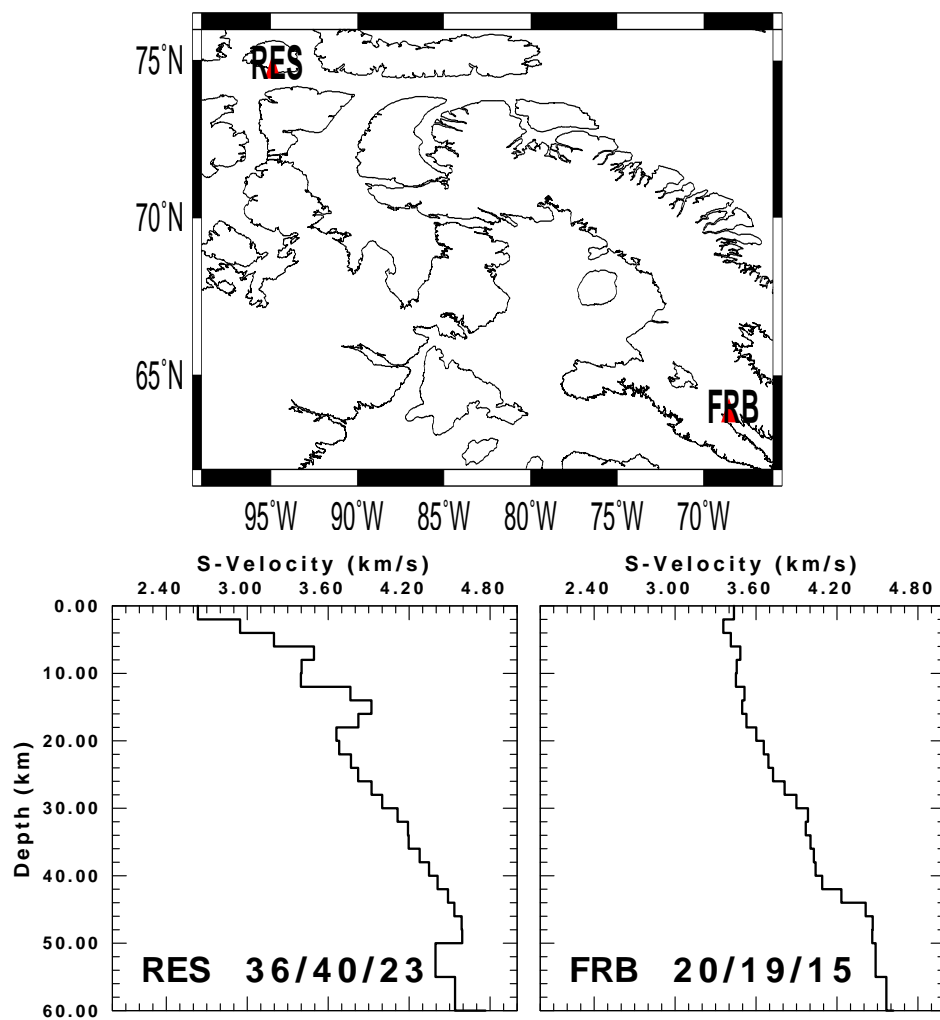


Figure 4.5: The final shear velocity model inverted from receiver function and surface-wave dispersion of Rayleigh group and phase velocity. This model show two stations from CNSN on the Arctic Region

terozoic crustal blocks record episodic tectonothermal pulses with widespread orogenic activity in the period 1.8-2.0 Ga (Hoffman, 1988). Stations of the CNSN in western Canada include EDM (Edmonton, Alberta) and WALA (Walterton Lake, Alberta) within the western Canadian Sedimentary Basin, FFC (Flin Flon, Canada) and ULM (Lac Du Bonnet, Manitoba).

Two stations sampled the Central Canada Shield, FFC and ULM. The structure of the crust and upper mantle beneath these stations have been studied earlier by a seismic line crossed the Superior-Churchill geological boundary (Mereu and Hunter, 1969). They estimated the Moho under Lake Superior was at a depth of approximately 30 km and then rapidly dropped to a depth greater than 50 km under the eastern half. The surface rocks underlying these two stations belong to the Canadian Shield and are Precambrian in age. The crustal thickness beneath station ULM (32 km) is in a good agreement with the previous result (Figure 4.6). The inverted model shows that the surface shear velocity is about 3.2 km/sec for the first 2 km. The velocity increased rapidly to 3.6 km/sec at a depth of 4 km with a constant velocity for the next 6 km. The depths between 10 and 16 km show a high velocity layer in the middle crust of 3.7 km/sec. The lower crust extends from 16 to 32 km with an average velocity of 3.8 km/sec.

As we move to the north approaching the station FFC the crustal thickness increases to about 40 km with three distinct layers. The surface layer has a shear velocity of 3.2 km/sec. The crust mantle transition zone under this station is gradual from 3.8 at 32 km depth to 4.5 km/sec at 44 km.

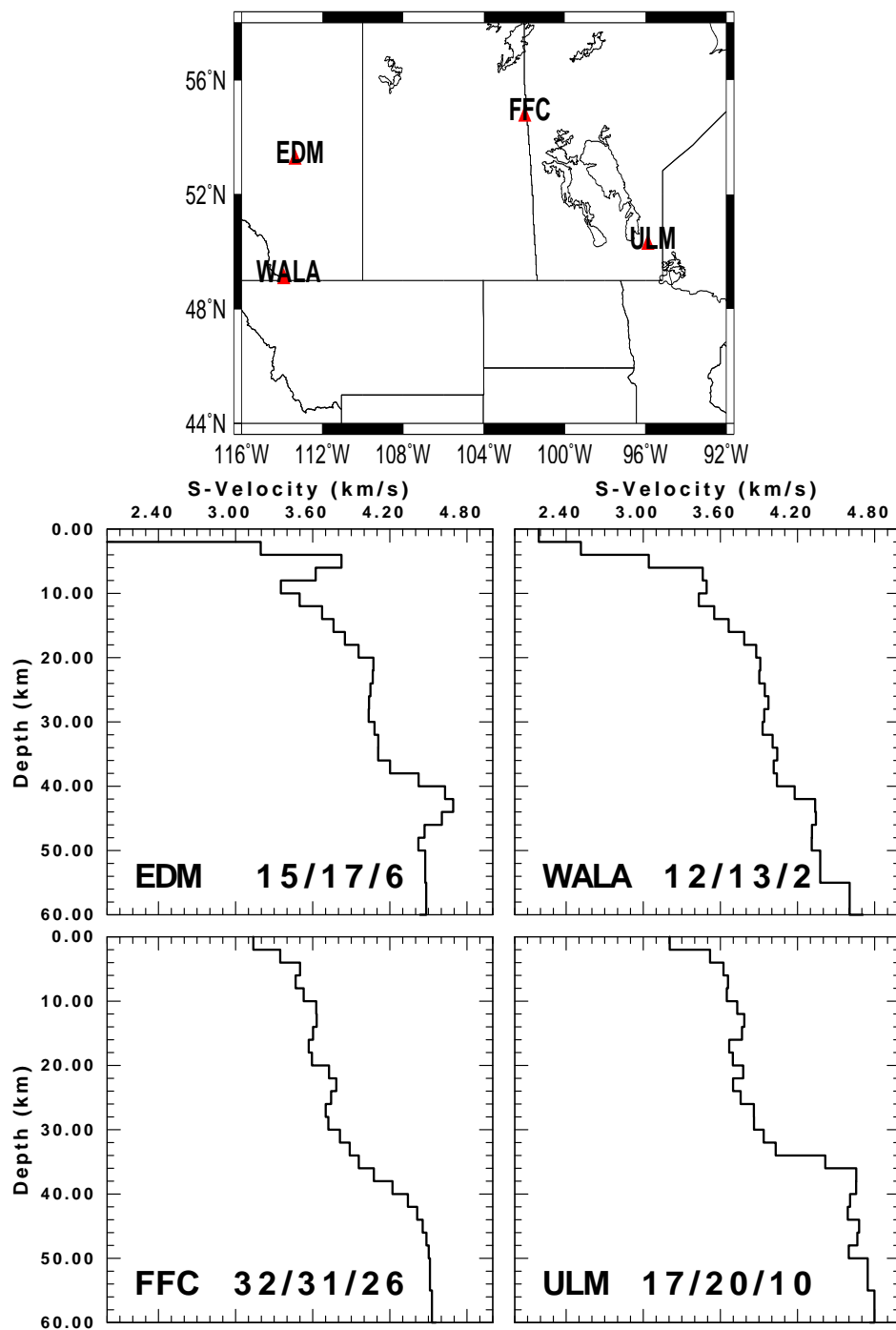


Figure 4.6: The final shear velocity model inverted from receiver function and surface-wave dispersion of Rayleigh group and phase velocity. This model compares four stations from the CNSN located in south-southwestern Canada.

The inverted shear velocity model at the station EDM (Figure 4.6), samples an area with low velocity at the surface, which is indicated a thick sediment layer. The velocity increases rapidly to about 3.8 km/sec at depth of 4 km and decreases to 3.3 km/sec at depth of 10 km. Ross et al. (1995) suggested the presence of mid-crustal reflections which may agree with inverted model for this station. The Moho discontinuity beneath the station is sharp with the maximum shear velocity of 4.7 km/sec at 40 km depth. The model, also, shows a low velocity zone at the depth of 10 km which have a composition similar to serpentinized peridotites that occur in ophiolites (Eaton et al. 1996).

Station WALA, located southwest of the station EDM, and has a similar velocity model except it does not have the high shear velocity in the upper crust. The surface shear velocity is about 2.2 km/sec which represents the thick sediment layer. The velocity increases rapidly to about 3.45 km/sec at 6 km depth. The upper crust has a gradational velocity from 3.45 to 3.85 km/sec for depths between 12 to 18 km. The middle crust has an average shear velocity of 3.9 km/sec and a total thickness of about 14 km. The lower crust extends from 32 to 40 km depth. The crust mantle transition is sharp with a total thickness of 2 km and the mantle shear velocity of 4.35 km/sec. Station FA28 is located almost between stations EDM and WALA. The inverted model for this station supports the features from the other two stations. For instance, the surface layer shows the same feature presented on both stations, a surface shear velocity is about 2.1 km/sec. Also, this model has a rapid velocity increase to about 3.75 km/sec at a depth of 6 km similar to station EDM. The shear

velocity decreases to about 3.4 km/sec at depths from 6 to 14 km.

4.4.4 Northwestern Canada

The Slave geological province, a relatively small Archean granite-greenstone in northwestern Canada, contains the oldest rocks on the Earth about 4.0 Ga (Fernandez and Clowes, 2003). Archean cratons such as the Slave normally include a deep, high seismic velocity root, believed to be composed of depleted mantle (Hoffman, 1990). The Slave province is spanned by all the POLARIS stations used on this study. Most of the volcanic and sedimentary rocks formed between 2.7 and 2.65 Ga (Kusky 1989). The refraction/wide-angle reflection survey (LITHOPROBE) interpreted by Fernandez and Clowes (2003) found the crustal velocity to range from 5.4-5.6 km/sec in the uppermost layer to 6.5 km/sec above the lower crust at about 20 km depth and to 6.9 km/sec above the Moho at about 35 km depth.

The POLARIS stations sampling the Slave province can be divided to four groups according to their location and the distance between them. First, a southwest group includes NODN, CAMN, SNPN, and IHLN (Figure 4.7). Of these stations NODN has the most receiver functions. The average surface shear velocity for this region is about 3.6 km/sec. All stations show the presence of a low velocity layer around 10 km depth. Two stations (CAMN and SNPN) have a sharp crust mantle transition of about 38 km depth, whereas, the other two stations (CAMN and IHLN) show a gradual transition at about 35 km depth. The central south group includes KNDN, MGTN, BOXN, and MLON

(Figure 4.8). All stations have just few receiver function. The velocity model for these stations show three distinct crustal zones and sharp boundaries between the upper and the middle crust. The average upper crust shear velocity is about 3.55 km/sec, the middle crustal velocity is 3.7 km/sec and the lower shear velocity 4.0 km/sec. Station MLON indicates the present of a slight low velocity layer at the base of the lower crust. Fernandez and Clowes (2003) suggested that the lower velocity layer is enigmatic and could be the result of lower grade metamorphic rocks.

The central group includes MCKN, LDGN, EKTN, and GLWN (Figure 4.9). The surface shear velocity 3.5 km/sec for the upper 4 km except at EKTN. The stations LDGN and EKTN have good receiver functions and their velocity models are characterized by two crustal layers with average velocity of 3.6 and 3.75 km/sec. The crust-mantle transition boundary is gradual with a total crustal thickness of 34-36 km. The highest shear velocity is about 4.45 km/sec at 40 km depth.

In the north of the Province are the stations ACKN, COWN, and YMBN (Figure 4.10). Two crustal layers can be identified with shear velocity of 3.6 km/sec for the upper crust and 3.9 km/sec for the lower crust. The crust-mantle transition boundary at these stations is sharp as indicated from the inverted model and the computed receiver functions.

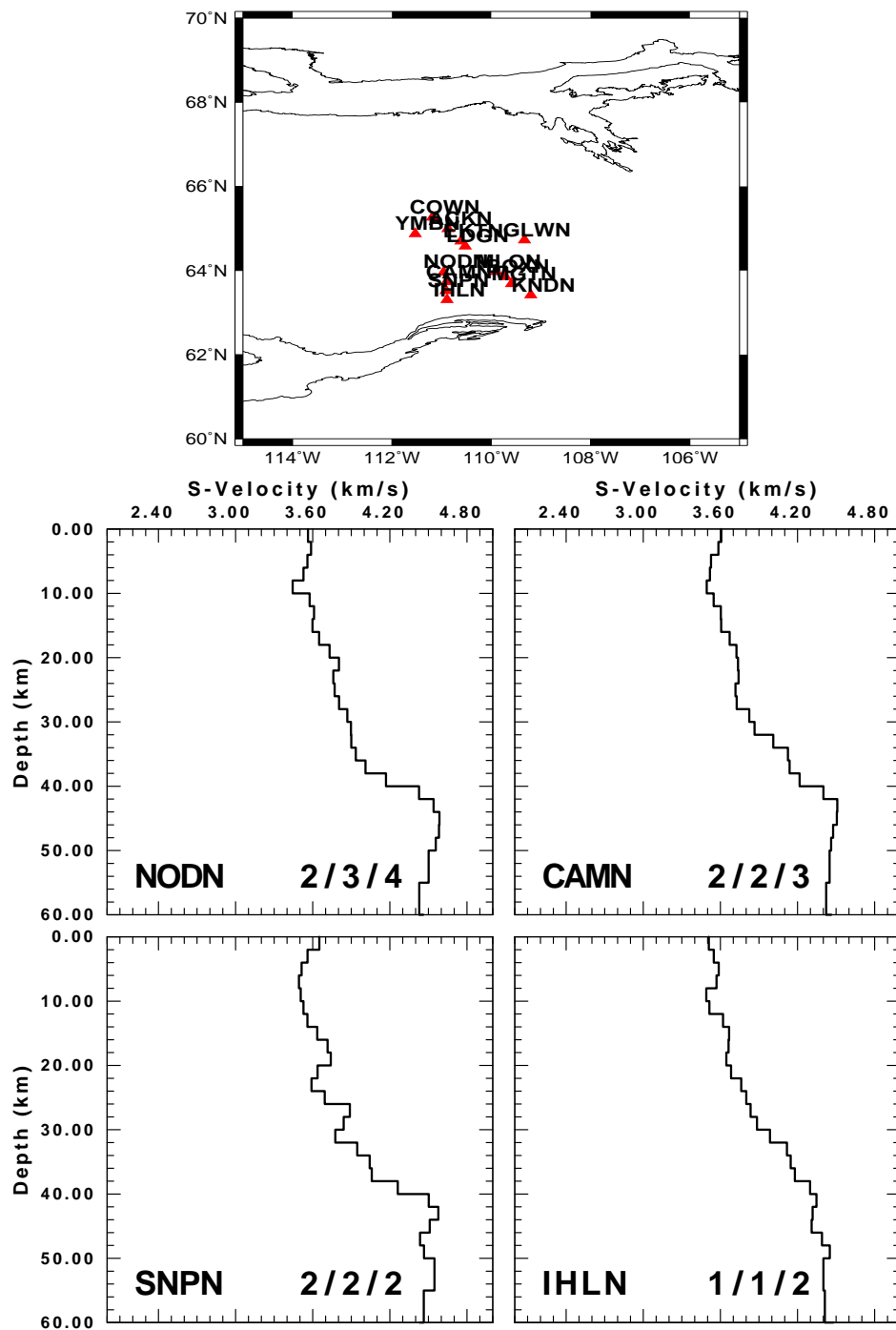


Figure 4.7: The final shear velocity model inverted from receiver function and surface-wave dispersion of Rayleigh group and phase velocity. This model compares four stations from POLARIS Network

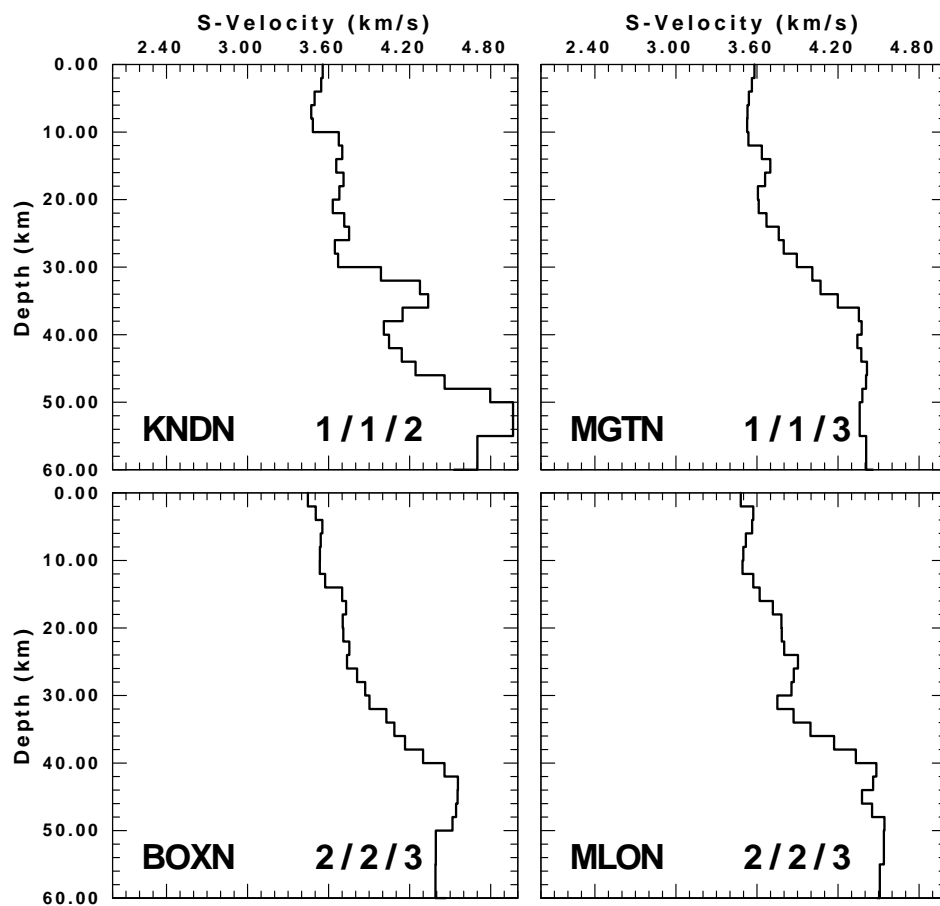


Figure 4.8: The final shear velocity model inverted from receiver function and surface-wave dispersion of Rayleigh group and phase velocity. This model compares four stations from POLARIS Network

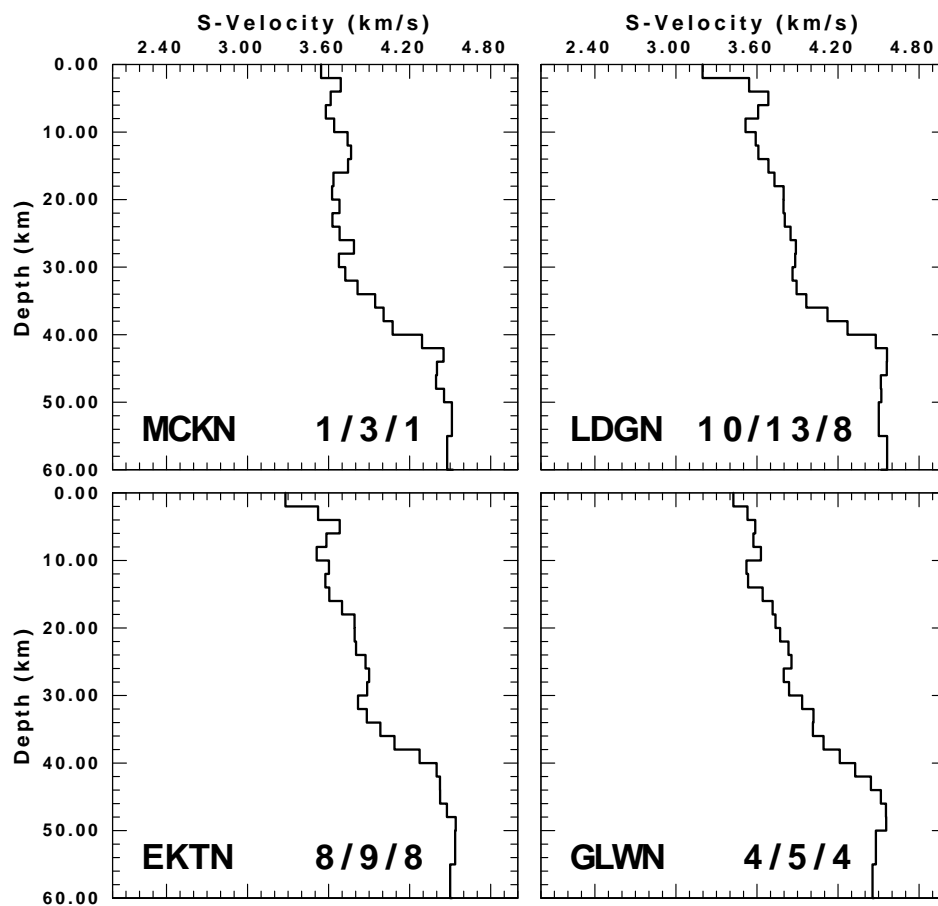


Figure 4.9: The final shear velocity model inverted from receiver function and surface-wave dispersion of Rayleigh group and phase velocity. This model compares four stations from POLARIS

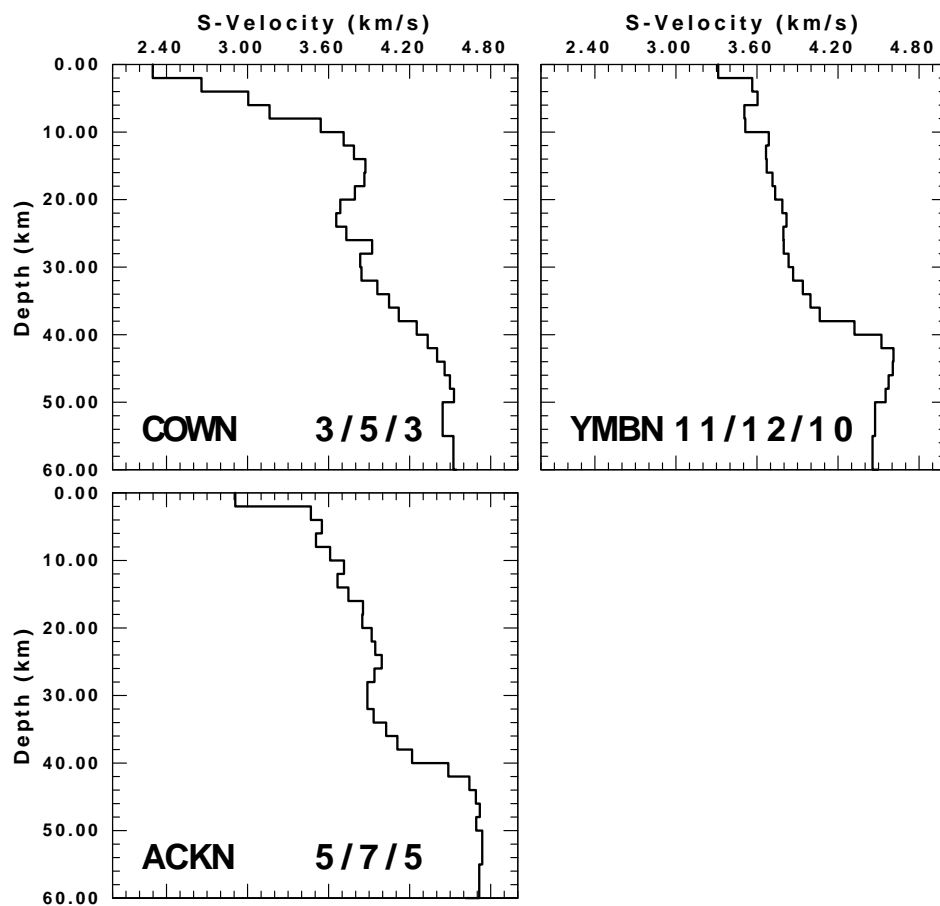


Figure 4.10: The final shear velocity model inverted from receiver function and surface-wave dispersion of Rayleigh group and phase velocity. This model compares three stations from POLARIS

4.5 Lithospheric Structure of the U. S. Sites

4.5.1 Coastal Plain

The Atlantic Coastal Plain Province is comprised of Upper Jurassic through Cenozoic sedimentary rocks which overlie much older Precambrian through lower Paleozoic basement rocks. The eastern United States results from a complex history involving successive accretions, orogenies, and continent breakup (Barruol et al., 1997). The coastal plain structure is sampled by the stations LBNH, HRV, GWDE, NHSC, DWPF, and HKT from the United State National Seismic System with MM01, FA01, and FA02 as a temporary stations. The inverted shear velocity model at LBNH (Figure 4.11), indicates a surface velocity of 3.25 km/sec and increases rapidly to 3.7 at 4 km depth. The upper crust beneath this station shows a low velocity zone. The low velocity layer has a thickness of about 6 km. The upper crust extends to 14 km depth with an average velocity of 3.7 km/sec. The crustal structure beneath this station is simple and consists of two layers (upper and lower) with the average velocity for the lower layer of about 3.85 km/sec and a total thickness 18 km extends from 16-34 km depth. The gradational crust mantle transition zone suggests a Moho at 36 km depth, with the maximum velocity of 4.5 km/sec is at 40 km depth.

The crustal structure beneath stations HRV, WES, and MM01 (Southern Appalachians) presents information on this area which has Paleozoic granitic intrusions and gneisses. Stations HRV and MM01 will be discussed because

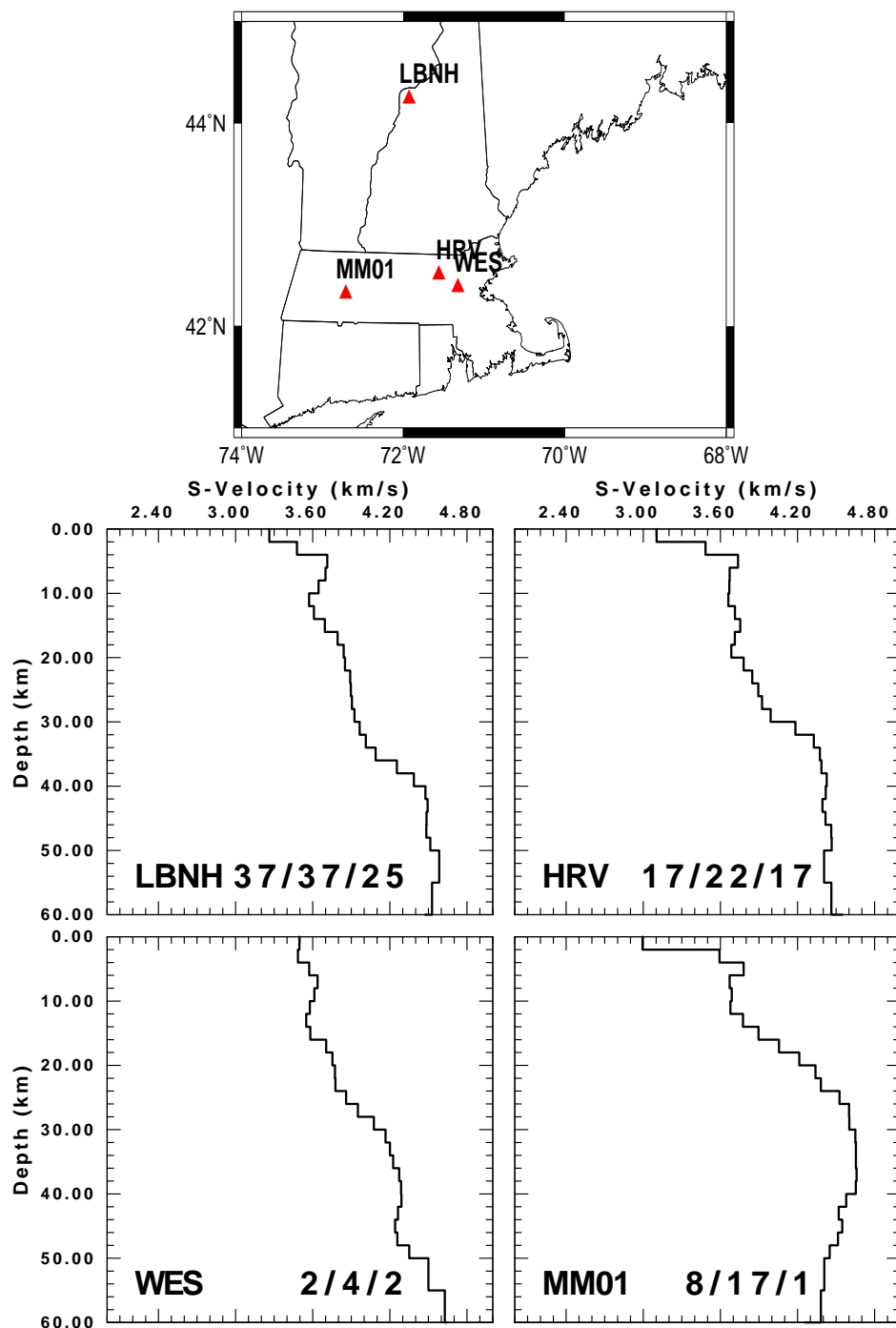


Figure 4.11: The final shear velocity model inverted from receiver function and surface-wave dispersion of Rayleigh group and phase velocity. This model compares stations located On the Coastal Plain East of the U.S.

they are based on more receiver functions (Figure 4.11). The model inverted at HRV and MM01 shows the a similar response with a surface velocity of 3.0 km/sec. The structure beneath these stations is simple and consists of upper and lower crustal layer. The upper crust extends to 16 km depth with a average velocity of 3.6-3.65 km/sec. The lower crust at these stations shows a gradational shear velocity from the top to the bottom of this layer with an average velocity of 3.7-3.8 km/sec. The models suggest a gradient crust mantle transition zone at depth of 28-30 km.

The southeastern Coastal Plain is covered by NHSC, DWPF, FA01 and FA02 (Figure 4.12). The joint inversion technique is not applicable at NHSC because of receiver function reverberations due to a thick shallow sedimentary layer beneath it. The receiver function computed at this station shows the ringing effect which resulted on the unstable shear velocity model. Kean and Long (1980) suggested a thick sedimentary layer of about 2.5 km which may give an interpretation of the ringing phenomena on the receiver function at NHSC. Kean and Long inferred that the crust along the coastal plain in the vicinity of South Carolina thickens to about 35 km. Regional seismic reflection profile across the Georgia and South Carolina Coastal Plain provide a detailed view into the internal structure of the buried Triassic-Jurassic South Georgia basin (McBride et al., 1989), and estimate the thickness of the basin of about 6 km. Since we do not have enough receiver functions at DWPF, more attention is focused on FA01 and FA02. The crustal thickness at this region is about 42 km as delineated by the Ps conversion phase. The inverted models for these

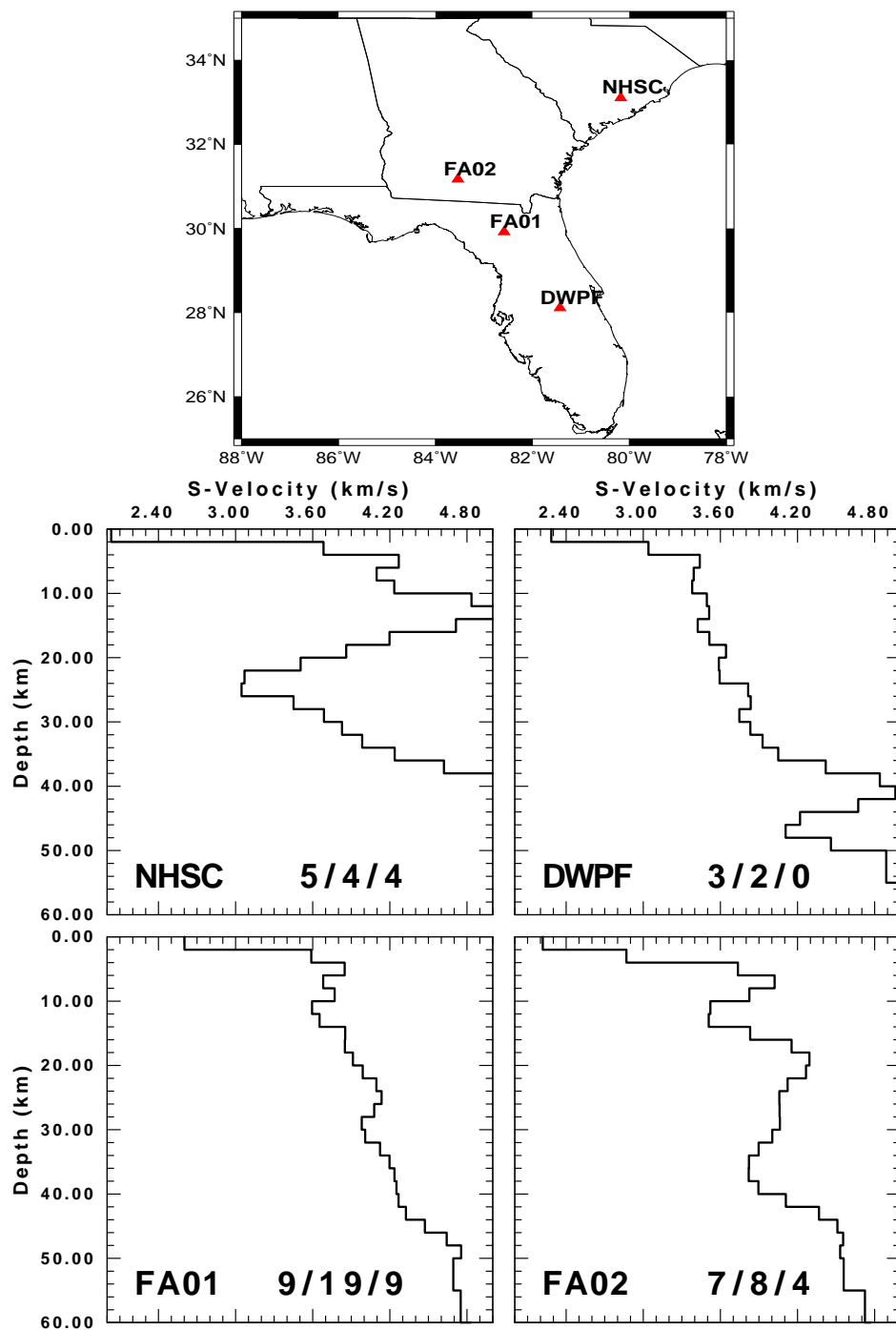


Figure 4.12: The final shear velocity model inverted from receiver function and surface-wave dispersion of Rayleigh group and phase velocity. This model compares stations located on southern coastal plain of the U.S.

stations indicate an average surface velocity of about 2.4 km/sec.

4.5.2 The Appalachian Orogen

The Appalachian Province consists of the eroded core of a Paleozoic mountain chain that extends from Newfoundland to the southeastern United States. The Appalachians may be divided into three regions (the northern and the central-southern Appalachians) in which metamorphic grade and implied depth exhumed to the surface increases from north to south, whereas the age of peak metamorphism and granite magmatism decreases (Michael Brown website). The Precambrian Grenville Province, exposed in the Adirondacks, extends southward in the subsurface west of the Appalachian mountain belt (Owens et al., 1987). The Adirondack Mountains (high-grade metasediments extensively intruded by granites and anorthosite) consist of a core of Precambrian Grenville rocks surrounded by gently dipping Paleozoic formation (Taylor, 1989). Taylor (1980) reported that in New York State, the Grenville crust appears to be uniform with thickness of about 36 km and velocity ranging from 6.4 to 6.6 km/sec.

P-wave ray-tracing modeling (Hughes and Luetgert, 1991) for interpreting refraction studies has been applied to data from the Appalachian Province. The resulting model shows that crustal thickness ranges from 36 km in east to 40 km in the west along the ONYNEX refraction seismic profile which traverses the southern Grenville province and the adjacent western New England Appalachian Orogen. They suggested that the Appalachian province exhibit an

increase in V_p/V_s values with depth, an observation that is consistent with the presence of quartz-bearing rocks in the upper crust and an expected decrease of silica content with depth. They conclude that the Appalachian crust shows a typical continental crust V_p/V_s ratio (1.70-1.77) at all depths with the lower crustal velocity of 6.7-7.0 km/sec and V_p/V_s ratio (1.77) indicative of an intermediate-to-basic composition and upper amphibolite to lower granulite metamorphic grades.

The northern Appalachians are sampled by the following stations NCB, MM02-MM04, BINY, and YSNY (Figures 4.13 and 4.14). Station NCB located in northern New York shows a crustal thickness of about 38 km. The inverted shear velocity model at NCB shows the same features that proposed by Owens et al (1987), two high velocity layers can be imaged beneath this station. From the surface, the velocity increases from 3.2 km/sec to 3.8 km/sec at depth of 4 km. A 4 km high velocity layer is present in the upper crust with a rapid decrease on the velocity to about 3.5 km/sec at 10 km depth. The middle crust has an average shear velocity of 3.6 km/sec and extended from 10 to 22 km depth. The middle crust is underlain by a broad high velocity layer with rapid increases in the velocity to about 4.35 km/sec, overlying a low velocity layer and a thick crust mantle transition zone.

The crust mantle transition zone extends from about 38 km (shear velocity is 4.1 km/sec) to 50 km (upper mantle shear velocity is 4.5 km/sec) depth. This station is located to the south - southeast of the station RSNY (modeled by Owens et al., 1987). The inverted model at NCB is similar to the south-

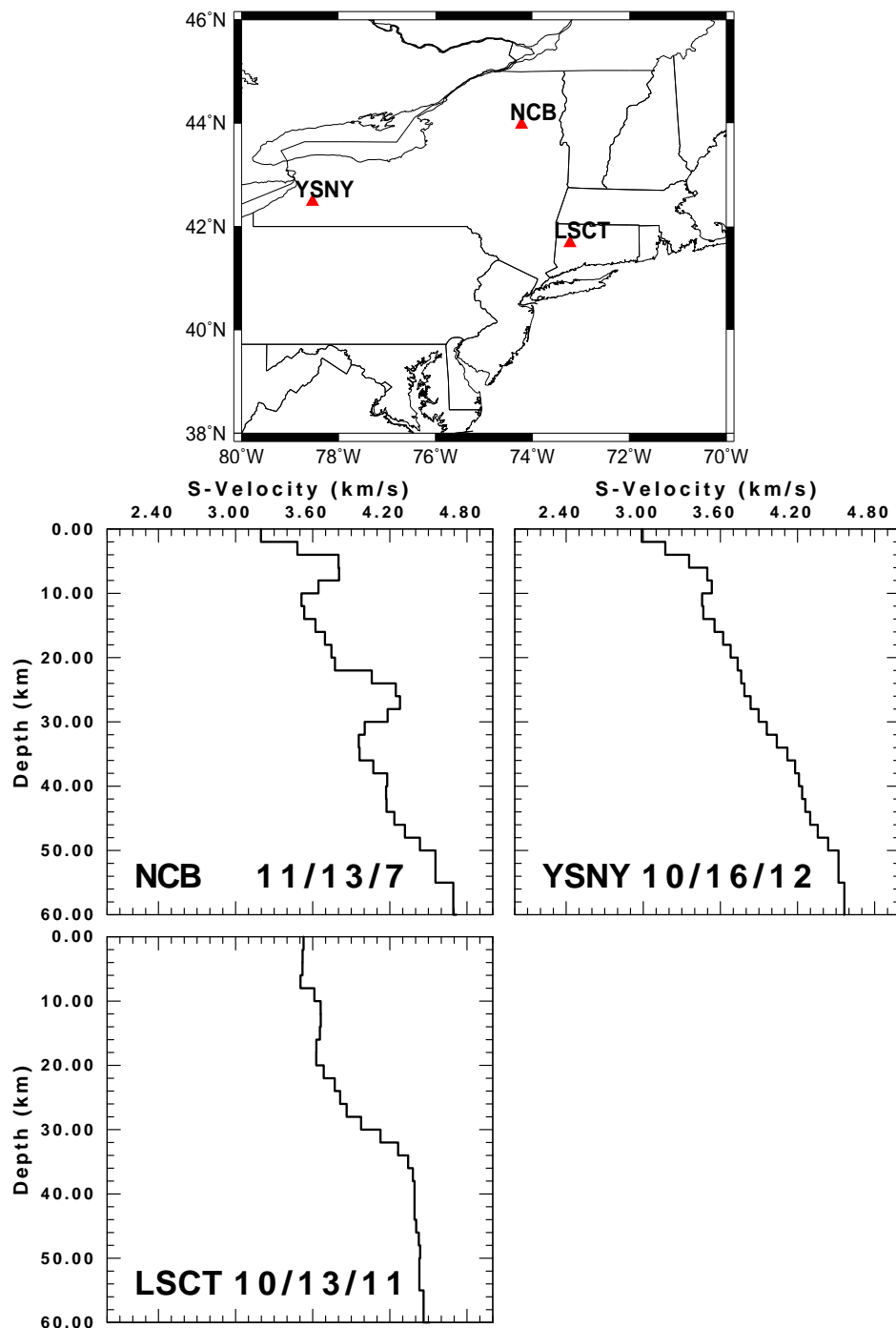


Figure 4.13: The final shear velocity model inverted from receiver function and surface-wave dispersion of Rayleigh group and phase velocity. This model compares stations located on the northern Appalachian

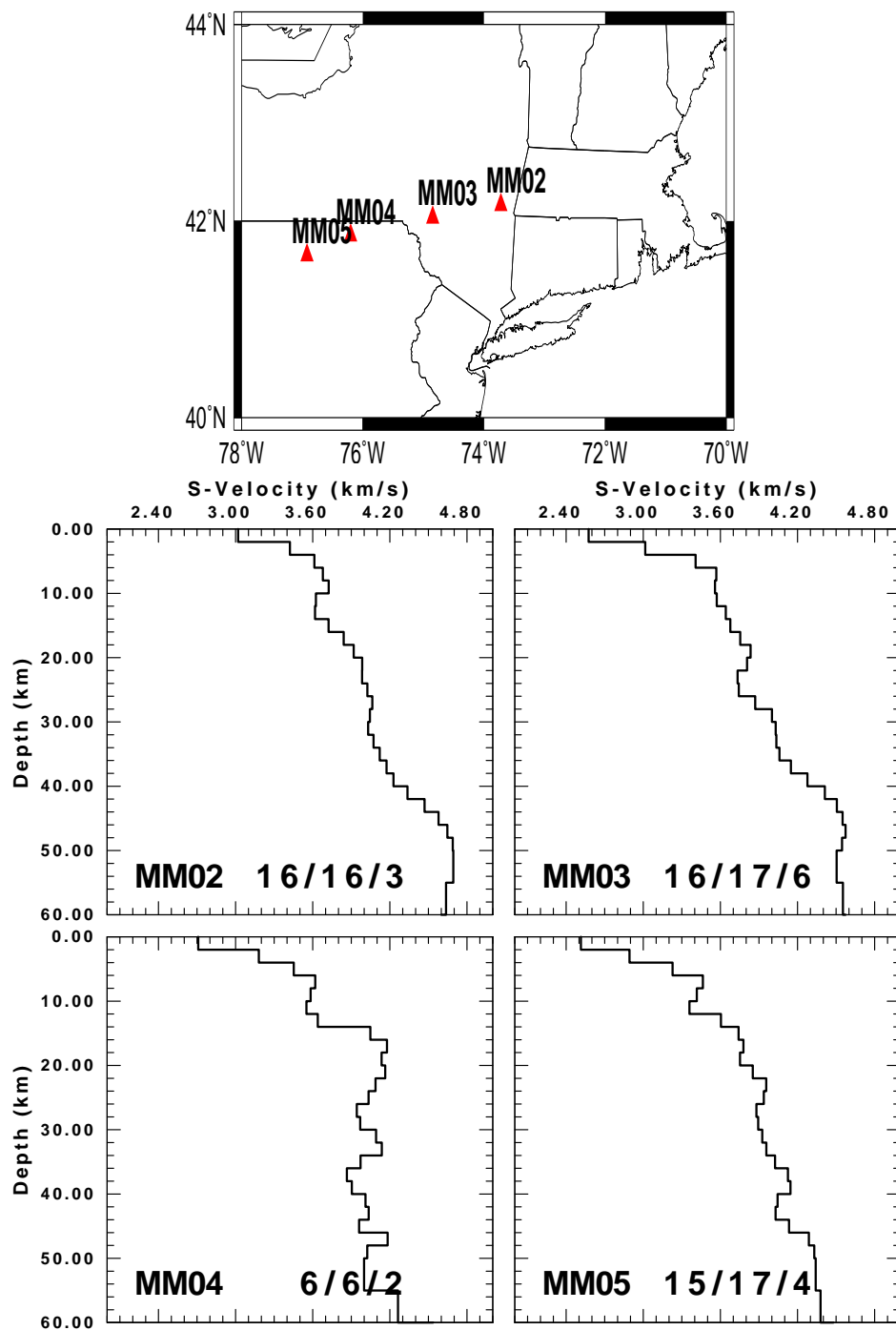


Figure 4.14: The final shear velocity model inverted from receiver function and surface-wave dispersion of Rayleigh group and phase velocity. This model compares stations located on the northern Appalachian

southeast inversion result by Owens et al. (1987) and in a good agreement with the seismic reflection profiling by COCORP (lines 7 and 11) which indicated a highly reflective zone at 18 to 26 km depth (Klemperer et al., 1985). The transition zone at this site differs from previous seismic studies which indicates that a sharp crust mantle transition should exist at about 35 km depth because these studies used only very small number of layer (two- or three-layer models).

To the south are located the stations MM02, MM03, and LSCT. According to Taylor and Toksöz (1979), the northern Appalachians can be divided into three units (western, central, eastern-belts). The western unit is mainly underlain by rocks of the Precambrian Grenville Province which are exposed in the Adirondacks. The central orogeny belt consists of the Connecticut Valley Synclinorium. The eastern belt consists of the Bronson Hill Anticlinorium which consists of a chain of elliptical gneisses domes. The central belt (of the Connecticut Valley Synclinorium), that characterizes by Amphibolite metamorphism facies is spanned by the station LSCT which (Zhu and Ebel, 1994). A sharp discontinuity can be seen from the inverted model with an average velocity anomaly ($\Delta V_s=0.2$ km/sec). The middle crust extends from 8 to 20 km depth with a constant velocity of 3.65 km/sec. Gradational in shear velocity is seen in the lower crust from 3.7 to 4.0 km/sec for depths between 20 and 28 km. The crust mantle transition zone is gradual with highest velocity of 4.45 km/sec at 36 km depth. The Moho discontinuity estimated from the Ps conversion phase is about 30 km depth which is consistent with average crustal thickness for the

eastern Appalachians.

Stations MM02 and MM03 sample the Adirondack massif in New York which is a southerly extension of the Grenville basement exposed in Quebec and is characterized by a complex assemblage of the lower granulite with high seismic velocity (Hughes and Luetgert, 1991 and Zhu and Ebel, 1994). The surface shear velocities at MM02 and MM03 are 2.58 and 3.2 km/sec respectively. Both models show a rapid increase in the velocity to 3.6 for the upper 4-6 km. At station MM02 a high velocity layer is seen at depth between 6 and 10 km with highest velocity of 3.72 km/sec. On the other hand, the inverted model at MM03 does show a high velocity layer, but for depth from 18 to 22 km shows a slight low velocity region. Station MM03 is located south of NCB and shows same feature of high velocity layer at depth from 18 to 22 km. The Moho depth estimated at this station at 38-40 km depth. The crust mantle transition for both stations MM02 and MM03 is gradual.

Stations MM04, BINY and YSNY are located along the Allegheny Plateau in northern Pennsylvania and southern New York. The inverted shear velocity beneath BINY and MM04 have the same surface velocity of 2.7 km/sec. The upper crust beneath BINY has a low velocity layer with velocity of 3.45 km/sec between 8 and 12 km depth. For the stations BINY and YSNY it is hard to identify the boundary between different crustal layers since the velocity gradually increases until reaching the Moho depth. The models for these stations estimate the Moho at 46 km depth. The crust mantle transition zone is gradual beneath YSNY and sharp beneath BINY.

Stations MM05-MM09 and ACSO are located in the central Appalachians (Figures 4.15 and 4.16). The earliest studies implemented in this area involve measurements of Rayleigh-wave phase velocities in the New York-Pennsylvania area over the Valley and Ridge and Adirondacks region (Oliver et al., 1961; Dorman and Ewing, 1962; Long and Mathur, 1972; Mitchell and Herrmann, 1979; Taylor, 1989). The estimated thickness at this area was 37-38 km, with an average crustal shear velocity of 3.6 km/sec and 4.7 km/sec in the uppermost mantle. The inverted models for stations MM05, MM06 and MM07 show a low surface shear velocity of about 2.3-2.5 km/sec and a rapidly increase in the upper 6 km to about 3.6 km/sec. All models show a low velocity layer at depth 10-12 km with shear velocity of 3.55 km/sec. On the other hand, all models inverted for stations MM05-MM09 show the same effect. The estimated thickness at stations MM05 and MM06 is 46 km. The crustal structure beneath MM05 and MM06 is characterized by a distinct four layers with a sharp boundary between each layers. As we travel to the west the crustal thickness increase from 48 km at MM07 to about 50 km at MM08 and MM09. A sharp crust mantle transition zone can be identified beneath MM05-MM09. Beneath the station MM07 a gradual transition is seen. The average shear velocity at this area is 3.6 km/sec for the upper 20 km, 3.9 km/sec for depths from 20-30 km, and 4 km/sec for the lower crust.

The southern Appalachians are sampled by the following stations SSPA, MCWV, BLA, CEH, MYNC, GOGA and FA03-FA07 (Figures 4.16-4.18). The crust in the Appalachian orogen can be divided to three major tectonic settings

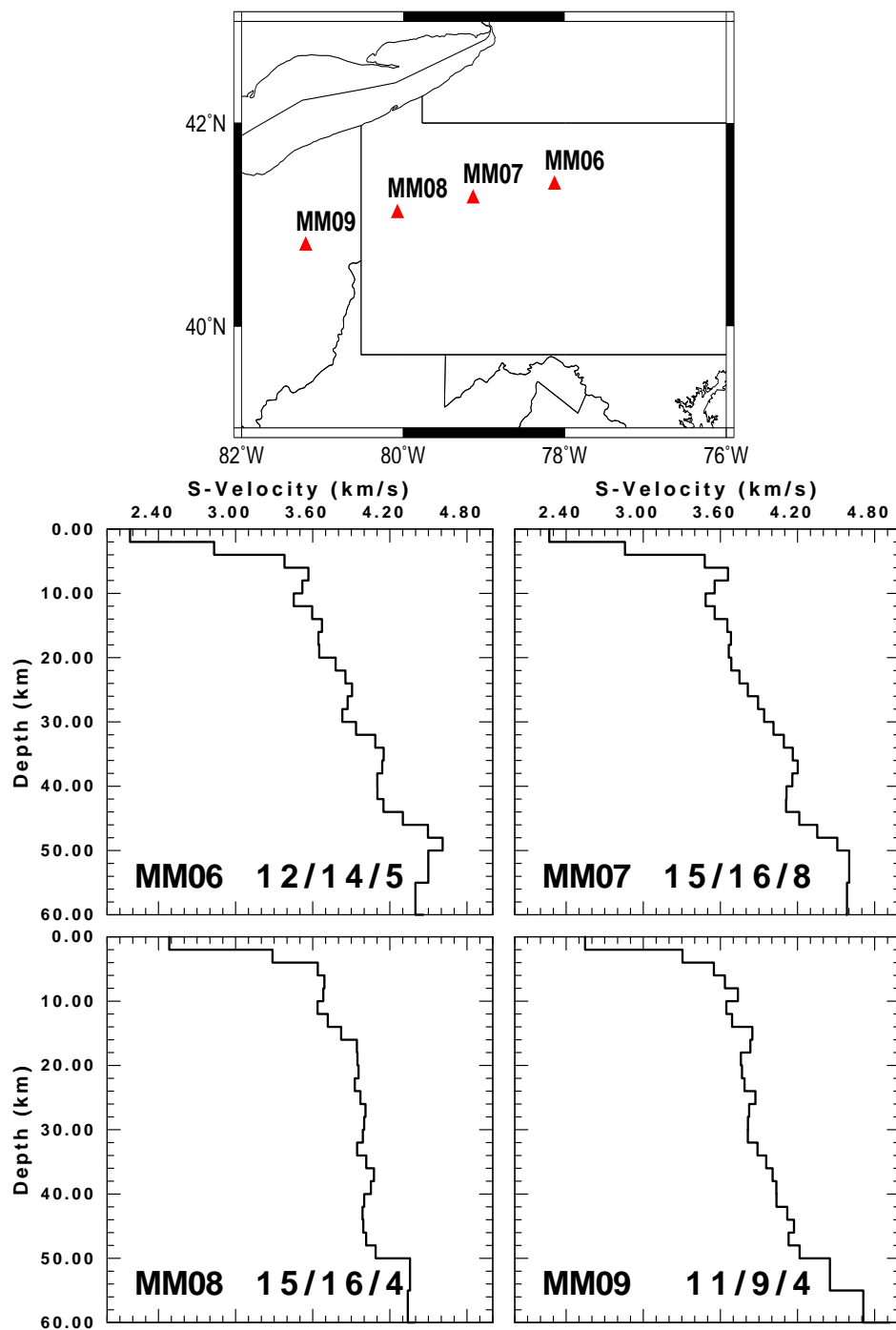


Figure 4.15: The final shear velocity model inverted from receiver function and surface-wave dispersion of Rayleigh group and phase velocity. This model compares stations located on the central Appalachian

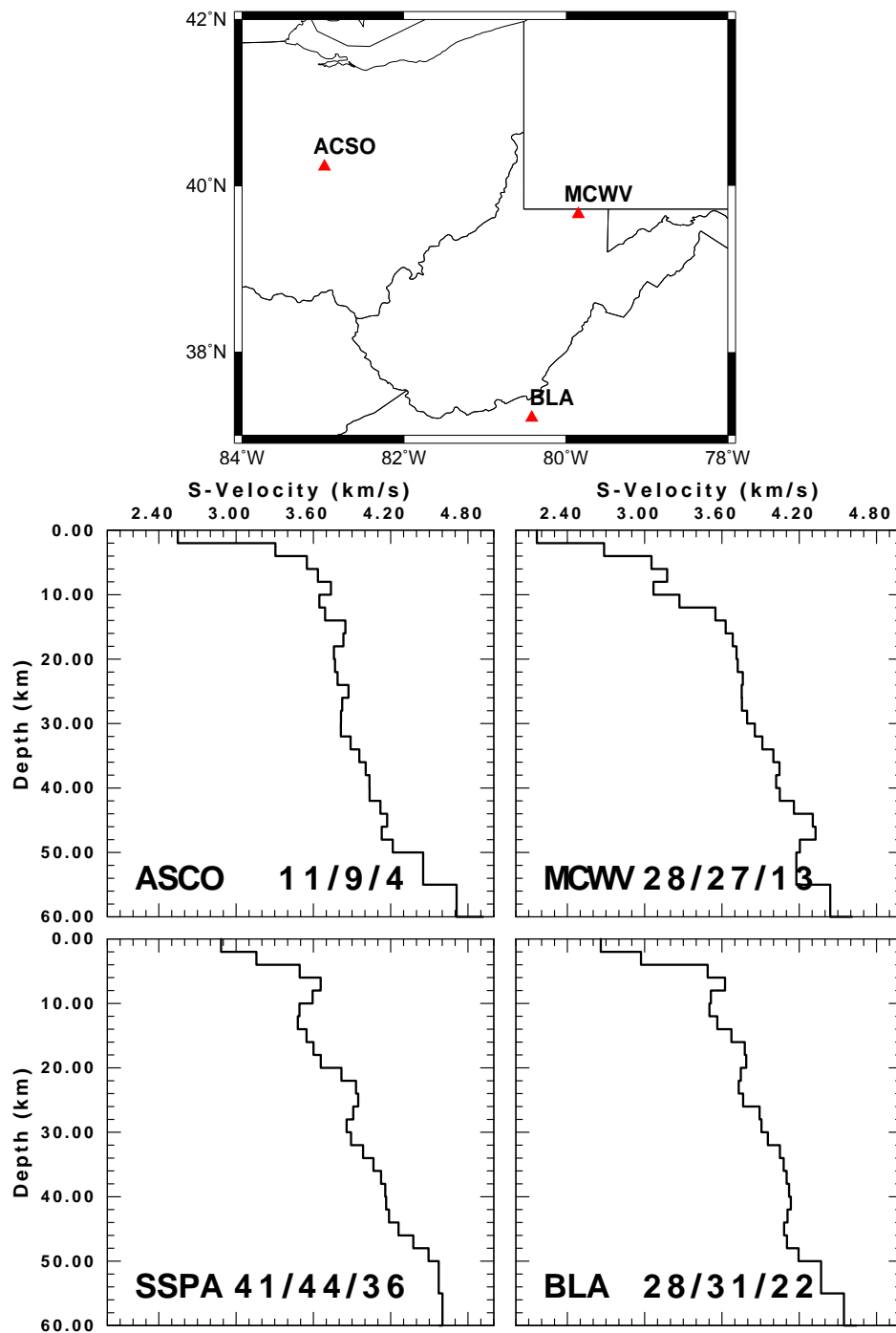


Figure 4.16: The final shear velocity model inverted from receiver function and surface-wave dispersion of Rayleigh group and phase velocity. This model compares stations located on the southern Appalachian

such as Piedmont, Valley and Ridge province, Cumberland Plateau (Costain et al., 1989). The area have been studied with different geological and geophysical techniques (Kean and Long, 1980; Manfred and Kalata, 1992; Owens et al., 1884, 1985, 1987, 1988; Prodehl et al., 1980, 1984; Taylor et al., 1984; Costain et al., 1989; Zandt and Owens, 1986; and Bollinger et al., 1980). The overall crustal thickness ranges from 33 to 55 km. The thinner crust is estimated under the Piedmont, whereas the thicker crust is observed in the Appalachian Mountains and the Cumberland Plateau province.

The Piedmont province (eastern Appalachian) consists of metamorphosed eugeoclinal rocks of lower and middle Paleozoic age which are associated with Paleozoic plutons of variable composition (Taylor, 1989). The station CEH is located to the east of the Piedmont. The crustal thickness at this station is about 34 km with surface velocity of 3.35 km/sec. According to Bollinger and Carts (1981), the average crustal velocity range from 3.47 to 3.76 km/sec. Based on the inverted shear velocity model, a crustal layer with velocity lower than 3.45 km/sec is observed near the surface. This model suggested a tow layer crust with the average velocity of 3.5 km/sec for the upper crust and 3.75 for the lower crust. The Bouguer gravity has been studied in the southern Appalachians and indicate a gravity anomaly in the Piedmont (Cook, 1984). The Piedmont gravity gradient has been interpreted as a transition from thicker crust (Appalachian mountain) to thinner crust (Piedmont), a southeast-dipping suture zone extending through the crust and separating the granitic crust to the west from the mafic crust to the east (Hatcher and Zietz, 1980), and a change

in crustal density associated with buried low-density silica Grenville crust and mafic crust of accreted microplates to the southeast of the Charlotte belt and Carolina slate belt.

The Valley and Blue Ridge province is spanned by the following stations BLA, GOGA, MYNC, FA04, and FA05. The Blue Ridge Thrust Belt Province underlies parts of eight States from central Alabama to southern Pennsylvania. Along its western margin, the Blue Ridge is thrust over the folded and faulted margin of the Appalachian basin, so that a broad segment of Paleozoic strata extends eastward for tens of miles, buried beneath these sub-horizontal crystalline thrust sheets (Harris and others, 1981). The province is bounded on the north and west by the Paleozoic strata of the Appalachian Basin Province and on the south by Cretaceous and younger sedimentary rocks of the Gulf Coastal Plain. It is bounded on the east by metamorphic and sedimentary rocks of the Piedmont Province. The deeply eroded Valley and Ridge is folded and has a sedimentary veneer approximately 4-8 km thick, separated from lower crystalline basement by horizontal thrust faults (Cook et al., 1979; Hatcher, 1987).

The inverted shear velocity model at the station BLA suggests a surface velocity of 2.65 km/sec. The model also shows a low velocity layer with shear velocity of 3.5 km/sec for depths from 8 to 13 km depth. The low velocity layer can be identified at all stations spanned this area for depths 6-16 km. Stations GOGA and MYNC are located close to each other and show a high velocity at the surface of about 3.65 and 4.0 km/sec respectively. The models beneath these stations suggest a four layer crust with high velocity contrast between

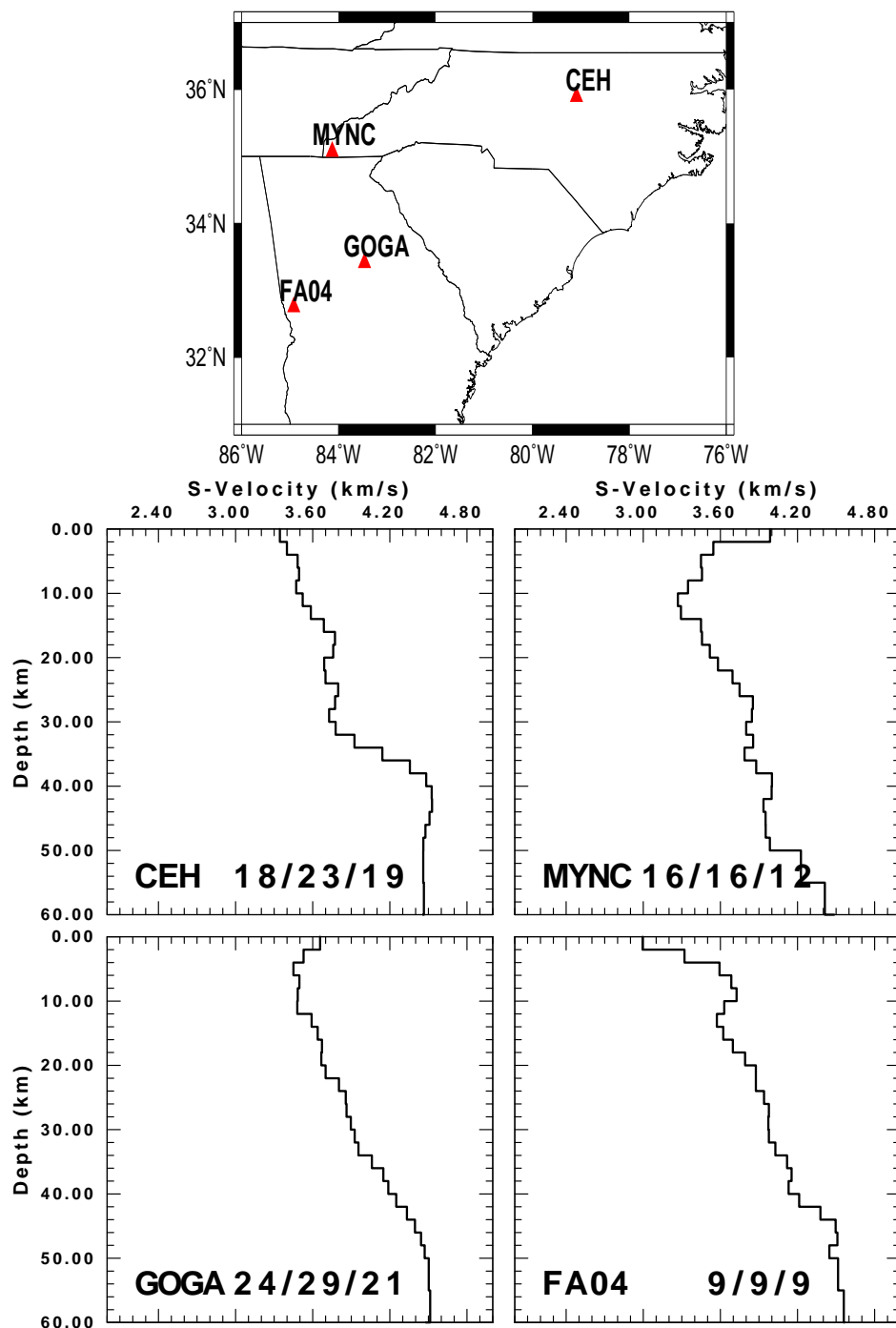


Figure 4.17: The final shear velocity model inverted from receiver function and surface-wave dispersion of Rayleigh group and phase velocity. This model compares stations located on the southern Appalachian

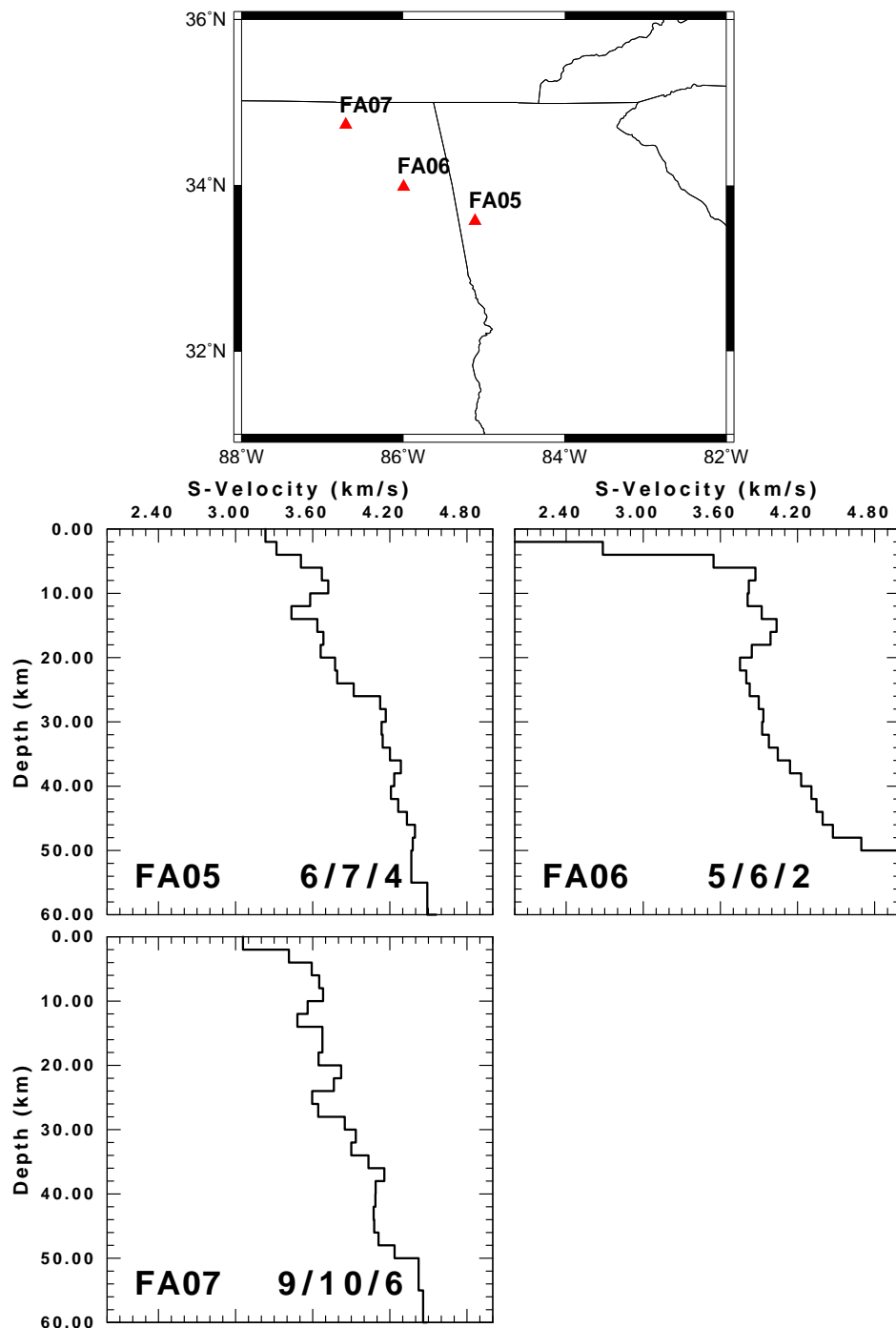


Figure 4.18: The final shear velocity model inverted from receiver function and surface-wave dispersion of Rayleigh group and phase velocity. This model compares stations located on the southern Appalachian

each layer with a sharp Moho at MYNC, FA04, and FA05 and a gradual crust mantle transition beneath GOGA. At stations with sharp Moho, the crustal thickness estimated underneath it is 50 km, whereas the crustal thickness at GOGA is 46 km. Although the crustal thicknesses at these stations are in agreement with the previous result, the suggested layering is different.

The Appalachian Plateau is a flat lying sedimentary sequence. In the middle of the Plateau is the Nashville Dome, which is a structural uplift with an eroded basin in the middle. East of the dome is the Cumberland Plateau, which is composed of Early Pennsylvanian sedimentary rocks and is bounded on the east side by a series of discontinuous northeast trending thin skin thrust faults (Bayer, 1983). Station FA07, located along the Plateau suggests a crustal thickness of 50 km. The surface velocity is 3.05 km/sec and increases rapidly to 3.7 km/sec at 10 km depth. The inverted model indicated the presence of low velocity layer between 10 and 14 km depth. The upper crust has average velocity of 3.6 km/sec and extends to 20 km depth. The middle crust has average velocity of 3.8 km/sec and extends to depth of 36 km and underlain by the lower crust (4.1 km/sec), which overlain a sharp Moho boundary at 50 km depth with shear velocity of 4.5 km/sec.

4.5.3 Central United States (late Proterozoic)

The Midcontinent of the United States is bounded approximately by the Appalachian Mountains on the east, the Front Range of the Rocky Mountains on the west and the Gulf Coastal Plain on the south. The definition of this

region coincides approximately with the edge of the stable craton, which has been relatively undeformed since Precambrian time. The data coverage (seismic studies) for this region is small, but some areas have good coverage to allow a more detailed view crustal structure. For the purpose of simplifying the interpretation of this region, I will divide it into central and western Conterminous.

The southern-central Conterminous United States, the Mississippi Embayment and surrounding areas are spanned by the following stations BLO, MM13-MM18, SLM, CCM, WCI, USIN, SIUC, WVT, UTMT, PLAL, OXF, MPH, and FA07-FA09. Previous studies suggested that the Mississippi Embayment is the site of a late Precambrian continental rift, which reactivated in the Mesozoic (Akinici et al., 1999; Kane et al., 1981, Mooney et al., 1982). The Mississippi Embayment, a spoon shaped trough, is a south plunging structural trough filled with unconsolidated sediments of Cenozoic and late Cretaceous age unconformable overlying Paleozoic carbonate and clastic rocks (Mooney et al., 1980). Other important geological structures surrounding the Mississippi Embayment include the Illinois basin to the north, the Ozark uplift to the northwest, and the Nashville dome and Cincinnati arch to the northeast. This area has the most seismically active zone, New Madrid, in the central and eastern United States which is located in the northern Mississippi Embayment. Southern Mississippi crustal structure is fairly complex because of the interaction of the Appalachian and Ouachita trends that meet there.

OXF (Oxford, Mississippi) and MPH (Memphis, Tennessee) are located east of the Mississippi River near an intersection of the Gulf coastal plain and the

interior plain (Figure 4.19). The crustal structure estimate beneath these two stations is not reliable because of the effect of the near-surface structure (reverberation between the surface and the bottom of the sedimentary layer) on the observed receiver function. The near-surface velocities is seen to increase as we travel from the middle of the Mississippi Embayment from 1.85 to 2.4 km/sec where the thickness of the sedimentary layer is decreases. The station UTMT is locate on the northeastern edge of the Mississippi Embayment. The surface velocity of the material beneath the station has a shear velocity of 2.3 km/sec.

Station PLAL (Pickwick Lake, Alabama) is located on the southwest edge of the Nashville Dome east of the Mississippi Embayment, whereas WVT is located northeast side of the Mississippi Embayment. Shear velocity of the surface layer beneath PLAL and WVT (Figures 4.19 and 4.20), reflect the thickness of the solid Paleozoic rocks east of the Mississippi Embayment. It is difficult to identify Moho depth from the inverted model for both stations because of the gradual increase of the velocity with depth and the absence of acoustic impedance contrast between the upper and the lower crust rocks.

The Illinois basin is located in the central and southern Illinois, southwestern Indiana, and western Kentucky. The greatest thickness of the Paleozoic sedimentary fill is in southern Illinois and western Kentucky which ranges in age from Early or Middle Cambrian to very Early Permian (Collinson et al., 1988). SIUC, USIN and WCI are located in the basin (Figure 4.20). The inverted shear model at WCI and USIN, located almost at the edges of the basin,

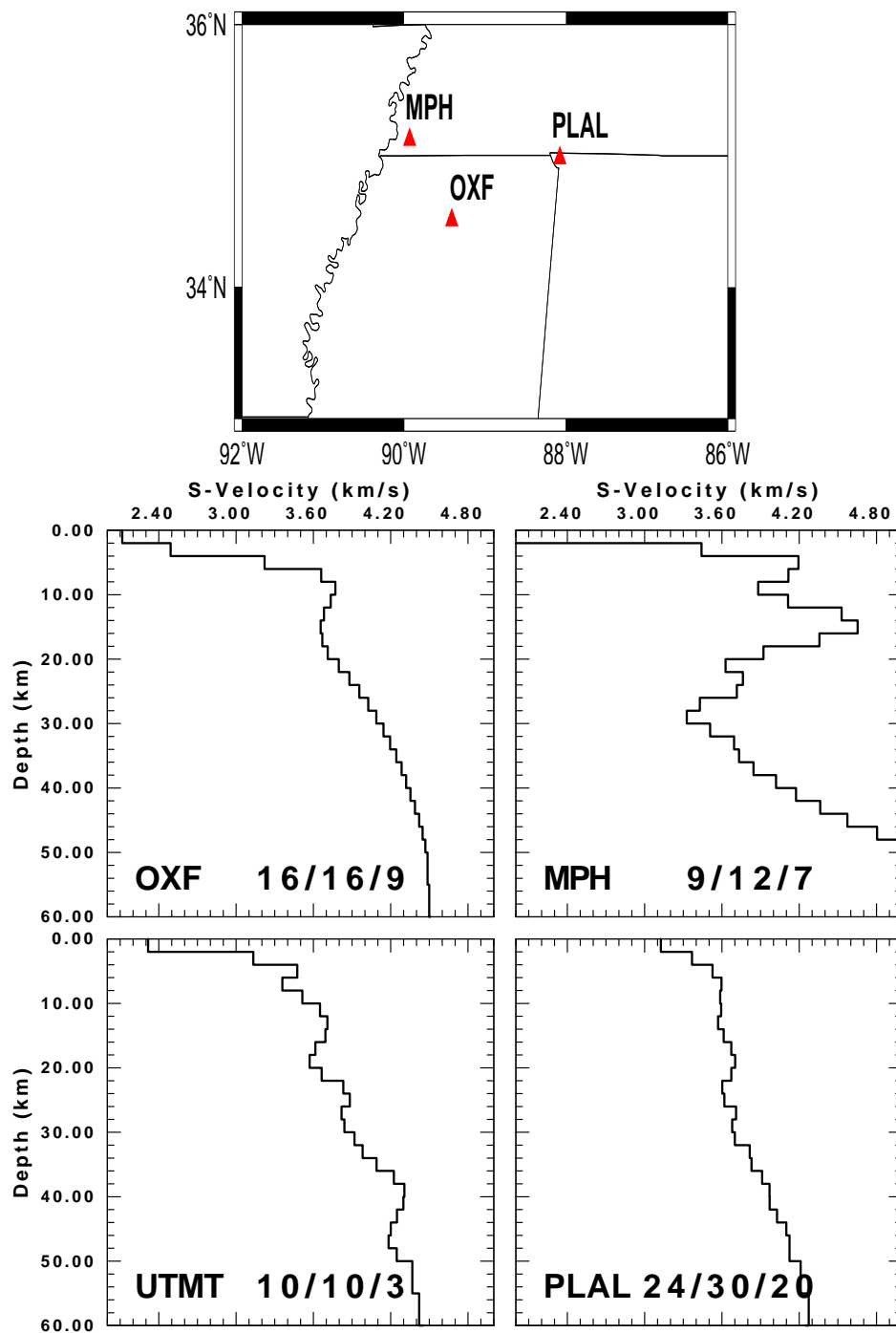


Figure 4.19: The final shear velocity model inverted from receiver function and surface-wave dispersion of Rayleigh group and phase velocity. This model compares stations located on the central Midcontinent

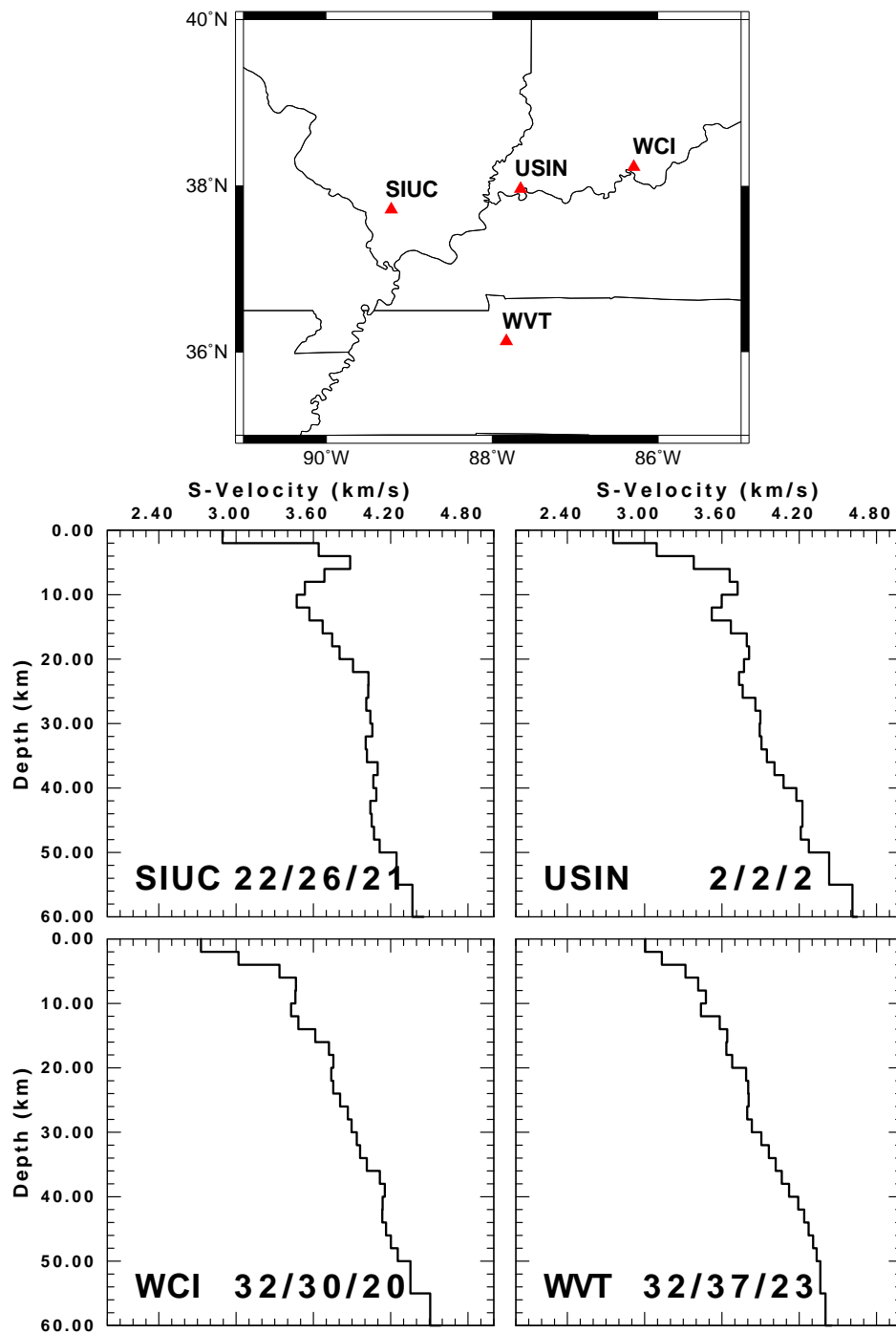


Figure 4.20: The final shear velocity model inverted from receiver function and surface-wave dispersion of Rayleigh group and phase velocity. This model compares stations located on the central Midcontinent

suggest that the velocity for the material beneath it ranges from 2.75 to 2.95 km/sec respectively. The crustal thickness is about 50 km deep. The crust beneath WCI may be divided into three distinct layers with shear velocity of 3.35, 3.75, and 3.9 km/sec respectively. The highest velocity of 4.5 km/sec (mantle shear velocity) occurred at 54 km depth.

The station FA08, located at the flank between the Mississippi Embayment and the Illinois basin, has a velocity value of 2.9 km/sec increases to about 3.35 km/sec at 4 km depth. This model suggests a low velocity layer on the lower crust of 3.8 km/sec up to 4 km thick at 30 km depth. Catchings (1999) indicated that most of the crust beneath the Illinois basin can be modeled as one layer. The crust beneath this station shows a gradational velocity with an average shear velocity of 3.85 km/sec with total crustal thickness of about 44 km.

The stations BLO, MM14-MM17 and SLM (Figure 4.21 and 4.22) form an array across the Illinois basin on the mid-continental platform (Paleozoic sediment resting on Precambrian basement) from the eastern flank of the Illinois basin (BLO) to the western flank (SLM). The velocity models estimated using joint inversion shows a crustal thickness of 40-45 km for all stations with relatively smooth velocity contrast except for the station MM16. The station MM16 inverted model was affected by the thickness of the sediment layer because it located above the thickest Paleozoic. The velocity for the surface materials ranges from 2.4 to 2.9 km/sec for the stations located along the basin. The SLM inverted model shows a higher surface velocity of 3.3 km/sec. The average velocity for upper crust of the Illinois basin is 3.65 km/sec, the middle crust

average velocity is 3.85 km/sec, and for the lower crust is 4.0 km/sec. All the stations on the Illinois basin show a low velocity layer with thickness of about 4 km on the upper crust.

Three more stations MM18, MO18 and CCM form another line across that passes over the Illinois basins. The sedimentary layer thickness ranges from about 0.5 at SLM to about 0 km at CCM (at Ozark Dome). The inverted model at SLM, MM18, and CCM almost shows the same velocity response for all depth. For example, the surface velocity is about 3.35 km/sec with smooth velocity gradually to 3.7 km/sec for the first 8 km. The crust beneath these stations show a three crustal layers with small contrast between each layer with a gradational crust mantle transition zone from about 36 km to 55 km depth.

The crustal structure along a line from the eastern flank of the Mississippi Embayment (latitude 35°) to the eastern flank of the Rocky Mountain Front can be studied by comparing the inverted model at stations UALR, MIAR, WMOK and ALQ (Figure 4.23). To the west of the Mississippi Embayment (western flank) the surface shear velocity is about 2.4 km/sec (beneath the station UALR), reflecting the effect of the sedimentary layer. The inverted model does not suffer from the thickness of the sedimentary layer as MPH and OXF. The velocity increases rapidly to about 3.1 for the upper 10 km. The crustal structure beneath this station shows a three layer crust. The upper crust extends to 12 km depth with an average shear velocity of about 3.1 km/sec, the middle crust extends to about 30 km depth with average shear velocity of 3.6

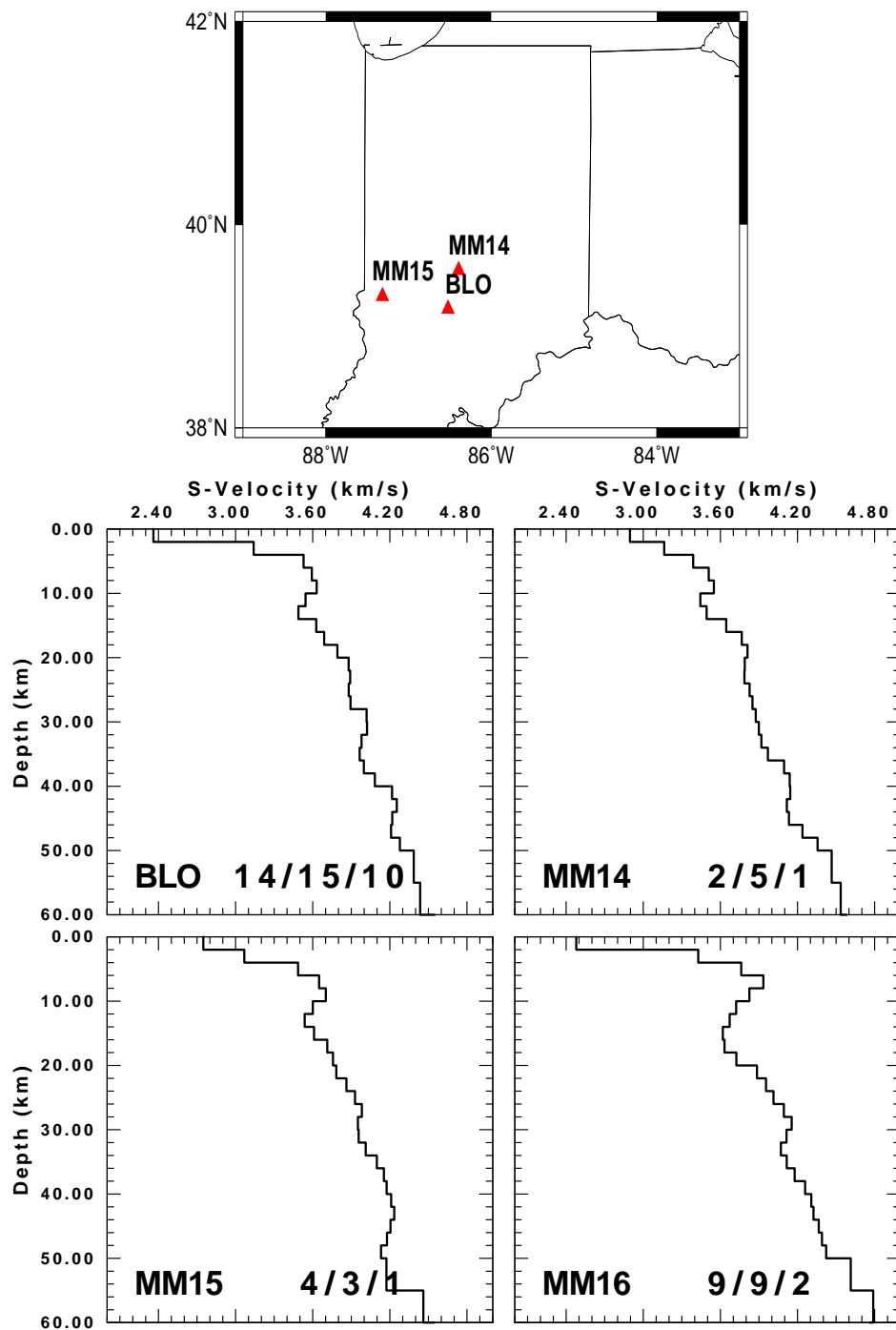


Figure 4.21: The final shear velocity model inverted from receiver function and surface-wave dispersion of Rayleigh group and phase velocity. This figure compares models for stations located on the central Midcontinent

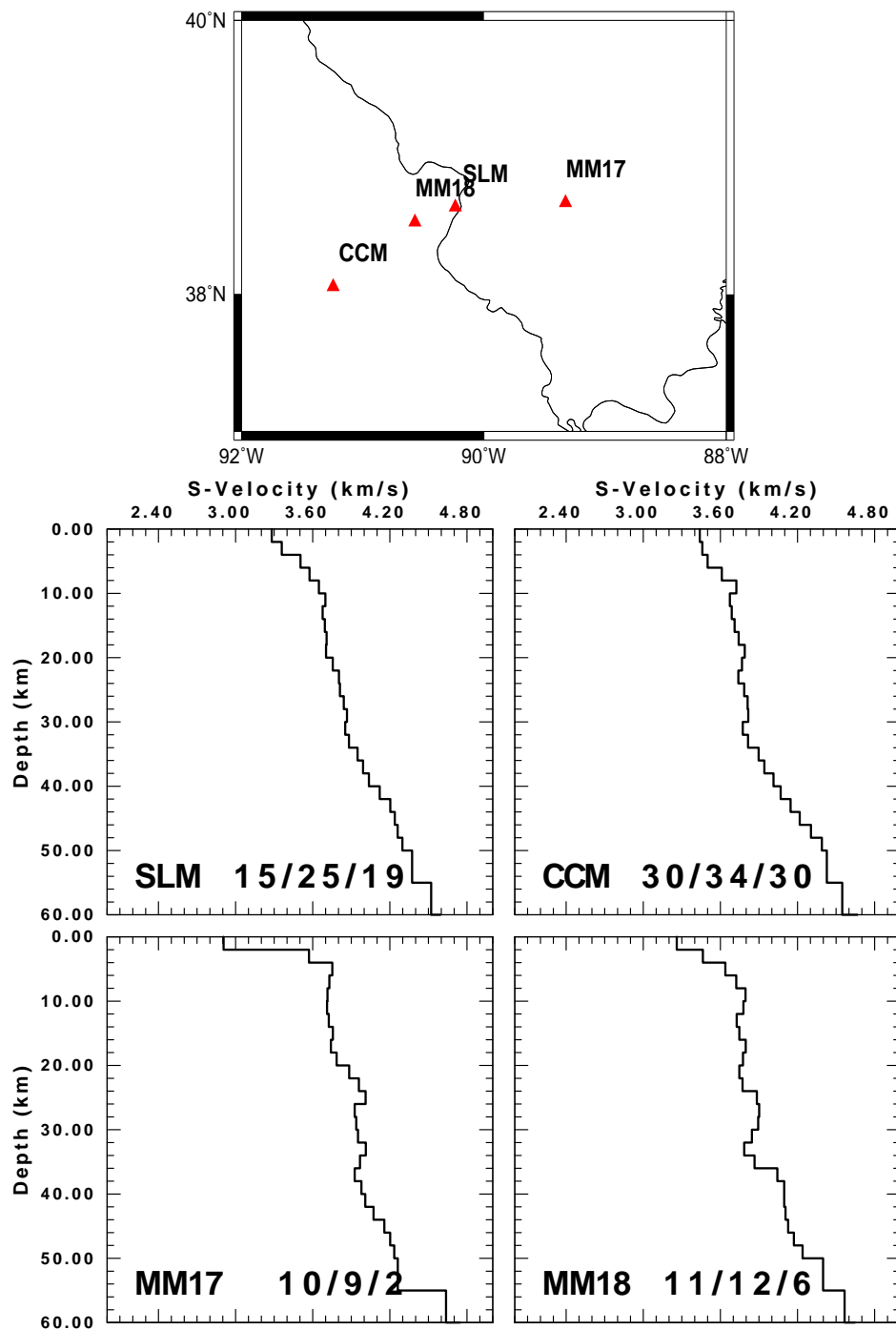


Figure 4.22: The final shear velocity model inverted from receiver function and surface-wave dispersion of Rayleigh group and phase velocity. This figure compares models at stations located on the central Midcontinent

km/sec, and the lower crust extends to about 42 km depth with average shear velocity of 4.0 km/sec. The model shows a sharp transition between the upper and the middle crust and a gradational transition between the middle and the lower crust. The crust mantle transition zone at this area is gradual with the highest shear velocity of 4.3 km/sec at depth of 50 km.

The station MIAR (southern part of the Arkoma Basin, Benton Uplift) is located on the southern part of the Grenville Province. A COCORP seismic reflection profile was performed long this area (Nelson et al, 1982). This study indicated that the Benton Uplift coincides with a broad antiformal structure occurring in the subsurface by uplifted North American Precambrian basement. The inverted model beneath this station shows significant features which may reflect the same structure. The surface shear velocity is low, (2.15 km/sec) for the upper two km. The upper crust extends to about 16 km depth with an average velocity of 3.0 km/sec. The model does not show a significant middle crust. A thick layer of about 8 km (16 to 24 km depth) is characterized by a rapid increase in the velocity from 3 km/sec at the top to about 3.8 km/sec at the bottom of the layer. The model presented by Nelson et al, (1982) may reflect the presence of the low velocity layer beneath this station at depth 10 to 16 km. They suggest that the North America basement and overlying Arbuckle facies carbonates continue to the south beneath Benton Uplift, where they are deformed into an antiformal basement arch.

In the vicinity of southwestern Oklahoma, a deep Proterozoic basin is filled with undeformed clastic and rhyolitic volcanic rocks 7-10 km thick (Keller et

al., 1983; Brewer et al., 1982). Several authors suggest that a failed-arm rift extends into the craton in the area of the early Paleozoic Tabosa basin (Keller et al., 1983). A gravity study of the area (Keller et al., 1980) delineates a large positive gravity anomaly which may be the result of a mafic intrusion beneath the central plain platform or a large thickness of volcanic and/or sedimentary rocks laid down early in the feature's history. The inverted model beneath WMOK (Wichita Mountain Oklahoma) shows a surface velocity of about 3.15 km/sec. The model delineates two crust layers with evenly the same thickness. The upper crust extends to depth of 22 km with an average shear velocity of 6.3 km/sec and the lower crustal thickness of about 24 km and shear velocity of 3.8 km/sec.

The station AAM (Ann Arbor, Michigan) is located to the north of these stations shows a surface velocity of about 2.9 km/sec increases rapidly to about 3.5 km/sec for the upper 6 km (Figure 6.24). The crust beneath this station shows a simple two layers with the upper layer extending to a depth of 20 km and average shear velocity of 3.55 km/sec. The lower crust extends to 42 km depth with average velocity of 3.95 km/sec. The crust mantle transition zone is gradual. The closest seismic profile was in northern Lake Michigan, mid-continent North America. Cannon et al. (1991) suggest that the lower crust is mostly mafic granulite with thickness 20-25 km. The upper crust is mostly Archean felsic gneisses and early Proterozoic supra-crustal rocks.

The north central region of the central Plains is spanned by the FLED stations several permanent stations such as JFWS, CBKS and RSSD. The in-

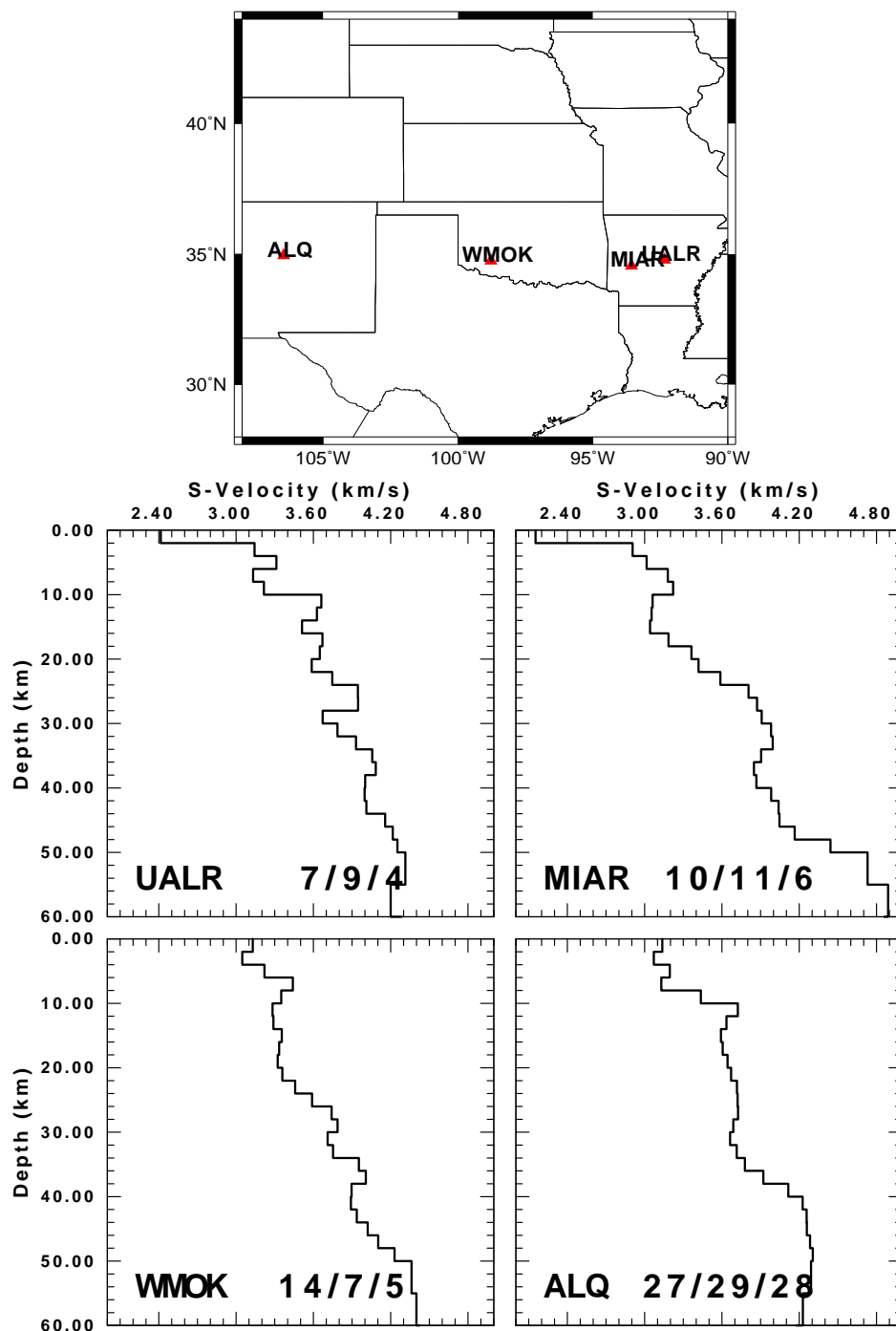


Figure 4.23: The final shear velocity model inverted from receiver function and surface-wave dispersion of Rayleigh group and phase velocity. This figure compare models for stations located on the central Midcontinent

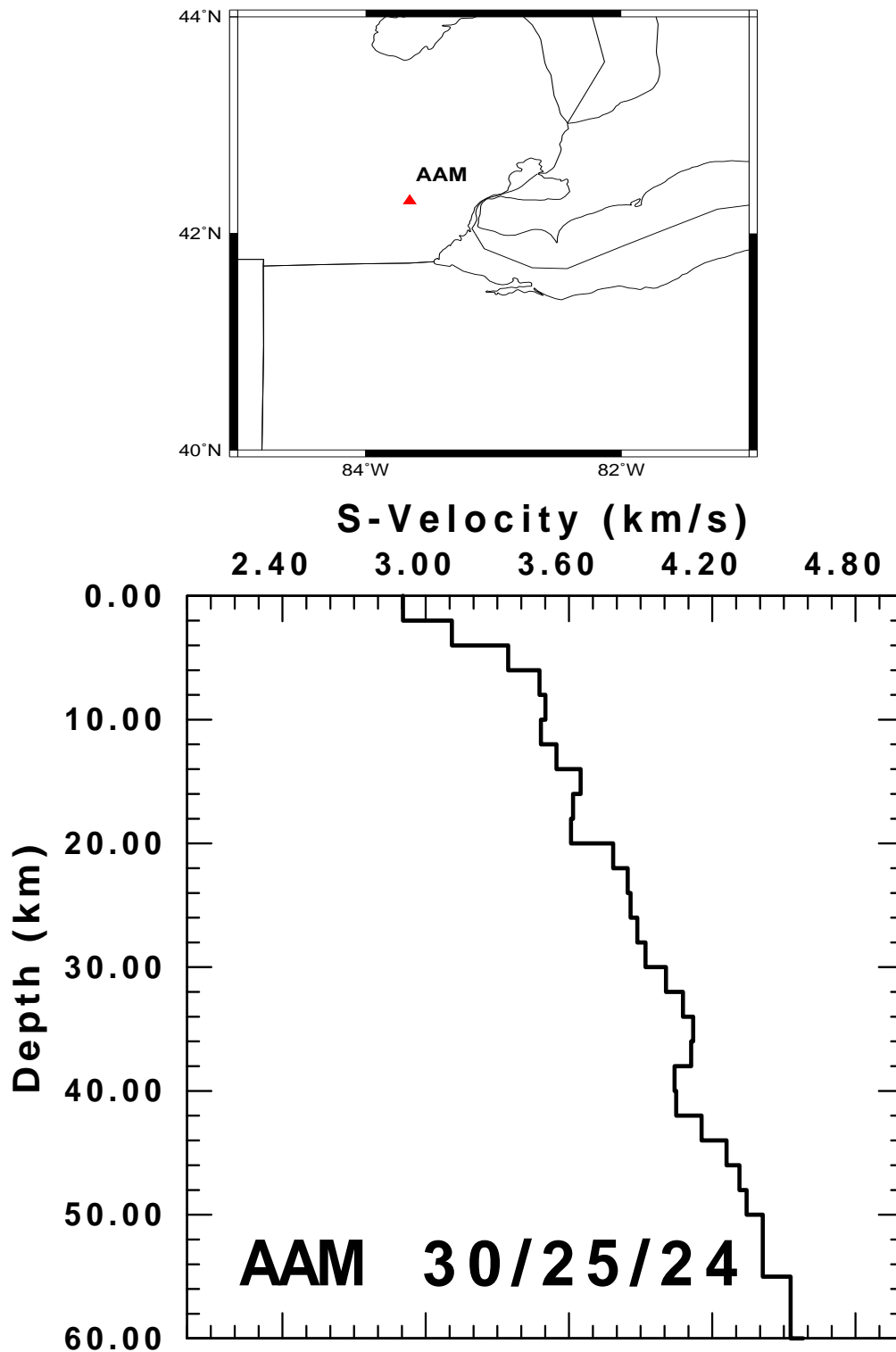


Figure 4.24: The final shear velocity model inverted from receiver function and surface-wave dispersion of Rayleigh group and phase velocity. This figure compares models for stations located on the central Midcontinent

verted models for most of the FLED stations (FA13-FA18) almost show a similar structure. For example, FA13, FA15, FA16, FA17 and FA18 have a gradual crust mantle transition zone with average depth of 46 km (Figures 4.25-4.28). These stations fall within the Precambrian Midcontinent Rift which was filled with by volcanic and intrusive rocks and then covered by sedimentary materials. All these stations show the presence of the low velocity layer at depth range from 18 to 26 km with a thickness of about 4-6 km. The crustal structure is constant and indicates two crustal layers with average velocity of 3.65 km/sec for the upper crust and 3.9 km/sec for the lower crust. The other stations crossing Iowa FA19, FA20 and FA21 delineate the same structure, but have a sharp crust mantle transition zone.

The stations FA21, FA22 and FA23 are located in South Dakota. The station RSSD has been studied intensively by Owens et al. (1984, 1987). The Black Hills form an elongated domal uplift exposing a core of Precambrian metamorphic and igneous rocks (Owens et al., 1987). The northeastern part of the range is thought to represent part of the basement upon which early Proterozoic sediments were deposited. The shear velocity models beneath these stations show a surface velocity of 3.4 km for the upper 10 km. The low velocity layer that was present beneath stations FA15-FA21 seems to be terminated at station FA21. The inverted model at FA22 does not show the low velocity layer. Generally, these stations show a simple crust with two distinct layers. The upper layer extends to a depth of 22 km with average velocity of 3.6 km/sec. The lower crust extends to the crust mantle transition boundary with an average velocity

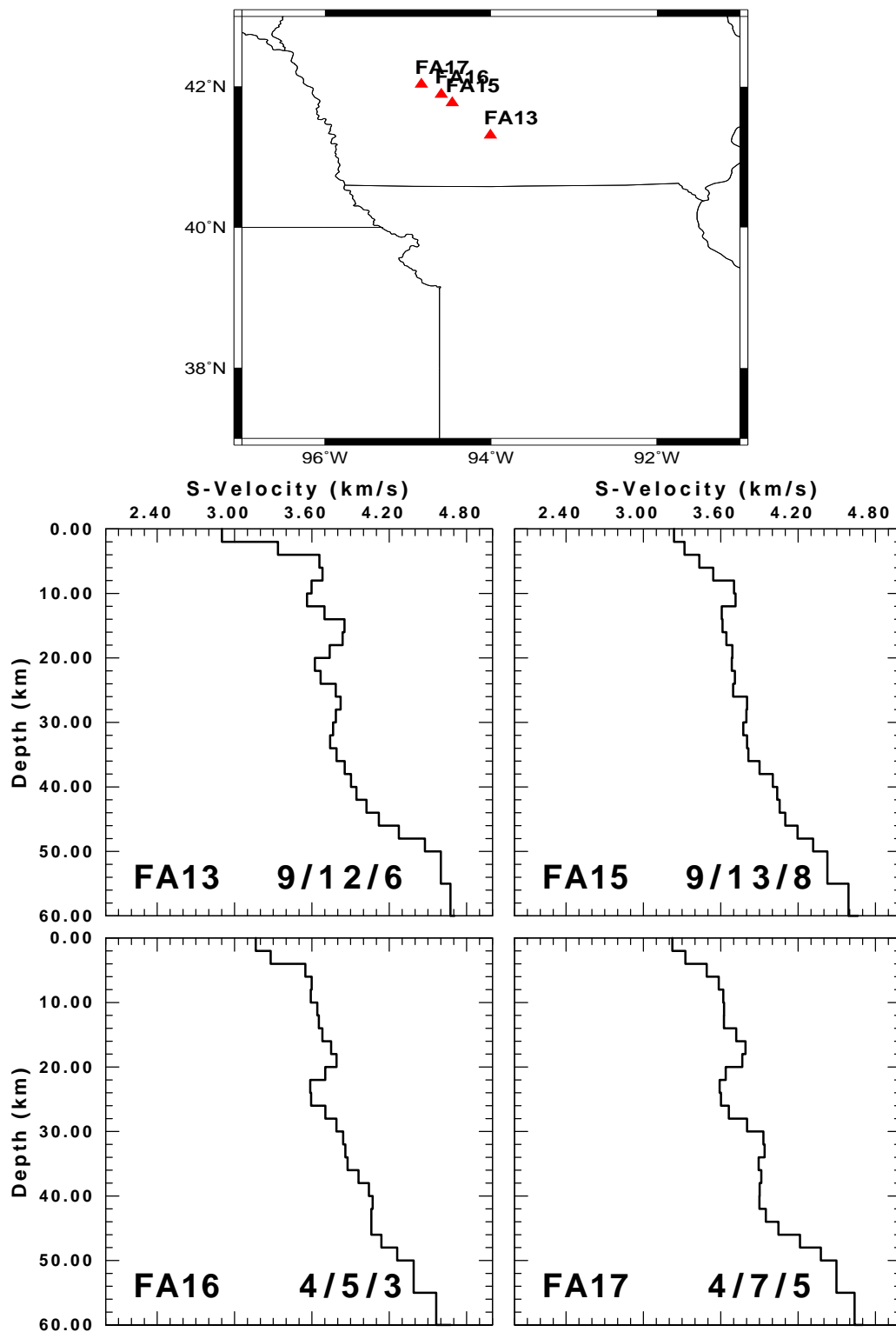


Figure 4.25: The final shear velocity model inverted from receiver function and surface-wave dispersion of Rayleigh group and phase velocity. This figure compares models at stations located on the central Midcontinent

of 3.8 km/sec.

The remaining stations of FLED are located along the Williston Basin. Stations FA23-FA27 are affected by the thick sedimentary layer. The Williston Basin is one of the major Cratonic basins of North America and lies close to the western margin of the Canadian Precambrian Shield (Hajnal et al., 1984). Within the United States the basin occupies greater portion of North Dakota, part of western South Dakota, and eastern Montana. The thickest portion of the sedimentary basin, about 4.8 km, is located in southeastern North Dakota. Among all those stations only station FA28 can reveal some information about the crustal structure. The surface shear velocity is about 3.6 km/sec and increases rapidly to about 3.5 at depth 4 km. The model also shows a sharp crust-mantle transition zone with the highest shear velocity of 4.55 km/sec at depth of 44 km.

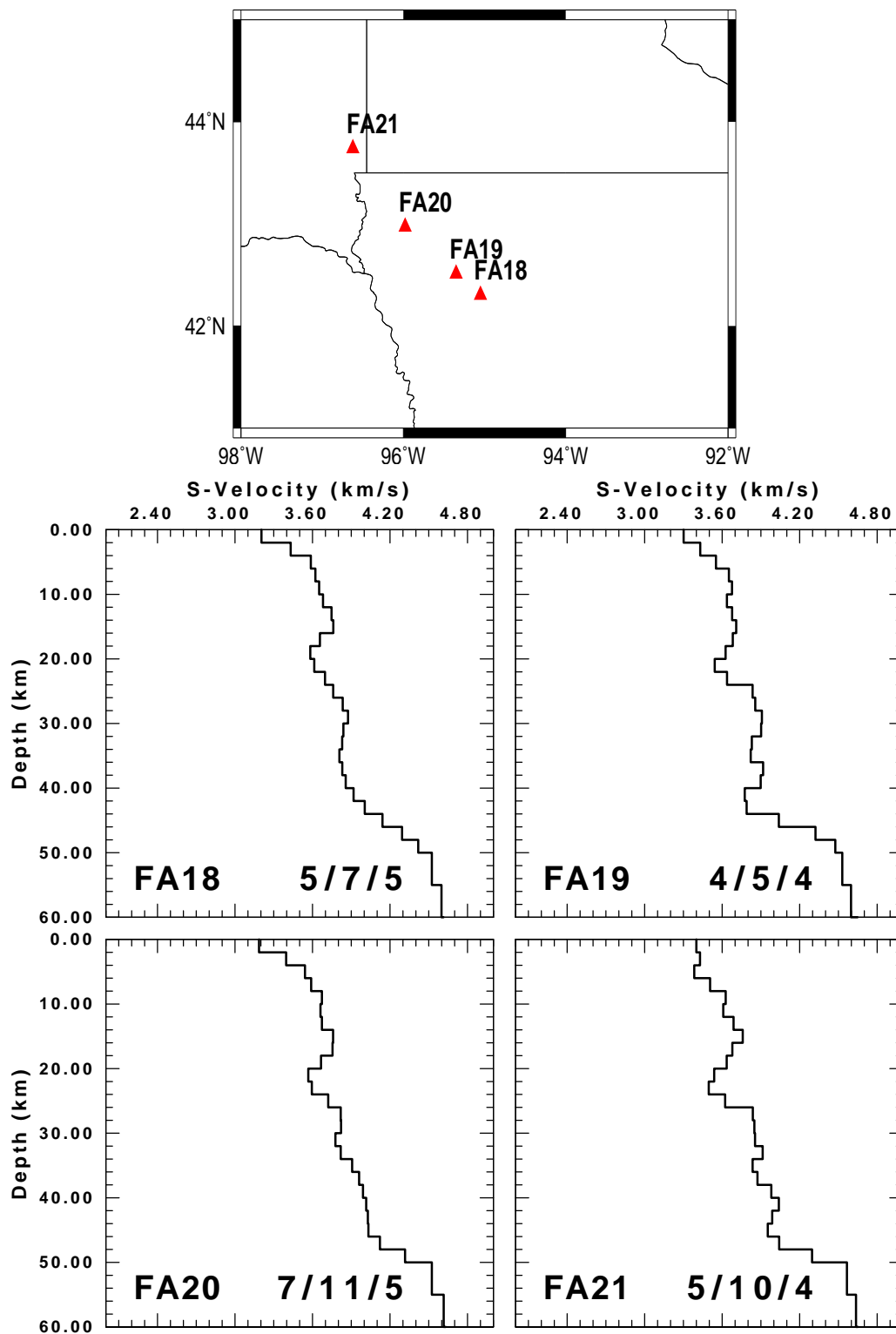


Figure 4.26: The final shear velocity model inverted from receiver function and surface-wave dispersion of Rayleigh group and phase velocity. This figure compares models for stations located on the central Midcontinent

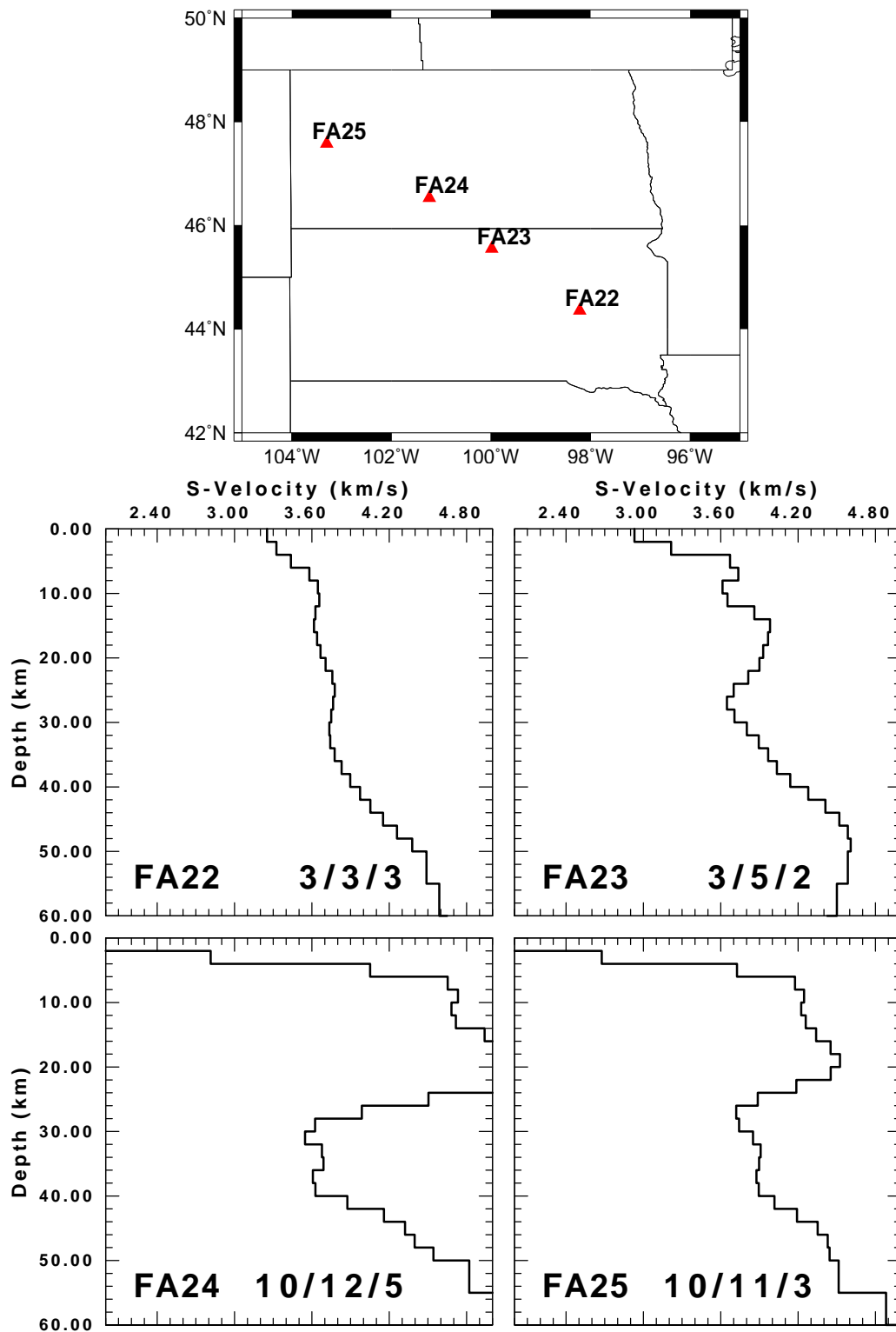


Figure 4.27: The final shear velocity model inverted from receiver function and surface-wave dispersion of Rayleigh group and phase velocity. This figure compare models for stations located on the central Midcontinent

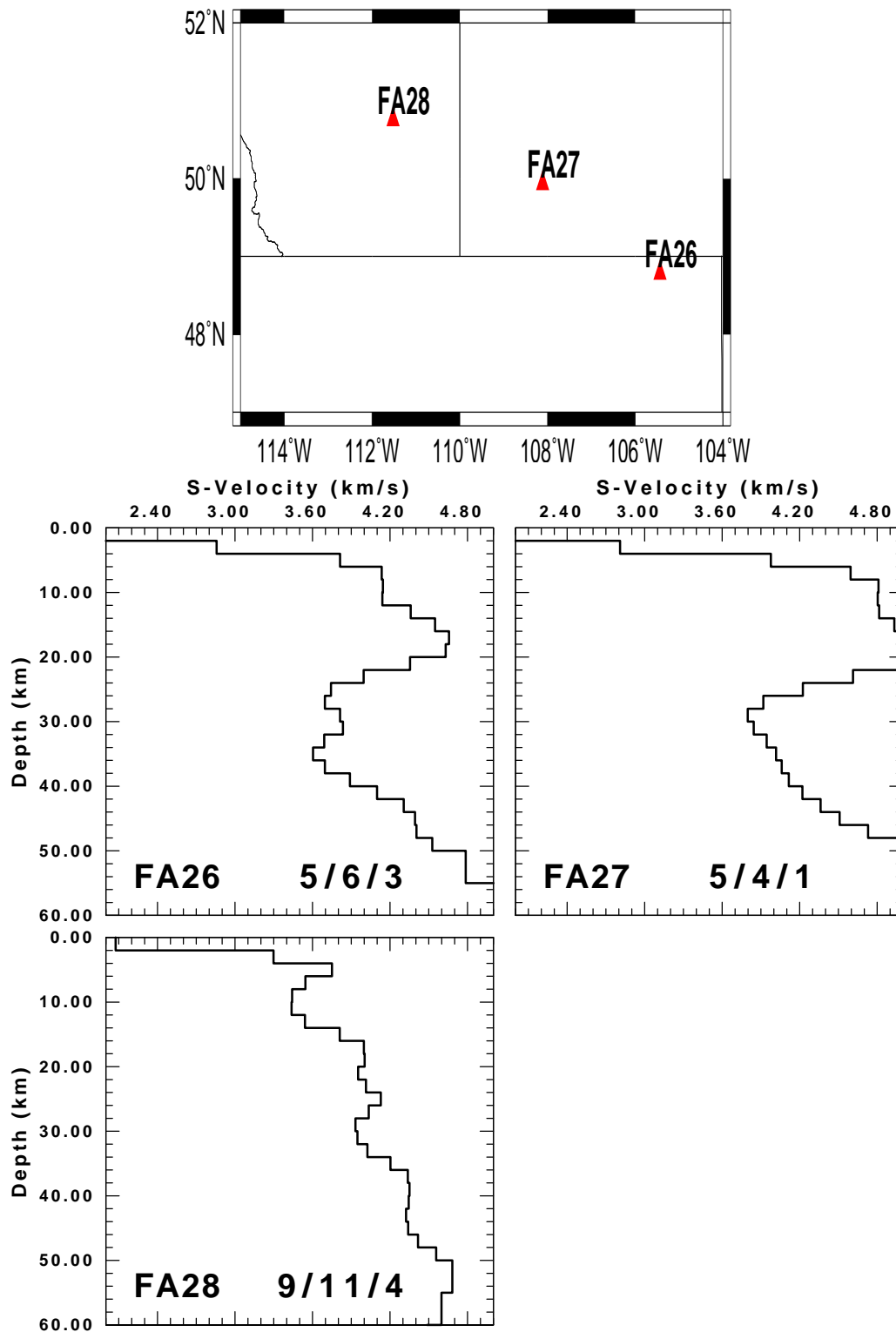


Figure 4.28: The final shear velocity model inverted from receiver function and surface-wave dispersion of Rayleigh group and phase velocity. This figure compares models for stations located on the central Midcontinent

Chapter 5

Conclusion

5.1 Crustal Structure

The purpose of this research was to apply a new technique, the joint inversion of surface-wave dispersion and P-wave receiver functions, to estimate crustal velocity profiles for 124 sites in eastern North America. To accomplish this, I determined receiver functions using the iterative time-domain deconvolution procedure of Ligorria and Ammon (1999). The interest in applying the joint inversion technique was to image the shear-wave velocities in the crust, especially near the Moho transition.

Because the focus of this research is on the nature of the shear-wave velocity distribution in the crust, I only considered one starting model and one set of constraints for the joint inversion. I recognize that even this inversion may not yield the true velocity model beneath a station because of data imperfections and the artifacts of the actual non-linear inversion procedure. Although there are inversion techniques that account for the effect of data noise on the final result, there is still the fundamental difficulty due to the nature of the data set used. The truth of the final model cannot be evaluated unless there are some other independent data to provide a critical evaluation. My joint inversion was constrained by an *a priori* upper mantle model that was based on body-wave studies to at least be consistent with global studies at depth. In a few loca-

tions the upper crustal velocities may be evaluated by comparing observed and predicted broadband seismograms of regional earthquakes in the 5 - 50 second period band. At other locations, it may be possible to compare model predicted P-wave first arrival times for known explosion sources. Finally, one can compare a crustal shear-wave model to a model derived from a crustal refraction or reflection survey. The data for such an evaluation are not available for most of the sites considered, but a critical comparison at a few sites may give confidence to the technique.

I was surprised to find that receiver functions vary in their ability to provide direct information about the Moho. As described in Chapter 3, this was apparent in the lack of P_s phase at some stations and the lack of evidence of crustal reverberation at others. Since the P_s phase can be associated with a velocity discontinuity in the Moho, the lack of this distinct converted phase in the receiver function is interpreted by the inversion procedure as a velocity gradient at the Moho, rather than as a sharp discontinuity. This does not mean that the change in velocities near the Moho is transitional, since scattering and Moho topography or spatial velocity heterogeneity may also make this phase less distinct in appearance. Again, other data, either from the use of wide angle refraction data or from the use of the transverse component of the receiver function, must be called upon to go beyond the limitations of the use of just the surface-wave dispersion and radial component P-wave receiver functions to image the Moho.

The following two sections will compare the Moho depth estimates for the

stations obtained using different techniques and compare the velocity model to crustal refraction models at three sites.

5.2 Crustal Thickness

In my study, the depth to the Moho was estimated in two ways. In Chapter 3, I used an assumed average crustal P-wave velocity and a data derived or assumed V_P/V_S ratio to make this estimate. In Chapter 4, I chose to use the depth at which the shear-wave velocity reaches 4.2 km/s as a proxy for the Moho depth. This velocity was chosen because this velocity corresponded to an inflection point in the velocity - depth profile at many sites that seemed to have a sharp Moho. I am also able to compare these depth estimates to those of Ligorria (2000) at a few sites. Table 5.1 presents this comparison. The different estimates of Moho depth are similar.

Table 5.1: A comparison of crustal thickness estimates

STA	h1 (km)	k1	h2 (km)	k2	h3 (km)
AAM	47.32 ±3.61	1.96 ±0.07	43.03 ±4.98	1.83 ±0.16	44
ACSO	47.94 ±2.10	1.86 ±0.03	—	—	50
ALQ	38.96 ±2.36	1.70 ±0.04	—	—	40
ALQN	—	—	—	—	40
ANMO	39.64 ±3.45	1.68 ±0.07	40.13 ±1.92	1.66 ±0.05	—
BINY	46.00 ±3.56	1.75 ±0.05	46.20 ±3.93	1.74 ±0.10	—
BLA	48.32 ±3.92	1.81 ±0.04	45.72 ±3.36	1.83 ±0.07	50
BLO	—	—	—	—	40
CARO	35.44 ±5.31	1.72 ±0.03	—	—	—
CBKS	43.10 ±3.94	1.83 ±0.06	44.10 ±2.64	1.81 ±0.09	—
CCM	43.93 ±3.70	1.79 ±0.04	41.77 ±5.65	1.86 ±0.16	44
CEH	35.57 ±3.29	1.74 ±0.04	36.16 ±2.01	1.75 ±0.07	36
DRLN	33.10 ±2.87	1.74 ±0.06	31.36 ±1.98	1.80 ±0.04	—
DWPF	35.94 ±4.76	1.91 ±0.07	—	—	36
EDM	37.05 ±3.35	1.79 ±0.10	38.39 ±6.21	1.84 ±0.12	38

continued on next page

Table 5.1: *continued*

STA	h1 (km)	k1	h2 (km)	k2	h3 (km)
EYMN	41.73 ±4.13	1.76 ±0.09	—	—	—
FA01	40.90 ±4.83	1.82 ±0.05	—	—	35
FA02	—	—	—	—	40
FA03	—	—	—	—	—
FA04	43.55 ±3.49	1.58 ±0.02	—	—	40
FA05	47.29 ±2.33	1.76 ±0.04	—	—	36
FA06	46.77 ±2.85	1.85 ±0.03	—	—	38
FA07	48.62 ±3.21	1.80 ±0.05	—	—	48
FA08	41.53 ±6.50	1.73 ±0.03	—	—	—
FA09	42.83 ±2.35	1.81 ±0.04	—	—	—
FA10	47.56 ±4.10	1.84 ±0.03	—	—	—
FA11	44.44 ±2.88	1.86 ±0.06	—	—	—
FA12	42.75 ±4.89	1.97 ±0.04	—	—	—
FA13	44.35 ±2.78	1.76 ±0.03	—	—	46
FA14	43.93 ±3.45	1.91 ±0.03	—	—	—
FA15	—	—	—	—	44
FA16	47.63 ±2.99	1.66 ±0.04	—	—	48
FA17	46.32 ±4.48	1.88 ±0.03	—	—	46
FA18	41.79 ±2.76	1.75 ±0.03	—	—	46
FA19	44.28 ±2.49	1.81 ±0.04	—	—	46
FA20	45.12 ±4.14	1.66 ±0.02	—	—	48
FA21	49.46 ±5.16	1.82 ±0.04	—	—	48
FA22	—	—	—	—	46
FA23	—	—	—	—	40
FA24	—	—	—	—	44
FA25	—	—	—	—	44
FA26	—	—	—	—	42
FA27	—	—	—	—	40
FA28	—	—	—	—	40
FCC	40.73 ±3.95	1.72 ±0.05	34.09 ±2.18	1.86 ±0.02	—
FFC	38.75 ±3.10	1.74 ±0.0	38.99 ±4.56	1.70 ±0.09	40
GAC	37.72 ±6.71	1.75 ±0.05	37.97 ±1.23	1.79 ±0.05	42
GOGA	38.94 ±4.63	1.76 ±0.05	37.52 ±4.86	1.80 ±0.14	39
GWDE	29.77 ±3.73	1.99 ±0.11	—	—	—
HKT	38.95 ±6.90	1.56 ±0.05	—	—	—
HRV	30.33 ±3.12	1.66 ±0.03	30.84 ±1.30	1.68 ±0.07	32
ISCO	46.69 ±16.26	1.56 ±0.04	45.35 ±6.09	1.73 ±0.13	—
JCT	43.79 ±3.62	1.87 ±0.06	—	—	—
JFWS	42.69 ±4.19	1.75 ±0.05	33.34 ±0.72	1.99 ±0.02	—
KAPO	41.62 ±5.79	1.76 ±0.06	—	—	44
KGNO	42.50 ±6.89	1.91 ±0.12	—	—	48

continued on next page

Table 5.1: *continued*

STA	h1 (km)	k1	h2 (km)	k2	h3 (km)
LBNH	30.97 ±5.71	1.99 ±0.16	—	—	36
LMN	39.13 ±3.76	1.75 ±0.04	44.42 ±5.25	1.68 ±0.01	—
LMQ	42.60 ±4.60	1.81 ±0.05	37.81 ±4.14	1.88 ±0.07	42
LRAL	43.84 ±4.03	1.82 ±0.04	—	—	—
LSCT	27.67 ±2.86	1.69 ±0.05	30.19 ±3.31	1.73 ±0.09	32
LTX	35.85 ±3.34	1.81 ±0.06	—	—	—
MCWV	43.23 ±4.11	1.80 ±0.05	38.53 ±5.62	1.96 ±0.12	44
MIAR	38.49 ±4.10	1.99 ±0.14	41.18 ±2.26	1.96 ±0.03	46
MM01	26.49 ±4.17	1.62 ±0.08	—	—	32
MM02	38.97 ±3.22	1.78 ±0.04	—	—	38
MM03	32.33 ±4.00	1.94 ±0.09	—	—	38
MM04	45.37 ±4.21	1.79 ±0.05	—	—	46
MM05	45.17 ±3.02	1.86 ±0.05	—	—	46
MM06	44.78 ±2.51	1.82 ±0.04	—	—	44
MM07	45.72 ±2.64	1.78 ±0.03	—	—	44
MM08	45.90 ±3.26	1.75 ±0.04	—	—	50
MM09	46.39 ±3.51	1.79 ±0.06	—	—	48
MM10	41.73 ±2.49	1.81 ±0.03	—	—	—
MM11	50.44 ±2.64	1.85 ±0.06	—	—	—
MM12	39.24 ±2.88	1.84 ±0.08	—	—	—
MM13	40.00 ±3.17	1.92 ±0.08	—	—	—
MM14	43.70 ±6.29	1.75 ±0.03	—	—	46
MM15	—	—	—	—	40
MM16	46.11 ±3.05	1.67 ±0.03	—	—	44
MM17	—	—	—	—	46
MM18	47.87 ±3.83	1.83 ±0.04	—	—	48
MO18	47.53 ±3.13	1.78 ±0.03	—	—	—
MPH	—	—	—	—	—
MYNC	47.87 ±5.57	1.77 ±0.06	48.88 ±1.32	1.79 ±0.04	50
NCB	37.99 ±3.63	1.91 ±0.05	—	—	—
NHSC	34.87 ±3.49	1.61 ±0.05	—	—	—
OXF	43.00 ±2.94	1.80 ±0.04	42.46 ±1.83	1.79 ±0.04	34
PAL	29.36 ±0.49	1.67 ±0.04	—	—	—
PAPL	38.43 ±1.66	1.78 ±0.04	—	—	40
PLAL	—	—	—	—	50
POP6	30.15 ±2.65	1.69 ±0.05	—	—	38
POUL	35.27 ±6.86	1.92 ±0.04	—	—	40
PQI	—	—	—	—	—
RSSD	—	—	—	—	—
SADO	36.68 ±2.74	1.79 ±0.04	35.88 ±5.66	1.82 ±0.16	38
SCHQ	45.89 ±6.24	1.78 ±0.05	40.04 ±7.87	1.90 ±0.15	44

continued on next page

Table 5.1: *continued*

STA	h1 (km)	k1	h2 (km)	k2	h3 (km)
SIUC	46.20 ±4.02	1.76 ±0.05	—	—	50
SLM	51.09 ±3.23	1.76 ±0.03	—	—	44
SSPA	43.26 ±4.47	1.81 ±0.06	40.38 ±9.07	1.88 ±0.20	44
SWET	—	—	—	—	—
UALR	35.34 ±5.39	1.93 ±0.06	—	—	46
ULM	33.25 ±2.11	1.74 ±0.03	32.13 ±1.51	1.79 ±0.03	34
UTMT	45.53 ±4.23	1.73 ±0.04	—	—	40
VSG4	36.68 ±2.38	1.94 ±0.09	—	—	34
WCI	47.45 ±4.24	1.81 ±0.05	—	—	46
WES	28.25 ±2.48	1.79 ±0.04	—	—	32
WMOK	48.40 ±7.64	1.65 ±0.05	44.17 ±3.75	1.90 ±0.06	48
WVL	32.94 ±1.87	1.78 ±0.05	—	—	—
WVT	45.02 ±4.00	1.78 ±0.06	—	—	42
YSNY	46.46 ±3.34	1.54 ±0.03	—	—	44

h1 - Moho depth from Chapter 3

k1 - Crustal V_P/V_S from Chapter 3

h2 - Moho depth from Ligorria (2000)

k2 - Crustal V_P/V_S Ligorria (2000)

h3 - Moho depth from joint inversion models of Chapter 4

Crustal structure constrained by modeling Moho conversions and reverberations shows a variation of Moho depth (Figure 3.23) from a minimum of 30 km near the Atlantic coast to depths of 44-49 km beneath the western Appalachian orogeny and 38-45 km beneath the mid-continent province. The average receiver function estimates of continental crustal thickness for ENA is 40 km. This agrees with the global average of 39.2 km (Christensen and Mooney, 1995) and is 3 km more than the 36.7 km average crustal thickness for North America (Chulick and Mooney, 2003). Thin (27-35 km) crust extends along the coastal plains. The thickest crust (40-50 km) occurs under the Appalachian orogeny and the central plains.

A rapid thinning of the crust between MM09 and MM13 west of the Ap-

palachian front may represent a Proterozoic age suture in the Grenville basement (Hoffman, 1989 ; Li et al., 2002). Li et al. (2002) found the same feature for stations MM09 and MM10, but there are some disagreements on the estimated depths between their study and mine which may be the result of using different underlying assumptions. Li et al. (2002) assumed both the V_P and the V_P/V_S ratio to estimate the crustal depths while I also estimated the V_P/V_S ratio; this may increase the uncertainties in their calculations. For other regions, the estimated crustal thicknesses show agreement with previous studies as explained in Chapter 4.

A comparison of my results with Moho maps inferred from interpolated refraction and reflection data, shows that the agreement is very good for some regions, while for other regions the interpolated values deviate from my observations. The largest deviations were found in southeastern Canada (Grenville front zone). Rivers et al. (1989) reported that the absence of a large gravity anomaly over this region of the Grenville Front is evidence that the crustal blocks are in isostatic equilibrium. Thus, the thinning of the crust at the Grenville Front must be accompanied by an increase in the average density of the middle to upper crust to preserve that isostatic equilibrium.

the estimated crustal thicknesses are somewhat correlated with the geologic ages of the eastern North America. Comparing the depth to the Moho shown in Figure 3.23 to the crustal age map in Figure 1.2 shows a pattern between the crustal thickness and the age. The Atlantic coastal plain which is known to be Paleozoic and younger is characterized by a thin crust (27-35 km). However,

the Appalachian province of Paleozoic age has a thicker crust which may reflect the Appalachian orogeny. The older Proterozoic-crust of mid-continent has the thickest crust on the study area.

5.3 Comparison of Joint Inversion Models to Crustal Refraction Models

In this dissertation I used the joint inversion technique to combine the average properties contained in surface-wave dispersion curves with the absolute properties of ray reflection and conversions provided by receiver functions. I have derived shear velocity crustal models for all available stations (permanent and temporary). Most of the derived models are simple in the sense that they may be simplified to no more than three layers. In the following discussion, I compare my final models to those of others at a few locations. Because most of the seismic refraction/ reflection studies give compressional velocity models, I will use the V_P/V_S ratio estimated in Chapter 3 to estimate the corresponding shear velocity.

5.3.1 Structure near DRLN

The station DRLN is located at the Humber zone in central Newfoundland (Northern Canadian Appalachian) and is close to a seismic refraction/wide-angle reflection profile between shot points 12 and 13 (Figure 5.1). Figure 5.1 compares the joint inversion model to the refraction interpretation. There is a good correspondence, but the joint inversion model has lower velocities in the upper 5 km and shows a transitional Moho. I created a simple model based

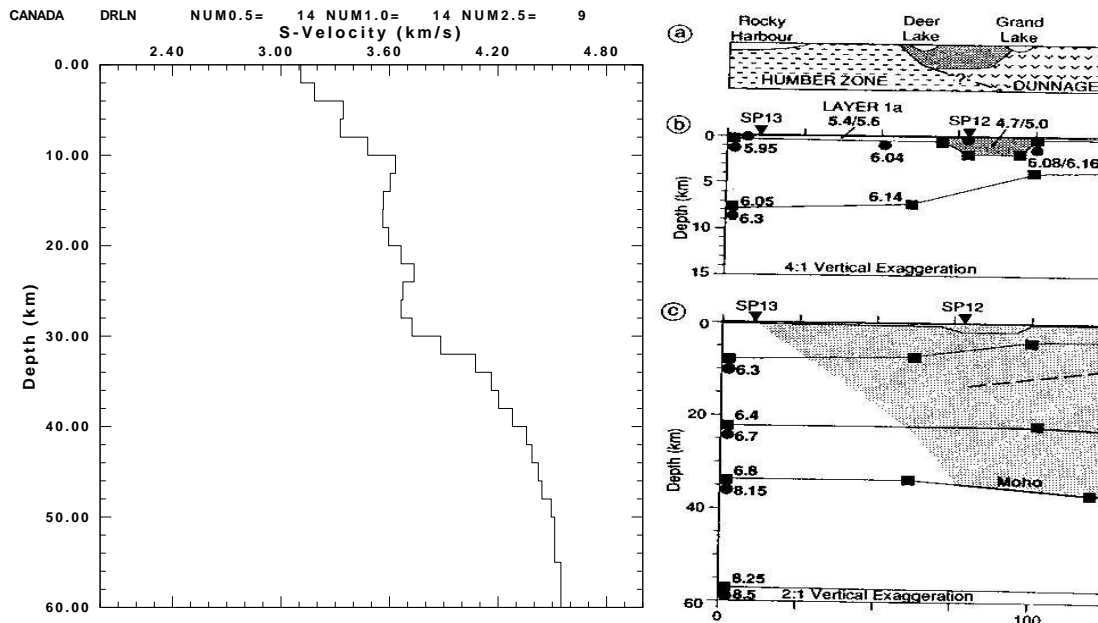


Figure 5.1: The model compares between the final model from this study with the final model from Hughes et al. (1992).

on the refraction model to generate a receiver function for $\alpha=1.0$. Figure 5.2 compares the receiver functions for the refraction model, the joint inversion model and a stack of observed receiver functions. The simple refraction model suffices to describe the observed receiver function to 10 seconds, but predicted the Moho bounce arrivals at 13 - 17 seconds are too large but do have the same arrival times. This difference can be explained by a slightly transitional Moho. Based on the good correspondence in the joint inversion and refraction model velocity depth functions shown in Figure 5.1, we would accept the joint inversion model.

5.3.2 Structure near GAC and NCB

The joint inversion models at stations GAC and NCB show a high velocity middle crust. Other crustal models at or near these stations are available from

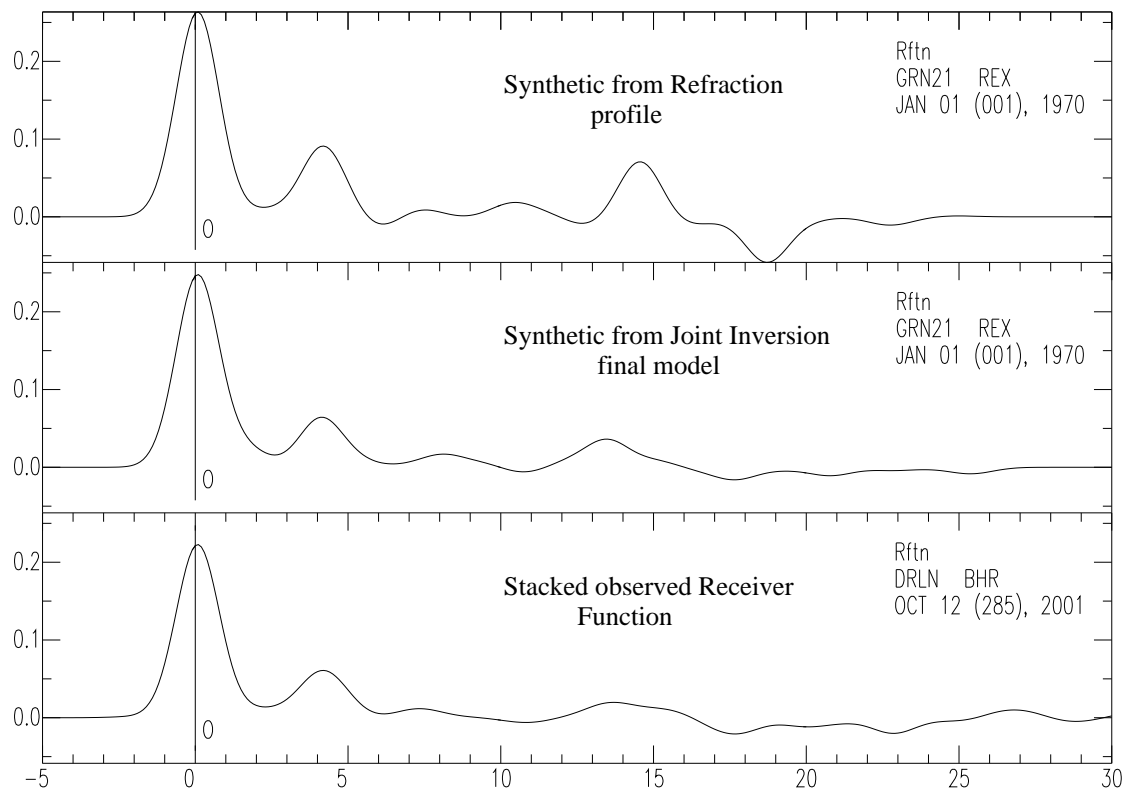


Figure 5.2: The model compares between the stacked receiver function for DRLN (ray parameter p 0.04-0.08 and $\alpha=1.0$) with the synthetic receiver function estimated from the final model from Hughes et al. (1992) and the final model from the joint inversion techniques (ray parameter $p=0.06$ and $\alpha = 1.0$).

an analysis of teleseismic receiver function (Owens, 1987), a seismic refraction profile O-NYNEX (Hughes et al., 1992) and an electromagnetic study (Connerney et al., 1980). The seismic models show a high P- or S-velocities at depths of 18-27 km (Figure 5.3). This high velocity was associated with a high conductivity anomaly in the middle crust, Tahawus Complex (Connerney, et al., 1980). Figure 5.4 compares the stacked observed receiver function to those predicted from the joint inversion and a simplified refraction model based on Hughes et al. (1992). The comparison focuses on a ray parameter of 0.06 sec/km. The refraction model synthetics do not agree perfectly with the observed because I used a simplified model of 3 layers over a halfspace. The timing of the direct and P_s pulses are predicted. The lack of agreement at 15-25 seconds, indicates that the simplified model has velocity boundaries that are too sharp. As expected the joint inversion model fits the observations better because this model must fit the receiver functions.

The joint inversion shear-velocity model shows a low velocity layer between the high velocity zone and the upper mantle. This is expected if the high conductivity layer is associated with the formation of serpentine, which would tend to reduce the seismic velocity.

5.3.3 Structure near SLM

Catchings (1999) presented a detailed study of the crust and upper mantle structure in eastern Missouri. The final result from this study is in good agreement with the inverted model from the joint inversion (Figure 5.5). The ob-

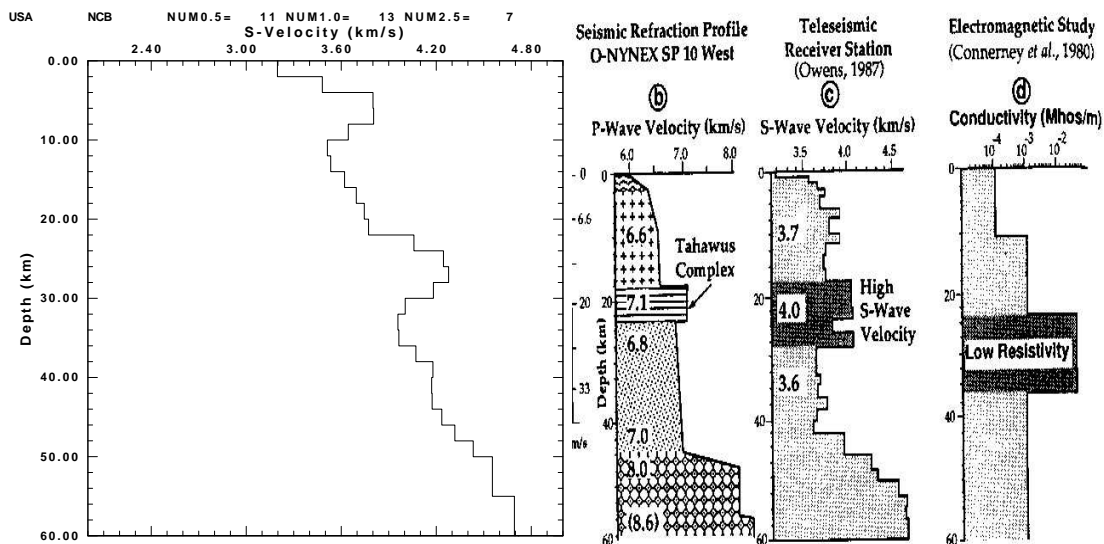


Figure 5.3: The plot compares the final model inverted from this study for NCB and different models as indicated by the model captions. All models reflect the present of the high velocity layer in the middle crust.

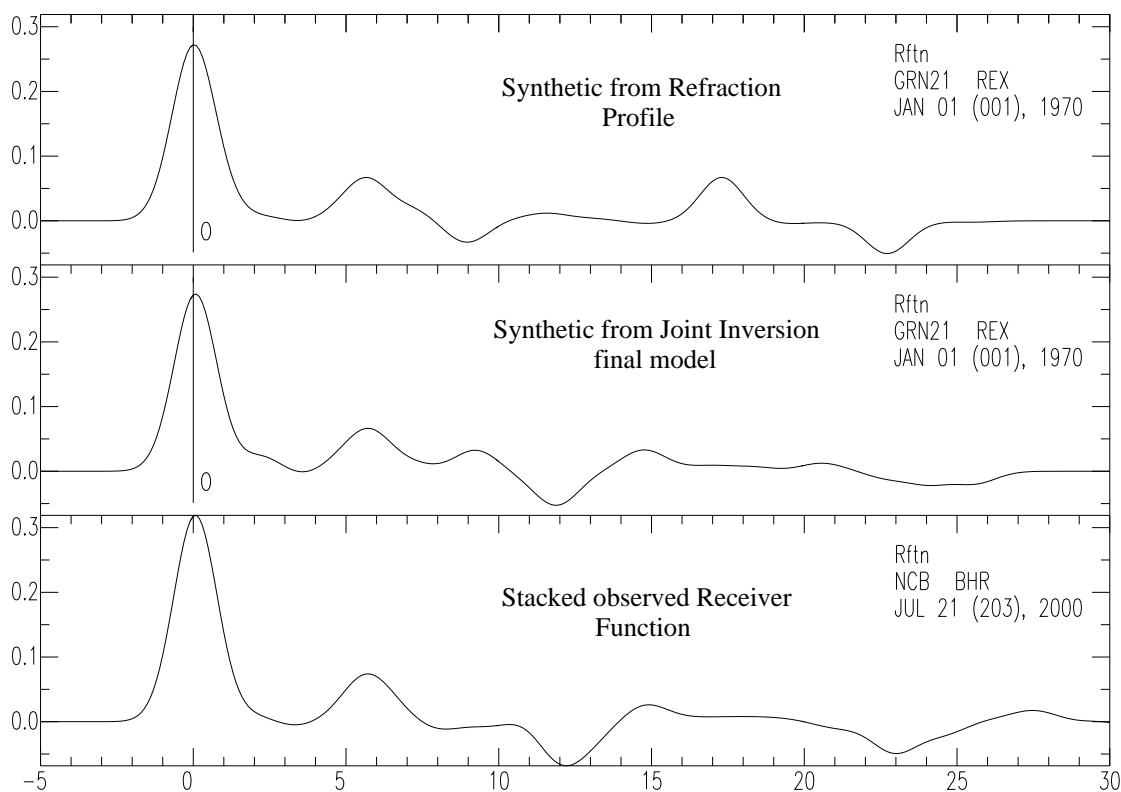


Figure 5.4: Compression between the synthetic receiver function computed from the refraction model and the joint inversion final model (ray parameter $p=0.06$ and $\alpha=1.0$) and the stacked receiver function for NCB station (ray parameter p 0.04-0.08 and $\alpha=1.0$).

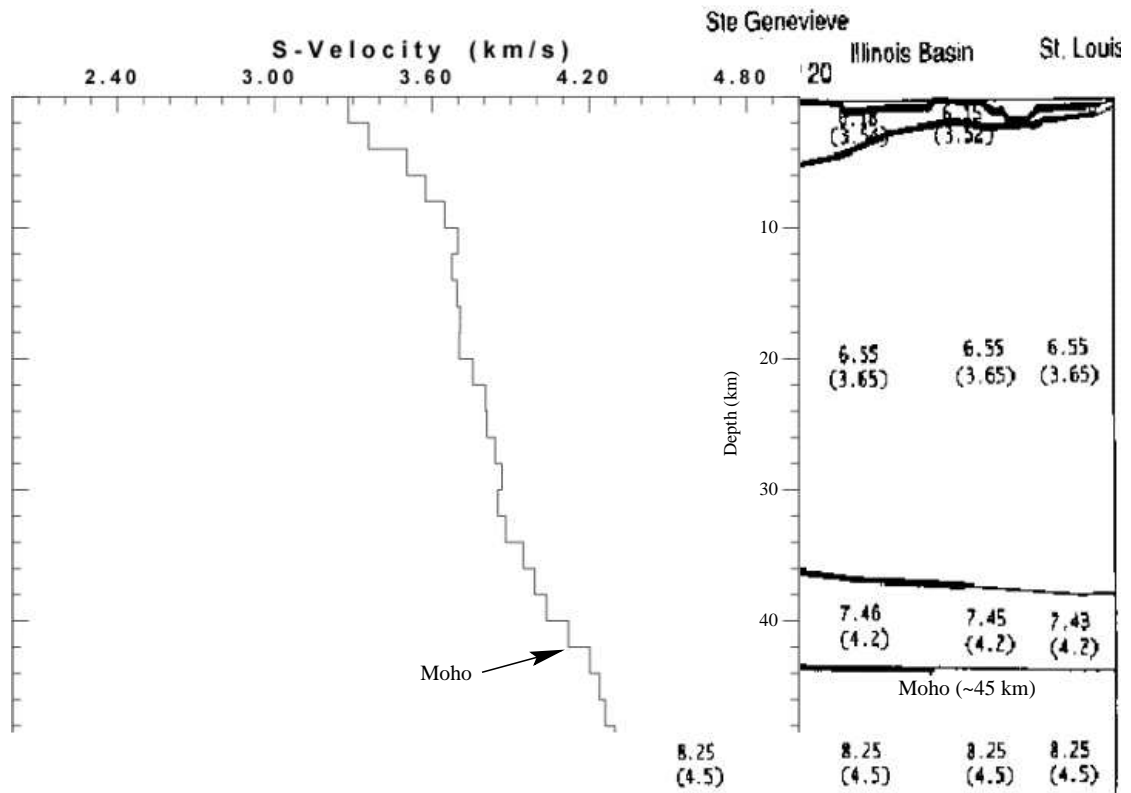


Figure 5.5: The final model inverted using joint inversion is in good agreement with the final model from Catchings (1999).

served and predicted receiver functions are compared in Figure 5.6. In fact they are much simpler than ones at NCB or even DRLN, pointing to the smoother crustal velocity-depth function. The striking feature of the SLM velocity models is the very uniform crust between 10 and 30 km.

These few examples show that the joint inversion method has yielded some acceptable shear velocity profiles. The final models may have features that may be the result of noise or the use of a uniform one-time inversion procedure. We have confidence that the joint inversion succeeds in imaging the crust and upper mantle precisely because it combines the receiver function sensitivity to velocity discontinuities with the uniform crustal velocity sampling of the sur-

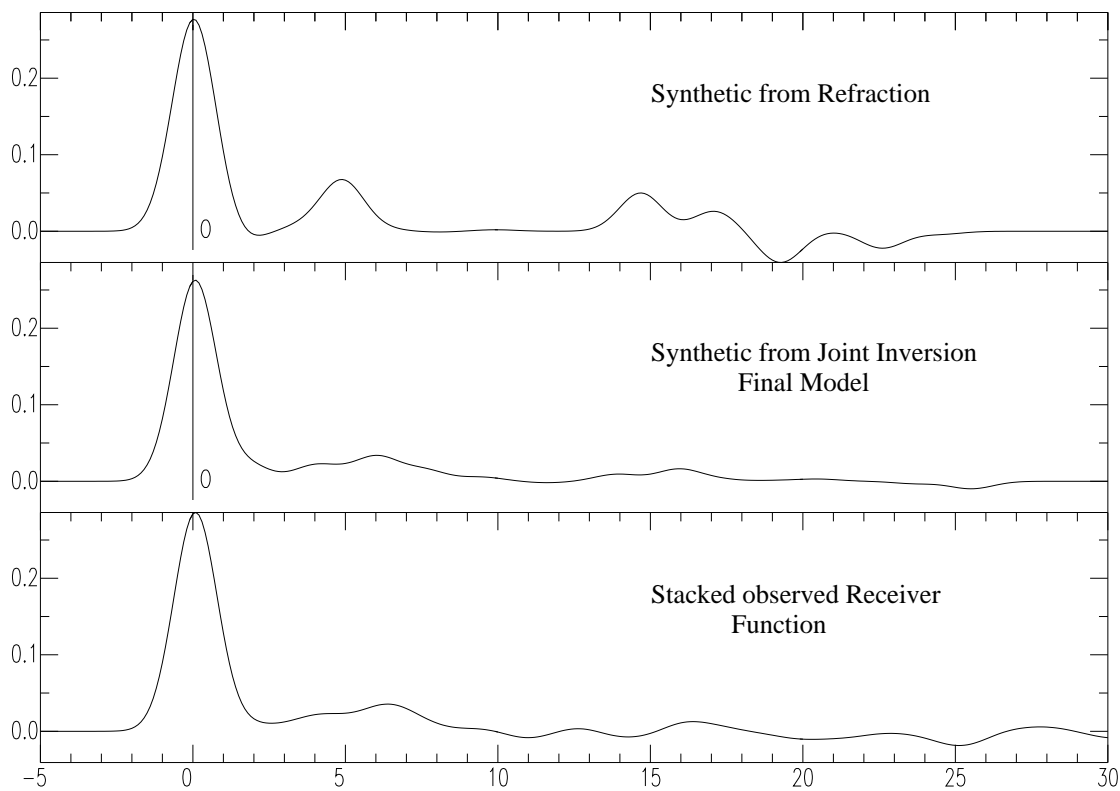


Figure 5.6: The synthetic receiver function computed from the final model for both refraction method (Catchings, 1999) and joint inversion techniques (ray parameter $p = 0.06$ and $\alpha = 1.0$) and the stacked receiver function for SLM as a function of ray parameter (ray parameter p 0.04-0.08 and $\alpha = 1.0$). Both receiver function have the same features with different amplitude.

face wave. The joint inversion does not work well in the cases that the receiver function has no such information because of the lack of a sharp Moho or because of an overwhelming signature of wave reverberation at shallow depth. Thus the joint inversion is a tool to be used to constrain crustal structure that may work in some regions.

5.4 Future Work

Recently the National Science Foundation funded a major research effort, USArray, that involves the deployment of hundreds of three-component broadband seismometers on a uniform grid that will cover the continental U.S. over a ten year period. In addition, support and instruments will be available for passive and active experiments to augment the transportable array. Besides providing the data to study the deep interior of the Earth, the data will also be used to image crustal structure of the continent. The teleseismic P-wave receiver functions and the dispersion across the array will be used to form this image.

Although the 125 locations used in this dissertation to study crustal structure are at least an order of magnitude less than the expected number of USArray sites, I believe the experience gained here is valuable. I have used station specific surface-wave dispersion estimates together with the receiver functions themselves. I have found sites at which the crustal phase signature is overwhelmed by shallow sedimentary structure. I expect that successful analysis of USArray data at these sites will require some imaginative signal processing

to be able to see the Moho. I have also found that there is spatial variability in the ability to image the Moho.

This study has demonstrated the usefulness of the three-component seismic data that are now available from different seismic networks. This research identifies several stations, e.g. FA22-FA28, NHSC, DWPF, and MPH, that were affected by the thick shallow sedimentary structure. This serves as a caution on a complete reliance on receiver functions for crustal structure determination. It is hoped that by illustrating some properties and applications of the receiver functions and joint inversion techniques, and by providing a comparison of the velocity models at these stations, this dissertation will encourage more detailed studies at these stations. Further studies would be most effective by incorporating a variety of geophysical techniques and would improve our understanding of the earth structure and tectonic evolution of the study area.

Appendix A

Stacked Receiver Functions for all Stations

Because of the large number of stations and receiver functions examined as part of this investigation, it is not possible to present them all because of size limitations. To evaluate the quality of the data for each station in the manner done in Chapter 3. It is useful, however, to show them in a concise manner. This is accomplished by stacking the receiver functions at a station, irrespective of the ray parameter or azimuth.

For each station, receiver functions used in the joint inversion are stacked. These receiver functions were required to satisfy the criteria that they explain at least 90% and 80% of the Gaussian filtered observed radial component, for Gaussian parameters of α of 1.0 and 2.5, respectively. In the plots to follow, both stacked receiver functions are plotted in two columns for the two α values. The plot time scale is -5 to 30 seconds. Ideally, the first pulse should be symmetric about a 0 second delay. The number of individual receiver functions used in the stack is plotted at the end of each trace.

There are some notable receiver function. The P-wave radial receiver functions FA02, FA21-27, GWDE, MPH, NHSC, OXF and UTMT exhibit a ringing character which is due to a shallow low-velocity structure beneath the site. The receiver functions for MM17, MM18, MO18 and HRV have observable Moho bounce phases.

It is hoped that this presentation serves to show environments where application of the receiver function technique for studying crustal structure may be difficult and also show sites where more data are required for a complete study.

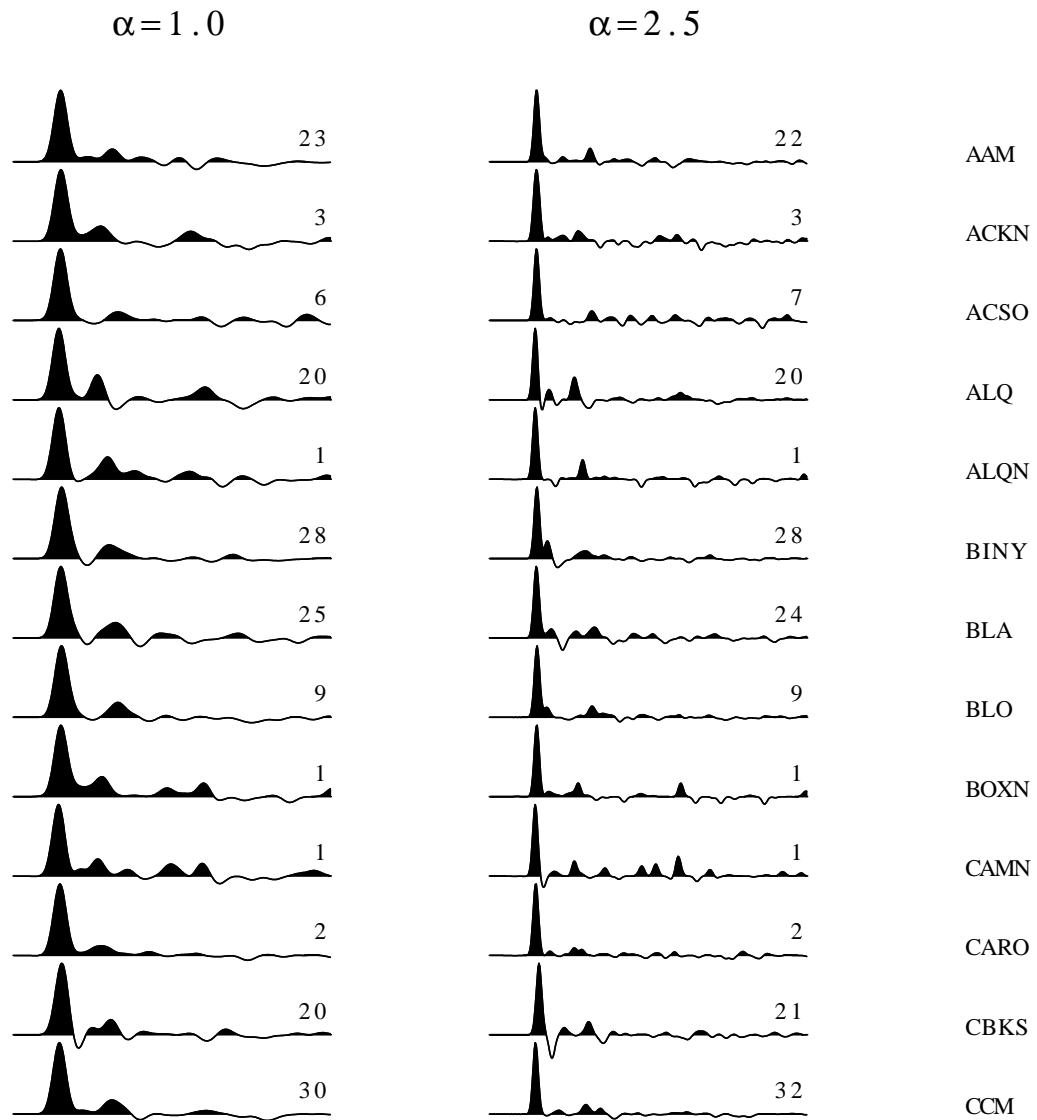


Figure A.1: Stacked receiver functions as a function of ray parameters.

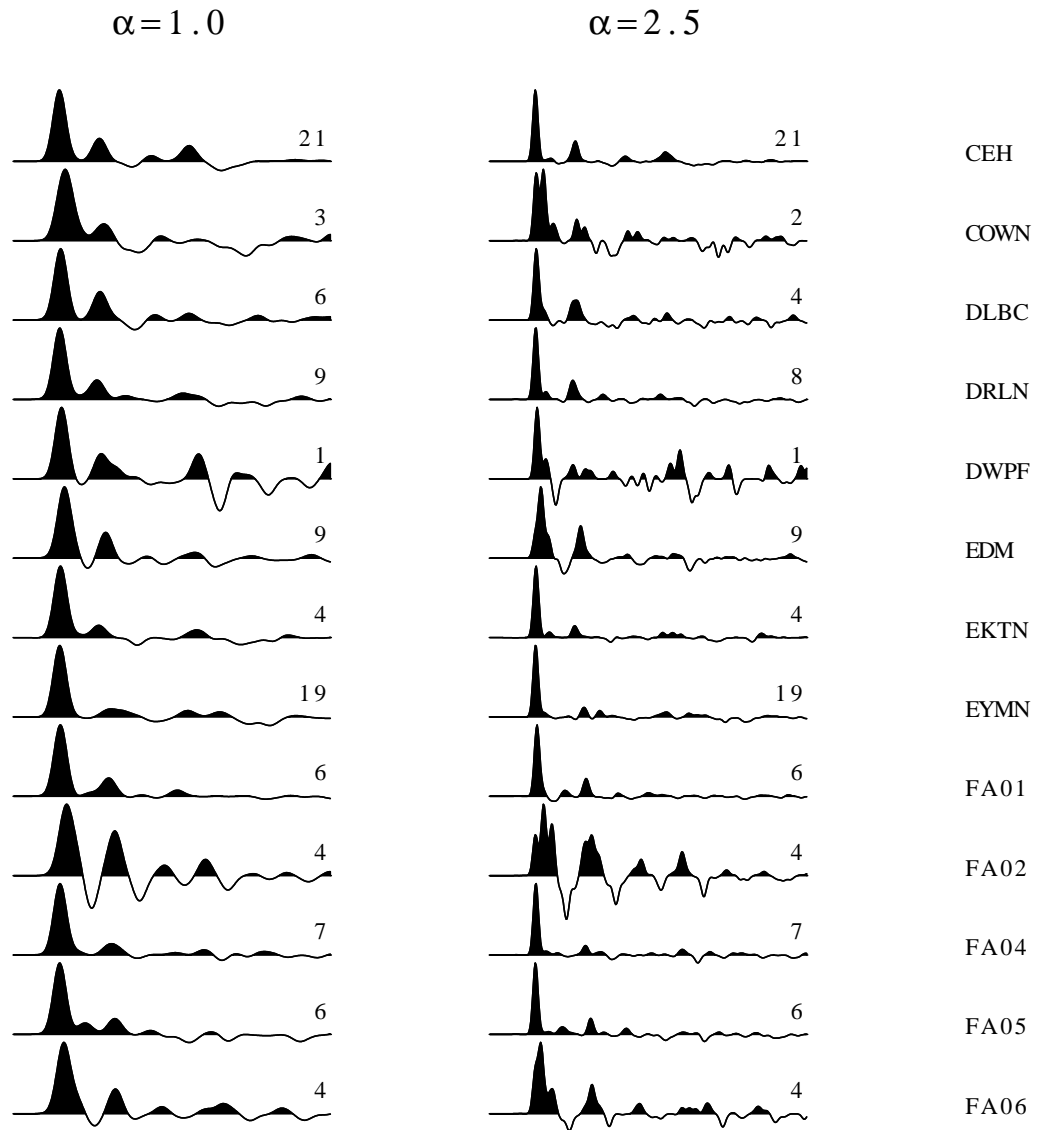


Figure A.2: Stacked receiver functions as a function of ray parameters.

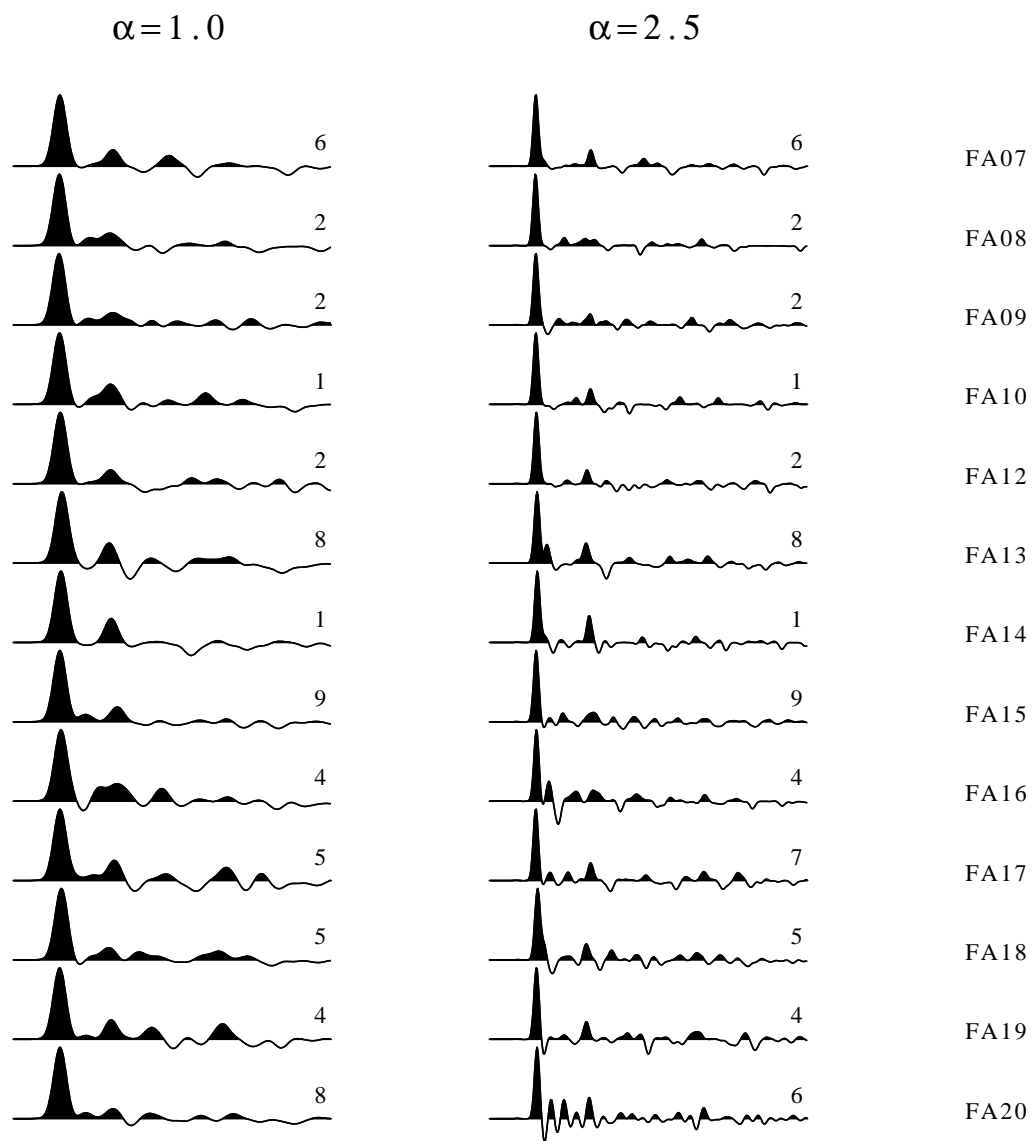


Figure A.3: Stacked receiver functions as a function of ray parameters.

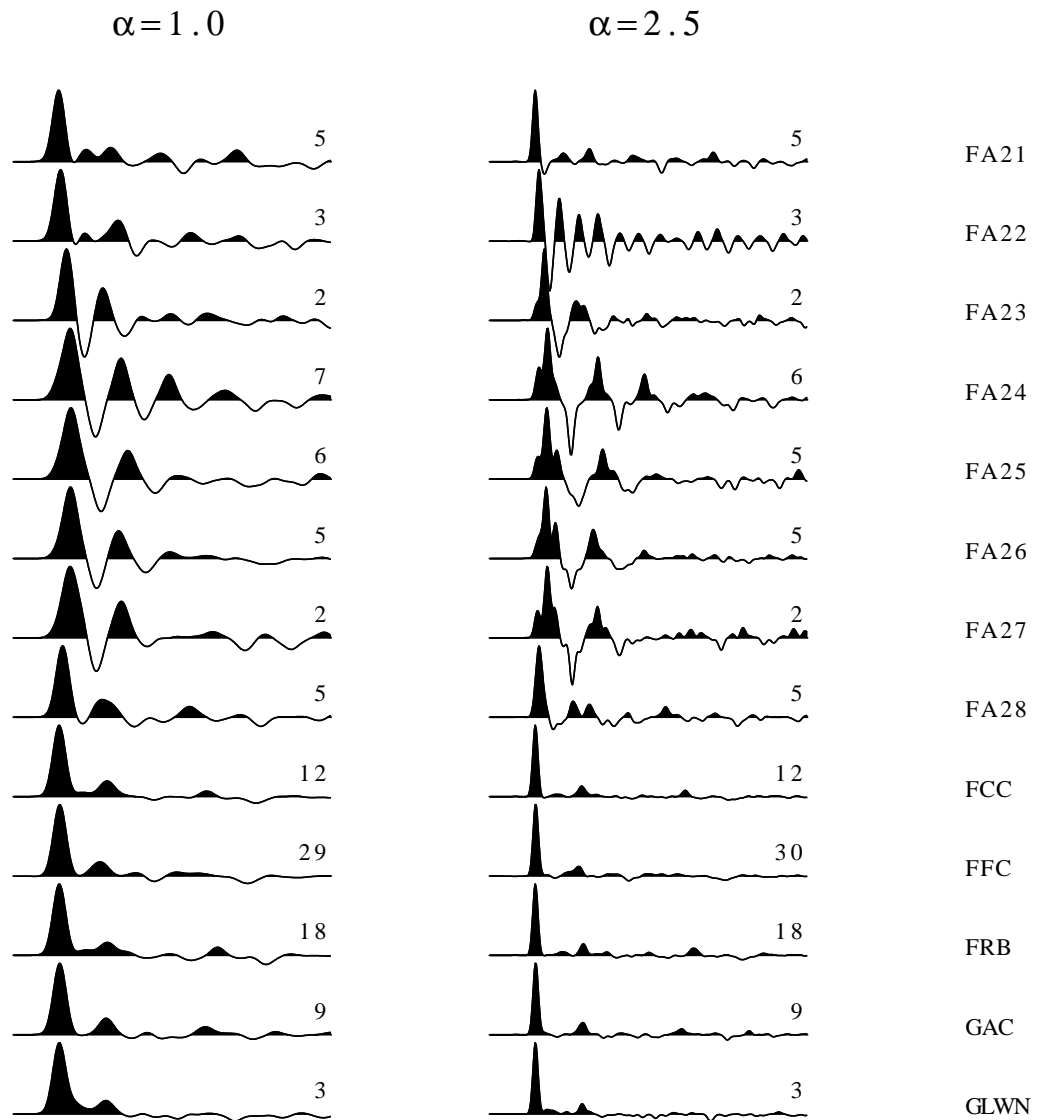


Figure A.4: Stacked receiver functions as a function of ray parameters.

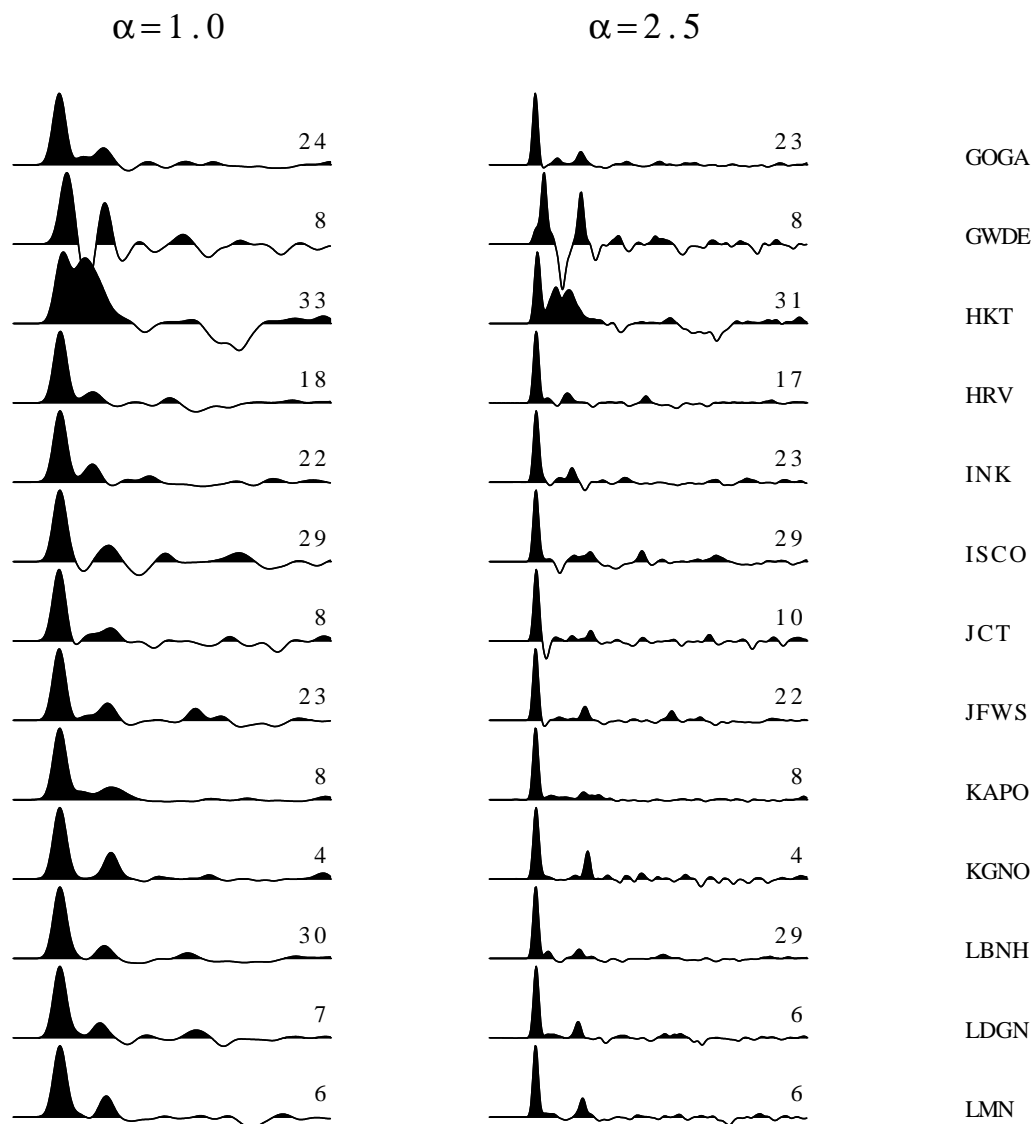


Figure A.5: Stacked receiver functions as a function of ray parameters.

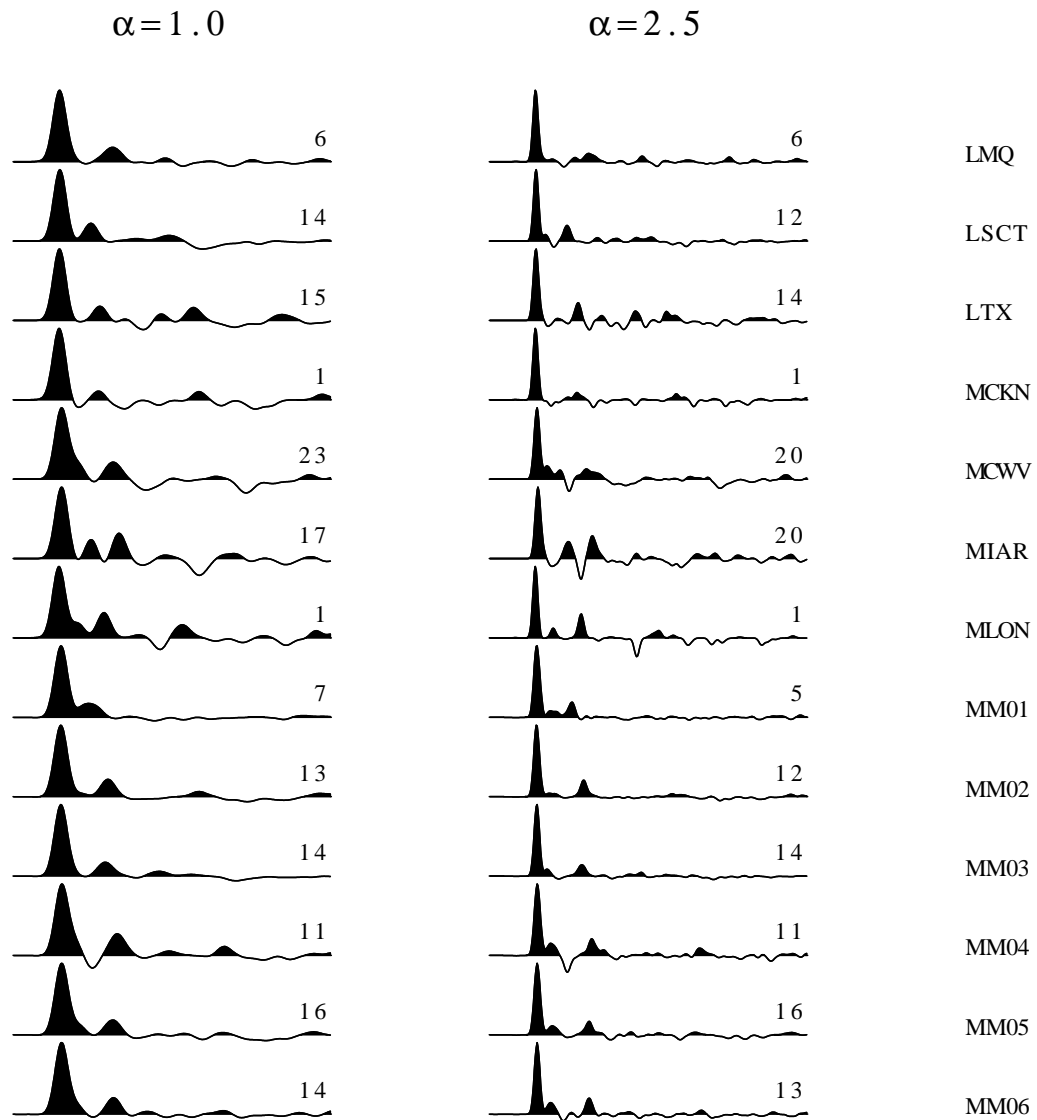


Figure A.6: Stacked receiver functions as a function of ray parameters.

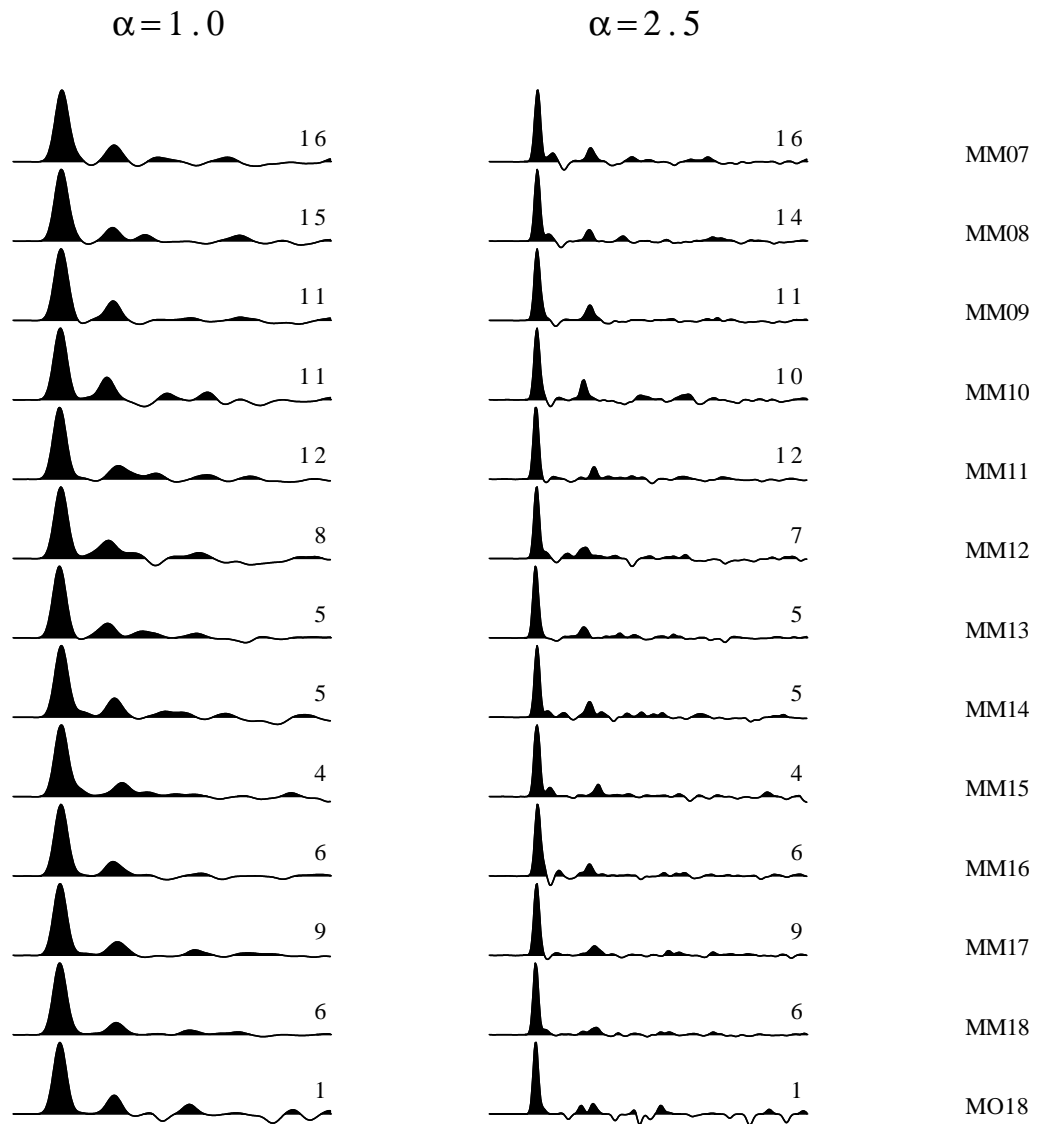


Figure A.7: Stacked receiver functions as a function of ray parameters.

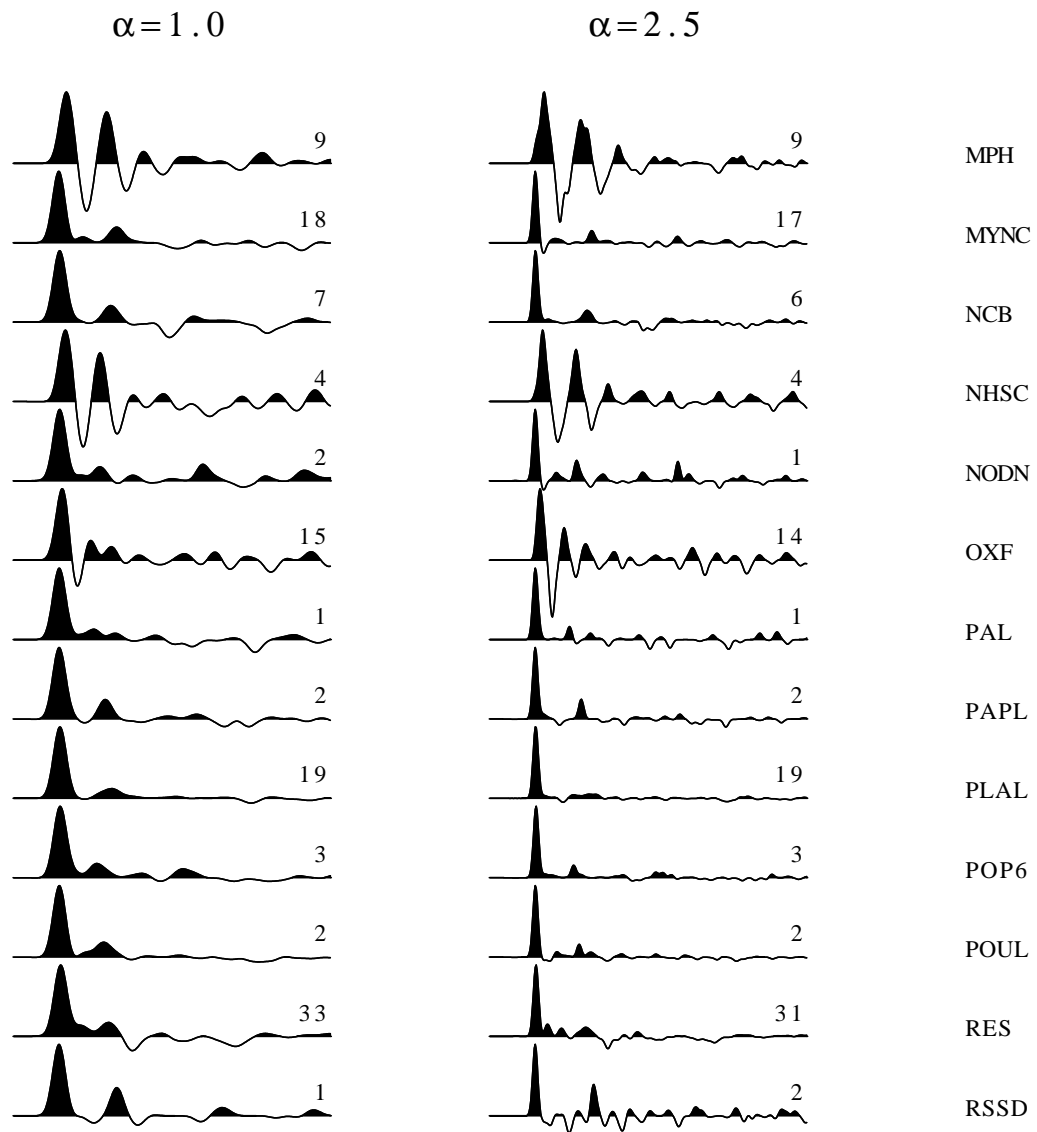


Figure A.8: Stacked receiver functions as a function of ray parameters.

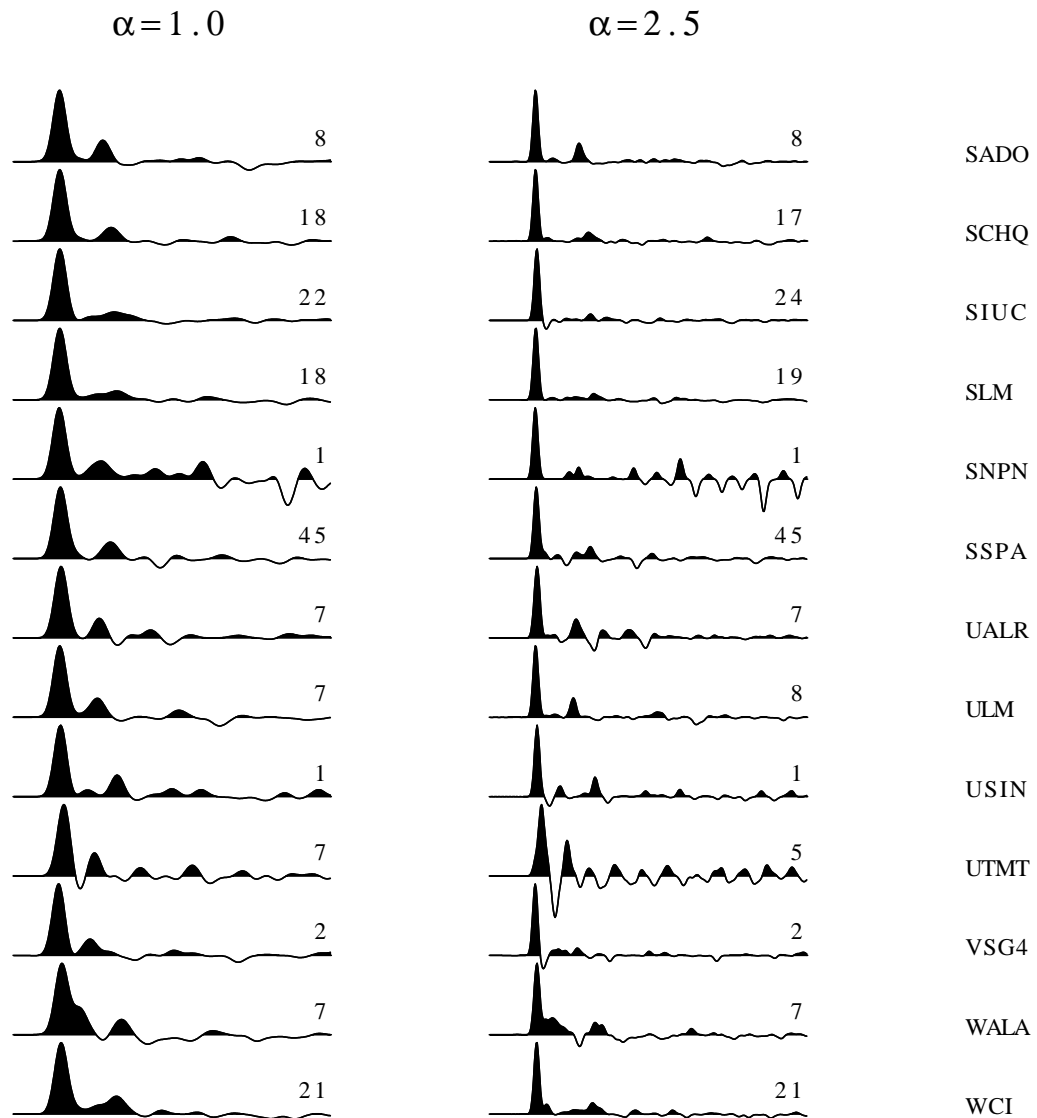


Figure A.9: Stacked receiver functions as a function of ray parameters.

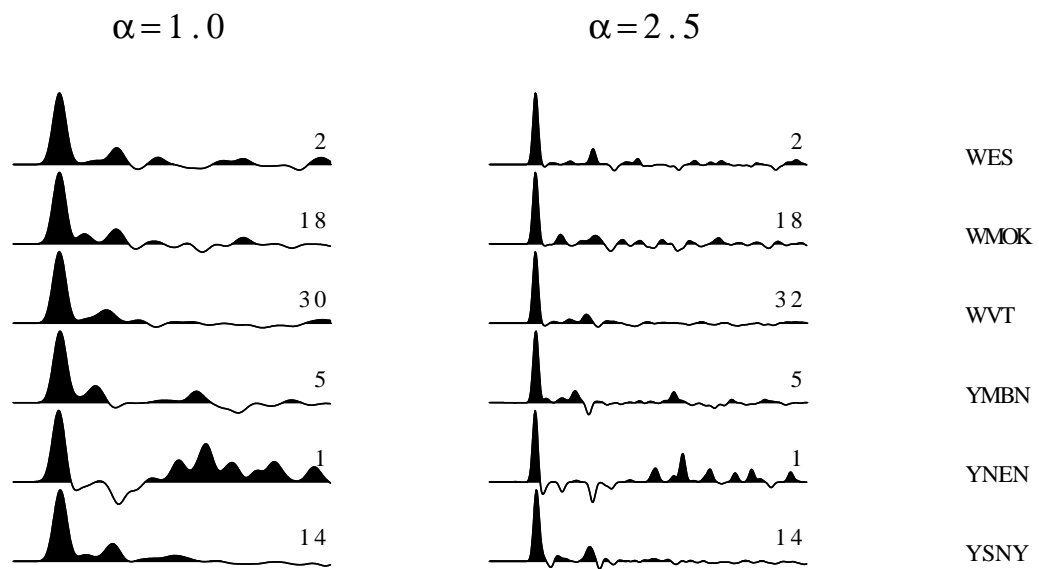


Figure A.10: Stacked receiver functions as a function of ray parameters.

References

- Adams, J. and P. W. Basham (1991). "The seismicity and seismotectonics of eastern Canada" In: Neotectonics of North America , D.B. Slemmons, E.R. Engdhal, M.D. Zoback, and D.D. Blackwell (eds), *Geological Society of America, Boulder, Colorado, Decade Map Volume 1*.
- Akinci, A., R. B. Herrmann, and N. Akyol (1999). Site Amplification at the Deep Sedimentary Deposits. Proceedings of the International Conference on Earthquake Hazard and Risk in the Mediterranean region, 18-22October, Nicosia, North Cyprus p:353-358.
- Ammon, C. J. (1991). The isolation of receiver effects from teleseismic P-waveforms, *Bull. Seism. Soc. Am.*, 81, 2504-2510.
- Ammon, C. J., G. E. Randall, and G. Zandt (1990). On the nonuniqueness of receiver function inversions, *J. Geophys. Res.*, 95, 15303-15318.
- Ammon C. J. and G. Zandt (1993). Receiver structure beneath the southern Mojave block, California, *Bull. Seism. Soc. Am.*, 83, 737-755.
- Bally, A. W. (1989). Phanerozoic basins of North America. In: Bally, A.W., and A. R. Palmer, eds. The Geology of North America-An overview. *Boulder, Co. Geological Society of America, The Geology of North America, v. A*.
- Bally, A. W. and A. R. Palmer, eds. (1989). The Geology of North America-An overview. *Boulder, Co. Geological Society of America, The Geology of North America, v. A*.
- Barruol, G., P. G. Silver, and A. Vauchez (1997). Seismic anisotropy in the eastern United States: Deep structure of a complex continental plate, *J. Geophys. Res.*, 102, 8329-8348.
- Baquer, S. A and B. J. Mitchell (1998). Regional Variation of Lg Coda Q in the Continental United States and its Relation to Crustal Structure and Evolution, *Pure and appl. geophys.*, 153, 613-638.
- Berry, M. J. and K. Fuchs (1973). Crustal structure of the Superior and Grenville Provinces of the Northeastern Canadian Shield., *Bull. Seism. Soc. Am.*, 63, 1393-1432.
- Bickford, M. E., W. R. Van Schmus, and I. Zietz (1986). Proterozoic History of the Midcontinent Region of North America. *Geology*, V. 14, pp. 492-496.
- Birch, A.F. (1958). Interpretation of the seismic structure of the crust in the light of experimental studies of wave velocities in rocks. In: *Benioff, V.H. (Ed.), Contributions in Geophysics. Pergamon, Oxford*, pp. 158 - 170.

- Birch, F., R. F. Roy, and E. R. Decker (1968). Heat flow and thermal history in New England and New York, in *Studies of Appalachian Geology: Northern and Maritime*, edited by E-an Zen, W. S. White, J. B. Hadley, and J. B. Thompson, Jr., pp. 437-451, Interscience, New York.
- Black, P. R. , and L. W. Braile (1982). Pn velocity and cooling of the continental lithosphere, *J.Geophys. Res.* , v. 87, 10557-10568.
- Blackwell, D. D., J. L. Steele, and L. S. Carter (1991). Heat flow patterns of the North American Continent; A discussion of the geothermal map of North America, p. 423-437, in *Neotectonics of North America*, ed. D.B. Slemmons, E.R., Engdahl, M.D. Zoback, and D.D. Blackwell, *Geol. Soc. Am. Decade of North Am. Geol., Decade Map V. 1*, 498 pp.
- Bloch, S. and A. L. Hales (1968). New techniques for the determination of surface waves phase velocities. *Bull. Seismol. Soc. Amer.*, 58, 1021-1034.
- Boland, A. V. and R. M. Ellis (1990). Velocity structure of the Kapuskasing uplift, northern Ontario, from seismic refraction studies. *Journal of Geophysical Research*, 94: 7189-7204.
- Bollinger, G. A., M. G. Hopper (1970). Virginia's two largest earthquakes december, 22 1875 and May, 31 1897. *Bull. Seism. Soc. Am.*, 61, 1033-1039.
- Bollinger, G. A., M. C. Chapman, and T. P. Moore (1981). Central Virginia regional seismic network; crustal velocity structure in central and southwestern Virginia: U.S. *Nuclear Regulatory Agency NUREG CR-1217*, pp 187.
- Braile, L. W., and G. R. Keller (1975), Fine structure of the crust, inferred from linear inversion of Rayleigh wave dispersion, *Bull. Seism. Soc. Am.*, 65, 71-83.
- Braile, L. W., J. Hinze, R. R. B. von Frese and G. R. Keller (1989). Seismic properties of the crust and uppermost mantle of the conterminous United States and adjacent Canada. In: Pakiser, L.C. and W. D. Mooney, eds. *Geophysical Framework of the Continental United States. Mem. Geol. Soc. Am.*, 172, 655-680.
- Braile, L. W. and C. S. Chiang (1986). The continental Mohorovicic discontinuity: results from near-vertical and wide-angle seismic reflection studies. In: Barangazi, M. and L. Brown, eds. *Reflection Seismology: A global Perspective. Geodyn. Ser. 13. American Geophysical Union.* 257-272.
- Brune, J.N. and J. Dorman (1963). Seismic waves and Earth structure in the Canadian shield. *Bull. Seism. Soc. Am.* , 53, 287-303.
- Burdick, L. J. and C. A. Langston (1977). Modeling crustal structure through the use of converted phases in the teleseismic body waveforms. *Bull. Seism. Soc. Am.*, 67, 677-692.

- Cannon, W. F., M. W. Lee, W. J. Hinze, K. J. Schulz, and A. G. Green (1991). Deep crustal structure of the Precambrian basement beneath northern Lake Michigan, Midcontinent North America, *Geology*, 19, 207-210.
- Catchings, R.D. (1999). Regional Vp,Vs, Vp/Vs and Poisson's ratios across earthquake source zones from Memphis, TN to St. Louis, MO, *Bulletin of the Seismological Society of America*, 89, 1591-1605.
- Cassidy, J. F. (1992). Numerical experiments in broadband receiver function analysis, *Bull. Seism. Soc. Am.*, 82, 1453-1474.
- Cassidy, J. F. (1995). A comparison of the receiver structure beneath stations of the Canadian National Seismograph Network. *Can. J. Earth Sci.*, 32, 938-951.
- Cassidy, J. F., R. M. Ellis, C. Caravas, and G. C. Rogers (1998). The northern limit of the subducted Juan de Fuca plate system, *J. Geophys. Res.*, 103, 26949-26961.
- Christensen, N. I. (1996). Poisson's ratio and crustal seismology, *J. Geophys. Res.*, 101, 3139-3156.
- Christensen, N. I. and W. D. Mooney (1995). Seismic velocity structure and composition of the continental crust: A global view, *J. Geophys. Res.*, 100, 9761-9788.
- Chulick, G. S. and W. D. Mooney (2002). Seismic structure of the crust and uppermost mantle of North America and adjacent oceanic basins; a synthesis. *Bull. Seismol. Soc. Amer.*, 92, 2478-2492.
- Clayton, R. W. and R. A. Wiggins (1976). Source shape estimation and deconvolution of teleseismic body waves. *J. R. Astr. Soc.*, 47, 151-177.
- Clowes, R. M. (1993). Variations in continental crustal structure in Canada from LITHOPROBE seismic reflection and other data. *Tectonophysics*, 219, 1-27.
- Cook, F. A. (1984). Towards an understanding of the southern Appalachian Piedmont crustal transition. *Tectonophysics*, 109, 77-92.
- Cook, F. A., D. S., Brown, L. D., Kaufman, S., Oliver, and R. D., Hatcher (1979). Thin skinned tectonics in the crystalline southern Appalachian-COCORP seismic-reflection profile of the Blue Ridge and Piedmont: *Geology*, 7, 563-567.
- Cook, F. A., K. H. van der Velden, and B. Roberts (1998). Tectonic delamination and subcrustal imbrication of the Precambrian lithosphere in northwestern Canada mapped by LITHOPROBE. *Geology*, 26: 839-842.

- Costain, J. K., R. D. Hatcher Jr., C. Coruh, L. P. Thomas, S. R. Taylor, J. J. Lithner, and I. Zietz (1989). Geophysical characteristics of the Appalachian crust, in *The Geology of North America*, vol. F-2, The Appalachian- Ouachita Orogen in the United States, edited by R. D. Hatcher Jr., W. A. Thomas, and G. W. Viele, pp. 385 - 416, *Geol. Soc. of Am., Boulder, Colo.*
- Crough, S. T. (1981). Mesozoic hotspot epeirogeny in eastern North America, *Geology*, 9, 2-6.
- Curtis, A., J. Trampert, R. Sneider, and B. Dost (1998). Eurasian fundamental mode surface wave phase velocities and their relationship with tectonic structures, *J. Geophys. Res.*, 103, 26919-26947.
- Curtis, A. and J. H. Woodhouse (1997). Crust and upper mantle shear velocity structure beneath the Tibetan Plateau and surrounding regions from interevent surface wave phase velocity inversion, *J. Geophys. Res.*, 102, 11789-11813.
- Dainty, A. M., C. E. Keen, M. J. Keen and J. E. Blanchard (1966). Review of geophysical evidence on crust and upper-mantle structure on the seaboard of Canada. *Amer. Geophys. Union Mono. Ser.*, 10, 349-369.
- Dart, R. D., and Zoback, M. L. (1988). Well-bore breakout-stress analysis within the continental United States, paper L, in 2nd International Symposium on Borehole Geophysics for Minerals, Geotechnical, and Groundwater Applications [Golden, Colorado, October 6-8, 1987], proceedings: *Society of Professional Well Log Analysts, Minerals and Geotechnical Logging Society Chapter-at-Large*, p. 139-149. Later published in 1989 as, Wellbore breakout stress analysis within the central and eastern continental United States: *The Log Analyst*, v. 30, no. 1, January-February, p. 12-24.
- Deninson, R. E., E. G. Lidiak, M. E. Bickford, and E. B. Kisvarsanyi (1984). Geology and geochronology of precambrian rocks in the central interior region of the United States, in Harrison, J. E. and Z. E. Peterman, eds., correlation of Precambrian rocks of the US and Mexico: *U.S. Geol. Survey Prof.*, Paper 1241-C, C1-C20.
- Delandro, M., and W. Moon (1982). Seismic structure of Superior-Churchill Precambrian boundary zone. *J. Geophys. Res.*, 87, 6884-6888.
- Der, Z., R. Masse, and M. Landisman (1970). Effects of observational errors on the resolution of surface waves at intermediate distances. *J. Geophys. Res.*, 75, 3399-3415.
- Dewey, J. W., D. P. Hill, W. L. Ellsworth, and E. R. Engdahl (1989). Earthquakes, faults, and the seismotectonic framework of the contiguous United States, in Pakiser, L. C., and Mooney, W. D., eds., *Geophysical Framework*

- of the continental United States: *Geological Society of America Memoir* 172, p. 541-576.
- Dewey, J. F., M. L. Helman, E. Turco, D. H. W. Hutton, S. D., and Knott (1989). Kinematics of the western Mediterranean. In Coward, M.P., Dietrich, D., and Park, R.G. (Eds.), Conference on Alpine Tectonics. *Geol. Soc. Spec. Publ. London*, 45, 265-283.
- Dorman, J. and M. Ewing (1962). Numerical inversion of seismic surface wave dispersion data. *J. Geophys. Res.*, 67, 5227-5241.
- Dueker, K. G., and A. F. Sheehan (1997). Mantle discontinuity structure from midpoint stacks of converted P to S waves across the Yellowstone hotspot track, *J. Geophys. Res.*, 102, 8313-8327.
- Du, Z. J. and G. R. Foulger (1999). The crustal structure beneath the north-west fjords, Iceland, from receiver functions and surface waves, *Geophys. J. Int.*, 139, 419-432.
- Dziewonski, A. and D. L. Anderson (1981). Preliminary reference Earth model, *Phys. of Earth and Planet Int.*, 25, 297-356.
- Dziewonski, A. and M. Landisman (1969). A technique for the analysis of transient seismic signals, *Bull. Seism. Soc. Am.*, 59, 427-444.
- Dziewonski, A. M. and A. L. Hales (1972). Numerical analysis of dispersed seismic waves, in *Methods in Computational Physics, Volume 11, Seismology: Surface Waves and Earth Oscillations*, B. A. Bolt (Editor), Academic, New York, 39-85.
- Eaton, D. W. and J. F. Cassidy (1996). A relic Proterozoic subduction zone in Western Canada; new evidence from seismic reflection and receiver function data. *Geophysical Research Letters*, 23, 3791-3794.
- Ebel, J. E. and A. L. Kafka (1991). Earthquake Activity in the Northeastern United States, in *Neotectonics of North America*, D.B. Slemmons, E.R. Engdahl, M.D. Zoback and D. Blackwell, editors, *The Geological Society of America, Decade Map Volume 1*, pp. 277-290.
- Ekström, G., A. M. Dziewonski, G. P. Smith, and W. Su (1996). Elastic and inelastic structure beneath Eurasia, in *Proceeding of the 18th Annual Seismic Research Symposium on Monitoring a Comprehensive Test Ban Treaty 4-6 September, 1996*, Phillips Laboratory Report PL-TR-96-2153, July, pp. 309-318, ADA313692.
- Engdehl, E. R., W. A., Rinehart (1988). Seismicity map of North America, Continent-Scale map-004, Decade of North America Geology, *Geological Society of America*, scale 1:5,000,000, 4 sheets.
- Engdahl, E. R., M. D. Zoback, and D. D. Blackwell Eds. GSA Decade Map v. 1.

- Ervin, C. P., and L. D. McGinnis (1975). Reelfoot rift: Reactivated precursor to the Mississippi embayment, *Geological Society of America Bulletin*, 86, 1287-1296.
- Ewing, M., and F. Press (1959). Determining the crustal structure from phase velocity of Rayleigh waves; part 3, The United States: *Geological Society of America Bulletin*, 70, 229-244.
- Fernández, F. G., Clowes, R. M. (2003). Lithospheric structure beneath the Archean Slave province and Proterozoic Wopmay orogen. Northwestern Canada, from LITHOPROBE refraction wide/angle reflection survey. *Geophys. J. Int.*, 153, 1-19.
- Forsyth, D. A. (1981). Characteristics of western Quebec seismic zone, *Can. J. of Earth Sci.*, 18, 103-119.
- Forsyth, D. A., B. Milkereit, C. A. Zelt, D. J. White, R. M. Easton and D. R. Hutchinson, (1994). Deep structure beneath Lake Ontario: crustal-scale Grenville subdivisions, *Can. J. Earth. Sci.*, 31, 225-270.
- Fowler, C. M. R. (1998). *The solid Earth: An introduction to global geophysics*, Cambridge University Press, Cambridge.
- Fountain, D.M., M. H. Salisbury, and J. A. Percival (1990). Seismic structure of the continental crust based on rock velocity measurements from the Kapuskasing uplift. *J. Geophys. Res.*, 95, 1167-1186.
- Gibb, R.A. and D. C., Thomas (1976). Gravity signature of fossil plate boundaries on the Canadian Shield. *Nature*, 262, p. 199-200.
- Godlewski, M. J., and G. F., West (1977). Rayleigh-wave dispersion over the Canadian Sheild, *Bull. Seism. Soc.Am.*, 67, 771-779.
- Goodacre, A.K. (1972). Generalized structure and composition of the deep crust and upper mantle in Canadian sheild, *J. of Geophys. Res.*, v. 77, p. 3146-3161.
- Green, A.G., B. Milkereit, A. Davidson, C. Spencer, D. R. Hutchinson, W. F. Cannon, M. W. Lee, W. F. Agena, J. C. Behrendt, and W. J. Hinze (1988). Crustal s tructure of the Grenville front and adjacent terranes: *Geology*, 16, 788-792.
- Gurrola, H., J. B. Minster and T. J. Owens (1994). The use of velocity spectrum for stacking receiver functions and imaging upper mantle discontinuities, *Geophys. J. Int.*, 117, 427-440.
- Gurrola, H., G. E. Baker and J. B. Minster (1995). Simultaneous time domain deconvolution with application to the computation of receiver functions, *Geophys. J. Int.*, 120, 537-543.

- Hale, L. D. and G. A. Thompson (1982). The seismic reflection character of the continental Moho discontinuity. *J. Geophys. Res.*, 87, 4625-4635.
- Hammer, R. M., R. M., Clowes, and R. M., Ellis (1997). ACCRETE crustal velocity structure across the transition between the Coast Plutonic Complex and Stikinia, LITHOPROBE SNORCLE Transect Workshop, *LITHOPROBE Report No. 56*, P. 160-168.
- Hannet, C. G., J. H., Luetgert, and R. A., Phinney (1991). The crustal structure in Central Main from coherency processed refraction data. *J. Geophys. Res.*, 96, 12023-12037.
- Harris, L. D., and K. C., Bayer (1981). Sequential development of the Appalachian orogeny above a master decollement; A hypothesis, *Geology*, 7, 568-572.
- Haskell, N.A. (1953). The dispersion of surface waves in multilayered media, *Bull. Seism. Soc. Am.*, 43, 17-34.
- Hatcher, R.D. (1987). Tectonics of the Southern and Central Appalachian Internides, *Annual Reviews of Earth and Planetary Sciences*, 15, 337-362.
- Hatcher, R.D., and I., Zietz (1980). Tectonic implications of regional aeromagnetic and gravity data from the Southern Appalachians, in Wones, D. R., ed., proceedings, The Caledonides in the U.S.A.; IGCP project 27:Blacksburg, Virginia Polytechnic Institute and State University Memoir 2, 235-244.
- Herrmann, R. B., (1973). Some aspects of band-pass filtering of surface waves, *Bull. Seism. Soc. Am.*, 63, 663-671.
- Herrmann, R. B. (1977). On the determination of the impulse response of seismograph systems with emphasis on the SRO system, *Earthquake Notes*, 48, No. 1-2, 3-23.
- Herrmann, R. B. (1979). Surface waves focal mechanisms for eastern North America earthquakes with tectonic implications. *J. Geophys. Res.*, 84, 3543-3552.
- Herrmann, R. B. (1987). Computer program in seismology, Volume IV, Saint Louis University.
- Herrmann, R. B. and C. J., Ammon (2002). Computer program in seismology; surface waves, receiver functions, and crustal structure, Version 3.15, Saint Louis University.
- Hinze, W. J., and L. W., Braile (1988). Geophysical aspects of the craton; U.S. in Sloss, L.L., ed, Sedimentary cover - North America craton, U.S.:Boulder, Colorado, Geological Society of America, *Geol. of North America*, D-2, 5-24.

- Hoffman, P. F. (1989). Precambrian geology and tectonic history of North America. In: Bally, A.W., and A. R. Palmer, eds. *The Geology of North America- An overview. Boulder, Co. Geological Society of America, The Geology of North America, v. A.*
- Holbrook, W.S., E.C. Reiter, G.M. Purdy, and M.N. Toksoz (1992). Image of the Moho across the continent-ocean transition, U.S. east coast, *Geology*, 20, 203-206.
- Holbrook, W.S., G.M. Purdy, J.A. Collins, R.E. Sheridan, D.L. Musser, L. Glover III, M. Talwani, J.I. Ewing, R. Hawman, and S.B (1992). Smithsonian, Deep velocity structure of rifted continental crust, U.S. mid-Atlantic margin, from wide-angle reflection/refraction data, *Geophys. Res. Lett.*, 19, 1699-1702.
- Hughes S, and J Luetgert (1992). Crustal structure of the southeastern Grenville province, northern New York and Eastern Ontario, *J. Geophys. Res.*, 97, 17455-17479.
- Hughes, S., and J. H., Luetgert (1991). The 1988 New England-New York seismic refraction profile: Crustal structure of the northern Appalachian and Adirondack mountains: *Journal of Geophysical Research*, v. 96, p. 16,471-16,494.
- Hughes, W. J. (1994). Magnetospheric ULF waves: A tutorial with a historical perspective, in *Solar Wind Sources of Magnetospheric Ultra-Low-Frequency Waves*, Geophysical Monograph 81, edited by M. J. Engebretson, K. Takahashi, and M. Scholer, Washington, D.C.: *American Geophysical Union*, 265.
- Hurich, C. A., S. J., Deemer, and A., Indares (2001). Compositional and metamorphic controls on velocity and reflectivity in the continental crust: an example from the Grenville Province of eastern Québec. *J. Geophys. R.*, 106, 665-682.
- Hutchinson, D.R., Grow, J.A., and K. D., Klitgord (1983). Crustal structure beneath the southern Appalachians: Non-uniqueness of gravity modeling: *Geology*, v. 11, p. 611-615
- James, D. E., T. J. Smith, and J. S. Steinhart (1966). Crustal structure of the Middle Atlantic states, *Journal of Geophysical Research*, 73, 1983- 2008.
- Jaupart, C., J. R., Mann, and G., Simmons (1982). A detail study of the distribution of heat flow and radioactivity in New Hampshire, U.S.A.: *Earth and Planetary Science Letter*, 59, 267-287.
- Jessop, A. (1990b). Geothermal evidence of climatic change, report AGU 1989 fall meeting: *EOS, Transactions, American Geophysical Union*, v. 71, no. 15, April 10, p. 390-391.

- Jessop, A. M. (1990a). Thermal geophysics: Elsevier, Amsterdam, Developments in Solid Earth Geophysics No. 17, 306 p.
- Juli, J., C. J. Ammon, R. B. Herrmann, A. M. Correig (2000). Joint inversion of receiver function and surface wave dispersion observations, *Geophys. J. Int.*, 143, 1-19.
- Kean, E. A., and L. T. Long (1980). A seismic refraction line along the axis of the southern Piedmont and crustal thickness in the northeastern United States, *Earthquakes Notes*, 51, 3-13.
- Keilis-Borok, V. I., (ed.) (1989). Seismic surface waves in a laterally inhomogeneous Earth, Kluwer Academic Publishers, Netherlands.
- Keilis-Borok, V. I. and T. B. Yanovskaja (1967). Inverse problems of seismology (structural review), *Geophys. J. R. Astr. Soc.*, 13, 223-234.
- Keller, G. R., E. G. Lidiak, W. J. Hinze, L. W. Braile (1983). The role of rifting in the tectonic development of the Midcontinent, U.S.A., *Tectonophysics*, 94, 391-412.
- Kellett, R. L., A. E. Barnes, and M. Rive (1994). The deep structure of the Grenville Front: a new perspective from western Quebec; *Canadian Journal of Earth Sciences*, 31, 282-292.
- Kennett, B. L. N., E. R. Engdahl, and R. Buland (1995). Constraints on seismic velocities in the earth from travel time. *Geophys. J. Int.*, 122, 108-124.
- Kikuchi, M. and H. Kanamori (1982). Inversion of complex body waves. *Bull. Seism. Soc. Am.*, 72, 491-506.
- Klemperer, S. L., L. Brown, J. E. Oliver, C. J. Ando, B. L. Czuchra, S. Kaufman (1985). Some Results of COCORP seismic reflection profiling in the Grenville - age Adirondack Mountains New York State: *Can. J. Earth Sci.*, 22, 141 - 153.
- Kovach, R. L. (1978). Seismic surface waves and crustal and upper mantle structure. *Reviews of Geophys. and space physics*, 16, 1-13.
- Kurita, T. (1973). Regional variation in the structure of the crust in the central United States from P wave spectra. *Bull. Seism. Soc. Am.*, 63, 1663-1687.
- Kusky, T. M. (1989). Accretion of the Archean Slave Province, *Geology*, 17, 63-67. Larson, E. W. F. and G. Ekström (2001), Global Models of Group Velocity, *Pure and Applied Geophys.*, 158, 1377 -1399.
- Langston, C. A. (1979). Structure under Mount Rainier, Washington, inferred from teleseismic body waves, *J. Geophys. Res.*, 84, 4749-4762.

- Langston, C. A. (1994). An integrated study of crustal structure and regional wave propagation for southeastern Missouri, *Bull. Seism. Soc. Am.*, 84, 105-118.
- Larson, E. W. and G. Ekström (2001). Global models of surface wave group velocity, *Pure Appl. Geophys.*, 158, 1377-1400.
- Larson, E. W. and G. Ekström (1999). Global models of surface wave group velocity, Manuscript submitted for publication.
- Last, R. J., A. A. Nyblade, C. A. Langston, and T. J. Owens (1997). Crustal structure of the East African Plateau from receiver functions and Rayleigh wave phase velocities, *J. Geophys. Res.*, 102, 24,469-24,483.
- Lay T. and T. C. Wallace (1995). *Modern global seismology*, Academic Press, San Diego.
- Levshin, A. L., M. H. Ritzwoller, and S. S. Smith (1996). Group velocity across Eurasia, in *Proceeding of the 18th Annual Seismic Research Symposium on Monitoring a Comprehensive Test Ban Treaty 4-6 September, 1996*, Phillips Laboratory Report PL-TR-96-2153, July, pp. 70-79, ADA313692.
- Li, A., K. M. Fischer, S. van der Lee, M. E. Wysession (2002). Crust and upper mantle discontinuity structure beneath eastern North America, *J. Geophys. Res.*, 107, 10.1029/2001JB000190.
- Ligorra, J. P. (2000). An investigation of the Mantle-Crust Transition beneath North America and Poisson's ratio of the North America crust. Unpublished Doctoral Dissertation, Saint Louis University, Saint Louis, Mo.
- Ligorra, J. P. and C. J. Ammon (1999). Iterative deconvolution and receiver-function estimation, *Bull. Seism. Soc. Am.*, 89, 1395-1400.
- Lond, L. T., U. P. Mathur (1972). Southern Appalachian crustal structure from the dispersion of Rayleigh waves and refraction data: *Earthquakes Notes*, 43, 31-39.
- Luetgert, J. M., C. H. Mann, and S. L. Klemperer (1987). Wide-angle deep crustal reflection in the northern Appalachina. *Geophys. J. Roy. Astro. Soc.*, 89, 183-188.
- Mangino, S. G., G. Zandt, and C. J. Ammon (1993). The receiver structure beneath Mina, Nevada, *Bull. Seism. Soc. Am.*, 83, 542-560.
- McCamy, K. and R. P. Meyer (1966). Crustal results of fixed multiple shots in the Mississippi Embayment, in *The earth beneath the continents*, ed. by Steinhart, J. S., and T. J. Smith, *AGU Geophys. Monog.* 10, 141-165.
- McNamara, D. E. and T. J. Owens (1993). Azimuthal shear wave velocity anisotropy in the Basin and Range Province using Moho Ps converted phases, *J. Geophys. Res.*, 98, 12003-12017.

- McNamara, D. E., W. R. Walter, T. J. Owens, and C. J. Ammann (1997). Upper mantle velocity structure beneath the Tibetan Plateau from Pn travel time tomography, *J. Geophys. Res.*, 102, 493-505.
- Mejia, J. A. (2001). Lithospheric structure beneath the Tibetan Plateau using simultaneous inversion of surface wave dispersion and receiver functions. Unpublished Doctoral Dissertation, Saint Louis University, Saint Louis, Mo.
- Menke, W. (1984). Geophysical data analysis: Discrete inverse theory, Academic Press, Orlando.
- Mereu, R. F., J. Brunet, K. Morrissey, B. Price, and A. Yapp (1986). A study of the microearthquakes of the Gobles Oil Filed area of southwestern Ontario., *Bulletin of the Seismological Society of America*, V76, pp 1215-1223.
- Mereu, R. F. and J. A. Hunter (1969). Crustal and upper mantle under the Canadian Sheild from project Early Rise data. *Seismological Soc. of America Bull.*, 59, 147-165.
- Minster, J.B., and T. H. Jordan (1978). Present-day plate motions, *Journal of Geophysical Research*, 83, 5331-5375.
- Miller, H.G., G. J. Kilfoil, and S. T. Peavy (1990). An integrated geophysical analysis of the Carboniferous Bay St. George Basin, western Newfoundland. *Bulletin Canadian of Petroleum Geology*, 38, 320-331.
- Mitchell, B. J., R. B. Herrmann (1979). Shear velocity structure in the eastern US from the inversion of surface-waves group and phase velocities. *Bulletin of the Seismological Society of America*, 69, 1133-1148.
- Mitchell, B. J., O. W. Nuttli, R. B. Herrmann, and W. Stauder (1991). Seismotectonics of the central United States. In: Slemmons, D. B., Engdahl, E. R., Zoback, M. D., and Blackwell, D. D., eds., *Neotectonics of North America, Boulder, Colo., Geological Society of America, Decade Map Vol. 1*, 245-260.
- Mitchell, B. J., L. Cong, and J. Xie (1996). Seismic attenuation studies in the Middle East and Souther Asia, St Louis University Scientific Report No. 1, PL-TR96-2154, ADA317387.
- Mooney, H. A., J. M. Bonnicksen, N. L. Christensen, J. E. Lotan, and W. A. Reiners (1980). Fireregimes and ecosystem Properties. USFS, GTR WO-26, pp. 421- 444.
- Mooney, H. A., S. L. Gulmon, P. W. Rundel, J. R. Ehleringer (1980). Further observations on the water relations of *Prosopis tamarugo* of the Northern Atacama desert. *Oecologia* 44, 177.

- Mooney, W. D., M. C. Andrews, A. Ginzburg, D. A. Peters, R. M. Hamilton (1983). Crustal structure of the northern Mississippi Embayment and a comparison with other continental rift zones, *Tectonophysics*, 94, 327-348.
- Mooney, W. D. and L. W. Braile (1989). The seismic structure of the continental crust and upper mantle of North America. In: Bally, A.W., and A. R. Palmer, eds. *The Geology of North America- An overview. Boulder, Co. Geological Society of America, The Geology of North America, v. A.*
- Mooney, W. D. and T. M. Brocher (1987). Coincident seismic reflection / refraction studies of the continental lithosphere - a global review. *Rev. Geophys.*, 25, 723-742.
- Mooney, W. D. and R. Meissner (1992). Multi-genetic origin of crustal reflectivity : a review of seismic reflection profiling of the lower crust and Moho, in : *Continental lower crust*, pp. 45-79, ed. Fountain, D. M., Arculus, R. and Kay, R. W., Elsevier, Amsterdam,.
- Mooney, W. D., and L. W. Braile (1989). The seismic structure of the continental crust and upper mantle of North America, in Bally, A. W. and A. R. Palmer, *The Geology of North America, vol. A, The Geology of North America: An Overview: Geol. Soc. Amer., Boulder, Colo.*, 39-52.
- Morel, L. P., A. G. Green, and C. J. Pike (1984). Crustal refraction survey across the Trans-Hudson Orogen/Williston Basin of south-central Canada. *J. geoph. R.*, 92, 6403-6420.
- Morgan, P. and W. D. Gosnold (1989). Heat flow and thermal regimes in the continental United States, *Geol. Soc. Am. Mem.*, 172, 493-522.
- Musacchio, G., W. D. Mooney, J. H. Luetgert, N. I. Christensen (1997). Composition of the crust in the Grenville and Appalachian provinces of North America inferred from Vp/Vs ratios, *Journal of Geophysical. Research*, 102, 15,225-15,241.
- Nelson, K. D., R. J. Lillie, B. De Voogd (1982). COCORP seismic reflection profiling in the Ouachita Mountains of western Arkansas: Geometry and Geology interpretation. *Tectonics*, 1,413-430.
- Nutli, O. W., G. A. Bolliger, and D. W. Griffiths (1979). On the relation between Modified Mercalli Intensity and body-wave magnitude. *Bull. Seism. Soc. Am.*, 69, 893-909.
- Oldenburg D. W. (1981). A comprehensive solution to the linear deconvolution problem, *Geophys. J. R. Astr. Soc.*, 65, 331-357.
- Oldow, J. S., A. W. Bally, G. G. Av; Lallemand, and W. P. Leeman (1989). Phanerozoic evolution of the North American Cordillera; United States and Canada, in *The Geology of North America, Vol. A, The Geology of North America: An Overview*, edited by W. Bally and A.R. Palmer, *Geol. Soc. of Am., Boulder, Colo*, pp. 139-232.

- Oliver, J., R. Kovach, and J. Dorman (1961). crustal structure of the New York-Pennsylvania area: *J. Geophys. Res.*, 66, 215-225.
- Owens, T. J. (1984). Determination of crustal and upper mantle structure from analysis of broadband teleseismic P-waveforms, Unpublished Doctoral Dissertation, University of Utah, Salt Lake City, UT.
- Owens, T. J. (1987). Crustal structure of the Adirondacks determined from broadband teleseismic waveform modeling, *J. Geophys. Res.*, 92, 6391-6401.
- Owens, T. J. and G. Zandt (1985). The response of the continental crust-mantle boundary observed on broadband teleseismic receiver functions, *Geophys. Res. Lett.*, 10, 705-708.
- Owens, T. J., S. R. Taylor and G. Zandt (1987) Crustal structure at regional seismic test network stations determined from inversion of broadband teleseismic P waveforms, *Bull. Seism. Soc. Am.*, 77, 631-632.
- Owens, T. J. and R. S. Crosson (1988). Shallow structure effects on broadband teleseismic P waveforms, *Bull. Seism. Soc. Am.*, 78, 96-108.
- Owens, T. J., and G. Zandt (1995). The response of the crust-mantle boundary observed on broadband teleseismic receiver functions, *Geophys. Res. Lett.*, 12, 705-708.
- Özalaybey, S., M. K. Savage, A. F. Sheehan, J. N. Louie, and J. N. Brune (1997). Shear-wave velocity structure in the northern Basin and Range province from the combined analysis of receiver functions and surface waves, *Bull. Seism. Soc. Am.*, 87, 183-199.
- Peng, X. and E. D. Humphreys (1997). Moho dip and crustal anisotropy in Northwestern Nevada from teleseismic receiver functions. *Bull. Seism. Soc. Am.*, 87, 745-754.
- Percival, J. A., G. F. West (1994). The Kapuskasing uplift: a geological and geophysical synthesis. *Cand. J. of earth Scie.*, 31, 1256-1286.
- Phinney, R. A. (1964). Structure of the Earth's crust from spectral behavior of long period body waves, *J. Geophys. Res.*, 69, 2997-3017.
- Prodehl, C., J. Schlittenhardt, and S. Stewart (1984). Crustal structure of the Appalachian Highlands in Tennessee. *Tectonophysics*, 109, 61-76.
- Ramesh, D. S., R. Kind, and X. Yuan (2002). Receiver function analysis of the North America crust and upper mantle. *Geophys. J. Int.*, 150, 91-108.
- Randall, G. E. (1989). Efficient calculation of differential seismograms for lithospheric receiver functions, *Geophys. J. Int.*, 99, 469-481.

- Randall, G. E. and T. J. Owens (1994). Array analysis of the large-aperture array of the 1988-89 PASSCAL Basin and Range passive-source seismic experiment. *Geophys. J. Int.*, 116, 618-636.
- Richardson, R. M., S. C. Solomon, and N. H. Sleep (1979). Tectonic stress in the plates. *Rev. Geophys.*, 17: 981-1019.
- Ritzwoller, M. H., A. L. Levshin, L. I. Ratnikova, and D. M. Tremblay, (1999). High resolution group velocity variations across Central Asia, in Proceeding of the 18th Annual Seismic Research Symposium on Monitoring a Comprehensive Test Ban Treaty 4-6 September, 1996, Phillips Laboratory Report PL-TR-96-2153, July, pp. 98-107, ADA313692.
- Rivers, T., J. Martignole, C. F. Gower, and A. Davidson (1989). New tectonic divisions of the Grenville Province, southeast Canadian Shield, *Tectonics*, 8, 63-84.
- Rondenay, S., M. G. Bostock, T. H. Hearn, D. J. White, and R. M. Ellis (2000). Lithospheric assembly and modification of the SE Canadian Shield: Abitibi-Grenville teleseismic experiment. *J. Geophys. Res.*, 105, 13735-13754.
- Ross, G. M., B. Milkereit, D. Eaton, D. White, E. R. Kanasevich, and M. J. A. Burianyk (1995). Paleoproterozoic collisional orogen beneath the western Canada sedimentary basin imaged by Lithoprobe crustal seismic-reflection data. *Geology*, 23, 195-199.
- Ryberg, T. and M. Weber (2000). Receiver function arrays: a reflection seismic approach, *Geophys. J. Int.*, 141, 1-11.
- Sato, H. and M. C. Fehler (1998). Seismic wave propagation and scattering in the heterogeneous Earth, Springer, New York.
- Savage, M. K. (1998). Lower crustal anisotropy or dipping boundaries? Effects on receiver functions and a case study in New Zealand, *J. Geophys. Res.*, 103, 15069-15087.
- Shearer, P. M. (1999). Introduction to seismology, Cambridge University Press, Cambridge.
- Sheehan, A. F., G. A. Abers, C. H. Jones and A. L. Lerner-Lam (1995). Crustal thickness variations across the Colorado Rocky Mountains from teleseismic receiver functions. *J. Geophys. Res.*, 100, 20391-20404.
- Sieh, K. E. and R. H. Jahns (1984). Holocene activity of the San Andreas Fault at Wallace Creek, California: *Geological Society of America Bulletin*, v. 95, p. 883-896.
- Smith, D. L. and W. T. Dees (1982). Heat flow in the Gulf Coastal Plain, *J. Geophys. Res.*, 87, 7687-7693.

- Smith, W.E.T. (1966). Earthquakes of Eastern Canada and adjacent areas 1928-1959, Publication of the Dominion Observatory, Ottawa, Canada, v. XXXII, p. 87-121
- Snoke, J. A., I. S. Sacks, and H. Okada (1977). Determination of the subducting lithosphere boundary by use of converted phases, *Bull. Seism. Soc. Am.*, 67, 1051-1060.
- Stevens, J. L. (1986). Estimation of scalar moments from explosion-generated surface wave, *Bull. Seism. Soc. Am.*, 76, 123-151.
- Stevens, J. L. and D. A. Adams (1999). Improved methods for regionalized surface wave analysis, *Proceeding of the 21th Annual Seismic Research Symposium on Monitoring a Comprehensive Test Ban Treaty*, September 1999, 1, 274-282.
- Stevens, J. L., and McLaughlin (1988). Regionalized maximum likelihood surface wave analysis, Maxwell Technologies Technical report submitted to Air Force technical applications center, SSS-TR-89-9953, September, San Diego.
- Stewart, S. W. (1968). Crustal structure in Missouri by seismic refraction methods, *Bull. Seism. Soc. Am.*, 58, 291-323.
- Takeuchi, H. and M. Saito (1972). "Seismic surface waves". In *Methods in computational physics*, Vol. 11: Seismology: Surface waves and Earth Oscillations, B. A. Bolt, (ed.), Academic Press, New York, 217-295.
- Tarkov A. P. and V. V. Vavakin (1982). Poisson's ratio behavior in various crystalline rocks: application to the study of the Earth's interior. *Phys. Earth Planet. Int.*, 29, 24-29.
- Taylor, S. R. and M. N. Toksoz (1979). Three-dimensional crust and upper mantle structure of the northeastern United States, 84, 7627-7644.
- Taylor, S. R., and M. N. Toksoz, (1982). Measurement of interstation phase and group velocities and Q using Wiener filtering. *Bull. Seism. Soc. Am.*, 72, 73-91.
- Taylor, S. R. (1980). Crustal and upper mantle structure of the northeastern United States [P.h.D.]: Cambridge, Massachusetts Institute of Technology, pp.288.
- Taylor, S. R. (1989). Geophysical framework of the Appalachian and adjacent Grenville Province. *Geological Society of America Memoir 172*, 317-348.
- Taylor, S. R. and T. J. Owens (1984). Frequency-Domain inversion of receiver transfer functions for crustal structure. *Earthquake Notes.*, 55, 7-12.
- Taylor, S. R. and S. M. McLennan (1995). The geochemical evolution of the continental crust, *Rev. of Geophys.*, 33, 241-265.

- Tomfohrde, D. A. and R. L. Nowack (2000). Crustal structure beneath Taiwan using frequency-band inversion of receiver function waveforms, *Pure Appl. Geophys.*, 157, 737-764.
- Vdovin, O. Y., J. A. Rial, Ritzwoller, and M. H., A. L. Levshin (1999). Group-velocity tomography of South America and the surrounding oceans, *Geophys. J. Int.*, 136, 324-330.
- Villeneuve, M. E. et al. (1993). Tectonic subdivision and U-Pb geochronology of the crystalline basement of the Alberta Basin, Western Canada. *Geological Survey of Canada Bulletin*, 447, p.1-25.
- Warren, P. H., P. Claeys, and E. Cedillo-Pardo (1996). Mega-impact melt petrology (Chicxulub, Sudbury, and the Moon): Effects of scale and other factors on potential for fractional crystallization and development of cumulates, *The Cretaceous-Tertiary Boundary Event and other Catastrophes in Earth History*, v. 307, p. 105-124.
- White, D. J., R. M. Easton, N. G. Culshaw, B. Milkereit, D. A. Forsyth, S. Carr, A. G. Green, and A. Davidson (1993). Seismic images of the Grenville Orogen in Ontario, Can. *J. Earth Sci.*, 31, 293-307. Williams, H. and Hatcher, R. D. Jr. 1983: Appalachian Suspect Terranes. In "Contributions to the Tectonics and Geophysics of Mountain Chains" Ed. R.D. Hatcher, H. Williams and I. Zeitz. *Geological Society of America Memoir*, 158, pp 33 - 53.
- Wiggins, R. A. (1972). The general linear inverse problem: Implication of surface waves and free oscillations for Earth structure, *Rev. Geophys.*, 10, 251 - 285.
- Williams, Harold and R. D. Hatcher (1983). Appalachian suspect terranes; in Contributions to the Tectonics and Geophysics of Mountain Chains, R.D. Hatcher, Jr., H. Williams and I. Zietz (eds.); *Geological Society of America, Memoir*, 158, 33-53.
- Wu, F. T. and A. Levshin (1994). Surface-wave group velocity tomography of East Asia, *Phys. of Earth and Planet Int.*, 84, 59-77.
- Wu, F. T., A. L. Levshin and V. M. Kozhevnikov (1997). Rayleigh group velocity tomography of Siberia, China and the vicinity, *Pure Appl. Geophys.*, 149, 447-473.
- Wysession, M.E., K.M. Fischer, T.J. Clarke, G.I. Al-eqabi, M.J. Fouch, L.A. Salvati, P.J. Shore, R.W. Valenzuela (1996). Slicing into the Earth: Seismic mapping with the Missouri-to Massachusetts broadband deployment, *EOS*, 77, 477, 480-482.
- Yao, Z. S. and R. G. Roberts (1999). A practical regularization for seismic tomography, *Geophys. J. Int.*, 138, 293-299.

- Zandt, G. and C. J. Ammon (1995). Continental crust composition constrained by measurements of crustal Poisson's ratio, *Nature*, 374, 152-155.
- Zandt, G., S. C. Myers and T. C. Wallace (1995). Crust and mantle structure across the Basin and Range-Colorado Plateau boundary at 37 N latitude and implications for Cenozoic extensional mechanism. *J. Geophys. Res.*, 100, 10529-10548.
- Zelt, C. A. and D. A. Forsyth (1994). Modelling wide-angle seismic data for crustal structure: southeastern Grenville province *J. Geophys. Res.*, 99, 11687-11704.
- Zelt, B. C., R. M. Ellis, and R. M. Clowes (1993). Crustal velocity structure in the eastern Insular and southernmost Coast belts, Canadian Cordillera, *Can. J. Earth Sci.*, 30, 1014-1027.
- Zhao, L. S. and C. Frohlich (1996). Teleseismic body waveforms and receiver structures beneath seismic stations, *Geophys. J. Int.*, 124, 525-540.
- Zhu, H., and J.E. Ebel (1994). Tomographic inversion for the seismic velocity structure beneath northern New England using seismic refraction data, *Journal of Geophysical Research*, 99, 15,331-15,357.
- Zhu, L. and H. Kanamori (2000). Moho depth variation in southern California from teleseismic receiver functions, *J. Geophys. Res.*, 105, 2969-2980.
- Zhu, L., T. J. Owens, and G. E. Randall (1995). Lateral variations in crustal structure of the northern Tibetan Plateau inferred from teleseismic receiver functions, *Bull. Seism. Soc. Am.*, 85, 1531-1540.
- Zoback, M.D., and Zoback, M.L., (1991). Tectonic stress field of North America and relative plate motions, chapter 19, in Slemmons, D.B., Engdahl, E.R., Zoback, M.D., and Blackwell, D.D., eds., *Neotectonics of North America: Geological Society of America, Decade Map Volume 1*, p. 339-366.

Vita Auctoris

Mohammed S. Fnais was born in Ahad Rofedah (Saudi Arabia) on December 30, 1969. He received a bachelor degree in geophysics from King Saud University in Riyadh in the fall of 1995. Mohammed is the second oldest brother among eleven (six brothers and five sisters) all of them are doing well in their lives. All his brothers and sisters have graduated from the university with a bachelor degree, except the youngest three. Mohammed's family has accounting, electrical engineering, geophysics, dentistry, Islamic-Studies, chemistry, and mathematics majors under one roof.

In the future "In shaalah" the family will have a doctor in medicine. In fall 1989, he moved to the capital city in Saudi Arabia to attend the university to do his bachelor in geophysics. Because of his high GPA, the department of geophysics sent him to pursue his graduate studies in United States. Mohammed taught one year as teacher assistant at King Saud University. Beside studying, Mohammed likes to play soccer where he used to play for the College of Science team.

In 1997 he began the masters program in geophysics at Tulsa University Tulsa, Oklahoma, and graduated on spring 1999. He moved to St. Louis for the purpose of completing his PhD program, at the Department of Earth and Atmospheric Sciences of Saint Louis University.

Mohammed is a faculty member at King Saud University in Riyadh, Saudi Arabia. By Spring 2004, he will start his new life experiencing the beauty of

teaching following the path of his father.